2

EGG-WTD-9807
August 1991

Idaho National Engineering Laboratory

Managed by the U.S. Department of Energy

INFORMAL REPORT

In Situ Vitrification Application to Buried Waste: Final Report of Intermediate Field Tests at Idaho National Engineering Laboratory

R. A. Callow
L. E. Thompson
J. R. Weidner
C. A. Loehr
B. P. McGrail
S. O. Bates

EG&G Idaho

Work performed under DOE Contract No. DE-AC07-76ID01570

This document contains new concepts or the author(s) interpretation of new calculations and/or measurements; accordingly, EG&G Idaho, Inc. is required by the United States Government to include the following disclaimer:

EGG-WTD--9807

DE92 003384

IN SITU VITRIFICATION APPLICATION TO BURIED WASTE: FINAL REPORT OF INTERMEDIATE FIELD TESTS AT IDAHO NATIONAL ENGINEERING LABORATORY

R. A. Callow
L. E. Thompson*
J. R. Weidner
C. A. Loehr
B. P. McGrail*
S. O. Bates

Published August 1991

Idaho National Engineering Laboratory
EG&G Idaho, Inc.
Idaho Falls, Idaho 83415

*Pacific Northwest Laboratory
Richland, Washington 99352

Prepared for the
U.S. Department of Energy
Office of Environmental Restoration and Waste Management
Under DOE Contract No. DE-AC07-76ID01570

IN SITU VITRIFICATION APPLICATION TO BURIED WASTE: FINAL REPORT OF INTERMEDIATE FIELD TESTS AT IDAHO NATIONAL ENGINEERING LABORATORY

EGG-WTD-9807

August 1991

Prepared by:

R. A. Callow — 8/26/91 Date

L. E. Thompson — 8/26/91 Date

J. R. Weidner — 8/26/91 Date

C. A. Loehr — 8/26/91 Date

B. P. McGrail — 5/26/91 Date

S. O. Bates — 5/26/91 Date

Approved by:

S. K. Merrill, Unit Manager, In Situ Vitrification — 8/27/91 Date

ABSTRACT

This report describes two in situ vitrification field tests conducted on simulated buried waste pits during June and July 1990 at the Idaho National Engineering Laboratory. In situ vitrification, an emerging technology for in-place conversion of contaminated soils into a durable glass and crystalline waste form, is being investigated as a potential remediation technology for buried waste. The overall objective of the two tests was to assess the general suitability of the process to remediate waste structures representative of buried waste found at Idaho National Engineering Laboratory. In particular, these tests, as part of a treatability study, were designed to provide essential information on the field performance of the process under conditions of significant combustible and metal wastes and to test a newly developed electrode feed technology. The tests were successfully completed, and the electrode feed technology successfully processed the high metal content waste. Test results indicate the process is a feasible technology for application to buried waste.

SUMMARY

During June and July 1990 two in situ vitrification (ISV) field tests were conducted at Idaho National Engineering Laboratory (INEL) to investigate the application of ISV to buried waste. The Intermediate Field Tests were a cooperative effort between INEL and Battelle, Pacific Northwest Laboratory (PNL) using PNL intermediate-scale processing equipment.

The Intermediate Field Tests were conducted as part of a treatability study investigating ISV as a potential remediation technology for use at the Subsurface Disposal Area (SDA) of INEL. The U.S. Department of Energy has identified the need to remediate waste disposed between 1954 and 1970 at the SDA. Concerns over the human health and environmental effects of the wastes disposed at the SDA have arisen due to the discovery of various contaminants, notably solvents, in groundwater underlying the site. In addition, organic contaminants and radionuclides have been detected in sedimentary interbeds and perched groundwater beneath the SDA, indicating migration away from the disposal area. As a result of these discoveries and other waste disposal activities, INEL was included in November 1989 on the U.S. Environmental Protection Agency National Priority List under the Comprehensive Environmental Response, Compensation, and Liability Act. This listing has led to the need for the remedial investigation/feasibility study (RI/FS) currently being conducted for the SDA. These tests were conducted as part of the RI/FS process.

The objectives of these field tests were the following:

- verify the operational suitability of the electrode feeding system
- verify acceptable vitrification in a region containing buried waste similar to that expected at the INEL SDA
- verify acceptable vitrification of a representative buried waste composition layer with minimum soil content

- verify acceptable vitrification of a buried waste layer with high metal content, approximately 11 wt% metal

- assess the potential for radionuclide transport during the vitrification of buried waste by using nonradioactive tracer materials such as dysprosium oxide, terbium oxide, and ytterbium oxide

- obtain engineering and scientific data necessary to assess the engineering capability of the ISV system, the safety of the process streams, and the suitability of the process as a remedial method for application to INEL buried waste.

Two test pits were constructed near the Water Reactor Research Test Facility at INEL. These pits contained simulated waste with no hazardous or radioactive material. Test Pit 1 was designed to simulate a waste region of randomly disposed drums and boxes intermixed with fill dirt. Test Pit 2 was designed to simulate a region of stacked drums and a stacked box region containing high metal content waste. The materials contained in the drums and boxes were similar to waste types contained within the SDA buried waste.

The first Intermediate Field Test started on June 12, 1990 and continued until June 15, reaching the depth of 2.4 m (8 ft). This test was more dynamic than previous ISV tests conducted by PNL. A series of pressure and temperature transient spikes occurred within the off-gas hood as cans of buried combustible material were encountered. Electrical imbalances occurred in the power transformer due to an unusually small volume of molten glass and the lack of sufficient electrode control due to electrode sticking. The small volume of molten glass resulted from the greater percentage of void space in regions of buried waste relative to the normally occurring void percentage in soil. The smaller amounts of molten glass magnify the effects of transients on the power supply system. The insufficient electrode control resulted from the electrode coating sticking to the cold cap formed on top of the melt, thus, reducing the effectiveness of the electrode feed system. The test was

terminated when the advancing molten glass melted away from one of the electrodes resulting in loss of power to the melt.

Based on the experiences of Test 1, several changes were instituted prior to initiation of Test 2. These changes included additional overburden soil placed on top of the waste layer to provide a larger volume of molten glass, noncoated electrodes to reduce sticking, additional operational control of electrodes using the electrode feed system to reduce the effects of transients on the power system, and an additional backup blower added to the air inlet side of the hood to reduce the severity of hood pressure transients.

The second Intermediate Field Test was conducted July 12-14, 1990. During this test the melt proceeded through the test pit to a depth of approximately 3.9 m (10.8 ft). The melt penetrated both the stacked can region and the stacked box region of high metal content waste. Hood pressure transients were much reduced relative to Test 1 due to the increased amount of overburden placed over the waste, the increased control over electrode insertion and melt rate, and the more uniform heating of the stacked can region that was observed. Electrical imbalances were also reduced relative to Test 1 due to the additional operational control of the electrode feed system and power transformer.

Upon completion of Test 2, the two ISV blocks were allowed to cool prior to excavation on September 10, 1990. A careful and systematic excavation of the ISV processed pits was conducted in order to obtain physical descriptions of the waste pit morphology, the processed waste, and the vitrified product. Additionally, samples were collected for chemical and physical analysis and durability testing. Cores were drilled into the waste form and metal that pooled in the bottom of each pit to obtain analytical samples.

The general shape of Test Pit 1 after ISV processing was a square shaft with rounded corners. The depth from ground surface to the uppermost glassy material in the pit bottom, as measured directly from ground level, was about 1.5 m (5 ft). Depth from ground surface to the monolith centered among the four electrodes, was found to be about 1.9 m (6.1 ft). The monolith was

approximately oval and about 1.5 x 1.8 m (5 x 6 ft) with the long axis under diagonal electrodes (SW to NE). The thickness of the monolith was about 0.55 to 0.61 m (1.8 to 2.0 ft). The total amount of processed waste form recovered was 8267 kg (18,225 lb).

The general shape of the Test Pit 2 waste form was approximately rectangular with rounded corners. A significant amount of subsidence was observed in Test 2 with an approximate 60% reduction in volume as a result of processing. The depth from ground surface to the monolith upper surface ranges from 2.2 to 2.3 m (7.2 to 7.5 ft), with the monolith being 0.98 m (3.2 ft) in thickness. The maximum dimension of the monolith rectangle was 3.35 m (11 ft) and minimum was 2.90 m (9.5 ft). The weight of the monolith was 13,109 kg (28,900 lb), and the total amount of vitrified waste recovered from Test Pit 2 was 17,430 kg (38,425 lb). All waste within the melt volume was processed.

The product from both pits generally consisted of a black (with green tints) glassy material containing variable amounts of bubbles and crystalline material. The amount of bubbles varied with position in the pits. Although the crystalline materials found in the products from the two test pits were very similar, the megascopic appearance of the materials was somewhat different. Glass was the principle phase found within the monoliths. The outermost portion of the monolith, the most quickly cooled portion, was glassy with little devitrification (crystals). The Pit 1 waste form was smaller, cooled quicker, and so had little devitrification. Most of the material in the Test Pit 2 monolith was quite different in appearance. The Test Pit 2 monolith consisted of an outermost zone of black glass about 5.1 cm (2 in.) thick followed by a white to beige to lavender zone with a very fine crystal structure (aphanitic) region 5.1 to 10.2 cm (2 to 4 in.) thick that graded into a courser crystal structure (phaneritic) material. During cooling, devitrification occurred within the glass monolith producing a feather-like crystalline phase called augite. The mineral augite, a variety of clinopyroxene, is a calcium-magnesium-iron rich silicate. Augite is a common, naturally occurring pyroxene found in volcanic rocks, such as the basaltic rocks found at the INEL, which have compositions and cooling histories similar to the vitrified material in the Intermediate Field Tests reported here.

A series of tests were performed to determine the dissolution behavior of product samples. The IFT waste forms do not exhibit hazardous characteristics of TCLP toxicity. Based on MCC-1 leach testing data, the durability of the IFT waste form is comparable to naturally-occurring obsidian and granite, and 4 to 10 times more durable than typical high-level borosilicate nuclear waste glasses. Preliminary results from intrinsic rate constant measurements showed that the dissolution rates of the ISV samples range from 0.01 to 0.06 $g/(m^2 \cdot d)$ at 90°C and pH 7. These values are 10 to 100 times smaller than measured for a typical borosilicate nuclear waste glass. Devitrified samples from these tests showed a trend to be more durable in dissolution behavior than amorphous samples of equivalent bulk composition. Solids characterization of the ISV products showed that the ISV melts are chemically reducing, resulting in Fe^{2+}/Fe ratios >90%. Under equivalent closed-system conditions, as might occur during the slow migration of water through cracks in the solid mass, the reaction of the ISV glass with water reduces the redox potential to the lower stability limit of water. Under these conditions, several redox sensitive elements such as Se and Pu are expected to be sequestered in an alteration layer on the glass surface resulting in a smaller predicted release rate than calculated from the matrix dissolution rate alone.

As part of these tests, a tracer study was conducted during testing to provide qualitative assessment of the potential for radionuclide release during ISV processing of buried waste. During preparation of the test pits, rare-earth tracer elements were added to selected waste containers. The added tracers were oxides of dysprosium, terbium, and ytterbium (Dy_2O_3, Tb_4O_7, Yb_2O_3).

After testing, the amounts of tracers were measured in the vitrified product, in the smears of interior hood and off-gas piping surfaces, in the scrub solution, and in soil adjacent to the melt. Quantitative determination of tracer amounts was hampered by sampling and analysis uncertainties. Nevertheless, results indicated that the majority of each tracer was retained in the vitrified product as anticipated. The tracers concentrations were relatively homogenous throughout the glass and crystalline product. Order-of-

magnitude estimates for amounts of tracer materials released into the off-gas system for Test 1 were several grams to several tens of grams. This corresponds to up to several percent of the amounts initially added to the pit.

The results of the tracer study suggest the need for further effort to estimate the potential for radionuclide release during ISV processing. Further data are needed to quantify the magnitude of element retention by the melt; however, the data suggest that during buried waste ISV processing the retention of rare-earth tracers in the melt may be less than values previously reported for plutonium retention during processing of contaminated soil. The more dynamic melt off-gassing processes observed in these tests may enhance element release from the melt. Extrapolation of tracer results into predictions of plutonium behavior is currently without empirical foundation under ISV conditions; this is an area needing further investigation, including both theoretical analysis of release mechanisms and additional experimental data.

Compared to previous ISV applications to contaminated soils conducted at other Department of Energy sites, ISV processing of buried waste at INEL resulted in a more dynamic process, especially with respect to melt off-gassing and electrical transients in the power system. Containment of off-gases within the hood may require a more robust hood and off-gas system than currently designed. An improved design for off-gas containment may also be required for other ISV applications capable of generating sudden gas releases, such as underground tanks. These engineering considerations do not imply limitations in the fundamental ISV process.

Analytical modeling of the hood off-gassing transients was conducted in an attempt to improve understanding of physical mechanisms of off-gassing. These efforts were of limited value because data collection was not sufficient to validate assumptions in the models used. However, based on the measurements and results of these tests, recommendations are made for future testing and data collection design to address off-gassing mechanisms.

Results from these tests indicate that the ability to add glass-forming materials during processing may be desirable for buried waste ISV. A significant volume reduction of the processed buried waste is attained; however, the resulting subsidence may result in uncovering adjacent waste. Potential hazards of posttest activities would be alleviated by adding sufficient material (soil) during processing to keep the waste from being uncovered. This additional material may also serve to reduce electrical instabilities by reducing the impact of events such as glass flow into adjacent containers in the melt. Additional material may also buffer off-gas release as suggested by a comparison of results from these two tests.

The successful completion of these tests indicates ISV is a feasible technology for application to buried waste. The process fully incorporated and dissolved simulated waste containers to produce a durable product. The electrode feed technology was successful in processing the high metal content waste. The technique developed for use of movable electrodes will be beneficial for other ISV applications.

Additional assessment of the ISV process for application to buried waste is being conducted at INEL using an integrated program of laboratory-testing, field-testing, and analytical modeling.

ACKNOWLEDGMENTS

The successful completion of the ISV Intermediate Field Tests resulted from the combined efforts of many people at several institutions. The authors gratefully acknowledge the support provided by staff members from PNL, INEL, and the Geosafe Corporation. Their support significantly contributed to the success of these tests.

Operating Crew:

PNL: C. E. Bigelow, T. D. Powell, J. T. Jeffs, R. D. Sharp, S. S. Koegler, C. M. Smith, C. H. Kindle, R. D. Gibby, R. E. Garcia, M. C. Miller

Geosafe: C. L. Timmerman, B. E. Campbell, J. G. Carter

INEL: B. M. Gardner, S. K. Merrill, C. T. Mullen, D. F. Nickelson, L. A. Shelley, P. A. Sloan, L. C. Rounds

Off-gas Hood Design and Engineering Support (PNL): C. E. Bigelow, J. M. Seay, G. L. Ketner, R. L. Bogart, J. L. Tixier, R. M. Burnside, M. R. Garnich, R. L. Richardson

Off-gas Hood Construction (PNL): W. A. Douglass

Data Acquisition System Engineering (PNL): K. D. Steele

Process Performance Analysis (PNL): D. R. Gibby

Safety Engineering Support (PNL): A. G. Minister, R. M. Gough

Scientific/Engineering Support: D. R. Haefner, D. H. Miyasaki, C. E. Slater, K. M. Olson (PNL), D. L. Thomas (PNL)

Graphics Support: C. C. McKenzie, D. K. MacLeod

Publications Support: J. J. Nelson, K. L. Grant

Project/Program Management: J. L. Landon, R. M. Schletter, S. K. Merrill, S. A Morreale (DOE-ID), G. A. Hula (DOE-ID)

CONTENTS

FIGURES

TABLES

ACRONYMS

CERCLA	Comprehensive Environmental Response, Compensation, and Liability Act
DAS	Data Acquisition System
DF	decontamination factor
DIW	deionized water
DOE	Department of Energy
EFS	electrode feed system
EPA	Environmental Protection Agency
HEPA	High-efficiency particulate air
IC	ion chromatography
ICPAES	inductively coupled plasma, atomic emission spectrometry
IFT	Intermediate Field Test
INEL	Idaho National Engineering Laboratory
ISV	in situ vitrification
MRL	miminum reporting limit
NIST	National Institute of Standards and Technology
ORNL	Oak Ridge National Laboratory
PCT	Product Consistency Test
PD	Priority Data
PNL	Battelle, Pacific Northwest Laboratory
QC	quality control
REE	rare-earth element
RI/FS	remedial investigation/feasibility study
RPD	relative percent difference
RWMC	Radioactive Waste Management Complex

SDA	Subsurface Disposal Area
TAN	Test Area North
TCLP	Toxicity Characterization Leach Procedure
TRU	transuranic
WRRTF	Water Reactor Research Test Facility
WTDD	Waste Technology Development Department

IN SITU VITRIFICATION APPLICATION TO BURIED WASTE: FINAL REPORT OF INTERMEDIATE FIELD TESTS AT IDAHO NATIONAL ENGINEERING LABORATORY

1. INTRODUCTION

The U.S. Department of Energy (DOE) has identified the need to remediate waste disposed between 1954 and 1970 at the Subsurface Disposal Area (SDA) of the Radioactive Waste Management Complex (RWMC) at Idaho National Engineering Laboratory (INEL). The discovery of various contaminants, notably solvents, in groundwater underlying INEL has raised concerns over human health and environmental effects. In addition, organic contaminants and radionuclides have been detected in sedimentary interbeds and perched groundwater beneath the SDA, indicating migration away from the disposal area.[1] In November 1989, as a result of these discoveries and other waste disposal activities, INEL was placed on the U.S. Environmental Protection Agency (EPA) National Priority List under the Comprehensive Environmental Response, Compensation, and Liability Act (CERCLA). This listing has led to the need for the remedial investigation/feasibility study (RI/FS) currently being conducted at the SDA.

As part of the RI/FS, EG&G Idaho Waste Technology Development Department is conducting a treatability investigation of ISV as a remedial technology for use at the SDA. In situ vitrification (ISV) represents a promising technology for application to buried wastes. The technology was developed by Battelle, Pacific Northwest Laboratory (PNL) in the 1980s for remediation of soils contaminated with transuranic (TRU) material. The process utilizes electrical resistance heating to melt soil in place and fixes radioactive contamination by incorporation into a glass and crystalline waste form. Successful testing by PNL has proven the general feasibility and widespread applicability of the process.

To assess the applicability of ISV to buried waste, a comprehensive testing and analytical program has been developed. Testing is being done in a progressive fashion and includes both laboratory and field testing as well as

evaluation of the vitrified products. Analytical modeling is being used to define the tests and predict results. In this way, ISV will be evaluated in comparison to other likely candidates for SDA remediation. The overall treatability investigation process is being guided by established EPA criteria.

Two INEL Intermediate Field Tests were conducted as part of the ISV treatability investigation and represented the first testing of the ISV process in buried waste. The tests were designed to provide data on overall process suitability, performance of equipment, and potential technical issues of concern. This report provides results of the INEL tests and is organized as follows. Section 1 provides background information on the SDA buried waste site, the ISV process, and the intermediate-scale ISV equipment. Section 2 outlines the test objectives and factors influencing the design of the tests. Information for Test 1 is presented in Section 3; this includes specific test objectives, details of test pit construction, and a detailed review and assessment of process data collected during the test. Similar information for Test 2 is provided in Section 4. Section 5 includes the observations and data collected during the posttest excavation of the two vitrified products, and results of product evaluation studies. Section 6 presents results of a study involving transport of tracer materials placed in the buried waste materials. A discussion of analytical modeling of hood transients is presented in Section 7. Conclusions are provided in Section 8.

1.1 Brief History of the Radioactive Waste Management Complex

The RWMC encompasses 144 acres in the southwest section of INEL, as shown in Figure 1. Formerly known as the Burial Ground, the SDA of the RWMC served as a disposal area for radioactive [intermediate- and low-level solid and liquid wastes and TRU and mixed-fission products] and nonradioactive

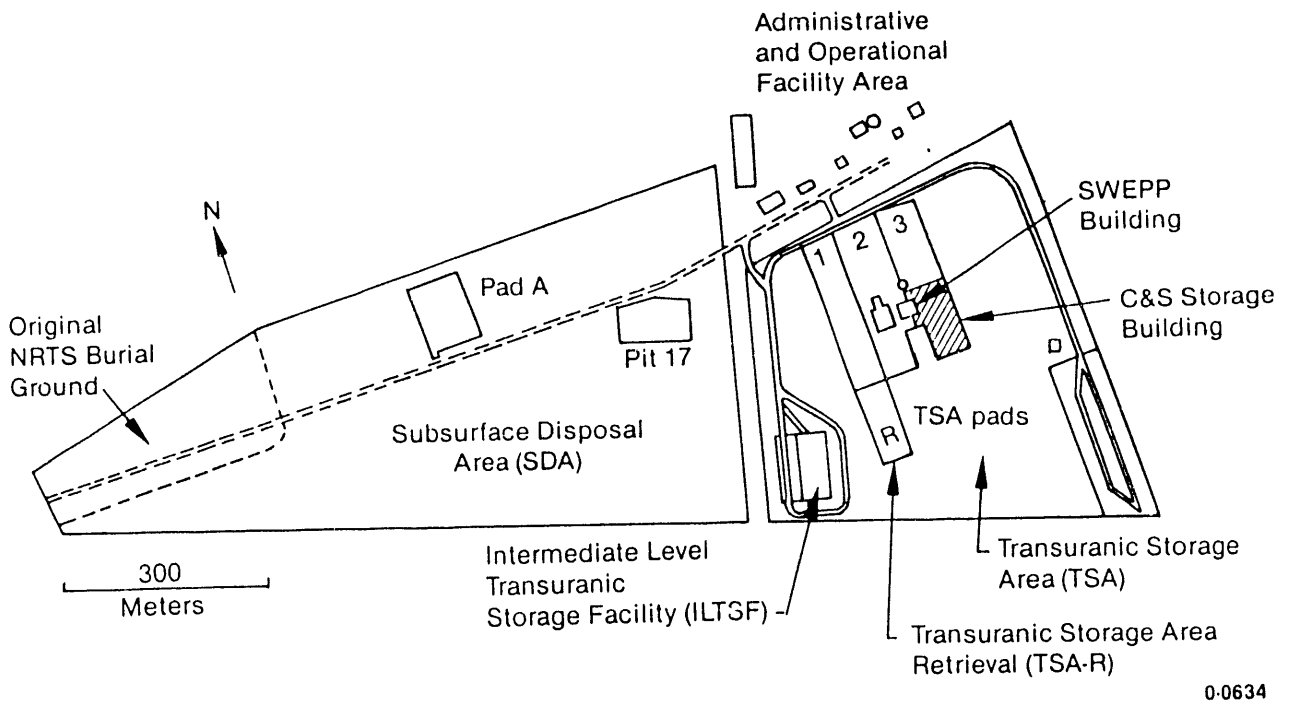

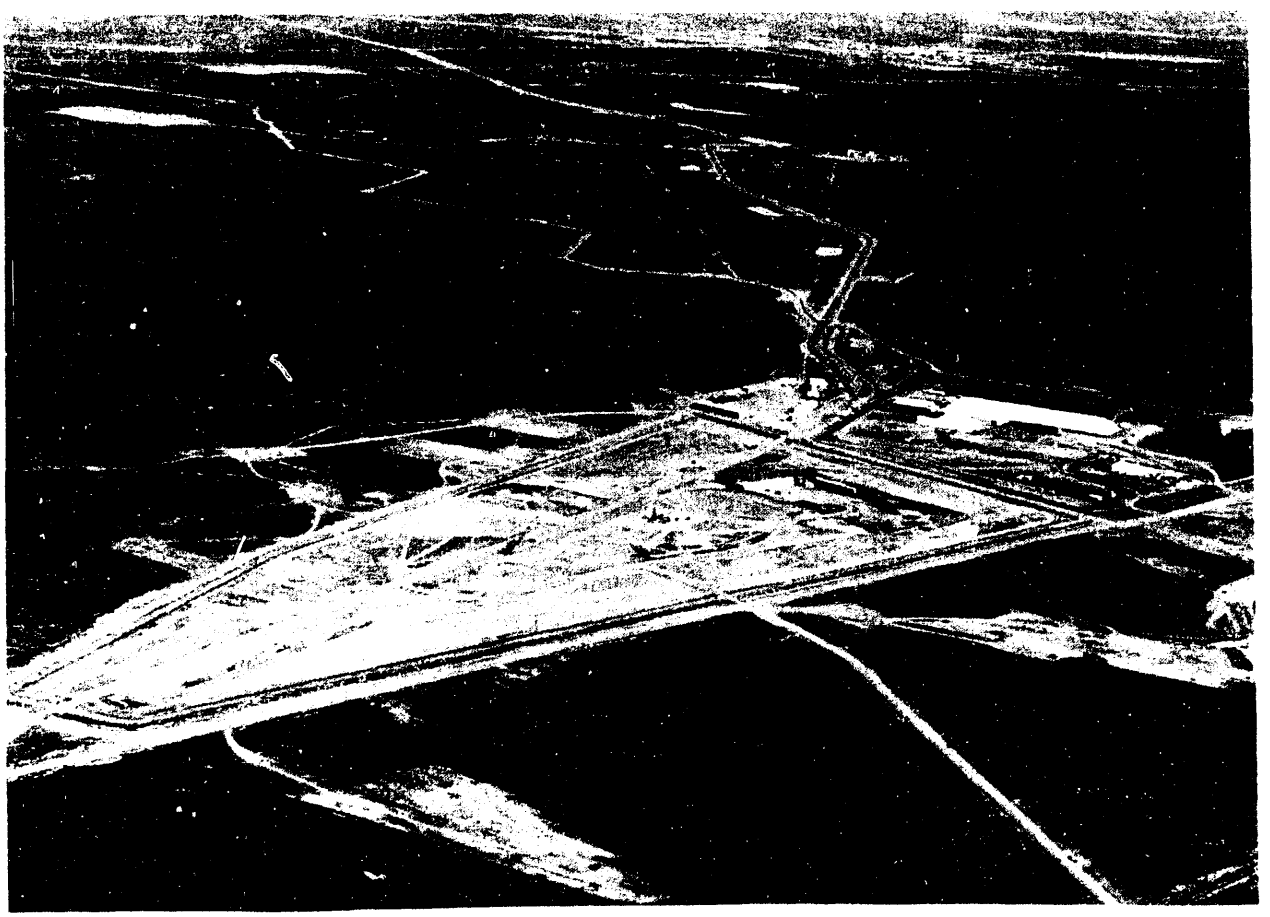

Figure 1. Radioactive Waste Management Complex.

hazardous wastes. The buried wastes were primarily generated by the DOE Rocky Flats Plant and INEL operations.

The SDA consists of belowground pits, trenches, and soil row vaults and one aboveground storage pad (Pad A). The pits are excavations that have surface areas of several acres and range in depth from 1.5 to 4.6 m (5 to 15 ft). In general, the pits were excavated to bedrock and covered with 0.61 m (2 ft) of soil, although some waste is believed to lay directly on basalt. Closure of a filled pit involved applying a final soil cover a few yards deep and planting stabilizing vegetation on the final cover.[1] Trenches at the SDA range in length from 30.5 to 305 m (100 to over 1000 ft) and were excavated approximately 1.5 m (5 ft) wide and an average of 3.7 m (12 ft) deep on 4.9 m (16 ft) centers. The waste was emplaced and usually, but not always, covered with at least 0.91 m (3 ft) of soil. The first trench at the Burial Grounds was opened for solid waste disposal on July 8, 1952. For about two years only mixed-fission product waste was buried. In April 1954 the first shipment of waste from the Rocky Flats Plant was received and buried in shallow pits and trenches with no segregation of TRU, mixed-fission product, and nonradioactive hazardous wastes. By 1957, ten trenches at the 13-acre site were nearly filled.

The site was then expanded to the 88-acre tract known today as the SDA. At that time, the use of large, open pits was initiated for the disposal of solid TRU wastes, with trenches reserved for the disposal of mixed-fission product wastes. Large, bulky items contaminated with mixed-fission product wastes were sometimes placed in the pits along with the TRU waste. During the 1960s, the SDA continued to receive TRU waste for disposal in the shallow land pits. Wastes in containers were deposited into the pits and trenches. Approximately 60% of the containers were steel drums (30 to 55-gal), 5% were plywood boxes, and 30% were cardboard and fiberboard containers.[1] Vehicles and large pieces of equipment were deposited without containers. From 1952 to 1963, the waste was stacked in the pits and trenches. From 1963 to 1969 the waste was randomly disposed into the pits to reduce worker exposure. This random placement continued until 1969, when stacking was reestablished. As a result, the distribution of wastes within the SDA is very heterogeneous,

making the characterization of any portion of the pits and trenches difficult. Disposal of TRU wastes in shallow pits and trenches at the SDA ceased in 1970. During the SDA operational period of 1952 through 1970, approximately 118,000 m^3 (4.2 million ft^3) of waste were disposed.

1.2 ISV Process Description and Development Status

ISV is a thermal treatment that melts contaminated soils and wastes into a chemically inert glass or crystalline substance. The process is initiated by a square array of four graphite electrodes inserted a few inches into the ground, as shown in Figure 2. Because soil is not electrically conductive, a mixture of flaked graphite and glass frit is placed among the electrodes to serve as a starter path. Once an electrical potential is applied to the electrodes, an electrical current is started in the starter path beginning the melt. The graphite starter path is eventually consumed by oxidation, and the current is transferred to the molten soil, which is processed at temperatures between 1450 and 2000°C. As the molten or vitrified zone grows, it incorporates or encapsulates any radionuclides and nonvolatile hazardous elements, such as heavy metals, into the glass structure. The high temperature of the process destroys organic components by pyrolysis. The pyrolyzed by-products migrate to the surface of the vitrified zone and combust in the presence of air. A hood placed over the area being vitrified directs the gaseous effluent to an off-gas treatment system. The waste is then allowed to cool, trapping waste in the vitrified substance.

The successful results of 59 tests conducted under a variety of site conditions and with a variety of waste types have proven the general feasibility and widespread applications of the process.[2] Table 1 shows the different scales of testing units that PNL used in developing and adapting ISV technology. In addition, economic studies have indicated tremendous economies of scale are attainable with the ISV process.[3] ISV technology, refined to the point of being commercialized for specific types of contaminated soil sites has been broadly patented within the United States, Canada, Japan, Great

In Situ Vitrification

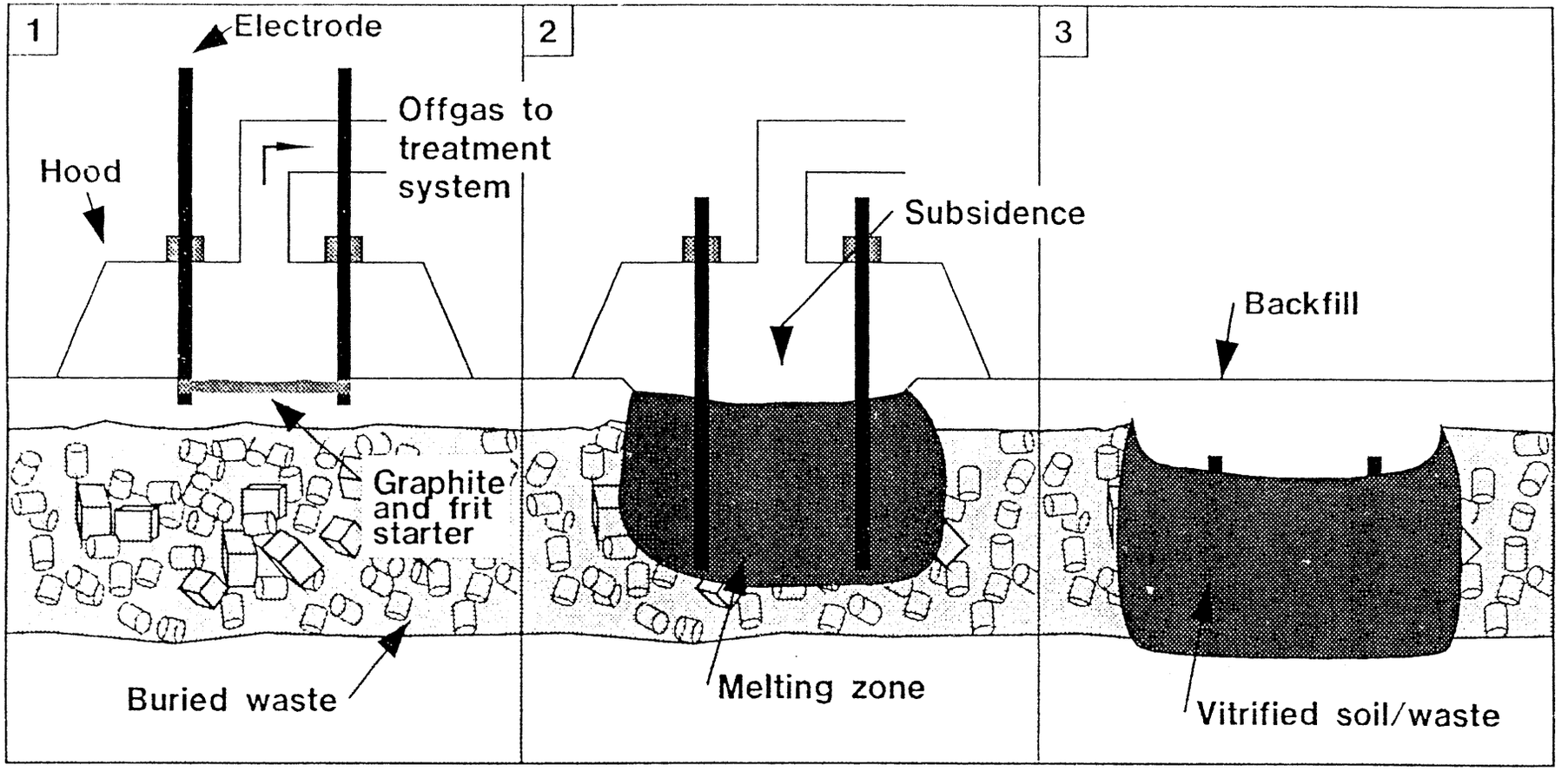

C9 2766

Figure 2. Electrode insertion during the ISV process.

Table 1. Testing units for developing ISV technology

Equipment Size	Electrode Separation, m	Block Size	Number of Tests Completed as of 12/1/90
Bench-scale	0.11	1 to 10 kg	19
Engineering-scale	0.23 to 0.36	0.05 to 1.0 t	33
Intermediate-scale	0.9 to 1.5	10 to 50 t	20
Large-scale	3.5 to 5.5	400 to 900 t	6

Britain, and France. Current emphasis is on developing the technology for buried waste and other subsurface inclusions such as buried tanks.

1.3 Intermediate-Scale Test System

The intermediate-scale test system consists of four graphite electrodes, a power control unit, an off-gas containment hood over the test site, and an off-gas treatment system housed in a portable semi-trailer, as shown in Figure 3. A layout of the ISV equipment at a typical site is shown in Figure 4. Figure 5 shows the system setup at the INEL Test Site.

1.3.1 Power System Design

The intermediate-scale power system uses a Scott-Tee connection to transform a 3-phase input to a 2-phase secondary load on diagonally opposed electrodes in a square pattern with a single potentiometer controlling both secondary phases, as shown in Figure 6 The 500-kW power supply may be either voltage or current regulated. The alternating current primary is rated at 480 V, 600 A, 3-phase, and 60 Hz. This 3-phase input on the primary side feeds the Scott-Tee connected transformer, providing a 2-phase secondary side (the secondary phases are denoted as phase A and phase B). The transformer

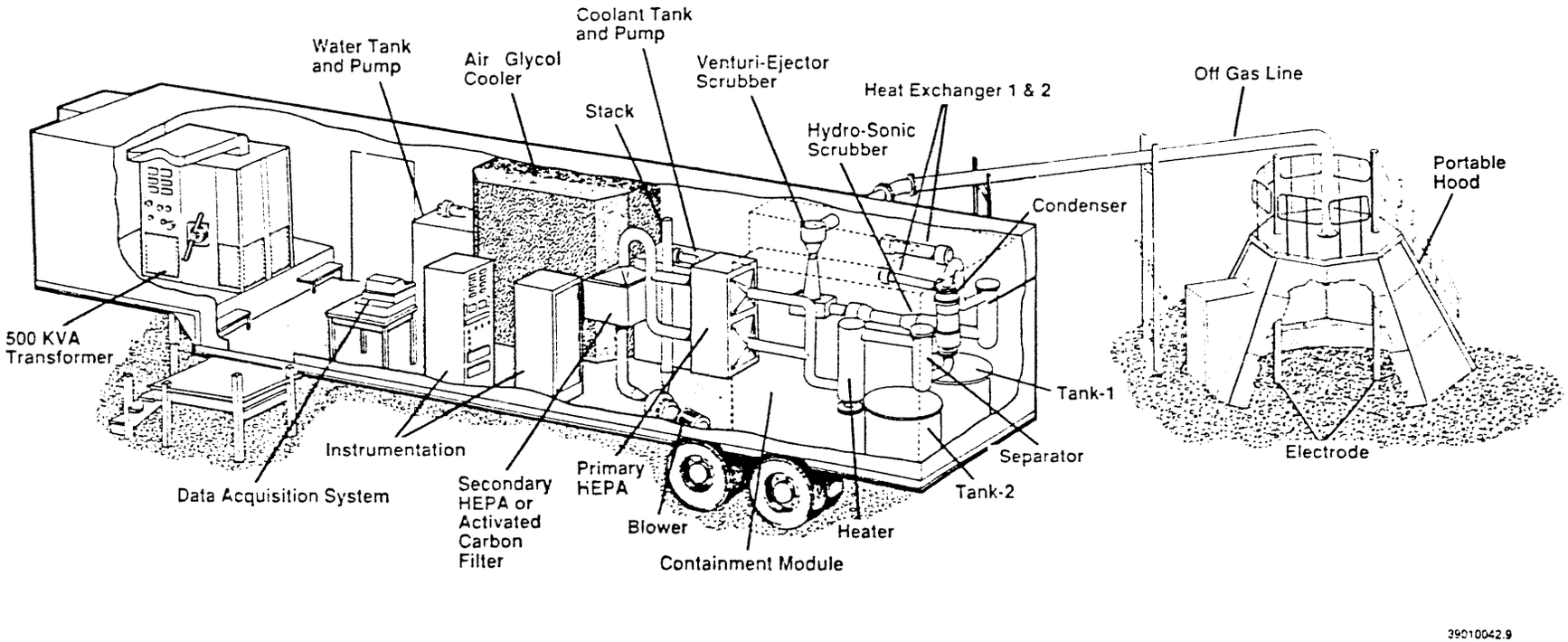

Figure 3. Cutaway view of the intermediate-scale process trailer and off-gas hood.

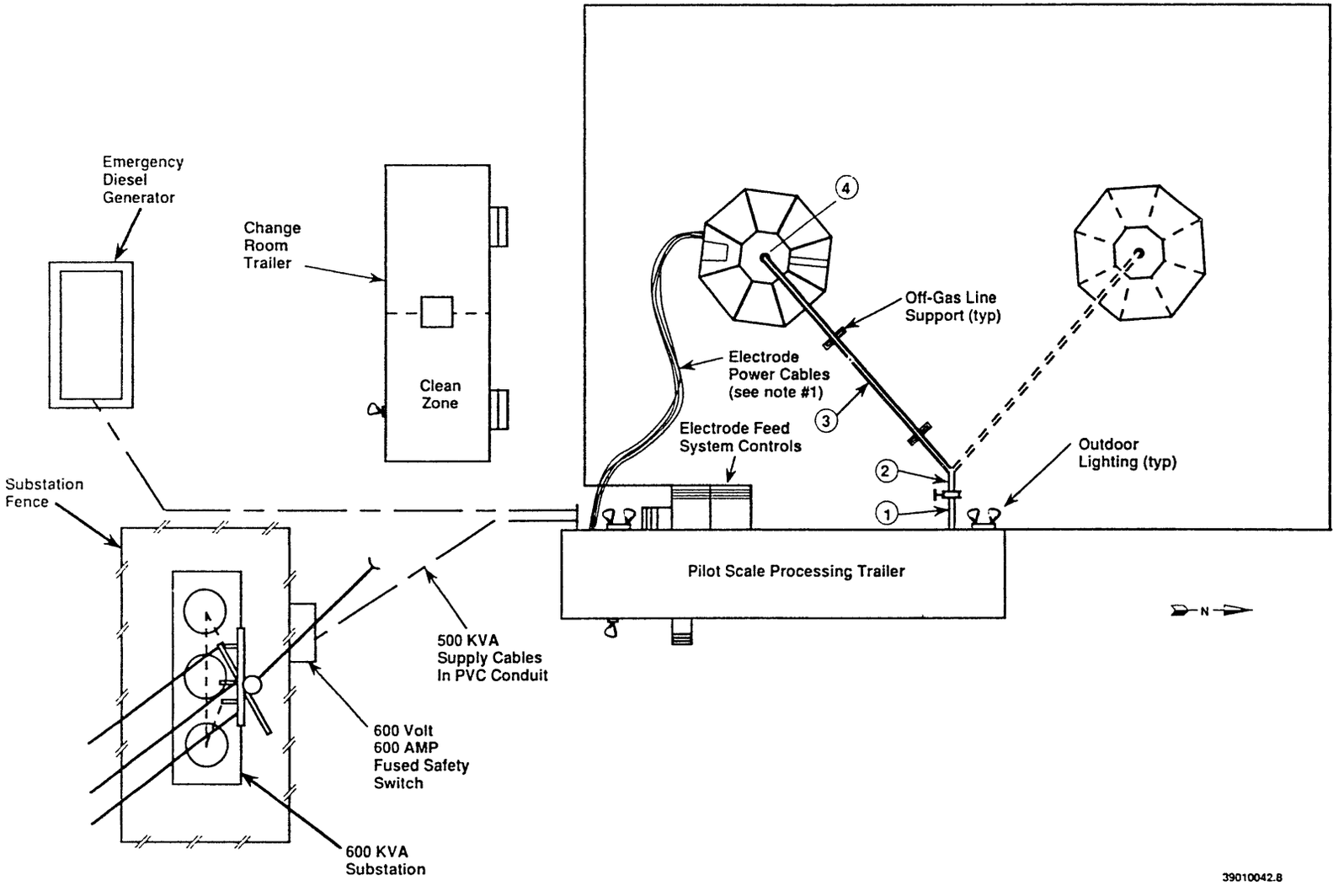

Figure 4. ISV equipment at a typical site.

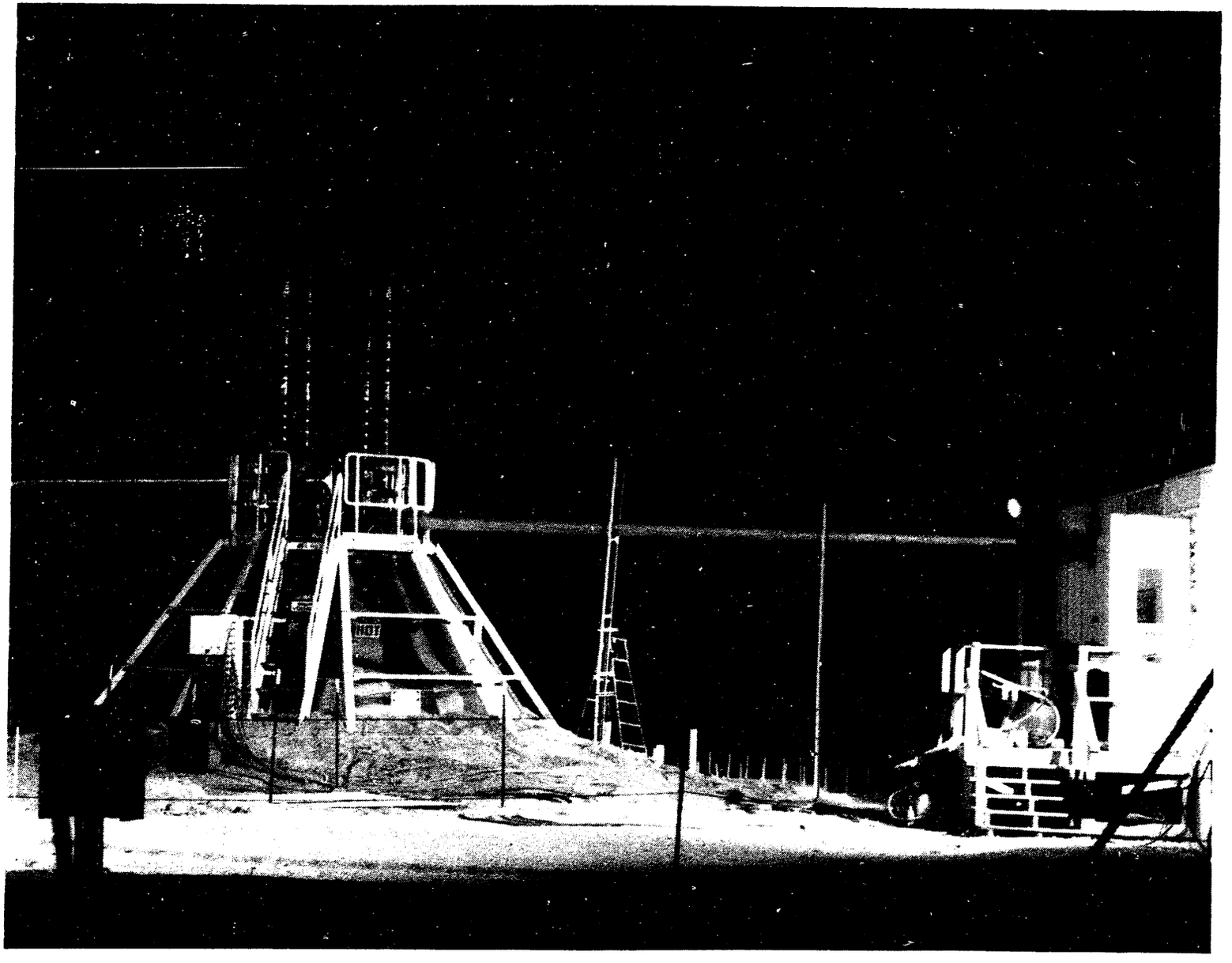

Figure 5. Intermediate-scale system setup at INEL Site.

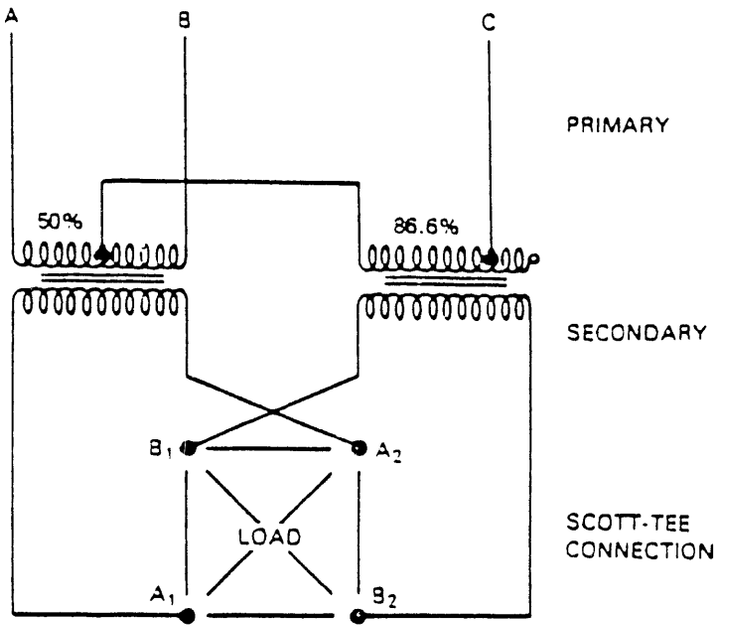

Figure 6. Scott-Tee electrical connection for the pilot scale ISV system.

has four separate voltage tap settings--1000 V, 650 V, 430 V, and 250 V. Each voltage tap has a corresponding amperage rating of 250 A, 385 A, 580 A, and 1000 A per phase, respectively. The amount of 3-phase input power delivered to the transformer is controlled by adjusting the conduction angle of the thyristor switches located in each of the three input lines. These switches, in conjunction with selectable taps on the transformer secondary, regulate the amount of output power delivered to both secondary phases. The Scott-Tee setup requires transformer taps at 50 and 86.6% of the primary transformer windings. The Scott-Tee connection provides an even power distribution when the molten zone approaches a uniform resistance load. The primary and secondary current is balanced for a Scott-Tee system when a balanced load exists.

1.3.2 Electrodes and Electrode Feed System

The graphite electrodes used to conduct current to the molten soil are 15.25 cm (6 in.) diameter and approximately 1.8 m (6 ft) long and are set up in a square array separated by a distance of 1.07 m (3.5 ft). Each electrode length is machined with female threads to allow connection of successive lengths via male threaded graphite connecting pins. The electrodes are initially buried to depths of 15 to 61 cm (6 to 24 in.), and the conductive mixture of starter path, consisting of graphite and glass frit, laid around and between the electrodes.

Electrodes are fed into the melt via a pneumatically controlled feed system. The electrode feed assemblies consist of four independently controlled, air-actuated systems with a feed system for each electrode. Each feed system has two air-actuated clamps and an air driven motor that provides vertical movement for one of the two air-actuated clamps. The moveable clamp allows the electrode to be inserted into or retracted from the melt. A second stationary clamp is provided to hold the electrode while the moveable electrode is being repositioned. Electrical contact from the power cables to each electrode is provided by a copper contact ring (brush), which is compressed to provide sufficient contact with the electrodes via a set of adjustable tension springs.

Normally, operations are conducted with the electrodes in a nongripped mode allowing the electrodes to rest on the bottom of the advancing melt front. As metallic objects, molten metal pools, or other electrically disruptive situations are encountered, the feed system is utilized to retract the affected electrode(s) until a stable electrical balance is achieved. Typically, a retraction of only 2 to 3 cm (1 to 2 in.) is needed to restore balance.

1.3.3 Starter Path

The starter path, consisting of a mixture of 35% glass frit and 65% graphite flake, is placed in a rectangular configuration with an electrode at each corner and a diagonal connecting the opposing electrodes. Preparations for laying the starter path involve ensuring the top soil of the area to be vitrified is free of coarse rock and other nonhomogeneous inclusions. The area is then covered with a 15 cm (6 in.) layer of sand. Next, a wooden form constructed of 2 x 4 in. studs cut to the length of the rectangular configuration is buried in the sand to the grade level and the area watered. Once the water has permeated the sand to at least the bottom of the studs, the studs are carefully removed leaving a trench with the approximate dimensions of 4 cm (1.5 in.) wide by 9 cm (3.5 in.) deep. In addition, hand-formed trenches of the same dimensions are formed around each of the four electrodes. At this point, a 2.5-cm (1 in.) deep layer of pure graphite flake is placed around the circumference of each electrode. Next, a 2.5 cm (1 in.) layer of the graphite/frit mixture is laid, and, finally, a 4 to 5 cm (1.5 to 2 in.) layer of the graphite/frit mixture is laid in the rectangular trench and also in the trenches of the diagonally opposing electrode pairs. Once the starter path is completed, it is covered with a 2.5 to 5 cm (1 to 2 in.) layer of fine soil or sand and is lightly patted in place. This layer of soil helps reduce the graphite particulate generation and carryover to the off-gas treatment system once powered operations are initiated.

Final preparations in the hood involve the placement of two layers of 1 in. thick KAO-WOOL insulation over the area to be vitrified. This silica insulation blanket is used to keep heat losses from the molten soil to a

minimum, especially during the early stages of operations. During the latter stages of operations, after the melt has achieved greater depths, the heat losses are limited by the formation of the naturally occurring cold cap, which is a frozen layer of glass covering the molten zone.

1.3.4 Off-Gas Containment Hood

The off-gas containment hood is designed to collect off-gasses emanating from the melt and to direct them to an off-gas treatment system. Typical operating conditions in the hood range from 1 to 2 in. of water vacuum and 200 to 400°C. The hood is operated at the slight vacuum, which is created by an induced draft blower, and has a volume of approximately 28.3 m^3 (1000 ft^3) to provide a surge capacity that minimizes vacuum loss during periods of sudden gas release. With a flow of between 10 and 15 m^3/min, gasses in the hood have a residence time of approximately 2 minutes.

The hood is an octagonal pyramid positioned above the containment shell and provides a working platform for the electrode feed system, access for maintenance personnel during nonpowered periods of operation, and support for the containment shell, as shown in Figure 3 (see p. 8). Off-gasses collected in the hood are directed to the off-gas treatment system via a 20.3-cm (8-in.) diameter off-gas pipe. The complete off-gas hood assembly is highly portable and can be assembled for operation in less than 1 day. The containment hood is constructed from 304L stainless steel sheet metal, with the side panels constructed from 18 gauge sheet metal and the top constructed of 14 gauge sheet metal. The containment hood is fitted with a removable door for entry prior to and following the test. A viewing window to observe the melt during processing is included as an integral part of the door design. Electrodes penetrate through the roof of the hood down to the zone to be vitrified, with seals composed of three independent layers of KAO-TEX 1000 (a tight-weave high silica fabric suitable for use in high temperature applications) around each electrode. The electrode seal is created by a press fit of the 15.25-cm (6 in.) diameter electrode through a 14 cm (5.5 in.) diameter hole in each of the fabric layers. This fabric configuration provides a relatively tight seal

around each electrode. The containment hood is sealed to the ground by piling soil around the base.

The hood design includes a seal pot assembly with a high-efficiency particulate air (HEPA) filter assembly. The seal pot assembly allows controlled air in-leakage into the hood for regulating vacuum and acts as a passive pressure relief system if the hood pressurizes from sudden gas releases. High pressure of approximately 1 in. of water causes a water seal to relieve and allows off-gases into the containment hood through the HEPA filter prior to venting the gases to the environment.

1.3.5 Off-Gas Treatment System

The off-gas passes through the off-gas treatment system, which consists of a Venturi-Ejector scrubber and separator, a Hydro-Sonic scrubber, a separator, a condenser, another separator, a heater, two stages of HEPA filtration, and a blower. The off-gas system is shown schematically in Figure 7. Liquid to the two wet scrubbers is supplied by two independent scrub recirculation tanks, each equipped with a pump and heat exchanger. The entire off-gas system has been installed in a 13.7-m long (45 ft) semi-trailer to facilitate transport to a waste site. Equipment layout within the trailer is illustrated in Figure 3 (see p. 8). All off-gas components except the final stage HEPA filter and blower are housed within a removable containment module. The containment module with gloved access for remote operations is maintained under a slight vacuum. This system was originally designed for testing radioactive-contaminated soil at the DOE Hanford Site.

The Venturi-Ejector scrubber serves as an off-gas quencher and as a high-energy scrubber. Heat is removed from the off-gas primarily via the Venturi-Ejector scrubber where aqueous scrubbing solution is sprayed into the off-gas stream. Heat removal from the scrub solution is accomplished by a closed loop cooling system, which consists of an air/liquid heat exchanger, a coolant storage tank, and a pump. A 50% water/ethylene glycol mix is pumped from the storage tank, through the shell side of the condenser, to the two

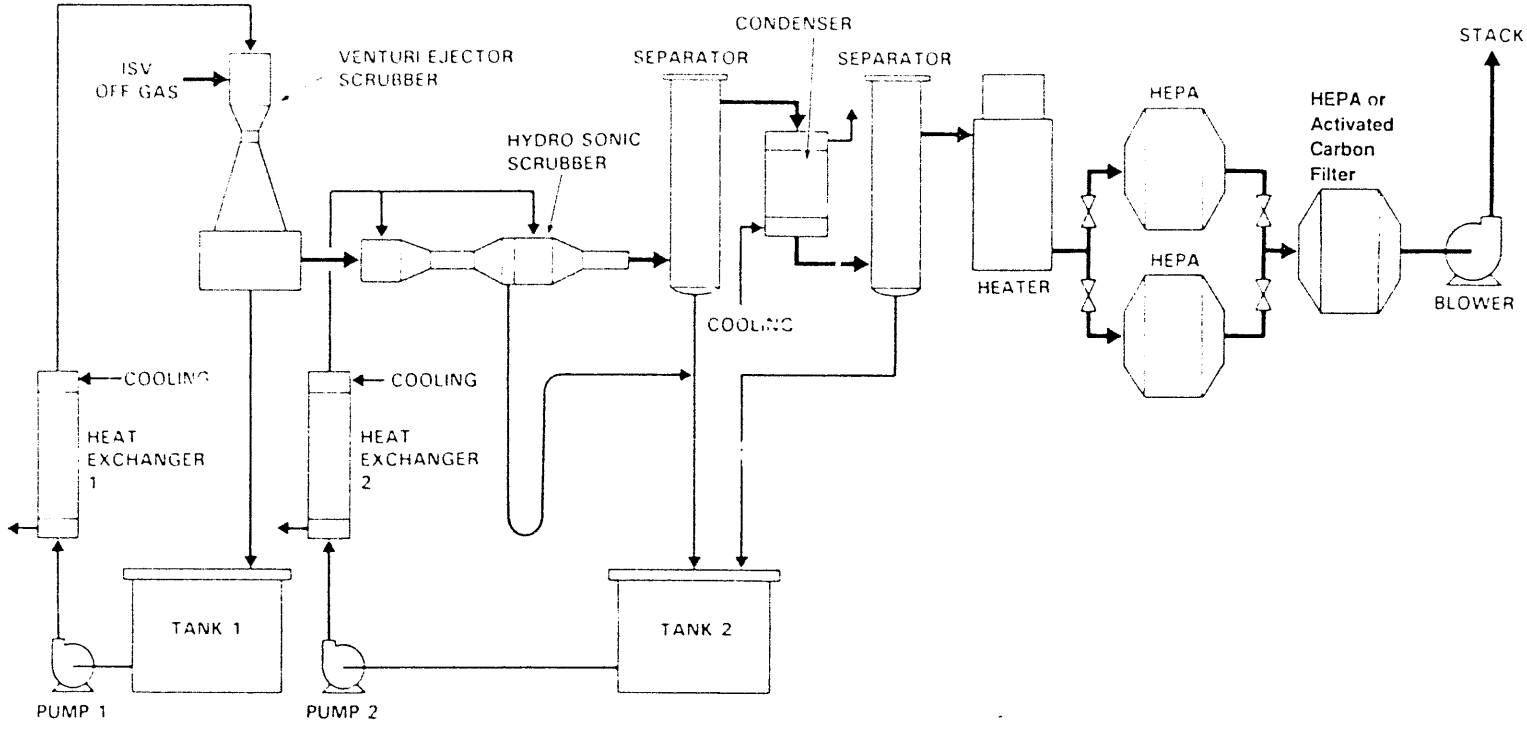

Figure 7. Schematic diagram of the intermediate scale ISV off-gas treatment system

scrub solution heat exchangers and then through the air/liquid exchanger where heat is removed from the coolant and discharged to the environment. The second scrubber is a two-stage Hydro-Sonic scrubber (tandem nozzle scrubber), as illustrated in Figure 8. The first stage condenses vapors, removes larger particles, and initiates growth of the finer particles so that they are more easily captured in the second stage. Particulate is captured when the gas is mixed with fine water droplets produced by spraying water into the exhaust of the subsonic nozzle. Mixing and droplet growth continue down the length of the mixing tube. Large droplets containing the particulate are then removed by a vane separator and drained back into the scrub tank. The unit is designed to remove over 90% of all particulate greater than 0.5 μ in diameter when operated at a differential pressure of 50 in. of water. Removal efficiency increases with an increase in pressure differential. Additional water is removed from the gas system by a condenser having a heat exchange area of 8.9 m^2 (96 ft^2) and a final separator. The gasses are then reheated ~25°C above the dew point in a 30-kW heater to prevent condensate in the HEPA filters.

The final components of the off-gas treatment system consist of two off-gas HEPA filters and an induced draft blower. The first stage of filtration consists of two 61 x 61 x 29-cm (24 x 24 x 11.5-in.) HEPA filters in parallel. During operation, one filter is used and the other remains as a backup in case the primary filter becomes loaded. The primary filter can be changed out during operation without process shutdown. The second-stage filter acts as a backup particulate filter in case a first-stage filter fails and is identical in construction and filtering efficiency as the initial-stage filters. The induced draft blower provides a total off-gas flow of between 10 to 20 m^3/min and creates a vacuum of approximately 100 in. of water.

1.3.6 Data Acquisition Systems

The Data Acquisition System (DAS) and associated instrumentation provide extensive process monitoring capabilities for ISV testing. For process control, inputs from process instruments are routed through a Hewlett Packard

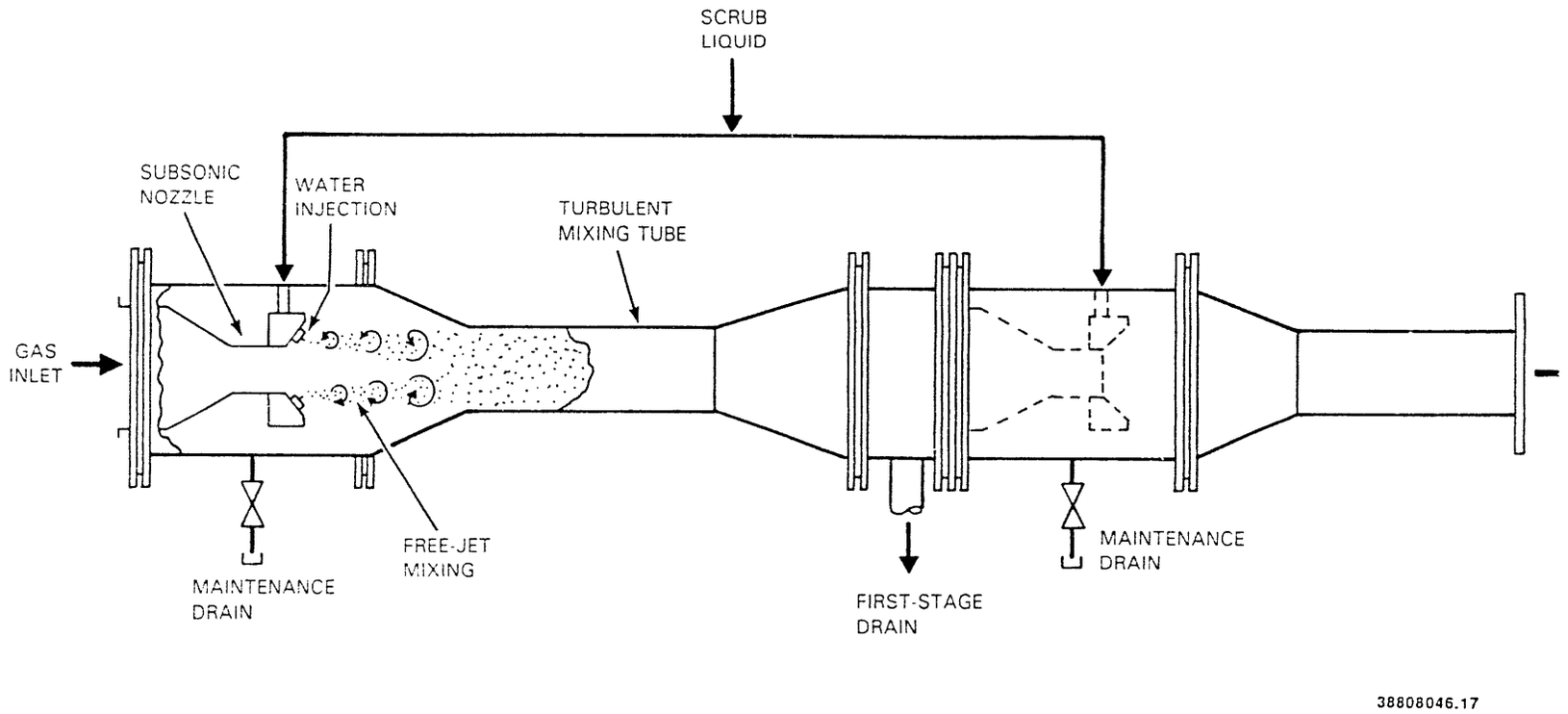

Figure 8. Tandem nozzle Hydo-Sonic Scrubber

model 3497A data acquisition and control unit linked to a MacIntosh II CX computer operating Lab View 2.0 software. The DAS scans, records, displays, and files process control informational data at the rate of twice per minute. The software allows essentially simultaneous manipulation of recorded data (for producing trend plots, etc.) while acquiring and storing data.

A second independent system, named the Priority Data (PD) system, scans, records, displays, and files critical process data at the rate of once per second. The PD system also features a visual alarm function to notify operators that operational limits (design parameters) have been reached. This system utilizes a second MacIntosh II CX computer operating Lab View 2.0 software to monitor the following eight data points associated with the off-gas containment hood.

- Two redundant hood vacuum points
- One plenum temperature
- One off-gas exit temperature
- Two wall temperatures (external and internal)
- Two roof temperatures (external and internal).

These eight parameters recorded by the PD system are sampled and stored at 1 second intervals; whereas the parameters recorded by the DAS are sampled and stored at 30 second intervals. As a result of this sampling frequency, the PD system provides better resolution of the maximum values of transient temperatures and pressures recorded in the hood. Inspection of the test data indicted the better resolution of the PD system was significant only in the recording of hood pressure transients because of the rapid spiking of pressure. In the case of pressure, the maximum value of pressure attained is more accurately recorded by the PD system. The rate of temperature change inside the hood was slow enough to be accurately resolved by either the DAS or the PD system.

The pressure transducers are Omega type transducers with a response time significantly better than 1 second. The range for the transducers is set to 5 in. of water vacuum to 5 in. of water pressure. The hood temperatures monitored by the PD system are acquired via 1/8-in. ungrounded stainless steel sheathed type K thermocouples.

2. TEST OBJECTIVES AND TEST DESIGN BACKGROUND

2.1 Test Objectives

Six major test objectives for the ISV Intermediate Scale Tests were identified.

- Verify the operational suitability of the electrode feed system (EFS)
- Verify acceptable vitrification in a region containing waste forms similar to those expected at the SDA
- Verify acceptable vitrification of a representative waste composition layer with minimum soil content
- Verify acceptable vitrification of a waste layer with high metal content
- Assess the potential for radionuclide transport during the vitrification process by using nonradioactive tracer materials
- Obtain engineering and scientific data necessary to assess the engineering capability of the ISV system, safety of the process streams, and suitability of the process as a remedial method.

Each of these objectives is justified as follows:

(a) Operational suitability of the EFS. All previous ISV tests have been conducted with the electrodes fixed at their maximum depth in the ground in predrilled holes. The EFS has been designed to allow the melt to be started with the electrodes inserted at depths of 15 to 61 cm (6 to 24 in.). As the melt progresses, the electrodes are fed down to their desired depth. This method of

operation (no predrilling) is highly desirable to reduce contamination spread and exposure at radioactive sites. The suitability of the EFS will be demonstrated at the intermediate-scale before a full-scale EFS is designed and built.

(b) Verify vitrification in a region containing waste forms similar to those found in the SDA. It is necessary to demonstrate the suitability of the ISV technology in producing acceptable vitrified product from soil and waste forms like those found in the SDA. Where applicable, information from SDA Pit 9 was used as a representative; however, it is recognized that there is significant uncertainty and variability regarding waste composition throughout the SDA.

(c) Verify vitrification of a waste layer with minimum soil content. Stacked boxes and drums in areas of the SDA could result in waste layers with reduced amounts of soil. It is necessary to verify the technique will provide suitable vitrification in these situations.

(d) Verify acceptable vitrification of a waste layer with high metal content. Areas of high metal content can potentially result in the formation of a metallic pool layer with subsequent shorting of the electrodes. It is necessary to verify the suitability of the ISV/EFS technique under such circumstances because large metallic objects and areas of high metallic content may occur in the SDA.

(e) Assess the potential for radionuclide transport. The intermediate-scale tests present an opportunity to assess the behavior of radionuclides by using nonradioactive, nonhazardous simulants. Potential problems can be identified and addressed prior to full-scale testing in radioactively contaminated waste.

(f) Obtain engineering and scientific data necessary to assess the engineering capability of the ISV systems, safety of the process streams, and suitability of the process as a remedial method.

Because these tests were the first field tests of ISV for buried waste applications, they provided an opportunity to discover potential issues of concern. Additionally, they provided product samples for characterization efforts.

Because the primary purpose of the ISV process is to stabilize and immobilize nuclear and toxic waste components, the chemical morphology and release characteristics of ISV products must be known to provide an accurate performance assessment. The properties of ISV products are directly related to the composition of the waste and surrounding soil and the thermal history of materials reacted during vitrification and cooling. The application of the ISV process to buried waste and soil at INEL presents unique conditions compared to the homogeneous soil/waste conditions previously tested at Hanford and Oak Ridge National Laboratory. Because the INEL soil and buried waste differ from previous ISV tests of soil and waste, a detailed characterization of the INEL ISV products is required.

It is necessary to collect data that will allow assessment of the engineering, safety, and environmental acceptability of the ISV process when applied at the SDA. Of particular concern is the off-gas transients that may occur during the processing of buried combustibles. There is little data available for this application. The presence of nonhomogeneous waste such as that which exists at the SDA and the amounts of combustible waste require a solid understanding of vitrification of different waste forms and gas releases from the melt be obtained. In addition, the engineering data obtained may be used to define design requirements for future testing or production systems.

2.2 Test Design Information

Two Intermediate Field Test pits were designed to meet test objectives described in Section 2.1. The first test was designed primarily to assess the performance of ISV in a region of randomly disposed waste. The second test was designed to assess performance in regions of stacked drums and in regions containing high-metal content wastes. A number of issues influenced the design of both tests and are described below.

2.2.1 Radionuclides and Hazardous Chemicals

Because the major objectives of the ISV Intermediate Field Tests were related to overall assessment of the ISV process on buried waste, radionuclides and hazardous chemicals were excluded. The exclusion of radionuclides was expected to have little effect on vitrification process parameters. The overall process behavior would be expected to be similar whether or not radionuclides were present. However, the exclusion of volatile organic materials was recognized to be a compromise in that vitrification parameters may be different in areas of the SDA where organic materials are present. Data collected as part of the ISV laboratory testing program will be used to assess potential areas of difference. Measurements of organic migration will be conducted in controlled conditions during laboratory testing.

2.2.2 Scaling Issues

The tests were conducted using PNL intermediate-scale equipment that mandated the test pits be scaled allowing test data to assess the expected performance of a large scale system at the SDA. PNL provided computer derived recommendations for electrode spacing for both the intermediate scale and large scale ISV systems. A 3.51-m (11.5-ft) distance between the large scale electrodes was recommended for a 6.10 m (20 ft) melt depth of INEL soil. The recommended intermediate scale value for electrode spacing was 1.07 m (3.5 ft) and was scaled from the large scale spacing to provide equal power density (kW/m^2) to the melt at each scale. The intermediate scale ISV system has a reduced power output relative to the large scale system.

The waste containers used in the intermediate-scale test were scaled representations of 55-gal drums and 1.2 x 1.2 x 2.4 m (4 x 4 x 8 ft) boxes. The linear dimensions were reduced by the ratio of the electrode spacing (3.5/11.5), therefore reducing the volume of waste containers by $(3.5/11.5)^3$. Standard containers with volumes closely approximating the calculated scaled volumes were used.

2.2.3 Waste Fractions and Disposal Efficiency

The intermediate-scale test pits were designed to include waste fractions similar to those found in the SDA.[4] Significant uncertainties exist regarding the distribution of waste throughout the SDA. The solid radioactive waste stored at the SDA is mixed with nonhazardous waste including broken equipment, lumber, paper, rags, plastic, and other solid debris. In addition, substantial amounts of organic waste from the Rocky Flats Plant exist in several pits. The test pit waste fractions for drums and boxes are found in Table 2. Separate waste materials were not mixed within individual drums (i.e., 50% of the drums consisted of entirely combustibles, 30% of entirely sludge, etc.).

Table 2. Volume of waste fractions

Container	Contents	Waste Fraction
Drums:		
	Sludge	0.30
	Combustibles	0.50
	Metals	0.08
	Concrete/glass	0.10
	Wood	0.02
Boxes:		
	Metal	0.80
	Concrete/glass/ wood	0.20

In addition, significant amounts of organic wastes contained in 55-gal drums from the Rocky Flats Plant are buried in Pits 5, 6, 9, and 10. Much of the sludge buried in Pit 9 consists of Organic Setups, Content Code 3, which was produced from treatment of liquid organic wastes generated by various plutonium and nonplutonium operations at Rocky Flats Plant.[5]

An important parameter of concern for the ISV process is the disposal efficiency ratio: waste volume/total volume. The same information can also be expressed in terms of soil to waste ratio. The relative amount of soil and waste is important for vitrification in order to produce a durable product and to ensure suitable amounts of soil to maintain conductance to the melt during the process. The soil-to-waste ratio limitations have not been defined for the ISV technology; therefore, the performance of the ISV process under

SDA-representative disposal efficiencies needs to be assessed. For Pit 9, a reasonable estimate of disposal efficiency is 0.25;[a] however, this is an average value for the entire pit. In local areas such as a stacked drum or box region, the disposal efficiency can be significantly higher.

2.2.4 Waste Materials Composition

The materials used in preparing the pit waste included steel drums and cardboard boxes. The 55-gal drums were simulated with carbon steel containers manufactured by Central Can Company of Chicago, Illinois. The containers were approximately 9.5 L (2.5 gal) capacity and 0.79 kg (1.75 lb). A lid was provided for each container and could be crimped to contain the waste; however, no effort was made to seal the cans. The boxes were simulated with standard cardboard boxes manufactured by Tharco Company of Salt Lake City, Utah. For structural strength, each box consisted of two boxes: an inner and outer box. The inner box measured 76 x 46 x 41 cm (30 x 18 x 16 in.), and the outer box measured 77 x 47 x 47 cm (30.5 x 18.5 x 18.5 in.). The combined weight of the boxes was 3.6 kg (8 lb).

The waste materials placed into the containers consisted of simulated sludge, combustibles, concrete/glass, metal, and wood. The combustibles consisted of computer paper and fabric used for combat fatigues. The concrete was obtained from a scrap pile 200-300 yards southeast of the INEL Water Reactor Research Test Facility (WRRTF) and was verified to be free of radioactive material by Test Area North (TAN) Health Physics. The glass was purchased from American Recycling in Idaho Falls, Idaho. Wood used as waste material was obtained from INEL cold waste dumpsters. The metal waste consisted of carbon steel and stainless steel from scrap piles on-site and at Pacific Steel. Much of the scrap carbon steel was rusted. Additionally, the carbon steel cans used to contain the waste were exposed to the weather prior to being placed in the pits and were rusted as well. It should be noted that previous retrieval projects at the SDA have resulted in the retrieval of badly deteriorated drums.[6,7] Most likely the containers used for the ISV

---

a. Engineering Design File, BWP-ISV-011

Intermediate Field Tests, even though slightly rusted, are in as good or better shape than most 55-gal drums likely to be found at the SDA.

Sludge was simulated by mixing 1.05 kg (2.31 lb) of MICRO-CEL E, 0.32 kg (0.70 lb) of FLOOR DRI, and 3.50 kg (7.71 lb) of water. MICRO-CEL E is the main ingredient used for solidification of Content Code 3 sludge. FLOOR-DRI is a dried clay material that simulates the clay material used in preparation of Rocky Flats Plant sludge. Table 3 provides a typical analysis of MICRO-CEL E and FLOOR-DRI. Hazardous organic materials were not added to the test pits; instead, the test pit sludge materials consisted of absorbent materials minus the organic materials. Water was substituted for the organic volume in order to provide a more realistic amount of vapor release into the off-gas system.

2.2.5 Test Pit Soil Material

The ISV test pits were built near the WRRTF at TAN, approximately 27 mi. northeast of the RWMC, as shown in Figure 9. In order to minimize the potential for processing difference resulting from different soil types found at the SDA and WRRTF, soil from the SDA lakebed (located near the RWMC but not part of the SDA area) was used for backfilling the ISV test pits. Soil from the lakebed was typically used as backfill soil within the SDA when additional soil was needed (e.g., to fill in subsided areas in the overburden or to supply additional overburden soil). Table 4 shows an analysis of the mineral constituents of the SDA lakebed soil.

2.2.6 Selection of Tracer Materials

Both test pits contained rare-earth tracers used to simulate the presence of plutonium. Test Pit 1 was spiked with three tracers: dysprosium oxide, ytterbium oxide, and terbium oxide. Test Pit 2 was spiked with dysprosium oxide. Detail on the Tracer placement and objectives of the Tracer is presented in Sections 6.3 and 6.4.

Table 3. Chemical composition of sludge

Element	Weight Percent
MICRO-CEL E[a]	
SiO_2	56.0
Al_2O_3	3.8
Fe_2O_3	1.0
CaO	26.0
MgO	0.7
Na_2O	0.6
K_2O	0.6
LOI[b]	11.3
FLOOR DRI[c]	
SiO_2	89.2
Al_2O_3	4.0
Fe_2O_3	1.5
CaO	0.5
MgO	0.3
Na_2O	0.25
K_2O	0.25
H_2O	4.0

a. The data for MICRO-CEL E were obtained from the manufacturer: Manville Corporation, Filtration and Minerals Division, Denver, Colorado 80217-5108 (303) 978-2000.

b. The loss on ignition (LOI) is assumed to include water and other nonhazardous volative materials.

c. The data for FLOOR DRI were obtained from Mr. Pat Flynn of Eagle-Picher, Reno, Nevada 89510, (702) 322-3331.

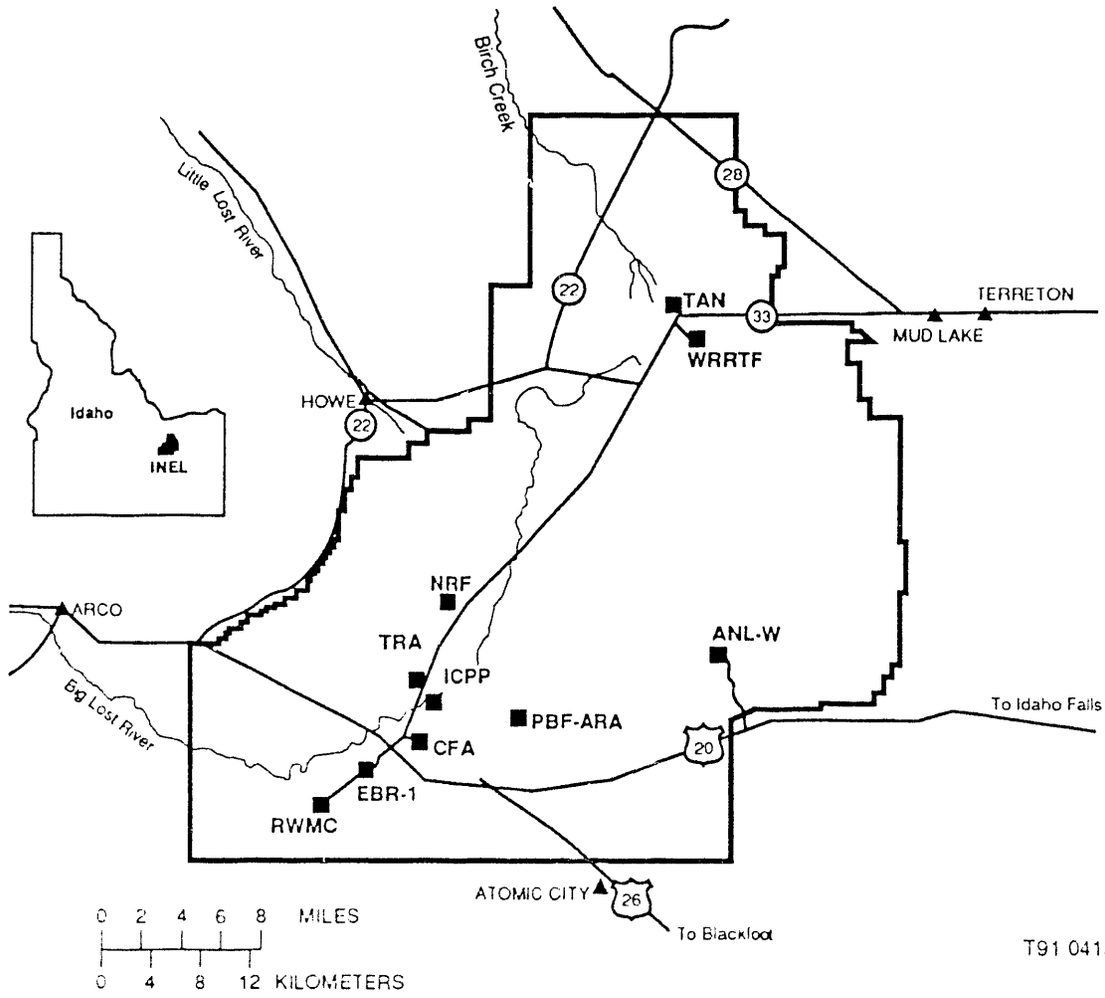

Figure 9. Map of INEL showing the WRRTF where the Intermediate-Scale Test took place.

Table 4. Chemical composition of SDA lakebed soil[a]

Element	Weight Percent
Silicon Oxide (SiO_2)	62.60
Aluminum Oxide (Al_2O_3)	11.85
Iron Oxide (Fe_2O_3)	4.25
Calcium Oxide (CaO)	3.68
Potassium Oxide (K_2O)	2.99
Magnesium Oxide (MgO)	1.72
Sodium Oxide (Na_2O)	1.37
Titanium Oxide (TiO_2)	0.68
Manganese Oxide (MnO_2)	0.10
Barium Oxide (BaO)	0.09
Zirconium Oxide (ZrO_2)	0.05
Boron Oxide (B_2O_3)	0.05
Nickel Oxide (NiO)	0.04
Strontium Oxide (SrO)	0.02
Chromium Oxide (Cr_2O_3)	0.02
Total Oxide	89.5
Water (H_2O)	7.50

a. Intermediate-Scale Testing of In Situ Vitrification, IS-INEL Test Plan, Rev. 1, Pacific Northwest Laboratories, March 1990.

2.3 Test Pit Construction Background Information

Two test pits were constructed for the ISV Intermediate Field Tests. In March 1989 a previously disturbed area (old baseball diamond) near the WRRTF was chosen for construction of the test pits. This area was chosen primarily because of the relative ease of supplying the required power. An environmental evaluation was performed prior to fieldwork activities. In May 1989 four holes were augured in the ground at the test site to verify that there was sufficient topsoil for construction of the test pits. In the area of the test pit there was 3.65 to 5.18 m (12 to 17 ft) of soil above basalt, with the topsoil at the western-most hole being 3.65 m (12 ft). Prior to test pit excavation, the test area was surveyed and staked, allowing correct placement of the two test pits relative to the position of the off-gas and administrative trailers. Construction of the test pits began on August 23, 1989. Test Pit 1 was filled on September 1-2, and Test Pit 2 was filled on

September 7-8. During pit digging and filling the weather was sunny and dry. After filling, the test pits were left undisturbed. No subsidence of the soil in the test pits was observed prior to the initial test operations in October 1989.

The waste containers for the test were filled in June - July 1989. After filling they were stored inside the WRRTF fence until the test pits were ready to be filled. The boxes were stored inside to protect them from the weather, and the cans were stored outside stacked on pallets. Rusting occurred on the exposed cans.

3. INTERMEDIATE FIELD TEST 1

This section presents information on INEL ISV Intermediate Field Test 1 and includes the specific objectives of the test, construction of the test pit, and description and assessment of the data collected during process operations. Product durability data are presented in Section 5. Results of the test tracer study are presented in Section 6. And information from analytical modeling based on off-gassing is presented in Section 7.

3.1 Test 1 Objectives and Test Pit Overview

This section presents objectives and design considerations specific to Test 1. General objectives applicable to both ISV tests are presented in Section 2.1 (see p. 21).

Test Pit 1 was primarily designed to test the ISV process in an area of randomly disposed waste that was representative of conditions expected to exist at the SDA. Due to the nonhomogeneous character of the SDA waste and the uncertainties regarding characterization of the waste, it was possible to represent SDA waste only in an overall sense. However, several key aspects of SDA buried waste were represented in order to collect applicable data for ISV processing performance, namely, buried combustible material and buried scrap metal in containers. Because all the waste was contained in cans and boxes, significant void space in containers existed due to constraints on packing scrap materials. Containers with void spaces are typical of what may be expected within SDA buried waste.

3.2 Test Pit 1 Construction Details

From bottom to top, Test Pit 1 consisted of 0.6 m (2 ft) of soil underburden, 1.8 m (6 ft) of a randomly-disposed box and can layer mixed with fill dirt, and 0.6 m (2 ft) of soil overburden. Figure 10 is a schematic of the completed Test Pit 1 with the hood in place.

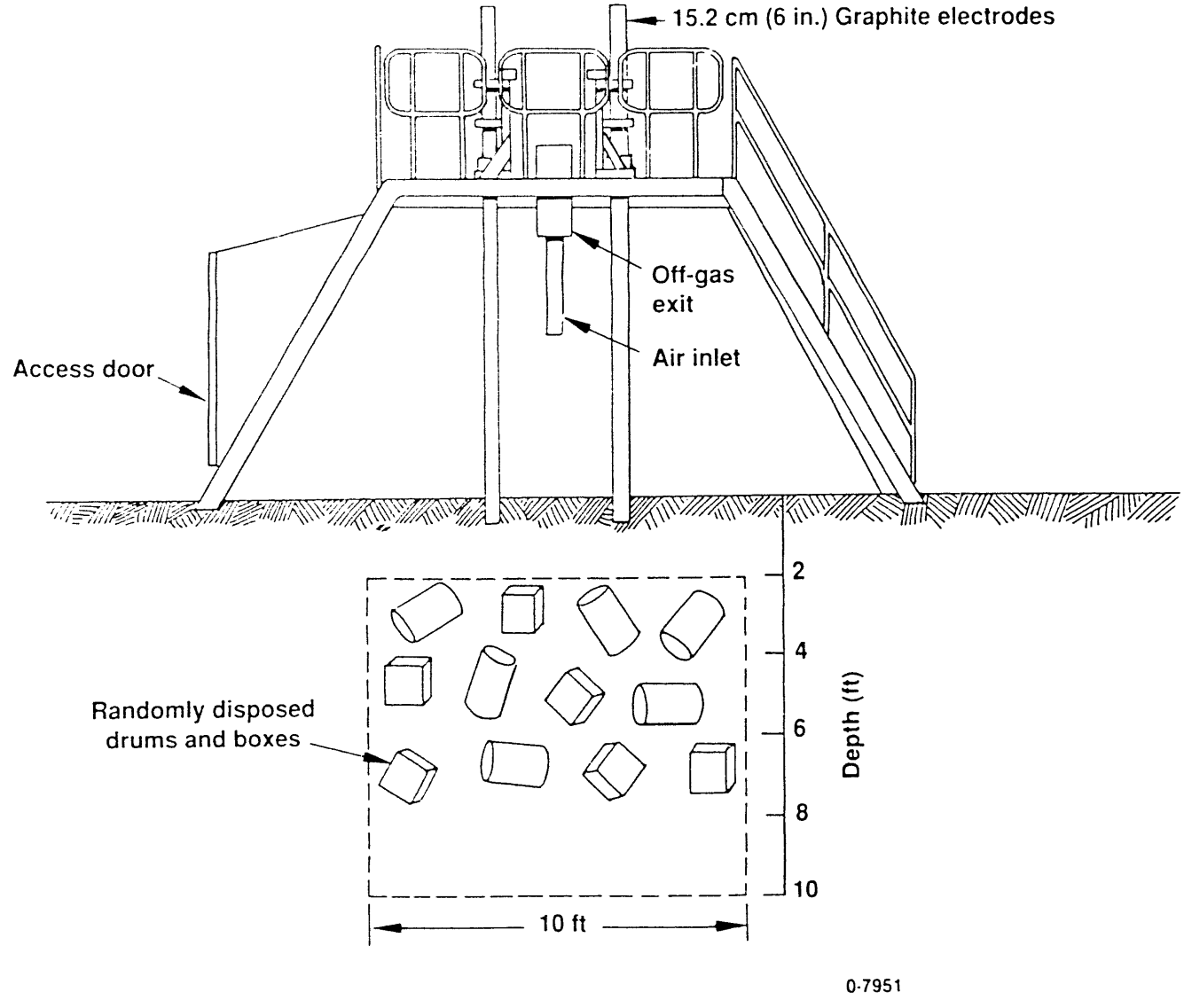

Figure 10. Schematic of completed Test Pit 1 with hood assembly covering the test site.

Test Pit 1 was built up in four layers with each layer consisting of approximately 5 boxes and 50 cans. The number of cans and boxes for each waste type in each layer is shown in Table 5. Tables 6 and 7 show the overall amounts of each waste type in the test pit. To obtain a random mixture of different waste types, a lottery was used to specify how many cans and boxes of each waste type would go into the specific layer being built. The cans and boxes were randomly placed into the test pit by hand with the exception of the cans containing tracers, which were hand-placed at specified levels and near the center of the pit.

Three types of tracer were place in Test Pit 1 in order to obtain data on possible effects of depth on tracer migration or release behavior. During Test Pit 1 filling, the three tracers were placed in three separate layers. Each tracer was added to six separate waste cans. The amount of tracer added to each can was approximately 225 g. The waste cans containing tracers were marked with orange spray paint and placed near the center of the pit to ensure that all tracer material would be within the melt zone. Figure 11 shows layer 4 (bottom layer of the four waste layers) after 5 boxes and 50 cans had been place. The boxes still banded to the wooden pallets contained concrete and glass; the other boxes contained scrap metal. Figure 12 shows layer 4 after backfill dirt has been added. Before starting on the next layer a hand compactor was used to compact the dirt. After compaction, layer 3 (second layer from the bottom of the pit) was placed containing 56 cans and 5 boxes. Figure 13 shows the cans and boxes for layer 2 (third layer from the bottom of the pit), which contained two tiers of tracer cans. The bottom tier of layer 2 contained tracer cans with ytterbium oxide, which were placed near the center of the pit. After placing backfill dirt over the bottom tier, the top tier was place with tracer cans containing terbium oxide, as shown in Figure 14. Figure 15 shows the can placement for layer 1 (the top layer), except for the tracer cans that contained dysprosium oxide.

During construction of Test Pit 1, two arrays of type K thermocouples were placed. A vertical array was place starting at approximately 15.2 cm (6 in.) from ground level and with the thermocouples spaced every 15.2 cm

Table 5. Depth view of Test Pit 1[a]

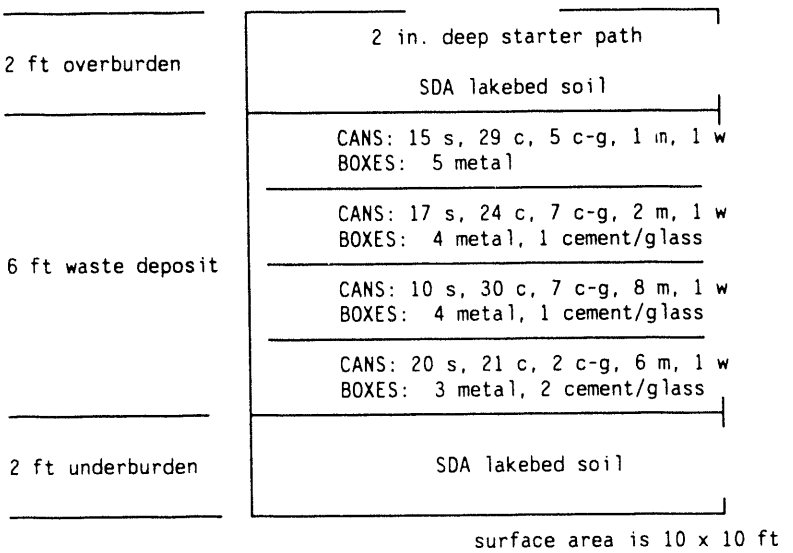

Where,

s is sludge cans

c is combustible cans

c-g is concrete/glass cans

m is metal cans

w is wood cans.

These designations indicate the contents of the cans. These cans contained the following, approximate amounts of material:

Sludge can (s) - 10.716 lb

(7.71 - H_2O, 0.70 - FLOOR DRI, 2.307 - MICRO-CEL E)

Combustible can (c) - 4.154 lb (1.637 - Cloth, 2.517 - Paper)

Concrete/glass can (c-g) - 17.440 lb (11.035 - concrete, 6.405 - glass)

Metal can (m) - 8.235 lb (4.118 - carbon steel, 4.118 stainless steel)

Wood can (w) - 4.875 lb

Pallet - 13.5 lb of wood

Boxes contained the following, approximate amounts of material:

Metal - 123.0625 lb (50% carbon steel)

Concrete/glass - 246.375 lb (158.75 - concrete, 87.625 - glass)

a. Engineering Design File, EDF-ISV-034.

Table 6. Test Pit 1 waste deposit material composition in pounds[a]

MATERIALS	TOTAL		ITEM WEIGHT	WASTE DEPOSIT LAYERS TOP	2ND	3RD	BOTTOM
COMBUSTIBLES:	665.5						
Cans:		451.5					
Paper			261.75	72.99	60.40	75.51	52.85
Cloth			170.25	47.47	39.29	49.11	34.38
Wood			19.50	4.88	4.87	4.88	4.87
Boxes:		214.0					
Cardboard			160.00	40.00	40.00	40.00	40.00
Pallet (wood)			54.00	0.00	13.50	13.50	27.00
SLUDGE: (cans only)	664.4						
Water		478.0	478.00	115.65	131.06	77.10	154.19
Floor Dri		43.4	43.40	10.50	11.90	7.00	14.00
Micro-Cel		143.0	143.00	34.50	39.20	23.10	46.20
METALS:	2,473.0						
Cans:		504.0					
Stainless			70.00	4.12	8.24	32.94	24.70
Carbon Steel			434.00	93.37	97.49	130.94	112.20
Boxes:		1,969.0					
Stainless			984.50	307.65	246.13	246.13	184.59
Carbon Steel			984.50	307.65	246.13	246.13	184.59
CONCRETE/GLASS:	1,351.75						
Cans:		366.25					
Concrete			231.75	55.18	77.25	77.25	22.07
Glass			134.50	32.03	44.83	44.83	12.81
Boxes:		985.5					
Concrete			635.00	0.00	158.75	158.75	317.50
Glass			350.50	0.00	87.62	87.63	175.25
TOTALS OF COLUMNS	5,154.65		5,154.65	1,125.99	1,306.66	1,314.80	1,407.20

a. Engineering Design File, EDF-ISV-034.

Table 7. Test Pit 1 waste inventory

Material	Mass (lb)	% of Total Mass
Combustible	666	1.1
Sludge		
Water	478	0.8
FLOOR-DRI	43	0.07
MICRO-CELL E	143	0.2
Metal	2473	4.1
Glass	485	0.8
Concrete	867	1.5
Soil (excluding underburden)	54,630	
Total	59,785	

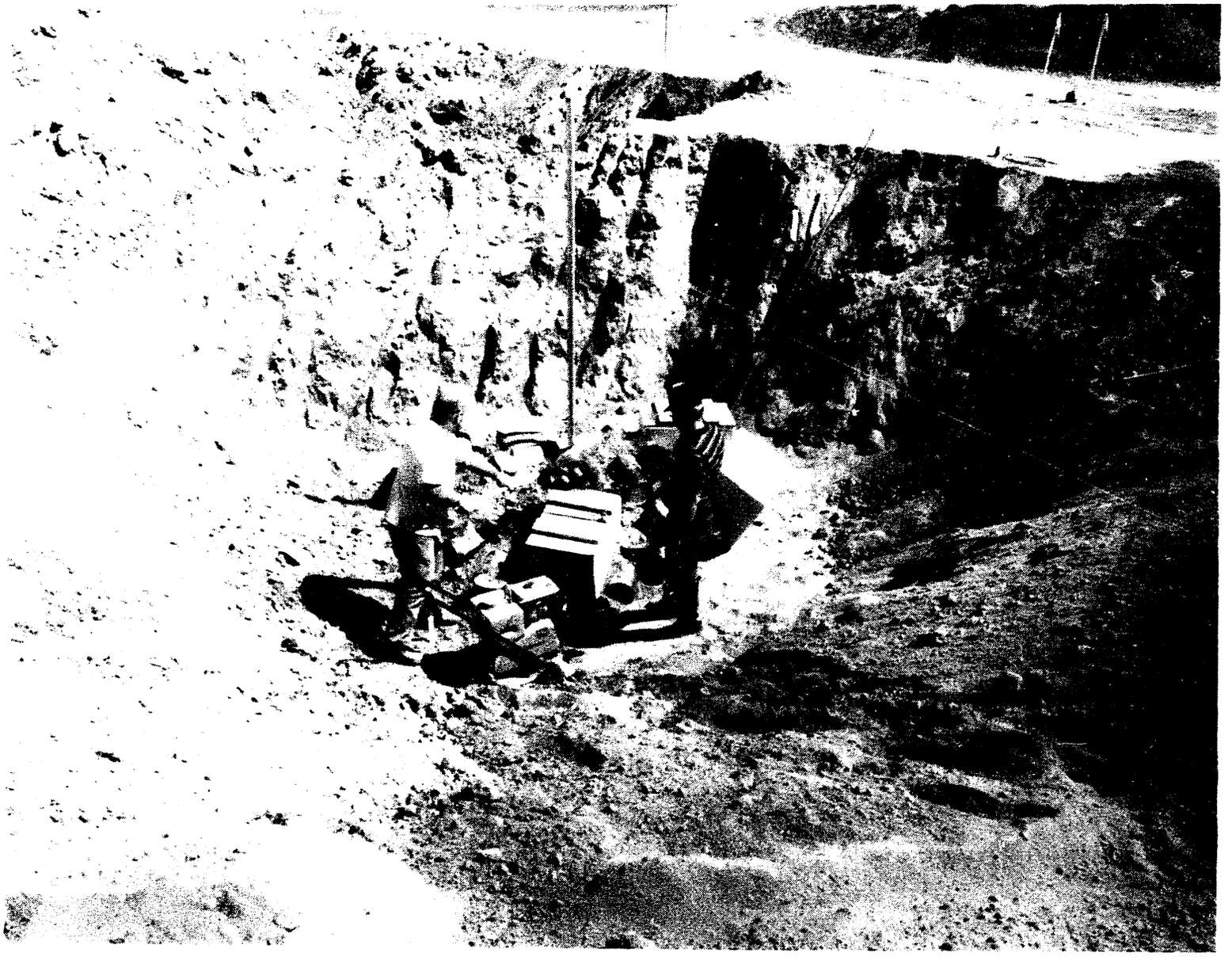

Figure 11. Cans and boxes placed in Test Pit 1, bottom layer (layer 4).

Figure 12. Test Pit 1 bottom layer covered with backfill.

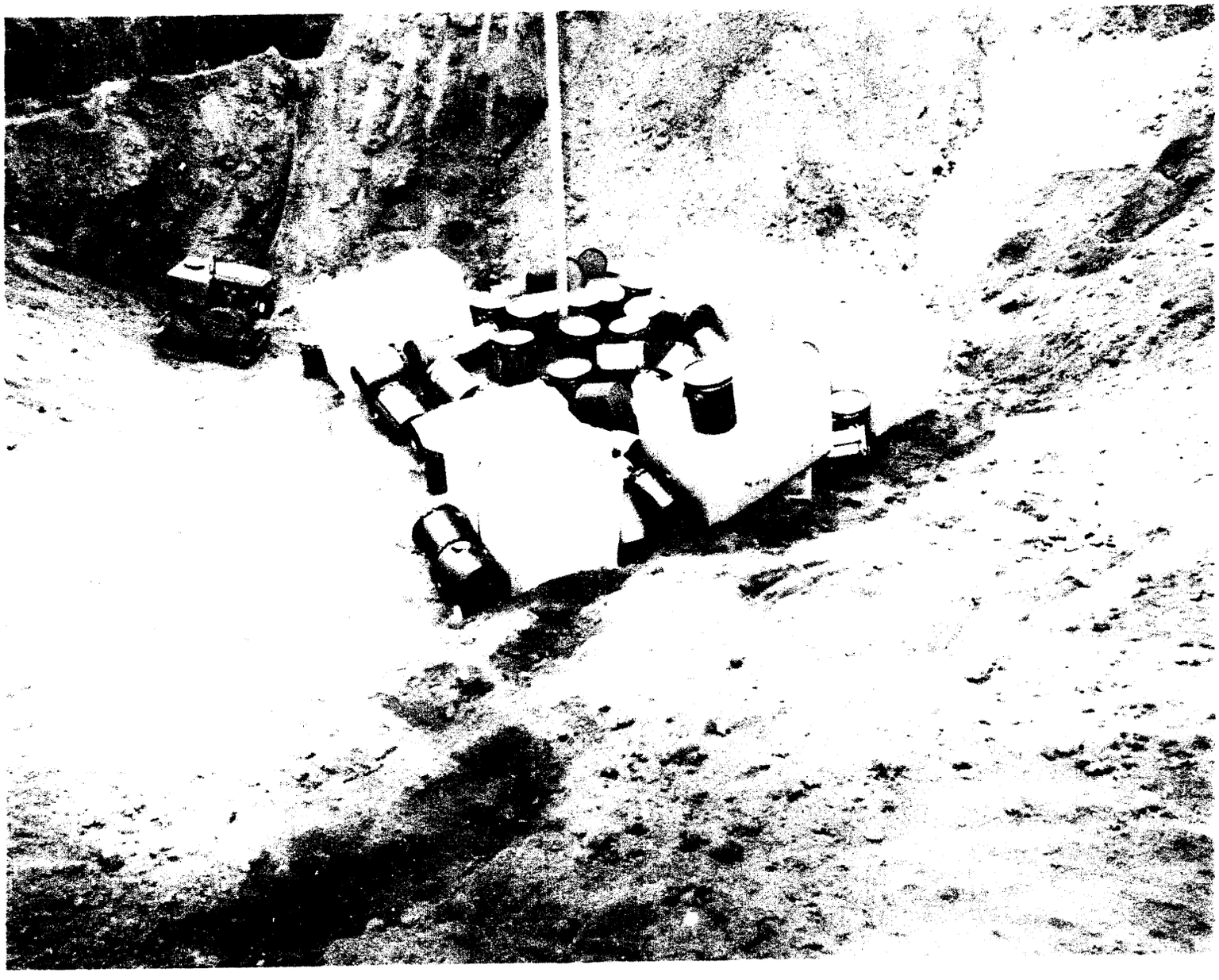

Figure 13. Cans, tracer cans contianing ytterbium oxide, and boxes placed in Test Pit 1, layer 2.

Figure 14. Backfill being placed over cans, tracer cans containing terbium oxides, and boxes in layer 2 of Test Pit 1.

Figure 15. Cans and boxes placed in Test Pit 1, top layer.

(6 in). A horizontal array was placed at approximately 1.4 m (4.5 ft) depth with thermocouples spaced 15.2 cm (6 in.) apart starting from the center of the pit. Unfortunately these thermocouples failed to perform during the test. The probable reason for failure was an unsuitable connecting wire leading from the thermocouples to the connection box at the process trailer. Part of this connecting wire was fiber braided and not coated with rubber. This was not suitable for outdoor use.

ISV testing on Test Pit 1 started October 18, 1989; however, hood failure occurred after approximately 14 hours of testing. As part of the accident investigation, a vitrified block approximately 48 cm (18 in.) deep was exhumed, and the soil overburden layer was excavated down to the tracer cans. The cans and the contents appeared unaffected by the melt. After excavation of the vitrified block, the soil overburden layer was replaced.

3.3 Test 1 Process Data Description

Test 1 operations were successful based on exceeding the target vitrification depth of 1.8 m (6 ft). This first field-scale test of a simulated buried waste site resulted in valuable operating experience and data relative to equipment design considerations and operating guidelines. As detailed later in this report, the information gained from Test 1 was utilized in Test 2 to improve operations. Generally, operations conducted on the random disposal orientation of Test 1 resulted in a very dynamic process that was extremely uncharacteristic of processing contaminated soil sites. Significant temperature and pressure spikes were observed in the hood throughout the test and appeared to be associated with each encounter of a buried can or box. Significant imbalances in the power supply routinely created electrical instabilities. Table 8 summarizes the sequence of events for the test.

Test 1 was initiated on June 12, 1990 at 1905 hours and had proceeded approximately 5 hours when a power cable in the Scott-Tee transformer failed. At that point a 46 to 51-cm (18 to 20-in.) layer of glass had formed with power at 103 kW. Operations were suspended for investigation, which revealed

Table 8. Test 1 - summary of events

Date	Time	Elapsed Time (hour)	Event
6/12/90	1905	0.0	Power to the electrodes.
6/13/90	0035	4.92	Transformer cable failure. Test aborted.
6/14/90	1546	-0.45	Data Acquisition System turned on.
6/14/90	1613	0.00	Power to electrodes. Restart initiated.
	1853	2.03	Melt resistance characteristics indicate melt is through starter path and into sand.
	2025	4.20	Tap change from 1000 to 650 V.
	2205	5.87	Average electrode depth 21 in.
	2215	6.03	Temperature and pressure spike noticed by operators. Electrode power reduced by operators.
	2301	6.80	Pressure/temperature spike. Hood made a loud "pop" sound. Smoke seen escaping through soil at base of hood, through air inlet HEPA, and around electrodes.
	2345	7.53	Pressure/temperature spike. "Bang" sound heard from hood. Resistance increased. Average electrode depth 25 in.
6/15/90	0000	7.78	Tap change from 650 to 1000 V.
	0021	8.13	Tap change from 1000 to 650 V.
	0033	8.33	Hood observation indicates flares and glass coming up around an electrode. Amperage dropping so tap change back to 1000 V tap.
	0120	9.12	Hood observation indicates glass shooting up vertically; yellow flares present.

Table 8. (continued)

Date	Time	Elapsed Time (hour)	Event
	0145	9.53	Pressure event. Amperage dropped 50% during event. Whole glass surface observed as molten with glass thrown 1.5-1.8 m (5-6 ft) in air. Large flames present.
	0320	11.12	Average electrode depth 34 in.
	0330	11.28	Power off to inspect cables around hood. Chunk of something (possibly wood) observed in melt, charred with ashes flaking off.
	0430	12.62	Average electrode depth 47 in.
	0523	13.17	Tap change back to 1000 V.
	0524	13.18	Sounds heard from within hood, cold cap disrupted by gas release and subsequently covered by molten glass.
	0550	13.62	Tap change from 1000 to 650 V.
	2650	14.62	Average electrode depth 60 in.
	0725	15.20	Tap change to 650 V.
	0830	16.28	Power off, transformer saturable core reactor fuses blown. All saturable core reactor fuses changed out. Electrodes stuck.
	0910	16.95	Power back on, using 650 V tap.
	0950	17.62	Transformer circuit breaker trip. Reset breaker. Electrodes gripped, no longer feeding by gravity alone. Electrodes still stuck.
	1000	17.78	Breaker trip. Reset.
	1010	17.95	Breaker trip. Reset.
	1020	18.12	Breaker trip. Reset.
	1022	18.15	Smoke from transformer, varistor failed, power off.

Table 8. (continued)

Date	Time	Elapsed Time (hour)	Event
	1100	18.78	Extension pieces to electrodes added.
	1155	19.70	Average electrode depth 71 in.
	1202	19.82	Power to electrodes for about 30 seconds, smoke from transformer, varistor failed.
	1405	21.87	Power back on, using 250 V tap. Electrodes are stuck, feed system cannot move them.
	1434	22.35	Tap change from 250 to 430 V. Phases not balanced. Phase B resistance is much higher than phase A.
	1450	22.62	Tap change from 430 to 650 V. Phases not balanced. Electrodes still stuck.
	1517	23.07	Power off to check fuses; they are OK. Power back on.
	1600	23.78	Average electrode depth 71 in.
	2220	30.12	Resistance of phase A increasing, power off, test terminated.

the cable received from the original manufacturer was undersized. A replacement cable was installed; all systems were inspected and tested; and preparations for restart were made, including relaying the starter path on top of the now frozen glass.

Test 1 was restarted at 16:13 hours on June 14, 1990. The power levels fluctuated during the test but generally averaged around 300 kW for the total test duration of approximately 18 hours and at the approximate total of 5400 kWh, as shown in Figure 16. Note that power is gradually increased over the first six hours to minimize possible disruptions in the starter path and to minimize the particulate generated by the oxidization of the graphite in the starter path. Hood plenum temperatures averaged around 300°C, which was slightly lower than predicted based on computer modeling. The lower-than-predicted temperatures were due to periods of nonpowered operations as a result of electrical imbalances associated with the power supply. Figure 17 illustrates the typical increase in resistance as the power distribution is transferred from the highly conductive starter path to the surrounding molten soil. As the molten soil zone grows, resistance decreases. The overall rate of downward melt growth averaged 4.6 cm/h (1.8 in./h), as illustrated in Figure 18. This average rate includes the final 15 hours of operation during which the downward melt growth rate was severely reduced due to the electrical imbalances described later in this report. The achieved melt depth was approximately 2.4 m (8 ft). Subsidence was measured at approximately 1.4 - 2.0 m (4.5 - 6.5 ft), leaving a 0.4 m (18 in.) layer of glass in the bottom of the vitrified area.

Gas releases from containers resulted in 14 separate events characterized by sharp temperature increases and/or pressure spikes in the hood. Many of these events also influenced other process off-gas components and the electrical system, as detailed in Section 3.3.2 (see p. 57). It is important to note that the pressure spikes were the result of either relatively slow gas releases from the melt or relatively slow expansions of gasses in the hood that occurred over a 10 to 30 second period. The pressure spikes were not rapid, which would be characteristic of a detonation or an explosion.

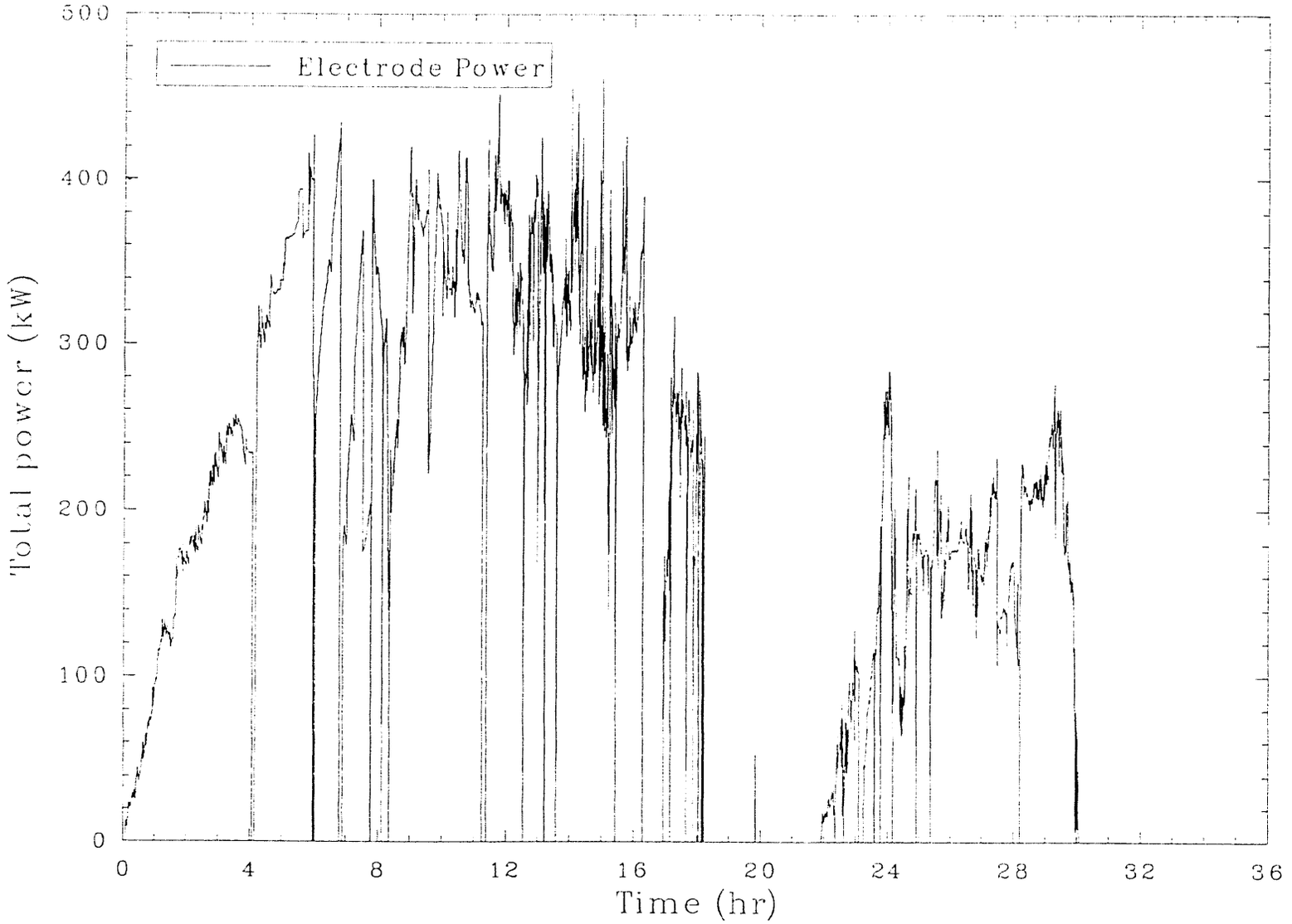

Figure 16. Total electrode power for Test 1.

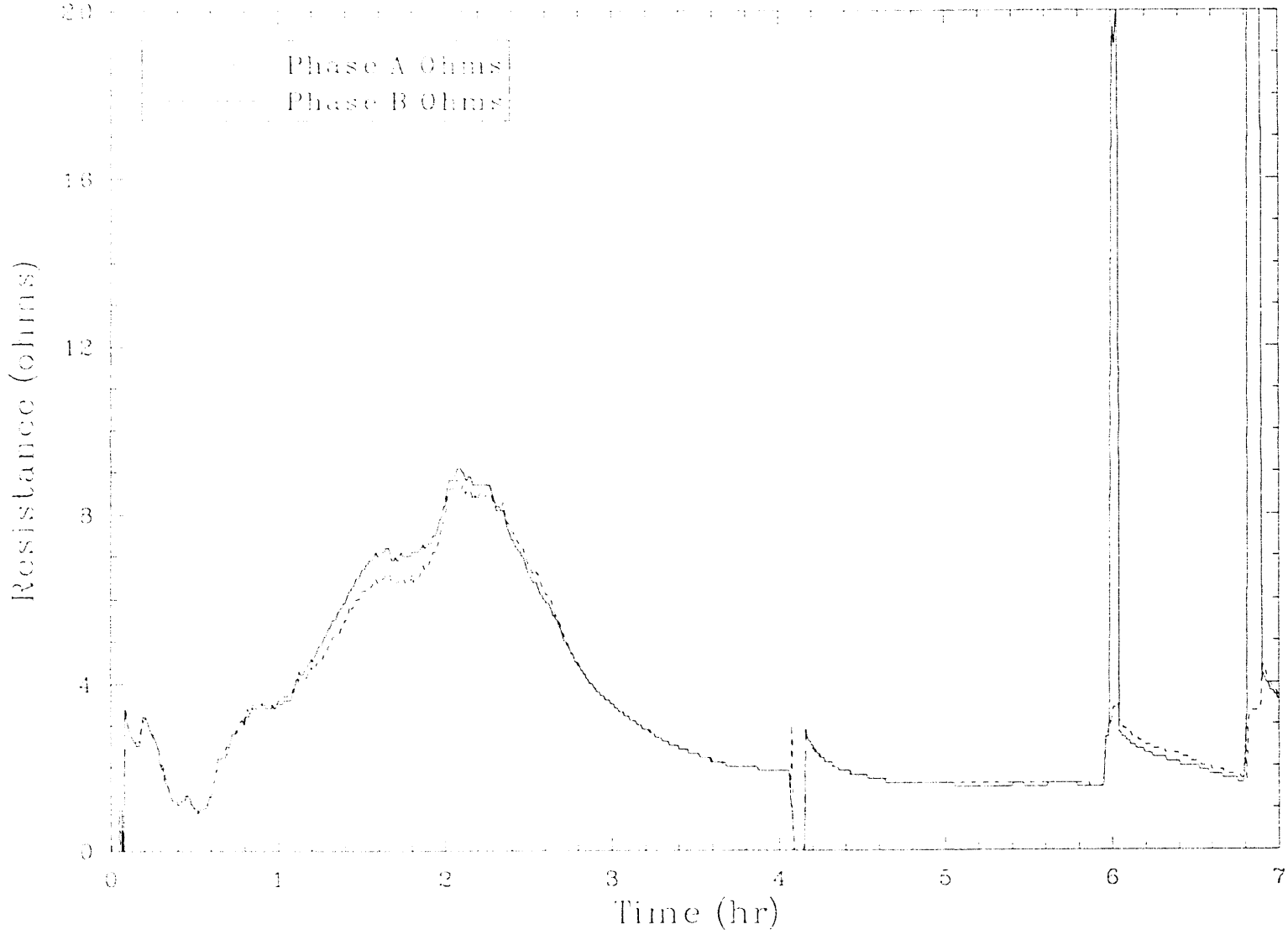

Figure 17. Phase resistance during startup for Test 1.

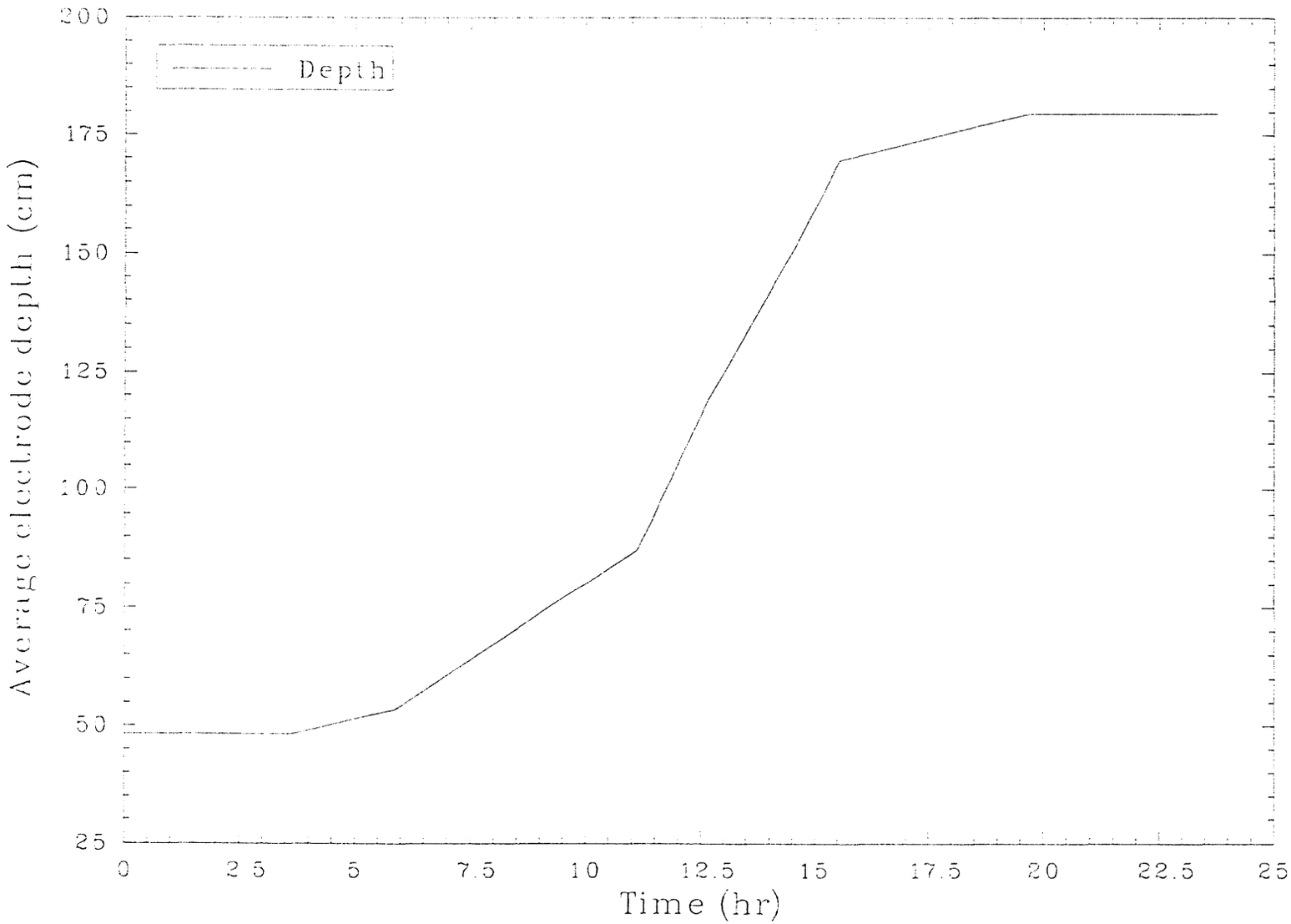

Figure 18. Average electrode depth for Test 1.

To fully analyze the ISV process operations and the behavior of buried waste processing, the following primary areas must be evaluated.

- Off-gas containment hood performance
- Power system and electrode performance
- Off-gas treatment system performance
- Off-gas system processing experiences
- Melt behavior at each event
- Electrical instabilities.

Note that the analysis of equipment performance is intended to serve as information supporting future design work for large-scale buried waste ISV processing systems.

3.3.1 Off-Gas Containment Hood Performance

The first intermediate-scale test of a simulated buried waste site resulted in a dynamic process, especially regarding conditions in the melt and off-gas hood. Surges in off-gas generation rates resulted in a loss of hood vacuum on several occasions; however, the hood was maintained at an overall average between 1.0 and 1.5 in. of water vacuum, and the plenum temperature maintained at an average of 300°C. Plots of the hood vacuum and the plenum temperature for the entire test are provided in Figures 19 and 20. A total of 14 significant temperature spikes were recorded, resulting in a net temperature increase ranging from approximately 50°C to over 300°C, as shown in Figure 20. The initial temperature spike in Figure 20 is biased high because this first event was observed to result in molten glass splashing up onto the tip of the plenum thermocouple. Other thermocouples in the hood suggest a true plenum temperature of approximately 700°C. The plenum temperature was generally the hottest temperature recorded in the hood because it is in the center of the hood cavity and was nearer to the molten glass than other thermocouples. Because the hood plenum thermocouple was not shielded from radiation, it is likely that radiant heat transfer was biasing these temperature values higher than true gas temperature. As shown in Figure 21, the cooler hood, roof, and wall temperatures parallel the plenum temperature.

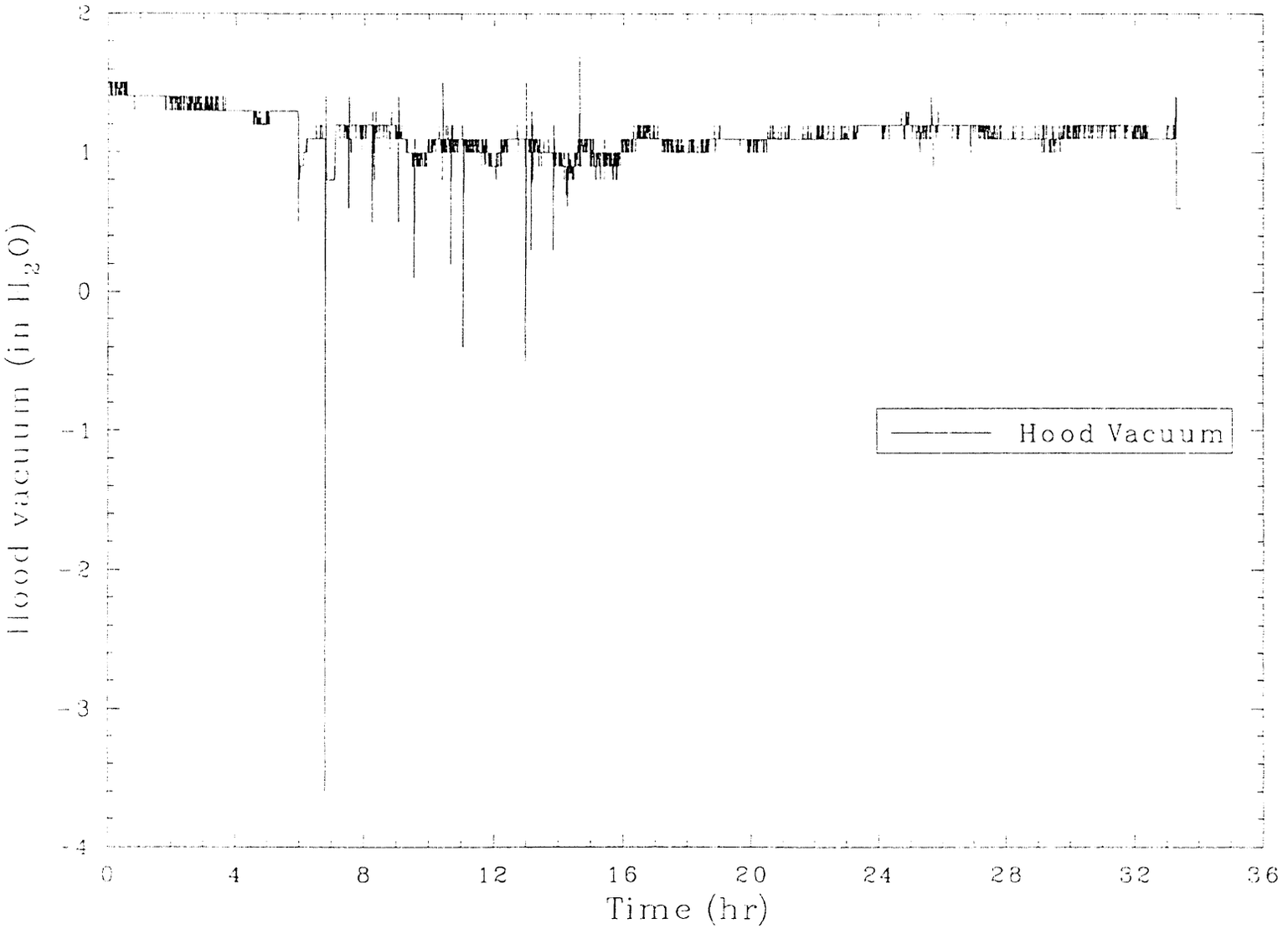

Figure 19. Hood vacuum plot showing pressure spikes for Test 1.

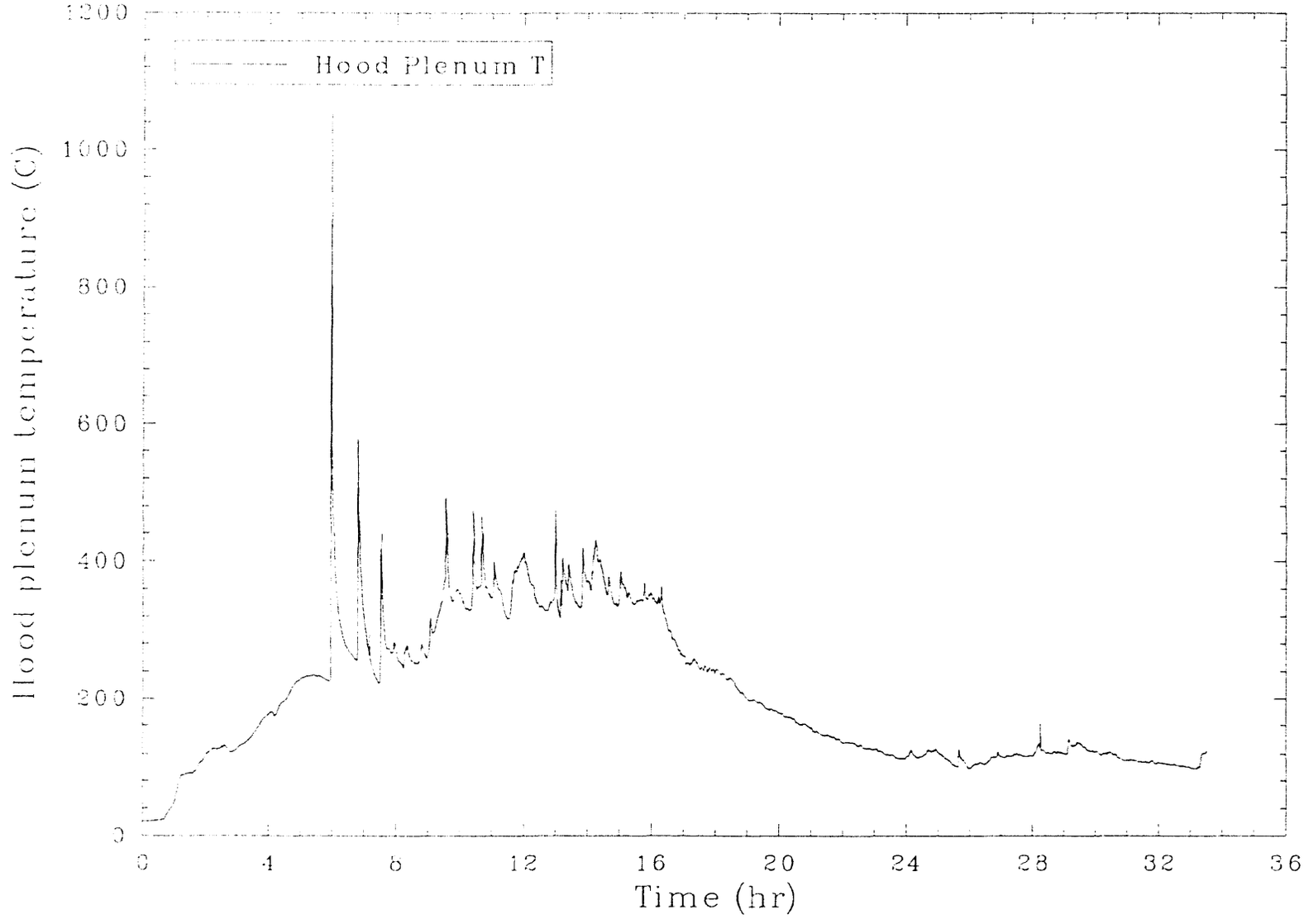

Figure 20. Hood plenum temperature plot showing temperature spikes for Test 1.

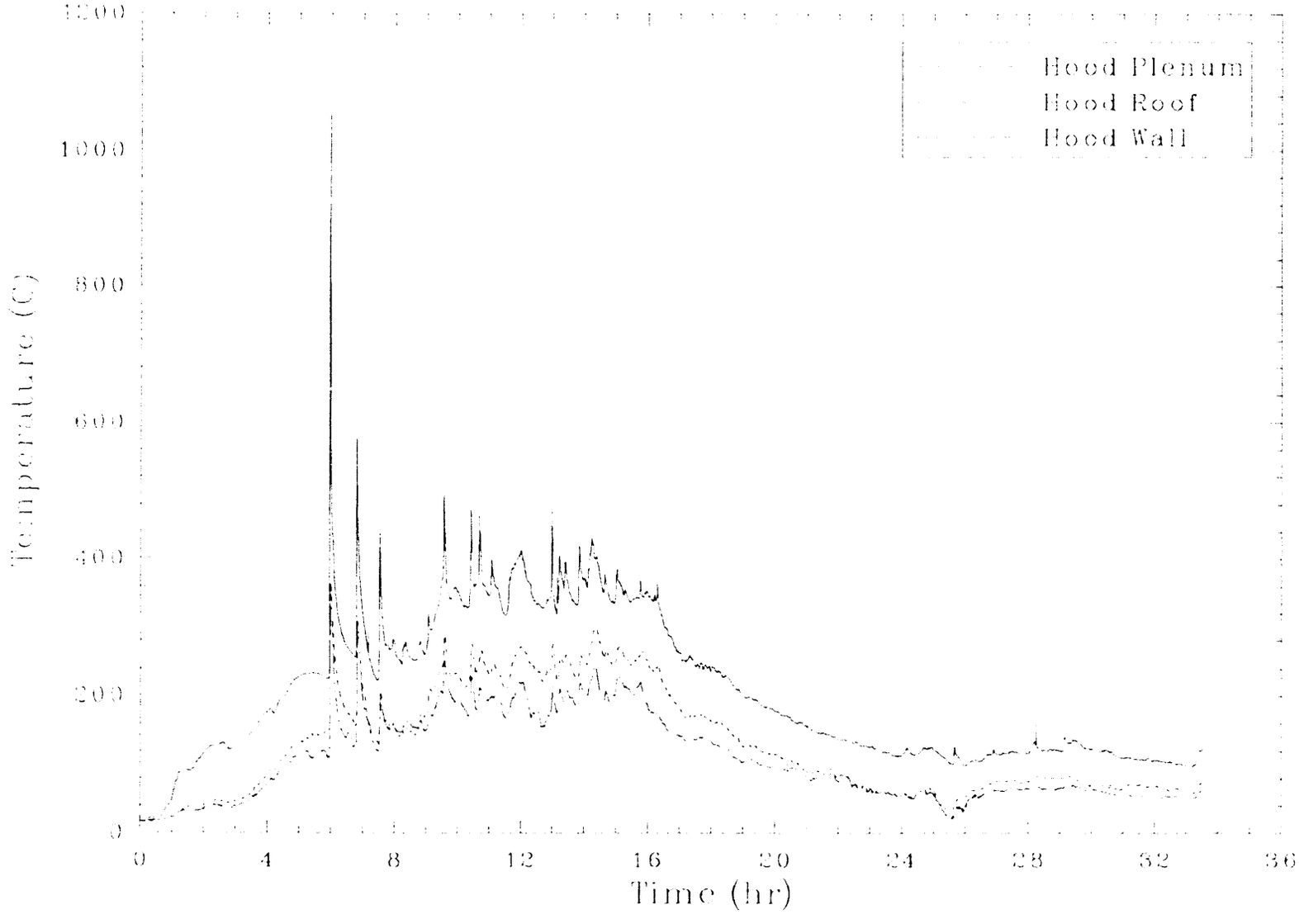

Figure 21. Hood Plenum, roof, and wall temperatures for Test 1.

Relative to the overall average processing temperature and temperature spikes, the off-gas hood performed as designed, maintaining its integrity throughout the test. On several occasions molten glass was ejected from the melt and contacted the hood containment panels, which resulted in significant localized heating. On at least two occasions during night operations, direct glass contact on the hood containment shell resulted in temporary localized heating that was observed by operators as a localized red glow. No significant thermally-induced structural degradations were observed following extensive examinations of the hood during and after the test. In addition, on several occasions, molten glass was ejected from the melt, contacting the high temperature fabric used for the electrode seals. This glass contact resulted in moderate degradation of the innermost layer, including a loss of structural strength due to partial melting of fibers. The outermost layers of fabric, however, were unaffected.

A high temperature sealant (RTV-106) was used as a test sealant compound for sealing some of the panel seams. The sealant remained pliant throughout the test and was used in locations on the containment hood that were directly exposed to the extreme temperatures inside the hood, as well as external seams that did not experience the extreme temperatures. Careful examinations following the test revealed no thermal degradation of the sealant on the external seams. Examinations of the internal seams revealed inconsequential surface degradation of the sealant that was directly exposed to the extreme temperatures to less than 1 mm (0.04 in.).

The intermediate-scale ISV system, appropriately sized for contaminated soil sites, was unable to contain transient pressure spikes in the containment hood on several occasions. This illustrates the need for a larger, more robust processing system for buried waste sites. These spikes were the result of relatively slow gas releases from containers, relatively slow gas generation created by the combustion of pyrolyzed products, and/or thermally induced expansions of existing gasses in the hood. The pressure spikes were not a sudden pressure spike characteristic of a detonation. Most pressure spikes occurred over a 10 to 30 second duration. In cases where the pressure in the hood did not exceed 1 in. of water, the gasses were contained within the surge volume in the hood and were subsequently drawn out to the process

off-gas treatment system. However, when pressures exceeded 1 in. of water, a portion of the gas was relieved through the HEPA filtered pressure relief system, with the balance being drawn through the off-gas treatment system. In extreme cases, when the pressure significantly exceeded 1 in. of water, the gas overcame the surge and pressure relief capacity of the hood and released through any available point including around the base of the hood and through unsealed panel seams. Figure 22 is a combined plot of temperature and vacuum versus run time. This plot illustrates the relationships between plenum temperature spikes and off-gas surges that resulted in sharp decreases in hood vacuum. As hot gasses are released from the melt and combust in the hood, temperatures in the hood increase. Additionally, as the gasses are released from the melt, the cold cap covering the molten glass is disrupted, resulting in a release of radiant heat to the hood. The resulting radiant heat loss from the molten glass causes the electrical resistance in the glass to increase. Figure 23 shows this effect for several gas release events.

3.3.2 Power System and Electrode Performance

The dynamic behavior of buried waste processing posed a variety of operational instabilities relative to the electrical power supply. As the melt encountered the buried containers, many of the sudden gas releases that affected the hood environment also affected the transformer. The primary cause for these disruptions was the minimal glass volume associated with the test. Inherent with any ISV process, the treated soil region is densified as water, soil gasses, and other decomposition products are driven off. This densification, or subsidence, typically ranges from 30 to 50% for a contaminated soil site. However, subsidence was significantly greater for this test (75%) involving a simulated buried waste site. It is expected that any buried waste site would result in at least 50% subsidence or greater primarily depending on the total void volumes and organic materials present.

Test 1 resulted in a total power level that varied typically between 300 and 400 kW. Plots showing amperage and volts for each phase are provided in Figures 24 and 25.

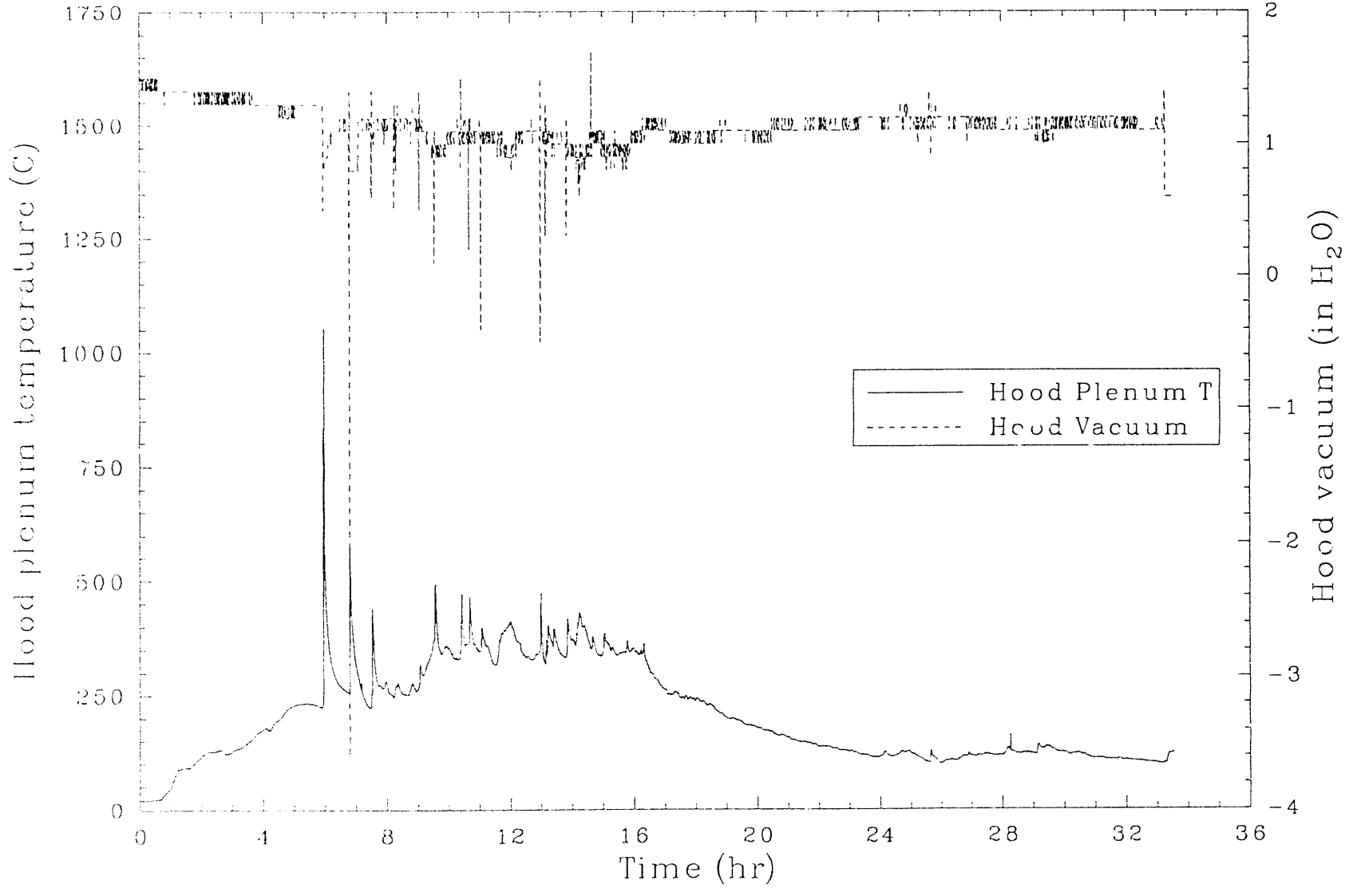

Figure 22. Hood vacuum and plenum temperature for Test 1.

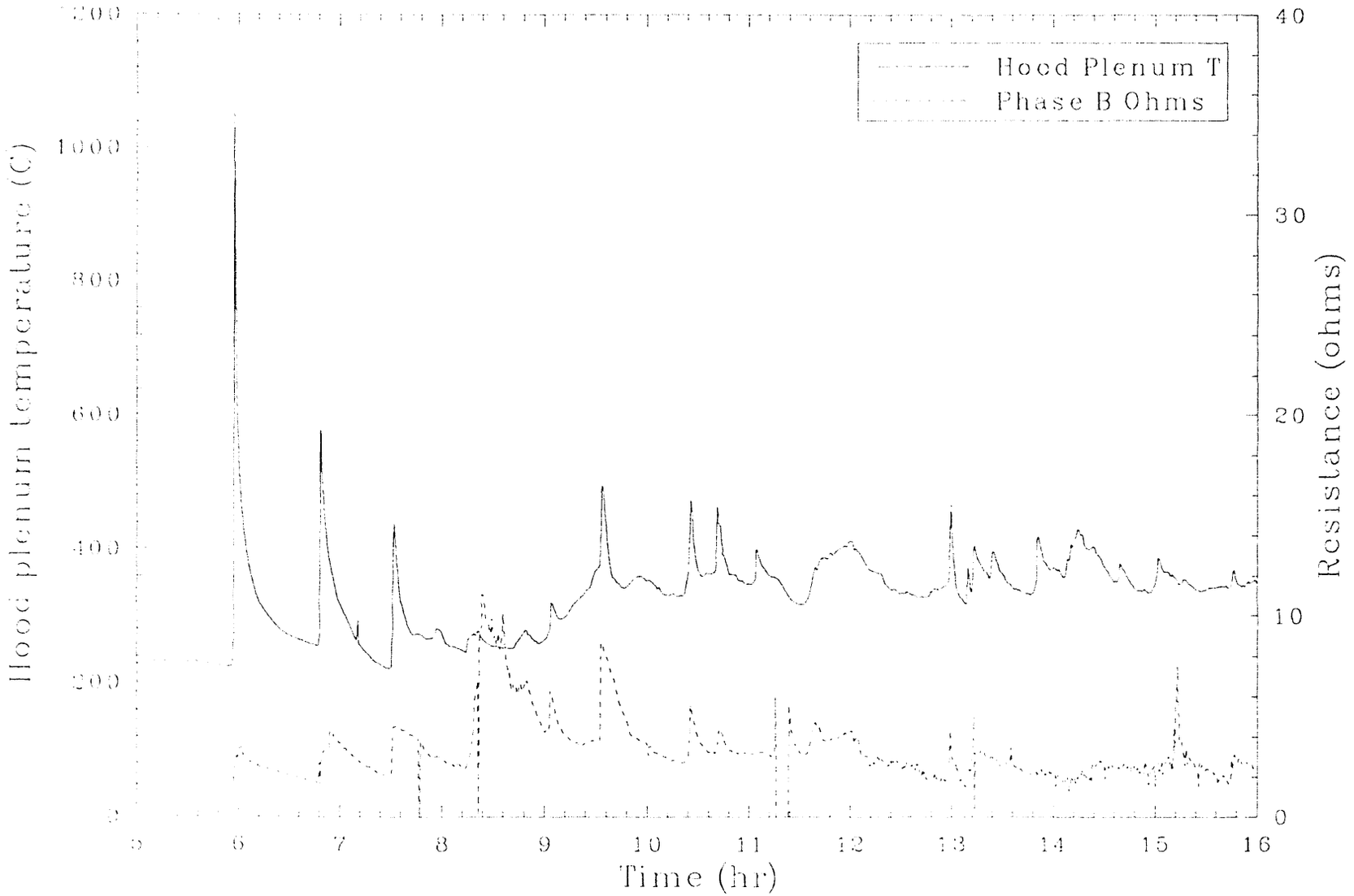

Figure 23. Hood plenum temperature and phase B resistance showing concurrent spiking in Test 1.

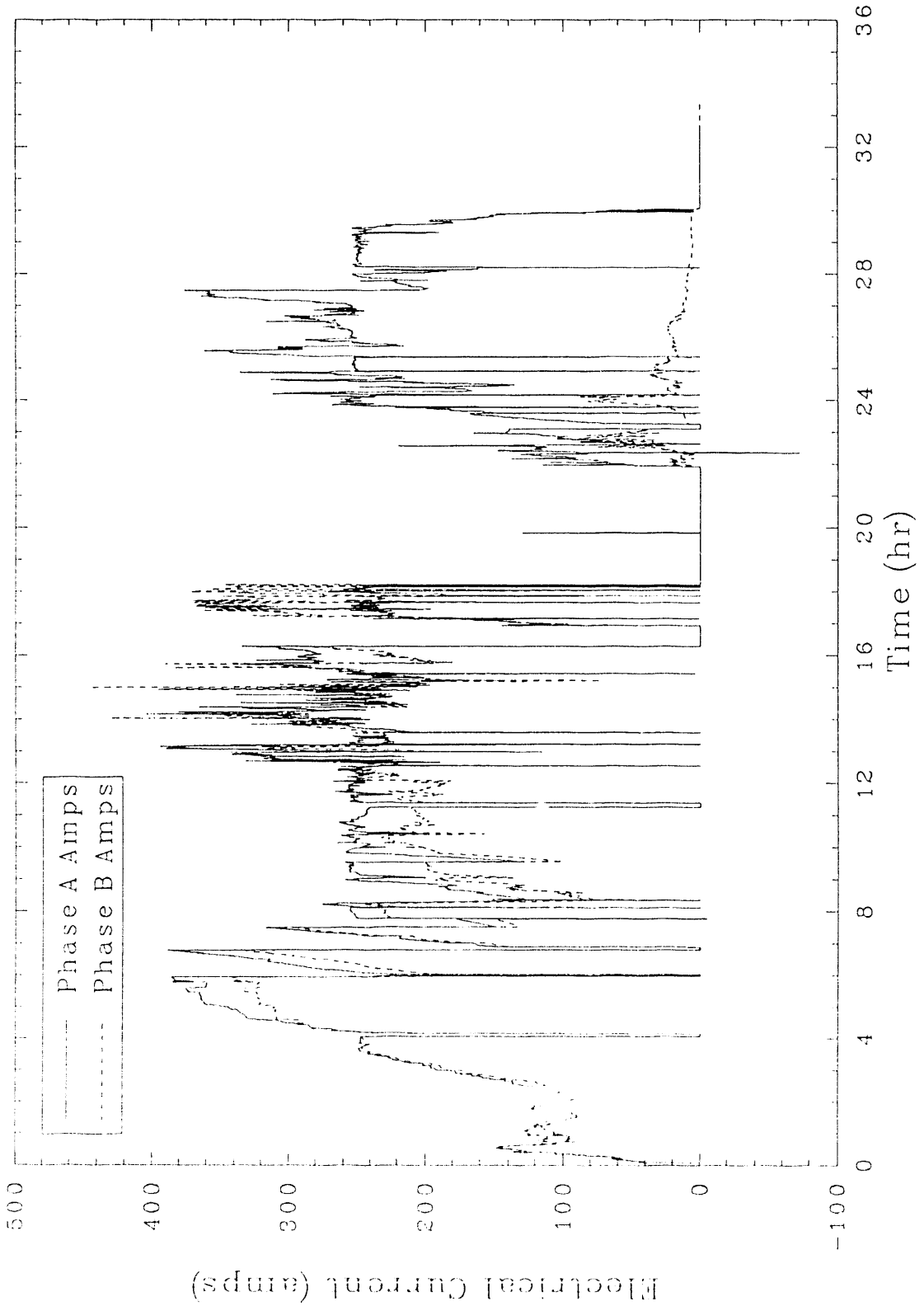

Figure 24. Phases A and B amperage for Test 1.

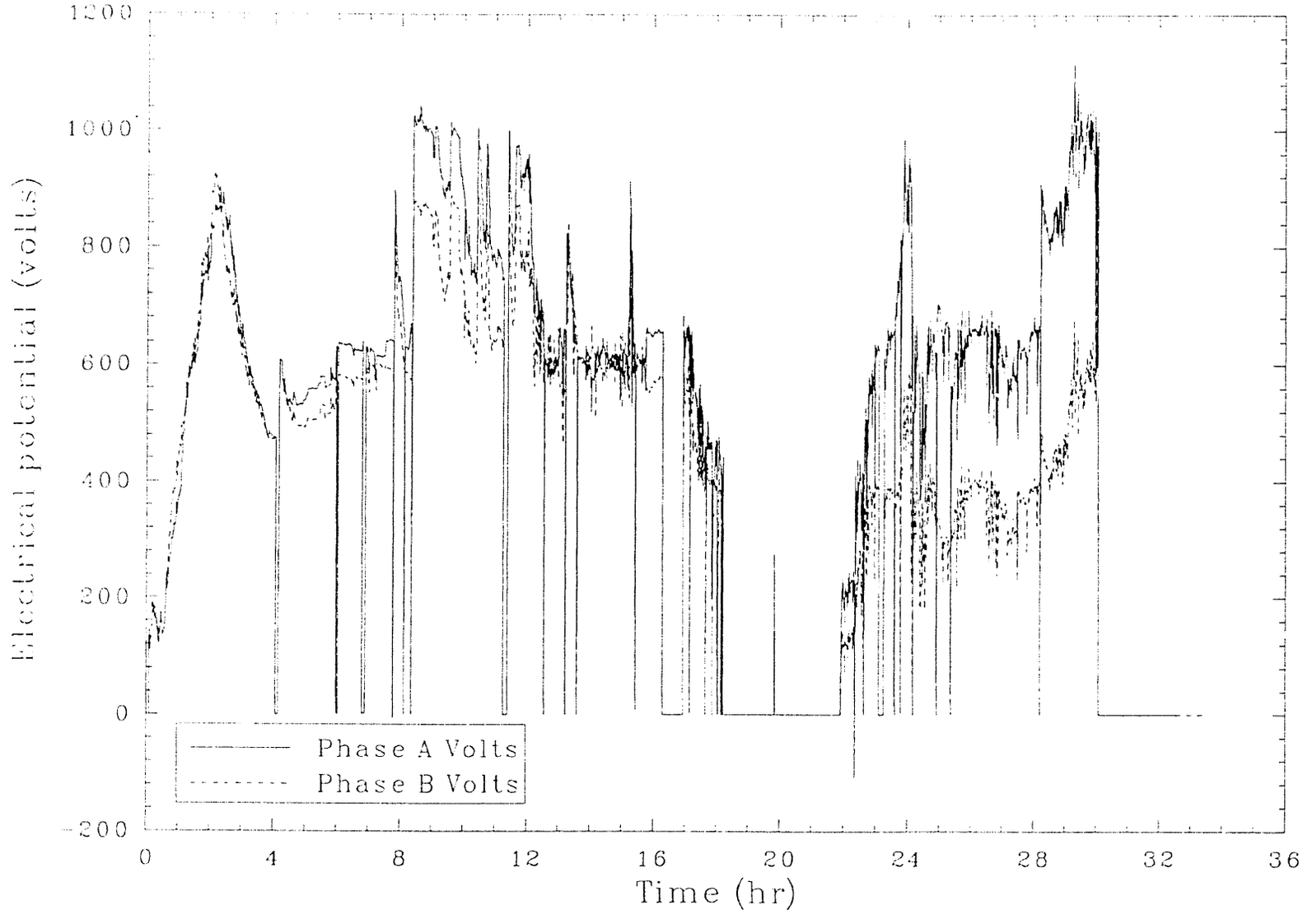

Figure 25. Phases A and B voltage for Test 1.

A minimal amount of glass available to the melt created electrical instabilities. For this test, only 0.61 m (2 ft) of soil overburden was available to provide a approximate 30 cm (12 in.) layer of glass before encountering the buried waste. As each waste container was encountered, glass would flow into the container, temporarily resulting in a net loss of glass between the electrodes available to conduct current. When containers near the edge of the melt were encountered, the glass would flow into the containers and freeze, thereafter being unavailable to the melt and resulting in a continual net loss of glass. With only a minimal level of glass to conduct the electrical current, the transformer was very susceptible to imbalances if one of the following conditions occurred.

- The electrodes were not inserted at an equal depth.
- Other nonelectrically conductive obstructions such as a partially dissolved waste container, a portion of the insulation blanket, ora piece of frozen glass dislodged from the cold cap, existed in the melt.
- Highly conductive objects, such as molten metal pools, created electrical short circuits between electrodes.
- Partially melted metallic objects contacting any of the electrodes effectively reduced the firing gap between the affected electrode and the opposing electrode.
- Sudden gas releases created electrically disruptive bubbles in the glass.
- Temporary localized area of cooled glass especially around an electrode resulted in increased resistance in that region. Glass cooling results from a cold cap disruption that allows molten glass to radiate heat to the hood environment. The radiant heat losses result in a net cooling of the molten glass in the localized area.

The resulting electrical instabilities appeared in a variety of forms and ultimately resulted in terminating the test shortly after the 1.8 m (6 ft) depth objective for the test was achieved. A key experience gained from this test involved the performance of the coating used to minimize oxidation of the graphite electrodes. Initially, the electrodes were painted with a silicon-based coating to help reduce oxidation. During ISV processing, the graphite electrodes tended to reduce in diameter at the air/melt interface due to the oxidation of graphite. The oxidation can lead to electrode failure if the electrodes are held in a static position for several hours. The use of the coating is a compromise in that, while the coating helps prevent oxidation, it tends to cause the electrodes to stick to the glass. Because this was the first field scale test of moveable graphite electrodes, it was determined that the use of the coating would be the prudent coarse of action. During the test, the electrodes became frozen to the cold cap and were unable to be moved (inserted or retracted) to compensate for electrical imbalances. The electrodes would become free from the cold cap whenever a container was encountered that disrupted or melted the cold cap with combustion or other sudden gas release and would free fall for typically 15 cm (6 in.) until they rested on the bottom of the melt. Ultimately, the test was terminated when the molten glass essentially melted away from the frozen electrodes during a period of time when no containers were encountered.

Electrical imbalances in the transformer resulted due to an unusually small volume of molten glass and the lack of electrode control caused by sticking. Because of the minimal glass volume, the effects of any transient condition in the melt was greatly magnified as compared to a situation involving several times the glass volume. For Test 1 the consequences of these problems included:

(a) 500 A saturable core reactor fuse failures due to imbalances on the primary side. Typically, operations for approximately 30 minutes in an imbalanced state of greater than 30% resulted in fuse failure.

(b) Thermal trips of the 750 A breaker to prevent overheating of the transformer. The excess heat was primarily caused by imbalances;

however, on a few occasions during the heat of the afternoon, the ambient conditions contributed significantly to the elevated transformer temperatures. The transformer automatically trips itself when temperatures in the secondary windings approach 150°C above ambient.

c) Amperage limit trips or magnetic trips of the 750 A breaker due to the electrodes shorting in a metal pool. Although no absolute electrical shorts occurred during the test, on several conditions the presence of molten metal or metal objects near one or more electrodes created a higher than normal amperage situation. Those near shorting conditions were typically short-lived and affected only one of the two secondary phases. Due to rapidly changing conditions in the melt and the inability to respond with electrode movement (retract electrodes from a molten metal shorting condition), a resulting amperage spike would trip the transformer. Any imbalance on the primary side amplified the effect of this type of trip. Therefore, the imbalance combined with the near shorting condition resulted in magnetic or high amperage trips.

(d) Thyristor switch failures due to imbalances in combination with amperage surges. The surges do not necessarily have to be associated with an absolute metallic shorting condition. An absolute metallic short will occur when two electrodes are shorted via direct contact with a pool of molten metal or if a solid metallic object simultaneously contacted two electrodes. Limited amperage surges combined with an imbalance can cause failure of the switches. A limited amperage surge will occur if a single electrode contacts a molten metal pool or metallic object, effectively resulting in a shorter electrical pathway through the resistive glass to an adjacent electrode.

A key conclusion drawn from Test 1 is that the silicon-based coating causes unacceptable sticking of the electrodes to the cold cap. Due to the coating on the electrodes, the EFS was largely ineffective. All of the lifting force available (over 1500 lb) was insufficient to free the stuck

electrodes from the frozen glass. At one point, in the final hours of the test, an additional lifting force of 1000 lb was provided by a mobile crane; however, after determining the combined lifting force was insufficient to free the electrodes, the additional lifting force was terminated to prevent damage to the electrodes. Occasionally, a stuck electrode could be moved 1 to 2 cm (0.4 to 0.8 in.) up or down, but the electrode would not break free.

Aside from being stuck in the glass due to the coating, the graphite electrodes performed satisfactorily. Oxidative losses on the four electrodes were negligible. This test likely represented a near worst case condition for the electrodes because the location of the air/glass interface relative to the electrode did not change significantly throughout the test. In typical operations, the electrode is inserted at a rate that exceeds the rate of subsidence. Therefore, the electrode area most susceptible to oxidative losses is always replenished by feeding (inserting) more electrode from above. Based on these results, electrodes would not be coated for Test 2. In addition, a deeper layer of cover soil would be added to increase the volume of molten glass to help reduce electrical instabilities.

3.3.3 Off-Gas Treatment System Performance

The first field test using ISV on a simulated buried waste site resulted in a dynamic process. As each container was encountered by the advancing melt front, the changes created by gaseous releases that affected the hood environment and transformer also affected the process off-gas treatment system. Overall, the off-gas treatment system performed well.

The performance of the Venturi-Ejector relative to heat removal is illustrated in Figure 26, which shows the gas temperature entering the Venturi-Ejector typically ranged from 200 to 300°C. The exit temperature (Hydro-Sonic entrance) was typically less than 50°C. Fluctuations in differential pressure for the Venturi-Ejector, shown in Figure 27, were due to corresponding hood vacuum fluctuations. The pressure on the upstream side of the Venturi-Ejector was measured on the off-gas line that was directly affected by fluctuating hood vacuums.

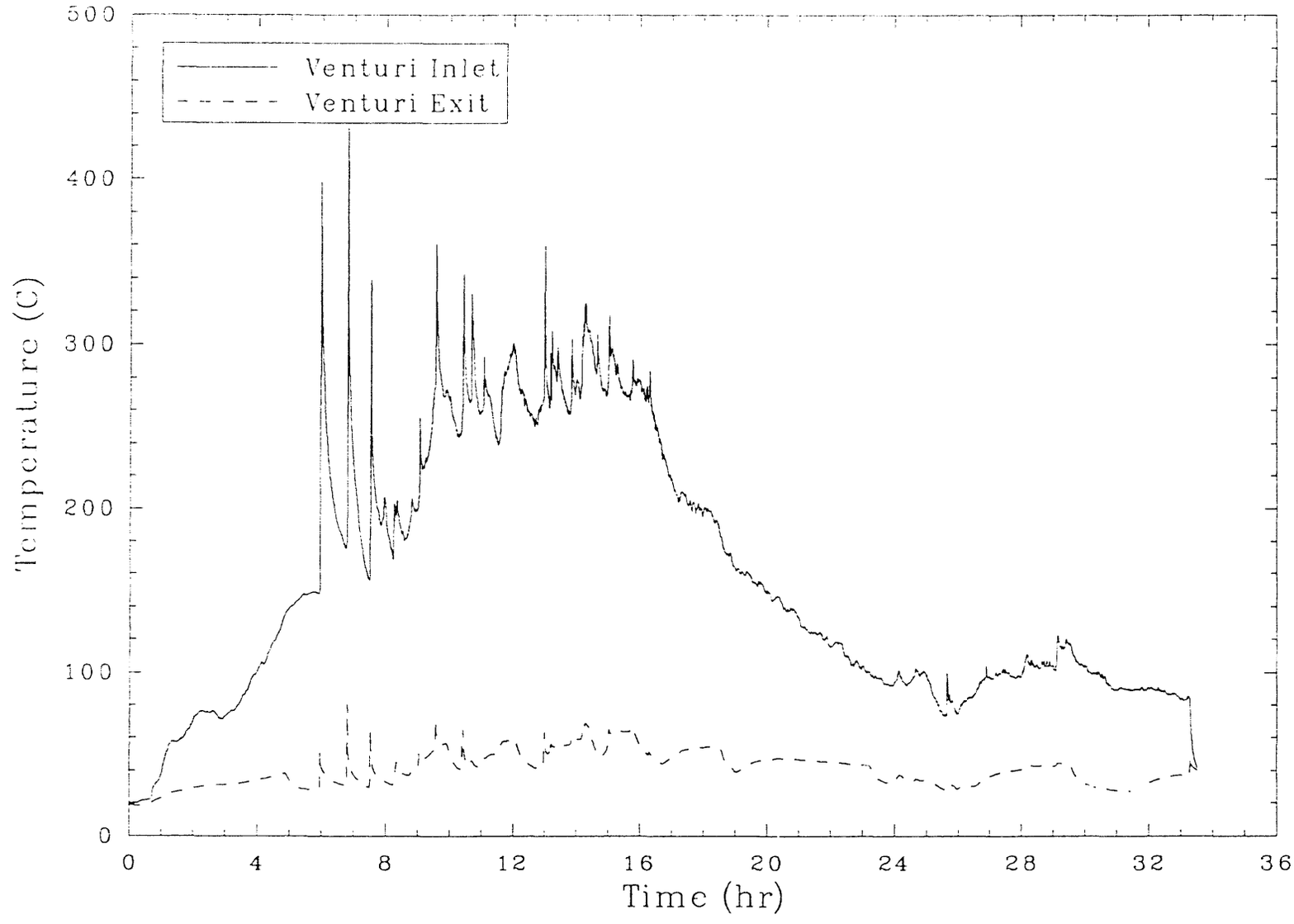

Figure 26. Temperature at inlet (off-gas at trailer) and exit of Venturi-Ejector for Test 1.

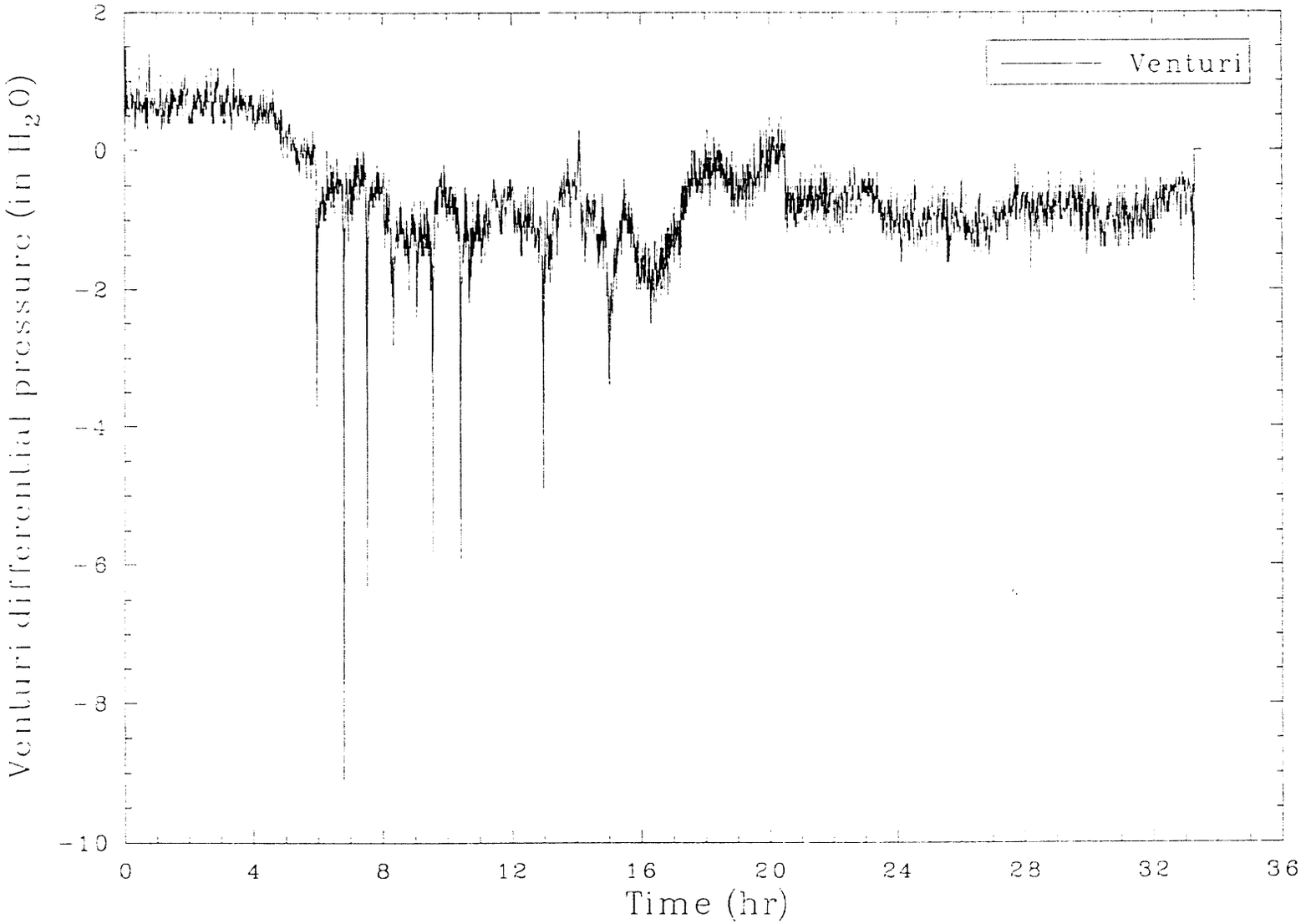

Figure 27. Venturi-Ejector differential pressure for Test 1.

The Hydro-Sonic scrubber differential pressure was maintained well above 50 in. of water throughout the test, as shown in Figure 28. By design, this should have resulted in a particulate removal efficiency of greater than 90% for particles sized greater than 0.5 μ. The fluctuations of differential pressure were due to fluctuations in total off-gas flow created by the automatic adjustment of the blower surge protection valve.

Differential pressure measured across the housing of the primary HEPA filter is shown in Figure 29. The differential pressure remained relatively constant throughout the test, indicating the scrubbers effectively removed the vast majority of particulate. Thus, a large-scale machine with a wet scrubbing system of comparable design could sufficiently remove particulate from the off-gas stream.

Total gas flow through the off-gas treatment system is shown in Figure 30. Total flow ranged from 12 to 22 m^3/min; however, periods where total off-gas flow exceeded 20 m^3/min coincided with the blower surge protection valve being opened, resulting in a false high reading. Later in the test, after 20 hours, off-gassing from the melt decreased due to the lower power input related to transformer imbalances. At the time the off-gas system was shut-down (approximately 3 hours after electrode power was terminated), the off-gas flow had decreased to approximately 12 m^3/min. Because off-gassing from the melt at this point in time would have ceased, this flow rate is largely the controlled in-leakage of air into the hood.

Concentrations of oxygen and carbon monoxide were monitored at the off-gas stack throughout the test. The oxygen concentration averaged between 20 and 21%, as can be seen in Figure 31. Short periods of reduced oxygen concentrations were measure at time periods consistent with gas releases from containers. This was consistent with the combustion of gasses in the hood upon release from containers in the melt. Carbon monoxide concentrations at the stack fluctuated throughout the test corresponding to gas releases from the containers in the melt and combustion activity in the hood. As shown in Figure 32, carbon monoxide concentrations ranged from 0.1 to 0.4%, with occasional spikes greater than 0.4%, up to a maximum of 1.1% at startup. The greatest concentrations of carbon monoxide are expected shortly after startup

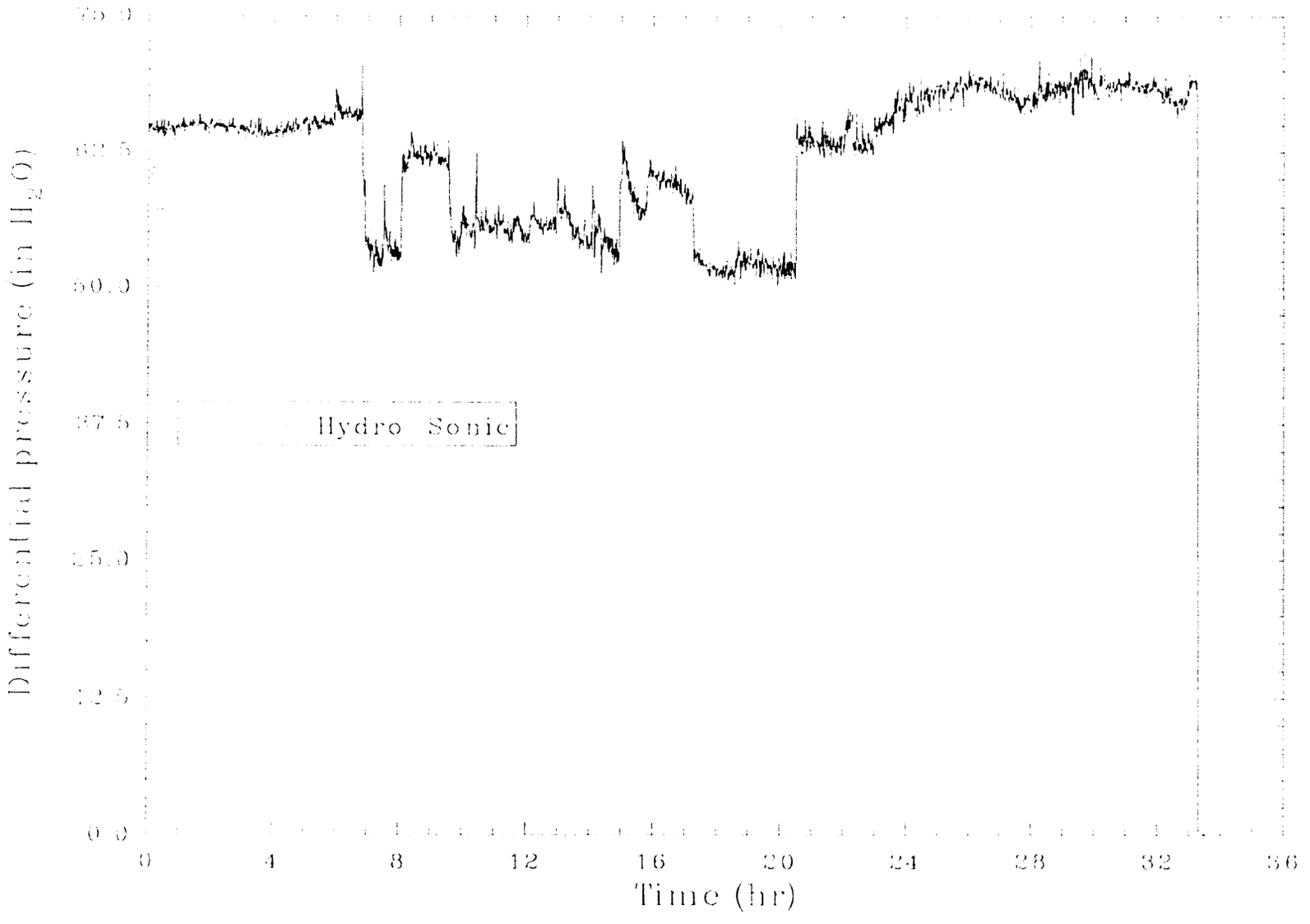

Figure 28. Hydro-Sonic scrubber differential pressure for Test 1.

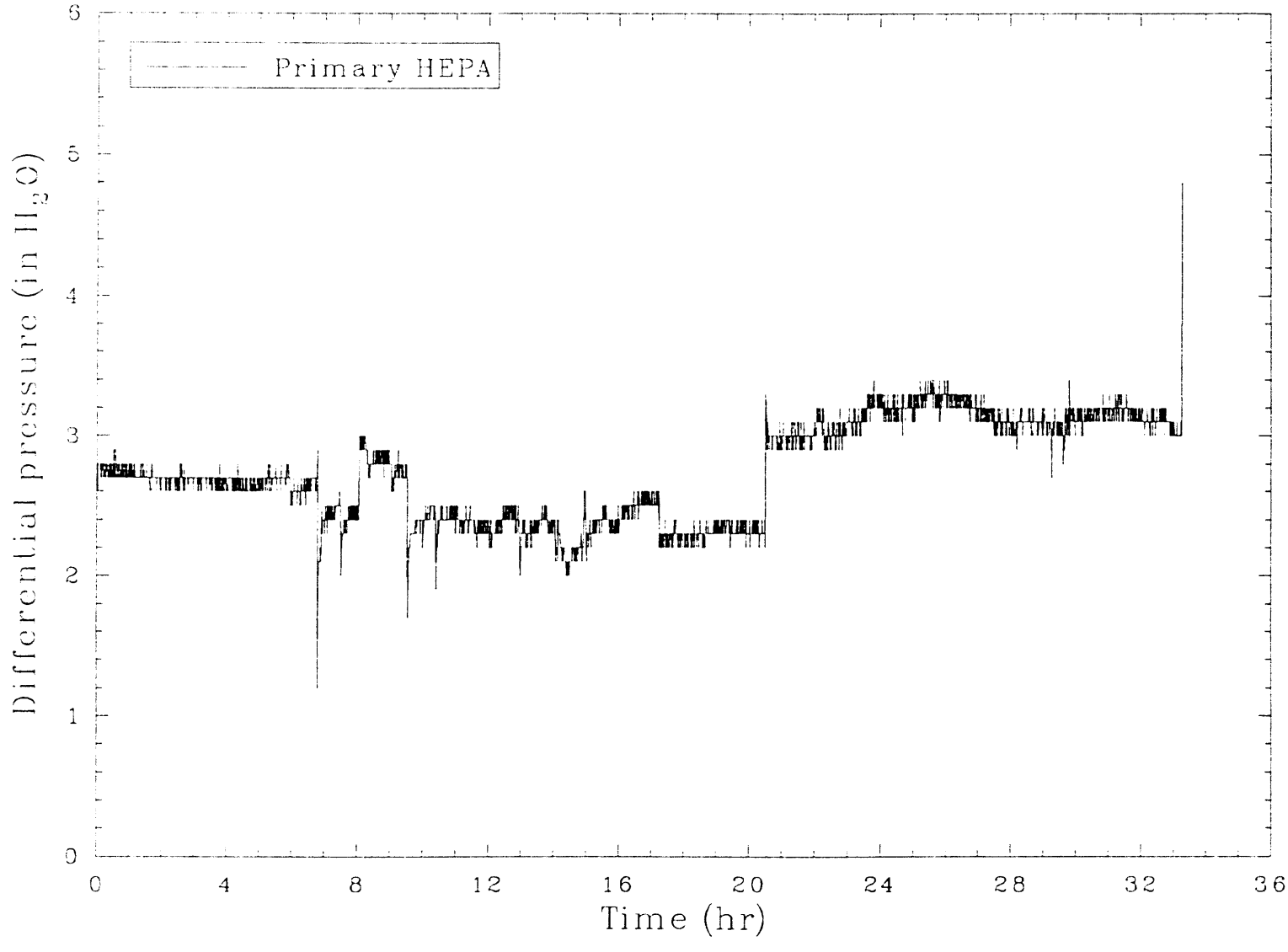

Figure 29. Primary HEPA differential pressure for Test 1.

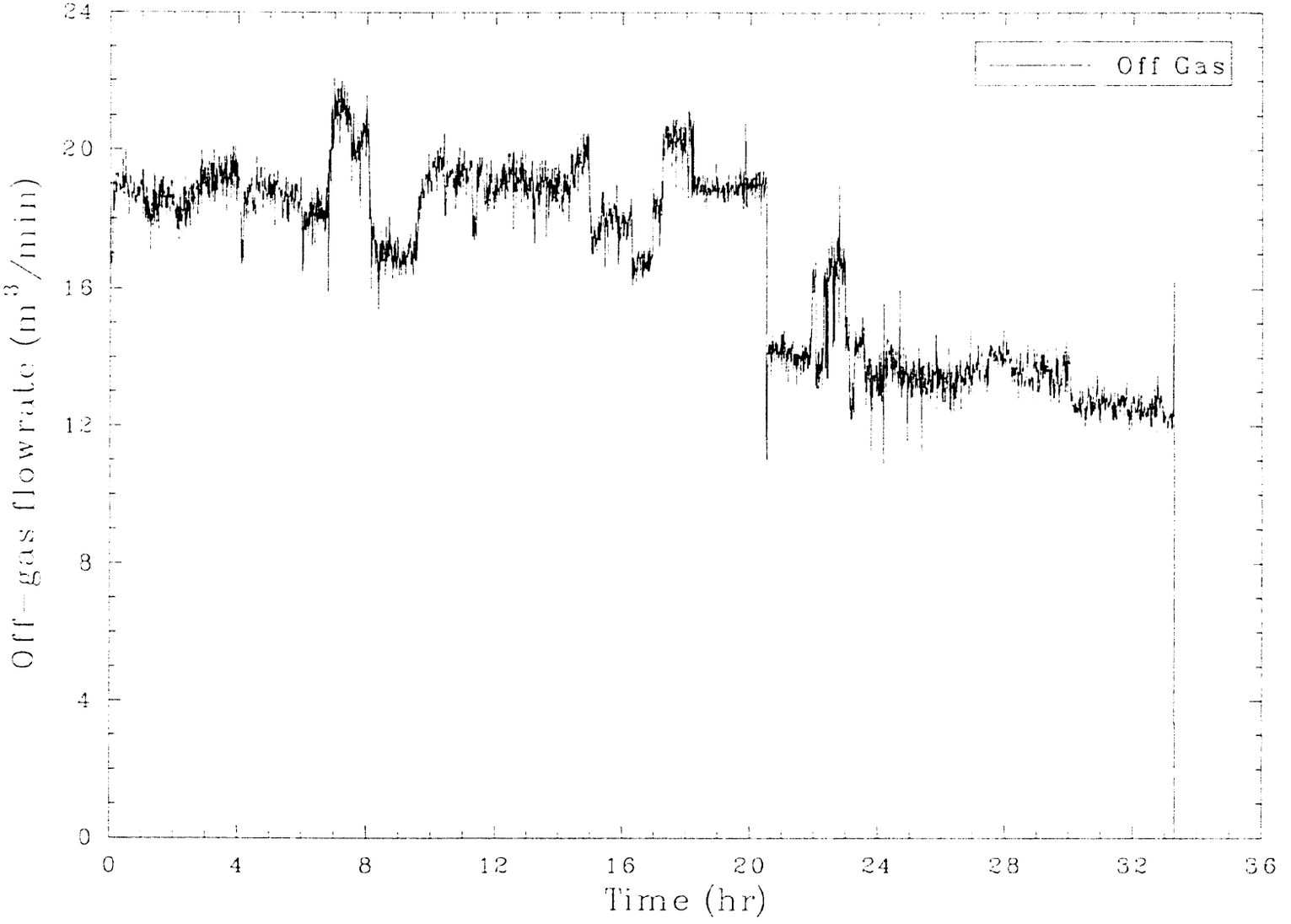

Figure 30. Total off-gas flow rate for Test 1.

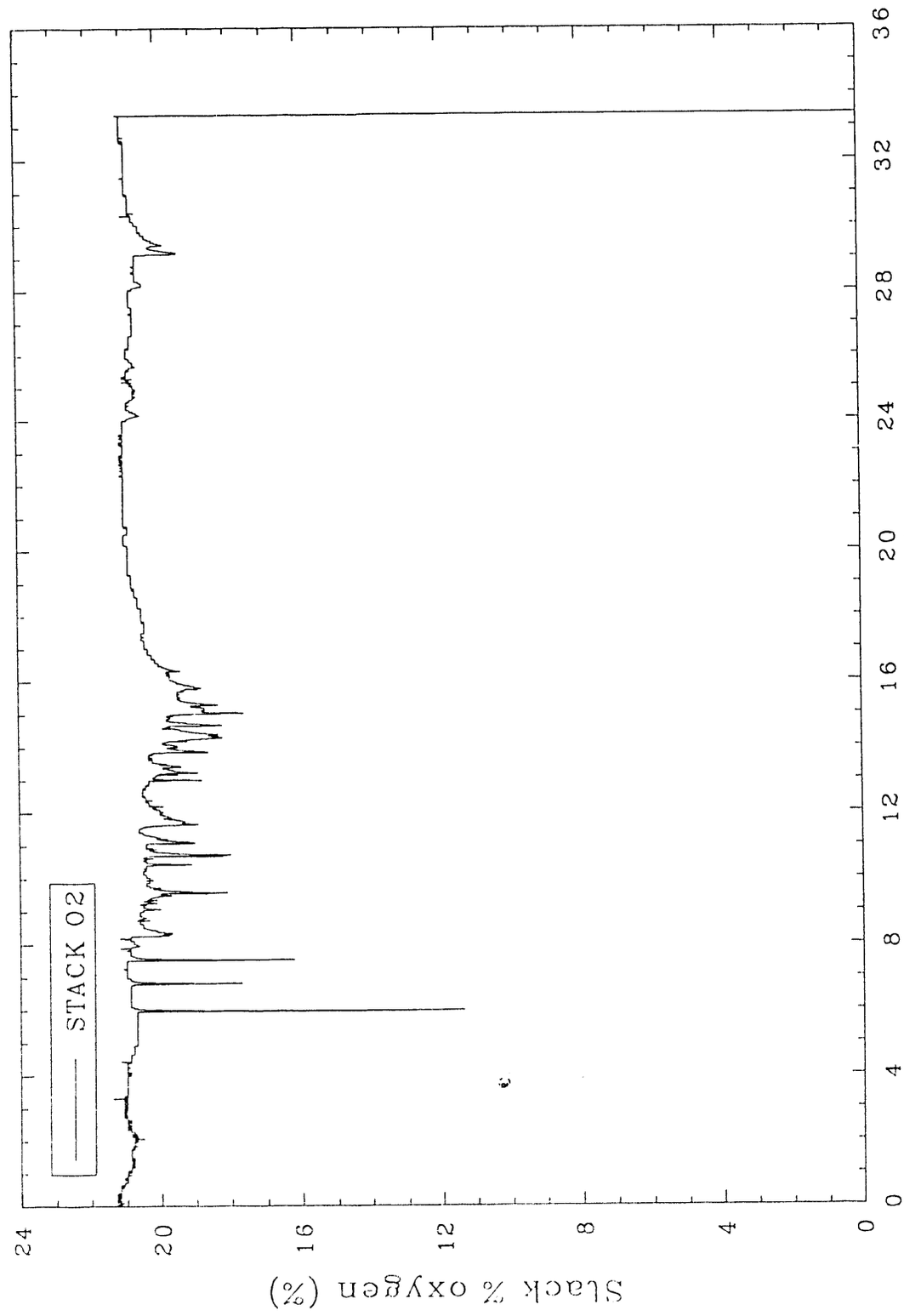

Figure 31. Stack oxygen concentration for Test 1.

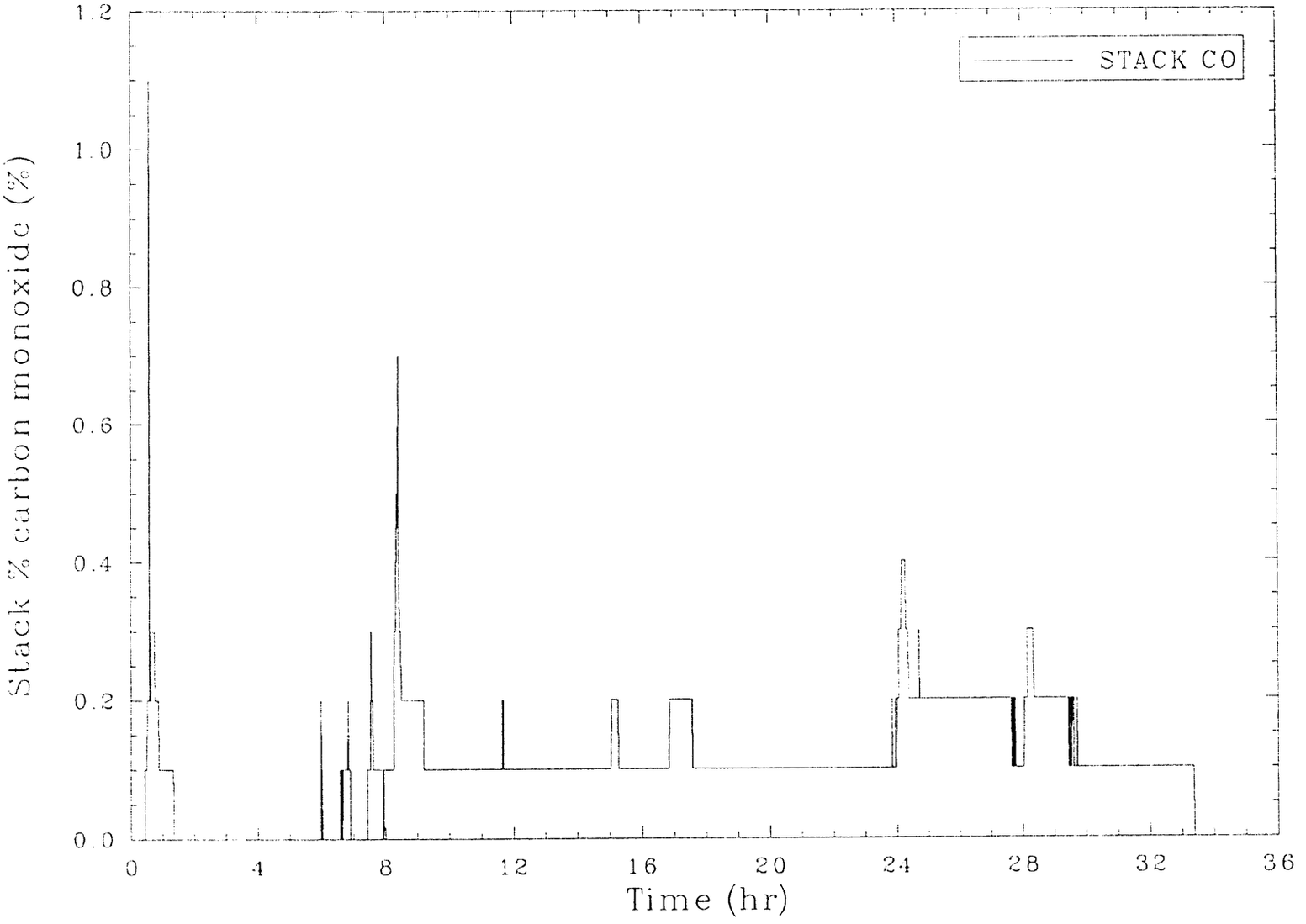

Figure 32. Stack carbon monoxide concentration for Test 1.

as the graphite starter path is consumed. Several pressure spikes resulted in a slight decrease in the oxygen concentration but were not accompanied by increases in carbon monoxide, as shown in Figure 33. It follows that the gas release from the melt in those cases was due to a release of steam or other noncombustible gas from a container, such as the noncombustible sludge cans that contained water. This phenomenon is explained by the release of noncombustible gasses from the melt, such as steam effectively displacing or decreasing the quantity of air entering the hood.

3.3.4 Off-Gas System Processing Experiences

The processing of the simulated buried waste site resulted in unusual off-gas processing equipment behavior and operating conditions relative to ISV processing of a contaminated soil site. The frequent temperature and vacuum fluctuations in the hood resulted in several operational consequences that appeared to be characteristic of processing any buried waste site. The key observations for Test 1 relative to the operation of the off-gas treatment system are summarized below.

- Increased melt rates resulted in more water vapor being introduced to the process off-gas system. As the melt progressed, water vapor in the soil was driven off as steam and condensed in the off-gas treatment system. With an increased melt rate, such as that seen in Test 1, the corresponding increased rate of water removal to the off-gas treatment system challenged the evaporative capability of the off-gas system. Consequently, the process scrub tank temperatures were operated near the maximum design limits to increase evaporative losses. It is important to try to maintain a water balance in the scrub solution tanks to prevent the undesired accumulation resulting in an increase in the secondary waste stream. This situation will result regardless of scale. Consequently, large-scale machines designed to process buried waste sites will require an improved evaporative capability to minimize the generation of secondary liquid wastes.

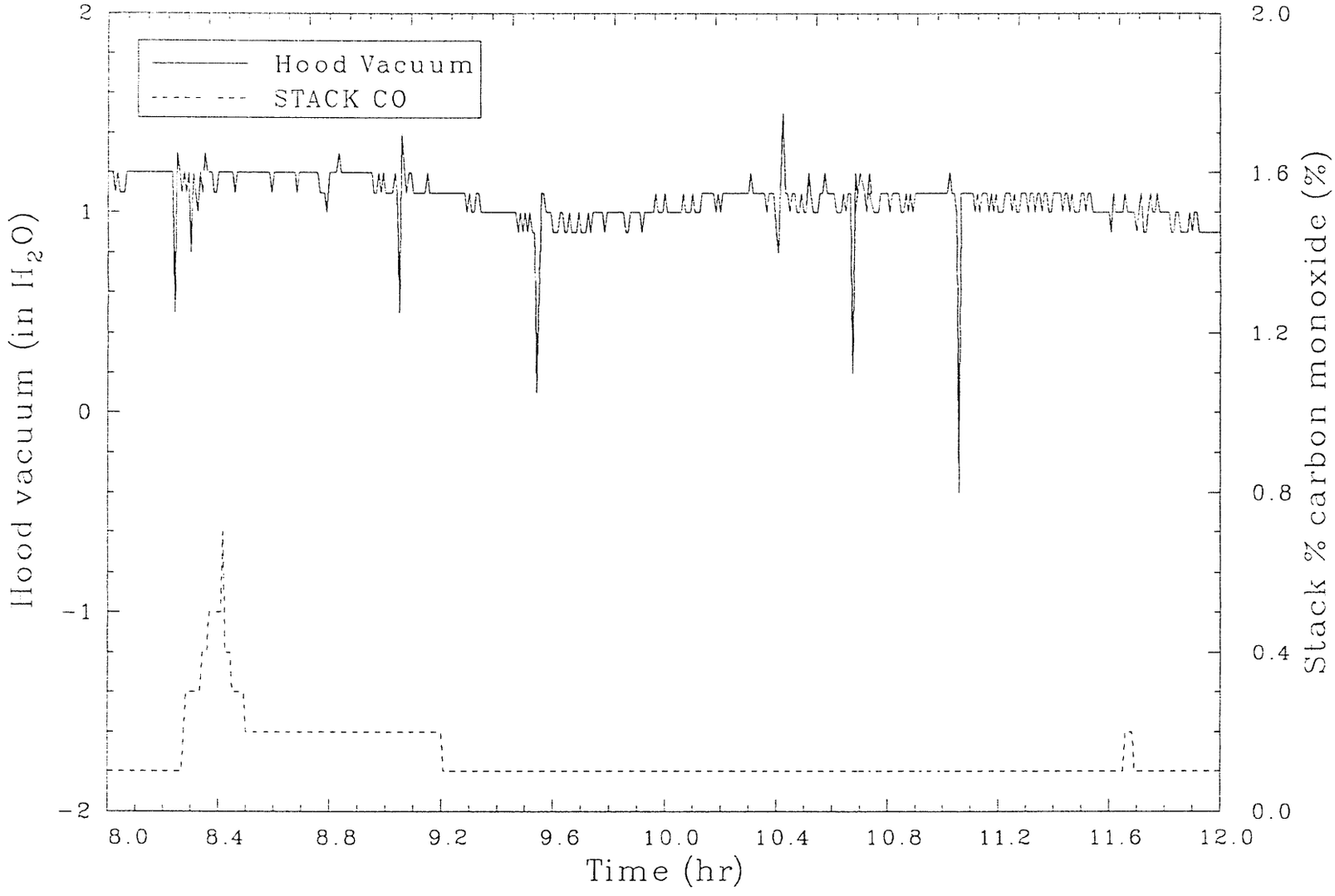

Figure 33. Hood vacuum and stack carbon monoxide concentration for Test 1, showing pressure events not concurrent with CO spikes.

- The off-gas temperatures in the hood fluctuated dramatically with each encounter of a container. As a result, the gas heater, designed to reheat the gas stream following wet scrubbing, required careful monitoring and frequent adjustment. Without this adjustment, excessively low gas temperatures would result in condensation in the HEPA filters, while excessively high temperatures would result in challenging the high maximum temperature limits for the blower. The present large-scale machine has an automatic set point controller that would effectively respond to these fluctuations.

- The rapidly fluctuating hood vacuum caused the automatic surge protection valve for the blower to continually readjust its position. The surge protection valve allows a controlled air flow into the blower to supplement the off-gas flow in cases of low gas flow from the hood. The effect of a low gas flow causes blower amperage to increase, potentially creating blower cavitation. When the surge protection valve was open, dilution of the off-gas flow resulted in a false high total off-gas flow value and a dilution of the off-gas stream prior to the stack measurements of CO, CO_2 and O_2.

3.3.5 Melt Behavior at Each Event

Understanding the behavior of the melt at each event is fundamental to understanding the processing impacts on the containment, off-gas treatment, and electrical system. This understanding is essential to proceed with full-scale operations on actual sites containing buried wastes. To fully detail the information gained from Test 1, qualitative visual observations are combined with measured data to provide a more explicit understanding of buried waste processing. Several of the events involving gas release from the containers are characterized below using the following key inputs.

- Hood temperature and pressure data

- Off-gas data including CO and O_2

- Amperage, voltage, and power to the electrodes
- Electrical resistance in the melt
- Visual observations during operations
- Posttest observations during excavation activities.

3.3.5.1 The Initial Event. The initial event occurred at approximately 5.9 hours into the test and resulted in the most dramatic temperature and pressure spikes for the test. In this event glass was ejected from the melt and contacted the hood surfaces at several locations including the tip of the plenum thermocouple. A hood vacuum plot of the event is provided as Figure 34. This event resulted in the most dramatic temperature spike (see Figure 23) even when accounting for glass contact on the plenum thermocouple. Figure 35 is a plot of roof and wall temperatures for several events and shows the dramatic temperature spike created by this initial event. The hood vacuum rapidly decreased during the event due to a rapid gas release from the melt, decreasing from an initial value of 0.9 in. of water to greater than 5.0 in. of water pressure. The pressure transducer range was from +5 to -5 in. of water; consequently, the exact magnitude of the pressure spike cannot be quantified. However, based on an estimate of the slopes when the data set is greatly expanded, the spike appears to have achieved a positive pressure of approximately 7 in. of water pressure.

At the time of the event, operators responded by deenergizing electrode power. Once power was reenergized, power levels had decreased approximately 100 kW, as shown in Figure 36. Resistance in the melt, as calculated from measurements in the secondary windings of the transformer, increased from 2 to 20 ohms on phase A and from 2 to 4 ohms on phase B, as shown in Figure 37. This difference in resistance on the secondary windings suggests the event had a localized effect adjacent to a phase A electrode. Resistance data both during startup and at later times in the test show the phases A and B resistance values agreed closely, as expected. Therefore, there is confidence in the resistance measurements indicating a localized effect on a phase A electrode. Resistance gradually returned to pre-event levels, approximately

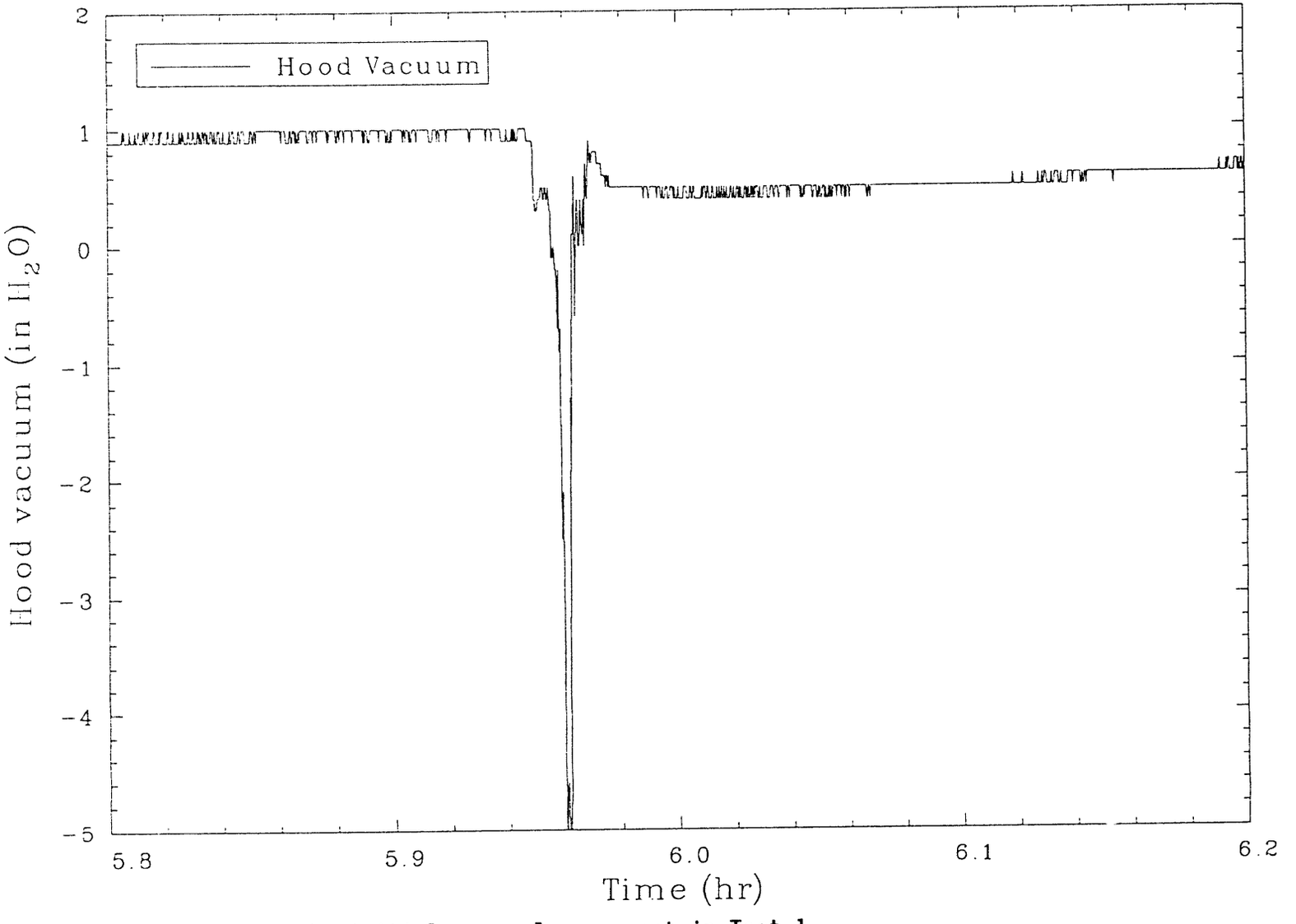

Figure 34. Hood vacuum for the initial gas release event in Test 1.

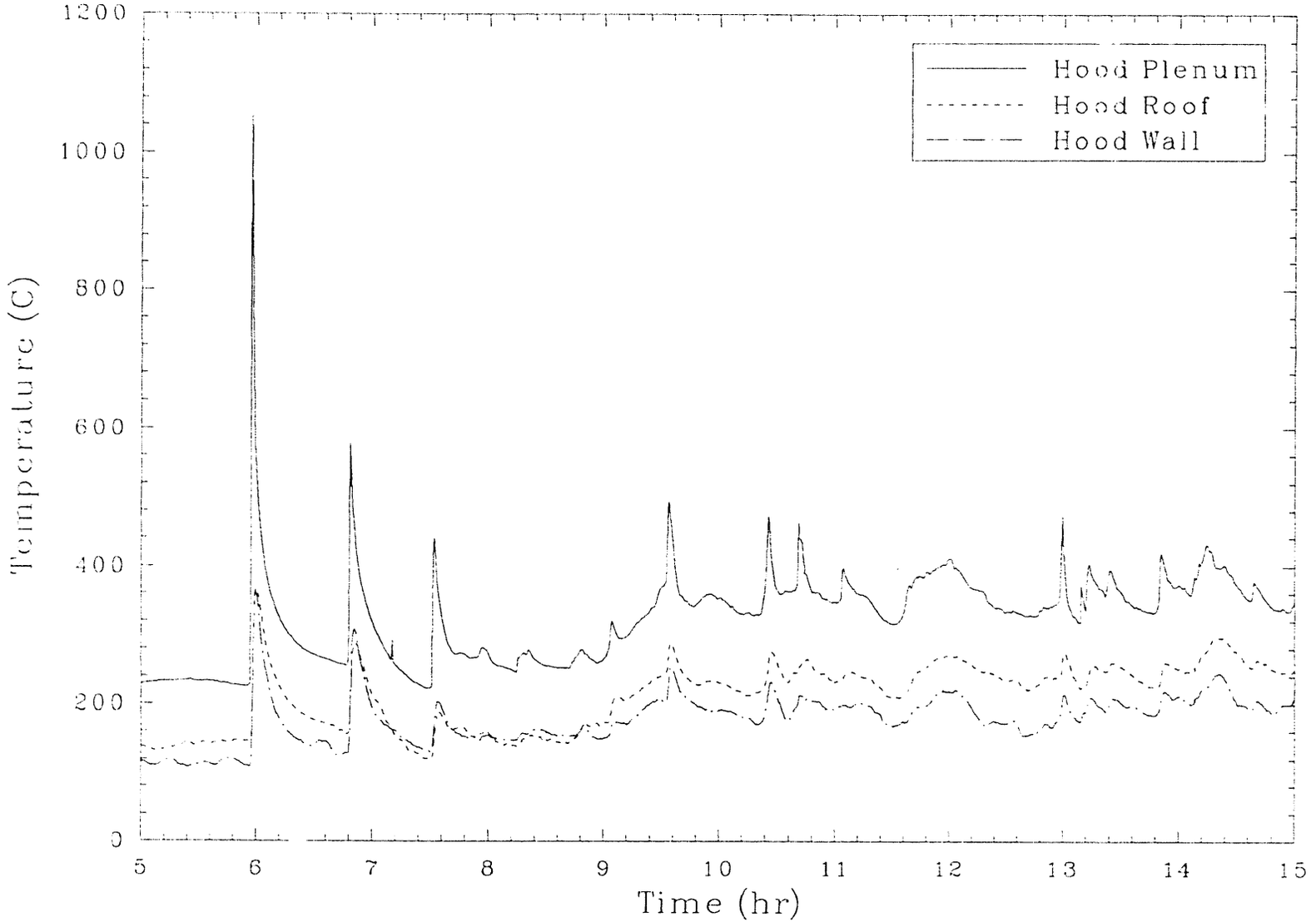

Figure 35. Hood, roof, and wall temperatures for several gas release events in Test 1.

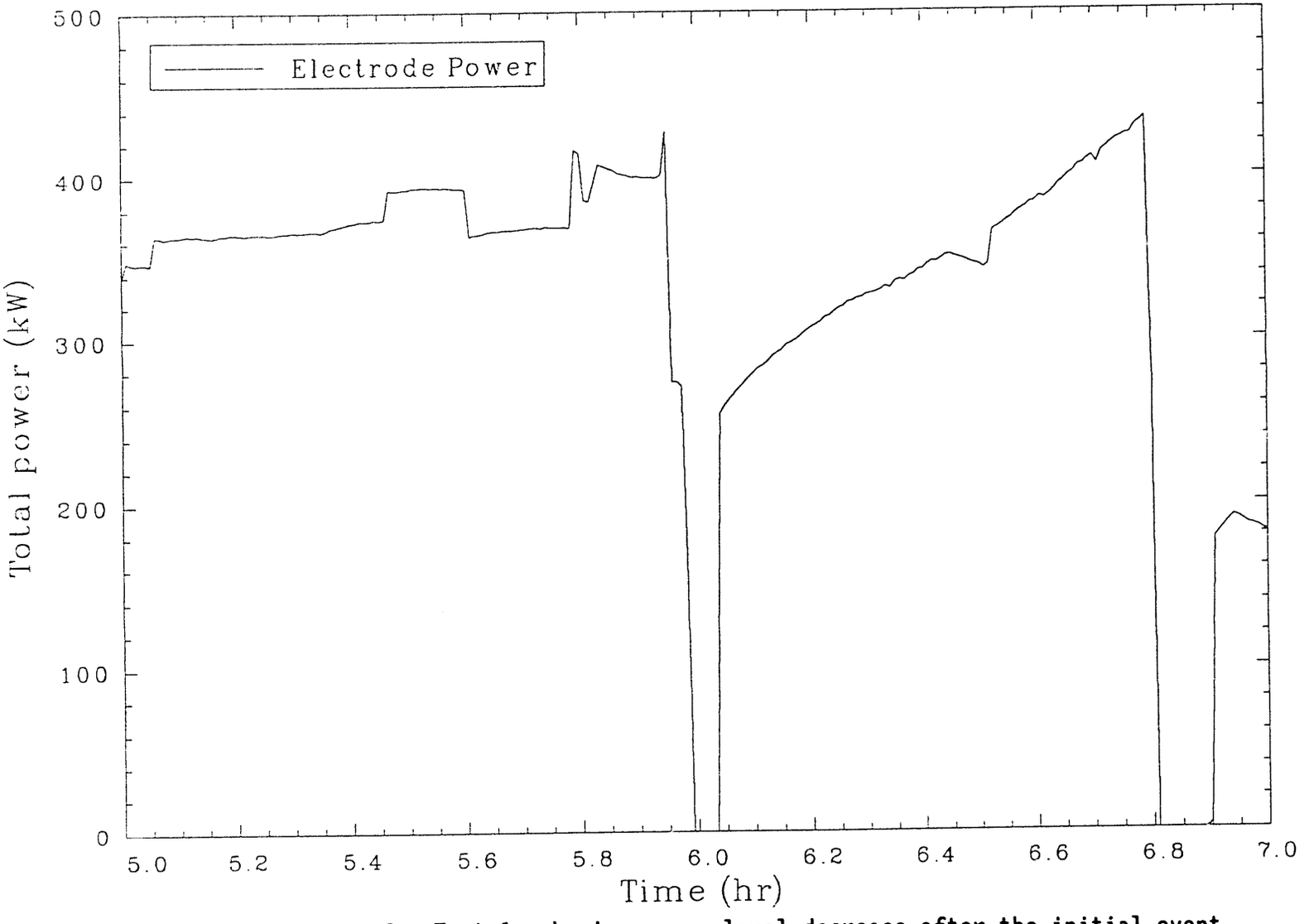

Figure 36. Total electrode power for Test 1, showing power level decrease after the initial event.

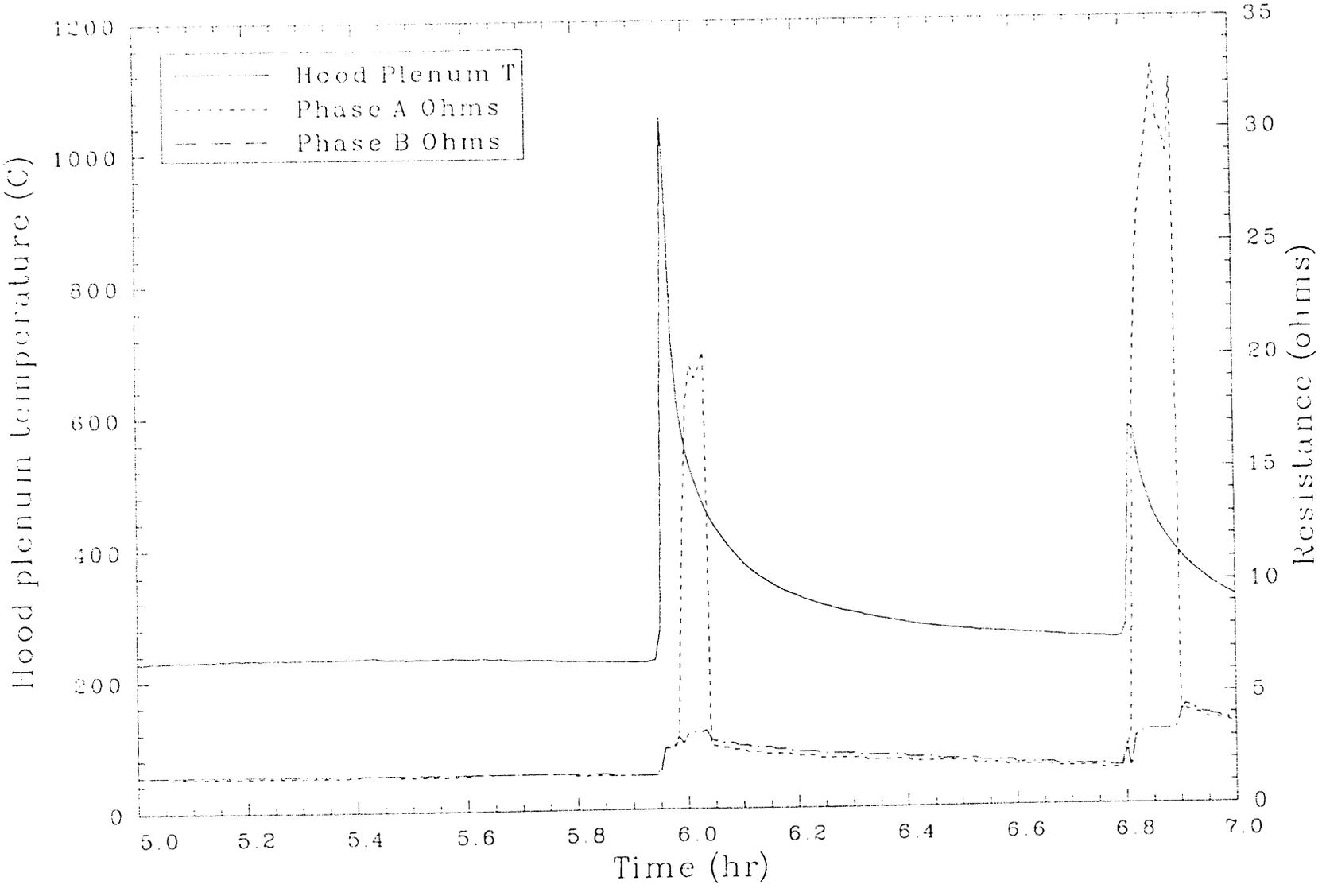

Figure 37. Phase A and B resistance during the initial gas release event in Test 1.

6 minutes after the event. Possible explanations for the single phase resistance increase include:

- The insulation blanket, placed during the laying of the starter path, subsided into the melt (as observed by the operating staff) and settled into a position that partially disrupted the firing pattern of a phase A electrode.

- A gas release caused a localized cooling effect on the glass. Any gas release through molten glass would act to remove heat from the glass and disrupt the cold cap, creating a situation where the molten glass could loose heat radiantly. Due to convective mixing currents in the melt, a localized area of cooled glass could be mixed, and increased resistance would be observed on both phases. As shown in Figure 37, resistance on phase B increased from 2 to 4 ohms.

- A portion of the frozen glass comprising the cold cap dislodged and caused partial disruption of the conductive path while serving to locally cool the glass. Once the frozen glass melted, the convective mixing currents in the melt would ultimately balance the resistance over both phases.

Other possible explanations that were discounted included the presence of electrically disruptive gas bubbles in the melt and the actual loss of glass volume due to ejection or glass flow into containers adjacent to the melt. These explanations are discounted because the bubbles would cause only a momentary electrical disruption before being released from the melt. In addition, glass flow away from the melt to an adjacent container would tend to affect both phases equally, as would the case where molten glass was ejected from the melt.

Carbon monoxide concentrations indicate that a significant volume of combustible gasses burned in the hood during the transient event. Carbon monoxide values at the stack spiked from 0 to 0.2% and then returned to 0%, as

shown in Figure 38. Oxygen concentrations dropped to just under 12%, which was the lowest level observed during the test.

Operating staff observed the following during and immediately after the event.

- A few localized points of glass contacting the interior surfaces of the hood were observed as glowing red spots from the exterior of the hood.

- The event caused the upper portions of the 304L stainless steel sheet metal panels on the hood to discolor to a bronze or copper color during the event.

- Visual observations through the viewing window in the hood immediately after the event revealed the insulation blanket had been covered by molten glass, causing the blanket to sink into the melt out of sight. Molten glass was ejected from the melt with sufficient force to contact most surfaces of the hood including the roof, plenum thermocouple, side panels, and the door.

This first event provided valuable information on the relationships of hood temperature and pressure relative to containment, resistance and power response data relative to a Scott-Tee transformer, and gas concentrations relative to the off-gas treatment system design. It is evident that the off-gas hood for a large-scale machine must be designed to handle dramatic temperature and pressure spikes and withstand direct contact with molten glass. Based on current large-scale transformer designs that include independent control on each phase of the secondary, imbalances on the secondary side of the transformer could be easily handled.

3.3.5.2 The Second Event. A second event occurred at approximately 6.8 hours into the test. This event resulted in the a dramatic hood pressurization similar to the initial event. Hood pressure spiked from 0.9 in. of water vacuum to over 5.0 in. of water pressure, as shown in Figure 39. The pressurization was followed by a temperature spike from 260 to 600°C.

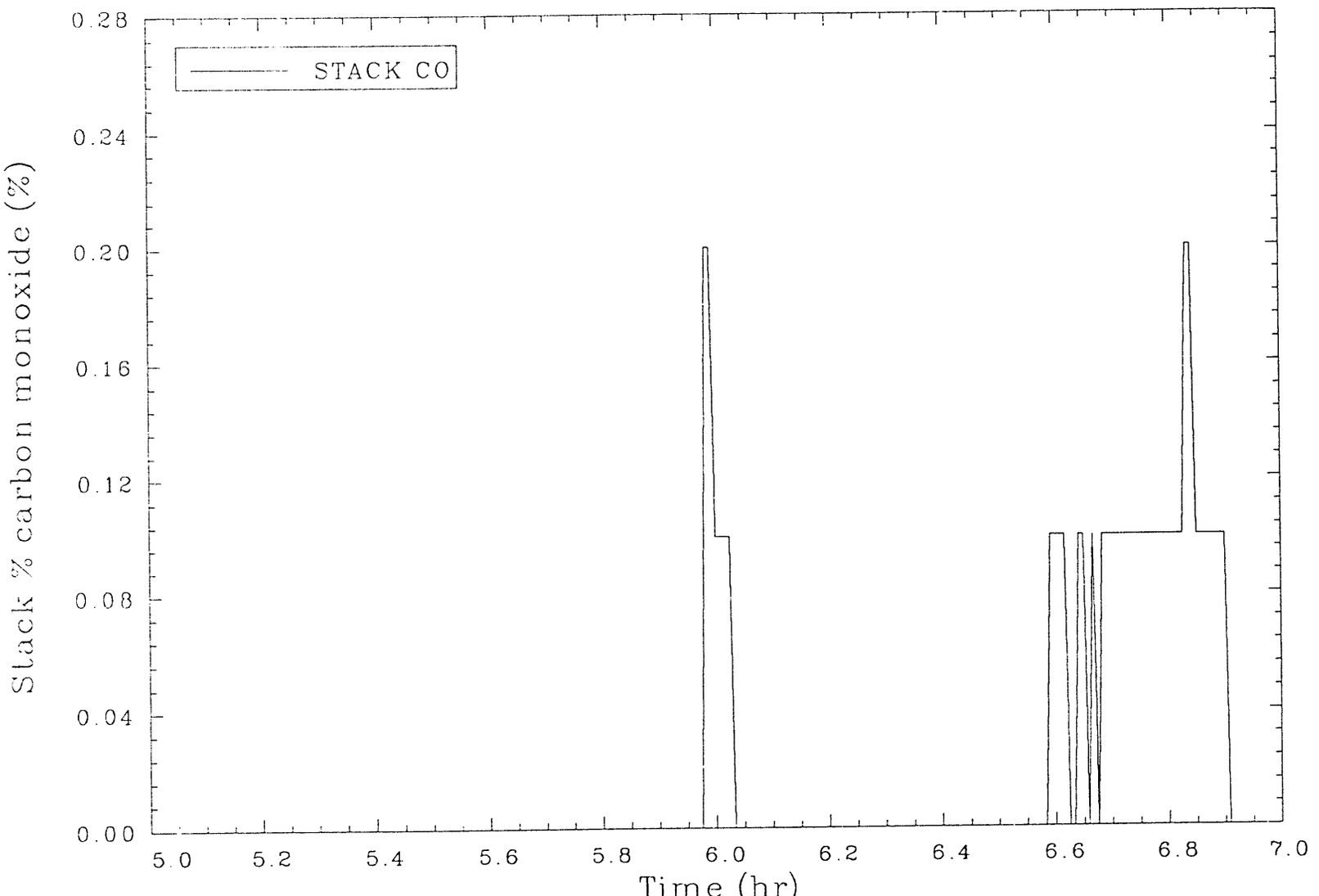

Figure 38. Stack carbon monoxide concentration during the initial gas release event in Test 1.

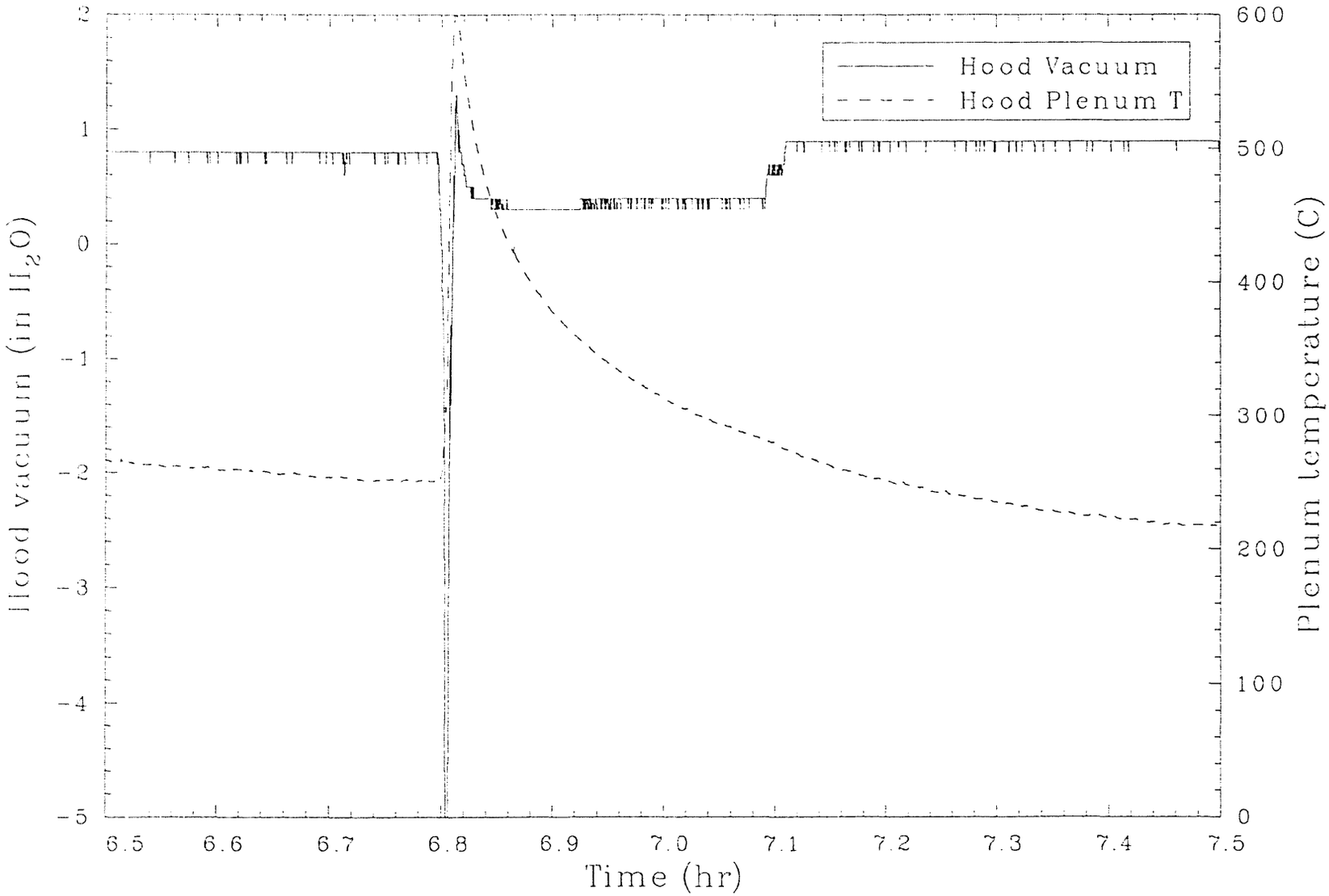

Figure 39. Hood vacuum and plenum temperature during the second event in Test 1.

Operators observed smoke escaping from the hood around the base of the hood and out through the HEPA filtered seal pot. Soil providing a seal at the base of the hood by the door was dislodged as pressure was relieved from the hood. Carbon monoxide concentrations at the stack increased from 0.1 to 0.2%, and oxygen concentration dropped from approximately 20.5 down to 17.5%, indicating that significant combustion occurred in the hood, shown in Figure 40.

Electrical resistance data from this event are similar to the initial event. Phase A ohms increased from 2 to approximately 33 ohms while phase B increased from 2 to 5 ohms, as shown in Figure 41. Phase A amperage decreased from approximately 400 to 160 A, as shown in Figure 42. Figure 43 illustrates the total power of the test decreasing from 440 to 180 kW as a result of the event. Even when accounting for a nonpowered period of operation immediately following the pressurization, phase A resistance dramatically increased, while phase B resistance increased only moderately. This again suggests a localized effect on one of the two phase A electrodes.

Like the first event, this second event provided valuable information on the relationships of hood temperature and pressure relative to containment. In addition, the magnitude of the pressurization identifies the need for a fast acting, high capacity pressure relief device that can effectively treat gases prior to their release from the hood.

3.3.5.3 The Third Event. The third event occurred at approximately 7.5 hours and resulted in only moderate plenum temperature and hood vacuum spikes relative to the first two events. The plenum temperature increased from approximately 220 to just over 440°C. The hood vacuum spiked from 1.2 to 0.6 in. of water. Figure 44 shows the temperature and vacuum relationship for this third event.

Electrical resistance data was balanced, unlike the previous two events. Phases A and B increased from 2 ohms to just over 4 ohms as a result of the event, shown in Figure 45. Power was not interrupted by operators during the event. Phase A amperage dropped from 320 to 160 A; and phase B amperage dropped from 300 to 140 A, as shown in Figure 46. Total power dropped from

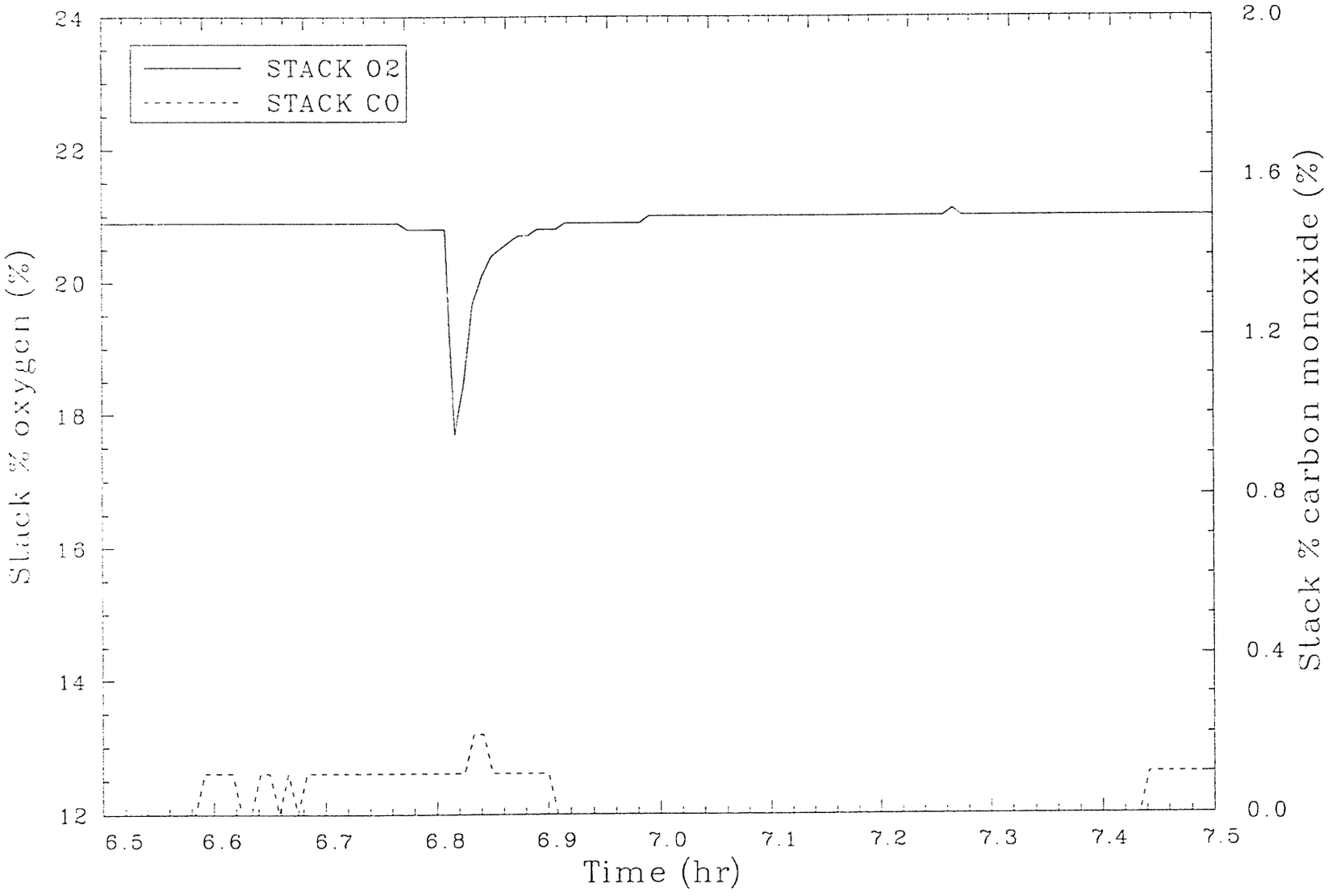

Figure 40. Stack oxygen and carbon monoxide concentrations during the second event in Test 1.

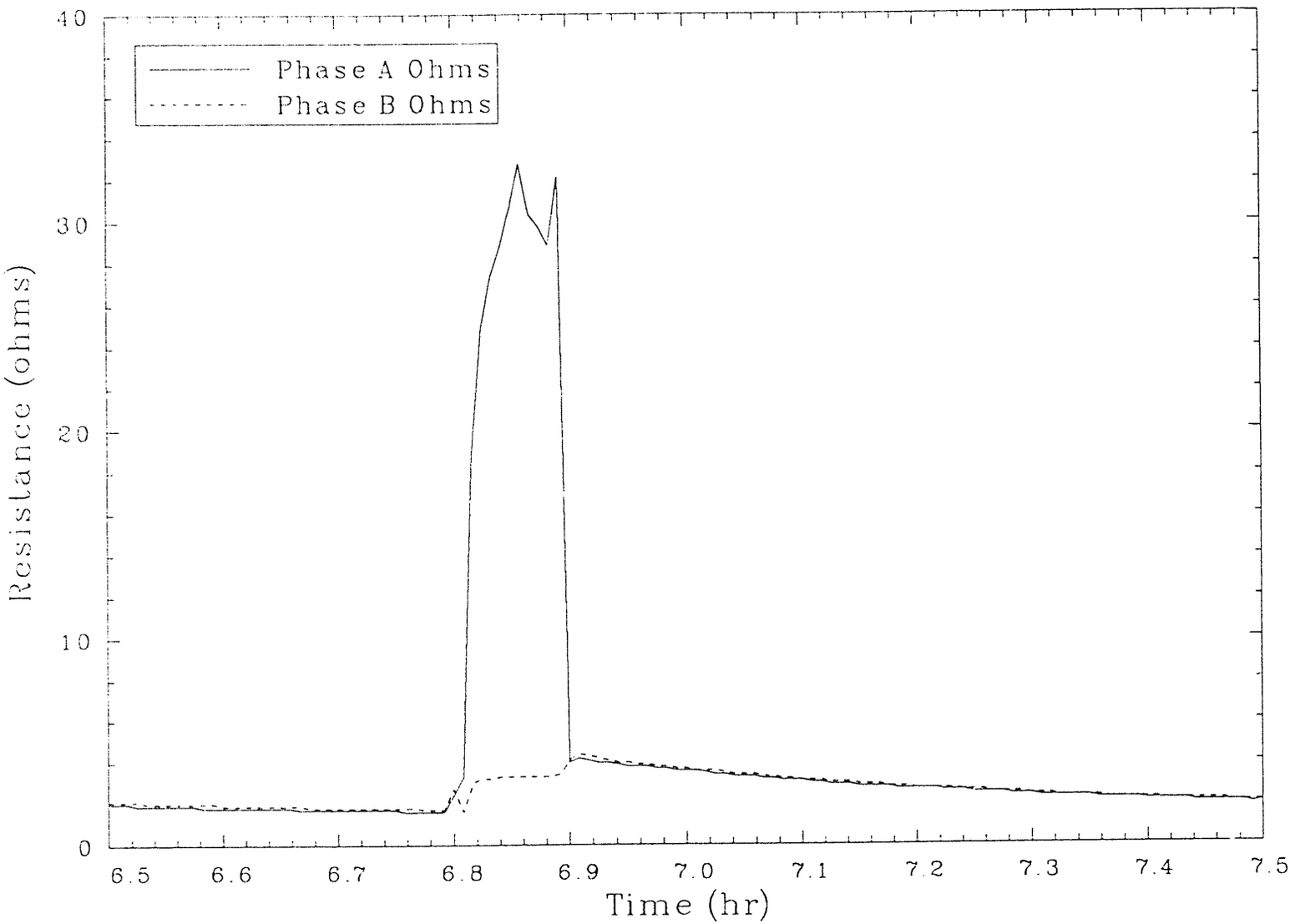

Figure 41. Phases A and B resistance during the second event in Test 1.

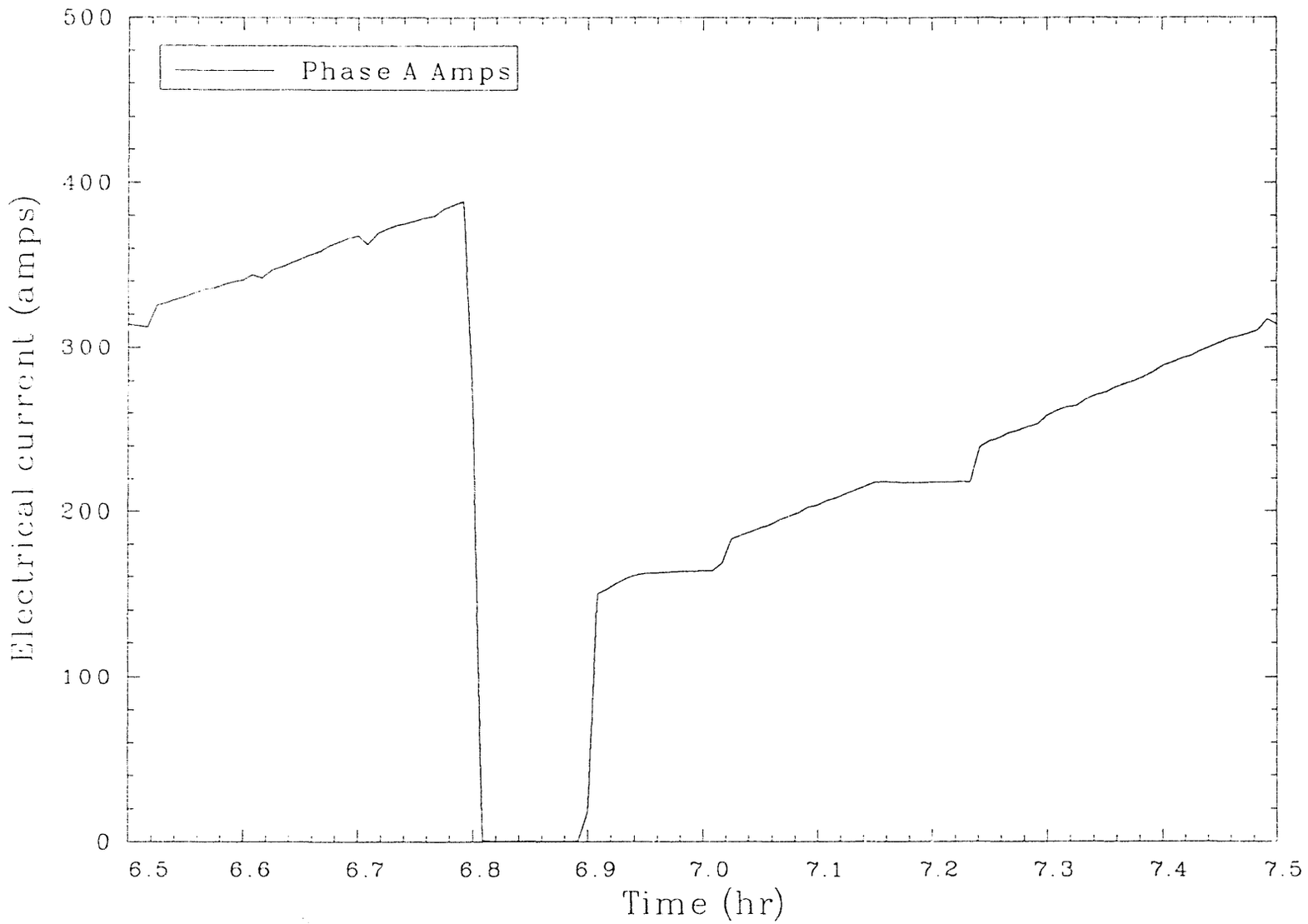

Figure 42. Phase A amperage during the second event in Test 1.

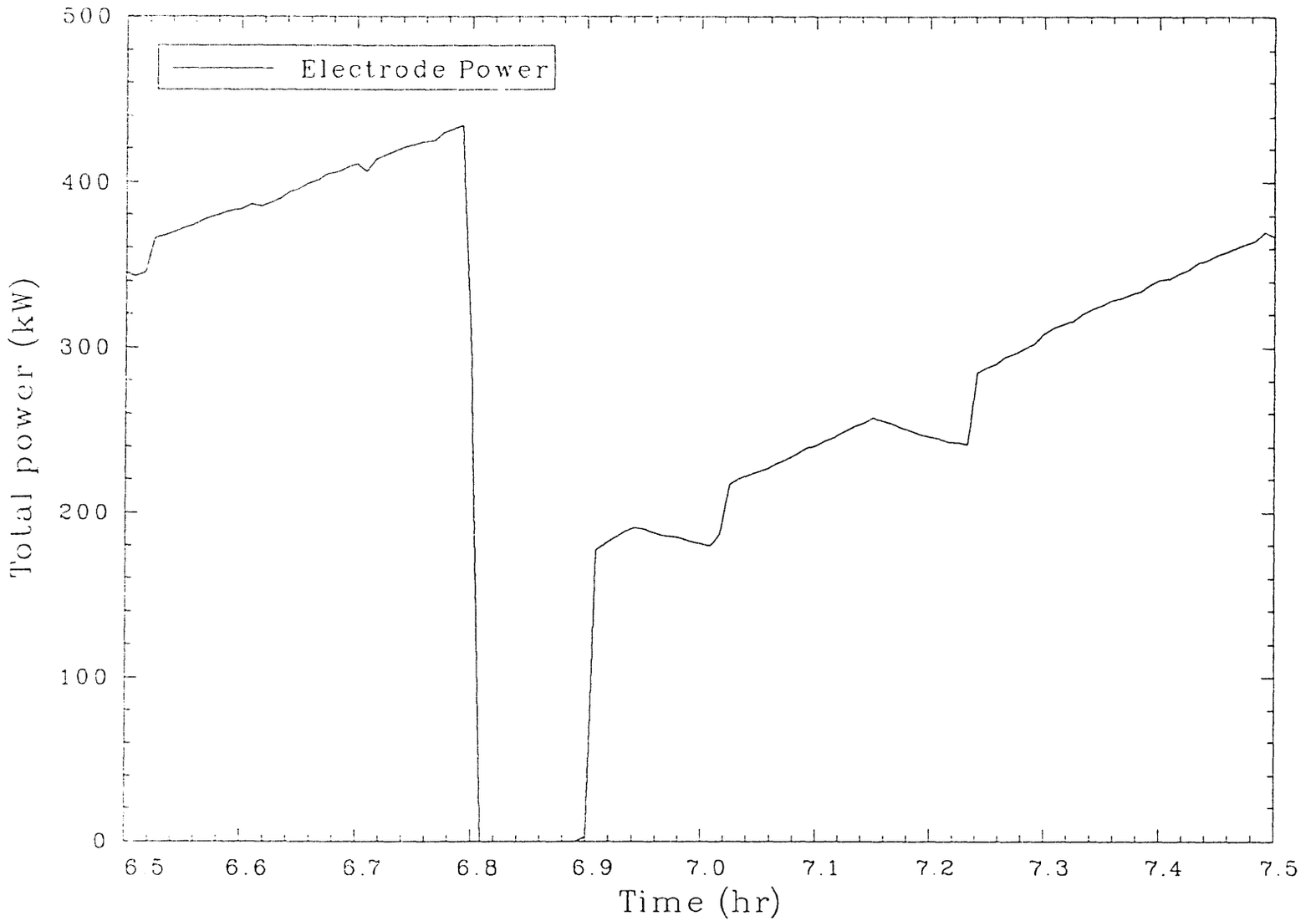

Figure 43. Total electrode power during the second event in Test 1.

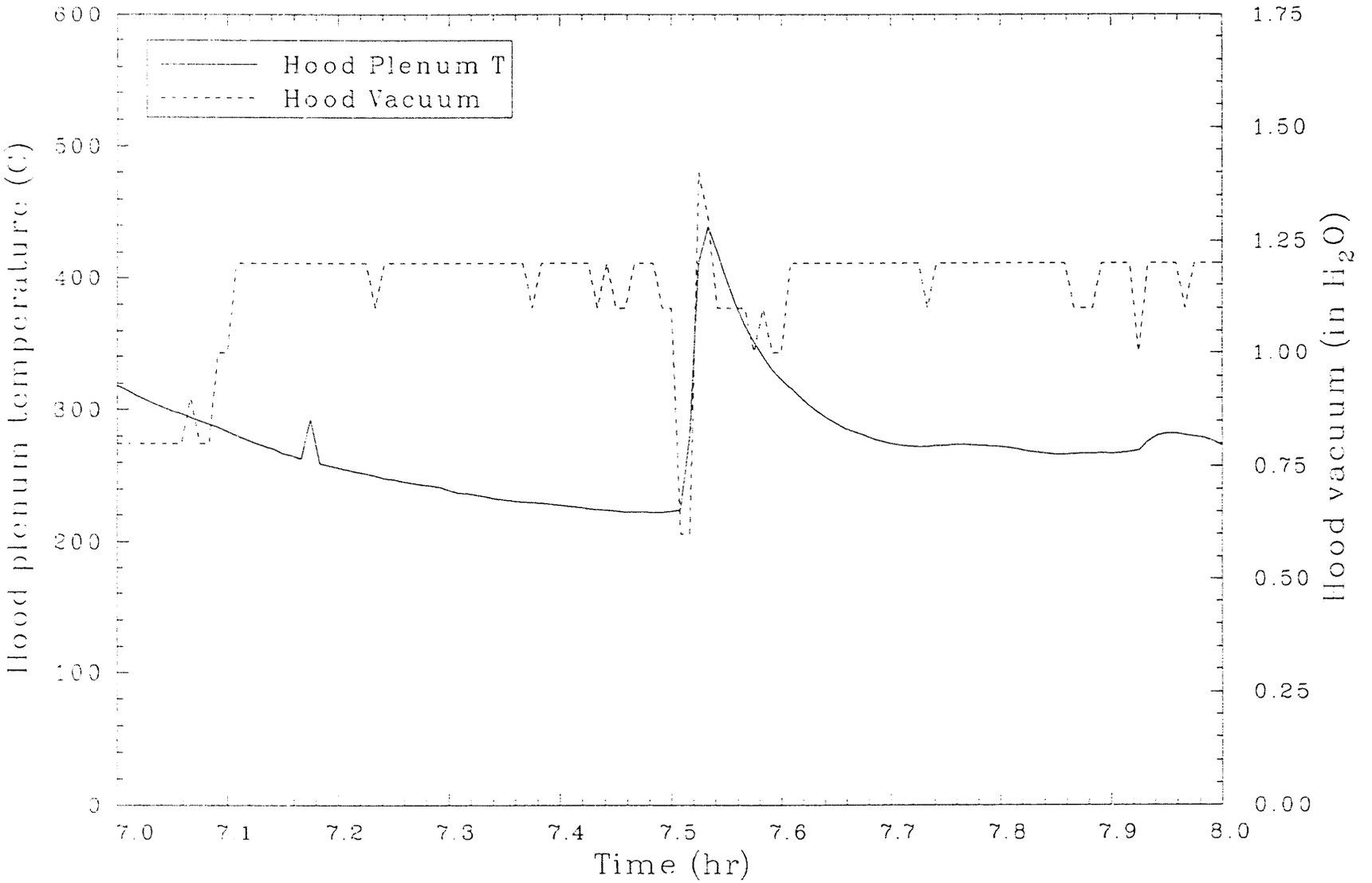

Figure 44. Hood vacuum and plenum temperature for the third event in Test 1.

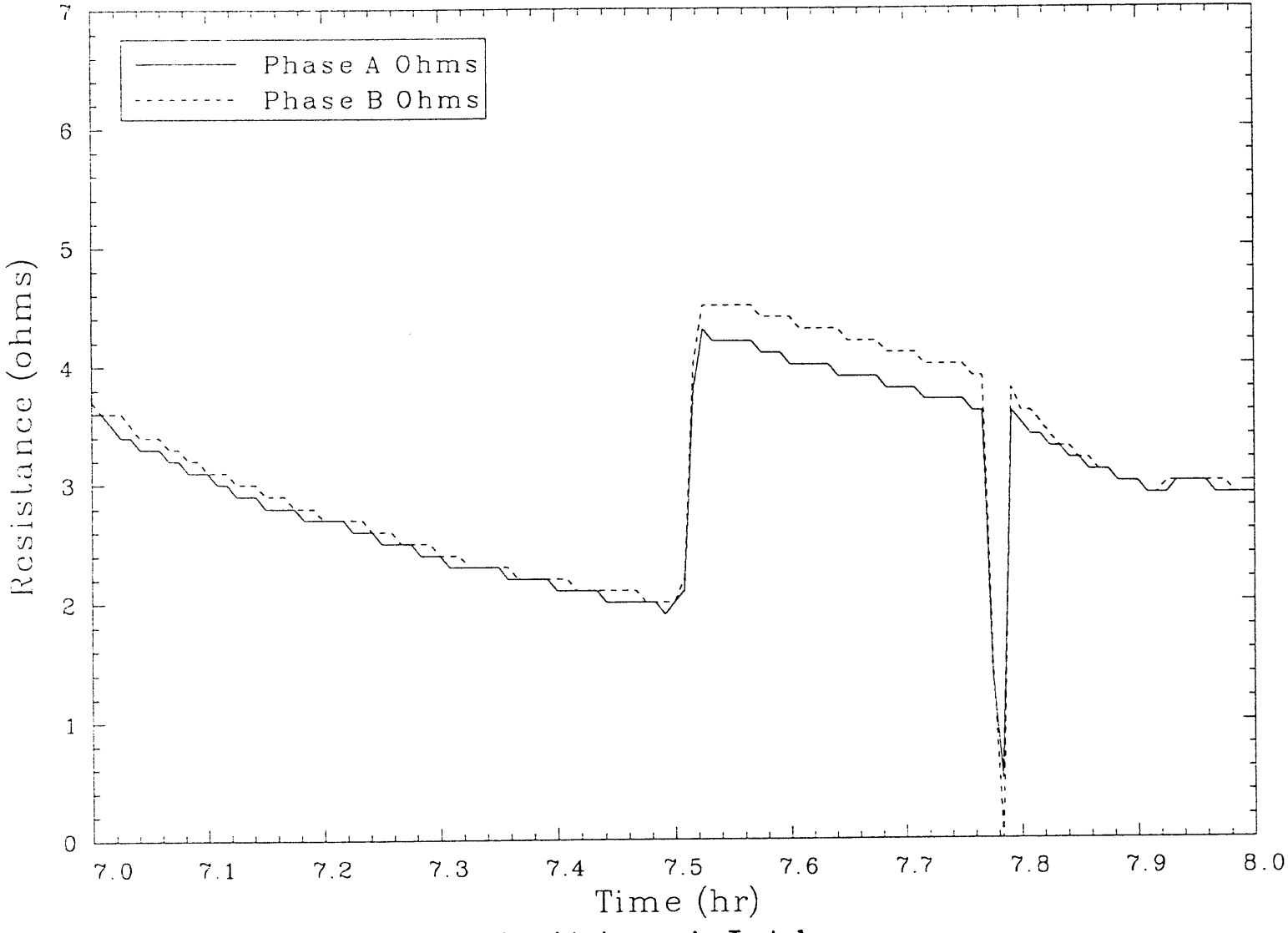

Figure 45. Phases A and B resistance for the third even in Test 1.

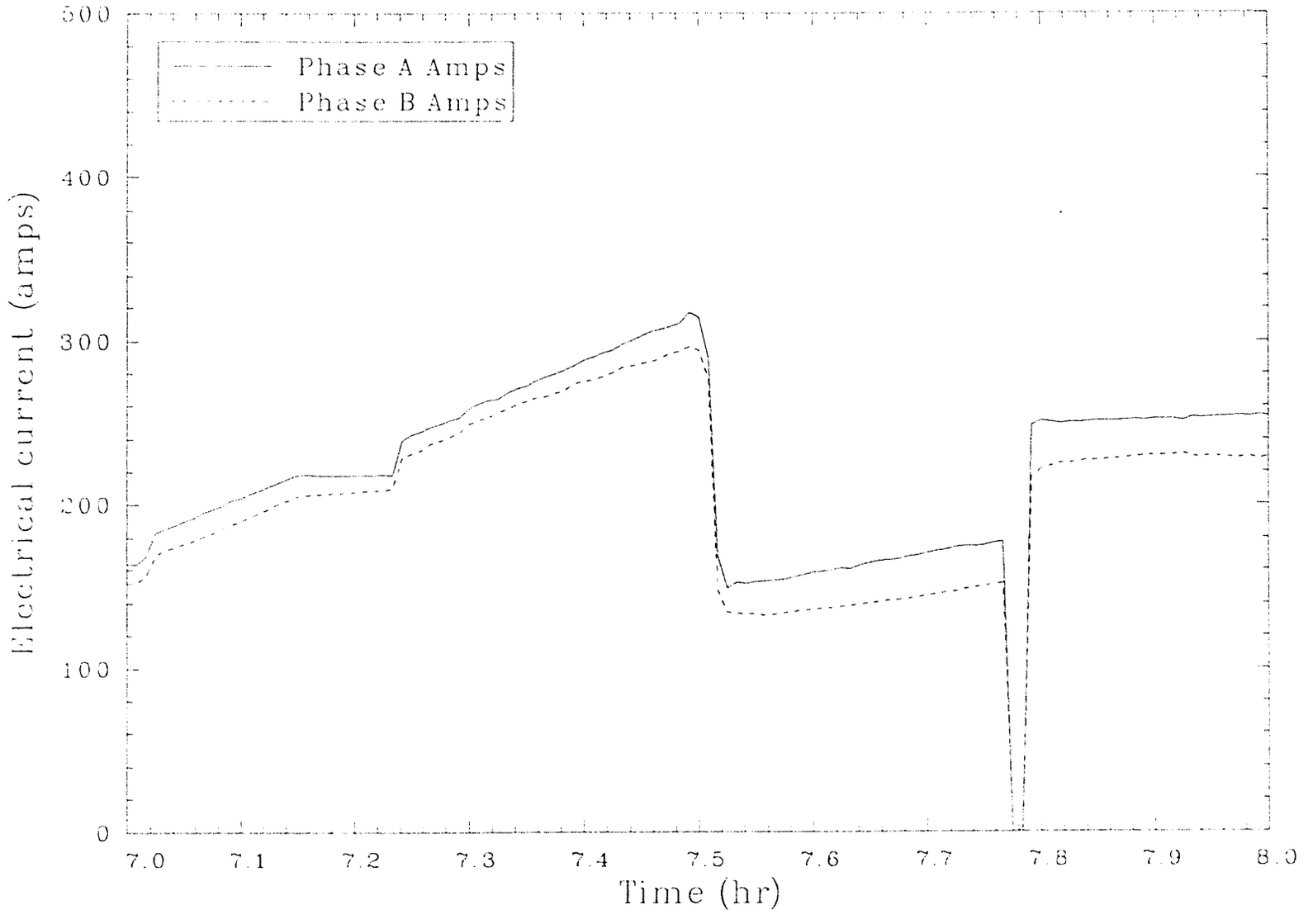

Figure 46. Phase A and B amperage for the third event in Test 1.

370 to 180 kW as a result of the event; this loss of power is illustrated in Figure 47. Radiant heat losses from the molten glass resulted in increased resistance in the molten glass as the glass cooled. This phenomenon occurred during essentially all gas releases (see Figure 23, p. 58).

Operators noticed resistance values rising sharply and immediately went to the hood to observe the event. A large opening, approximately 0.6 m (24 in.) in diameter, had formed in the center of the cold cap. Extremely hot molten glass was flowing up from the opening and covering the frozen cold cap. Within a few moments, the cold cap was completely covered by molten glass and disappeared from sight. Dissolution of the cold cap would explain the balanced increase in resistance on both phases because the overall melt temperature decreased with the introduction of pieces from the frozen glass layer into the melt.

The third event resulted in the stack oxygen concentrations to decrease from 20.9 to 16%, and carbon monoxide values to increase from 0 to 0.3%, shown in Figure 48. These values indicate the gas release resulted in combustion in the hood. An operator observed the event and noticed the hood appeared to be smoke filled. Flares were present.

3.3.5.4 Later Events. Several of the events later in the test involved hood vacuum fluctuations without any recorded change in the stack carbon monoxide concentrations. It is suspected the gas releases into the hood came from cans containing wet sludge. Once these cans were heated and pressurized, their resultant release to the hood consisted primarily of steam, hence, the steady state of carbon monoxide concentration. The oxygen concentration decreased from 20.3% to between 18 and 19% due to steam displacing the oxygen in the hood or to steam limiting the inflow of air to the hood during steam release from the melt (see Figure 31). Three events at approximately 9.5, 10.5, and 11.5 hours illustrate this phenomenon. Figure 33 is a plot of carbon monoxide concentration at the stack versus hood vacuum. The baseline carbon monoxide concentration of 0.1%, from 8 hours through 32 hours (see Figure 32), probably results from a gradual decomposition and combustion of organic materials from various cans and boxes; in particular, wood pyrolyzes more

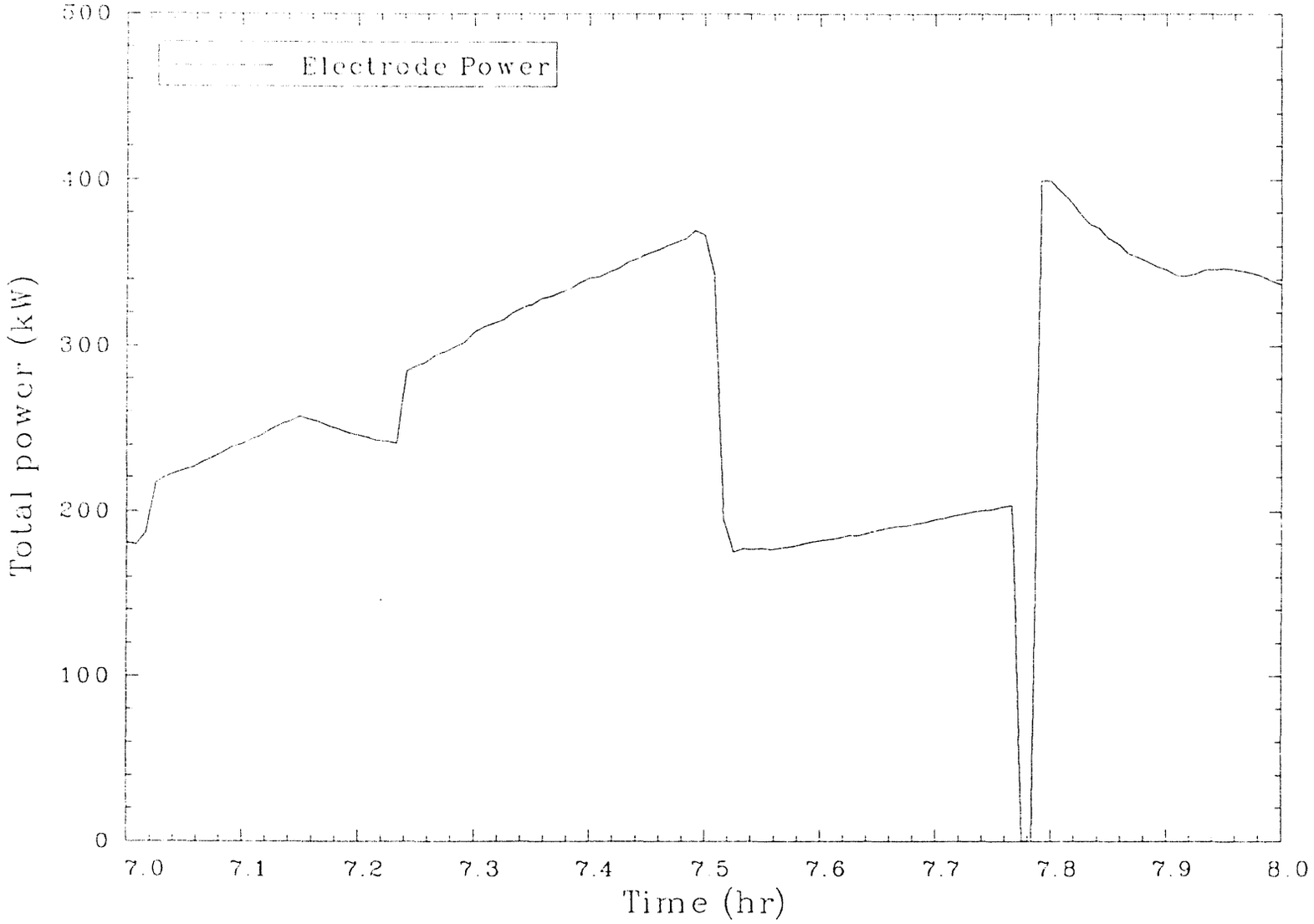

Figure 47. Total electrode power for the third event in Test 1.

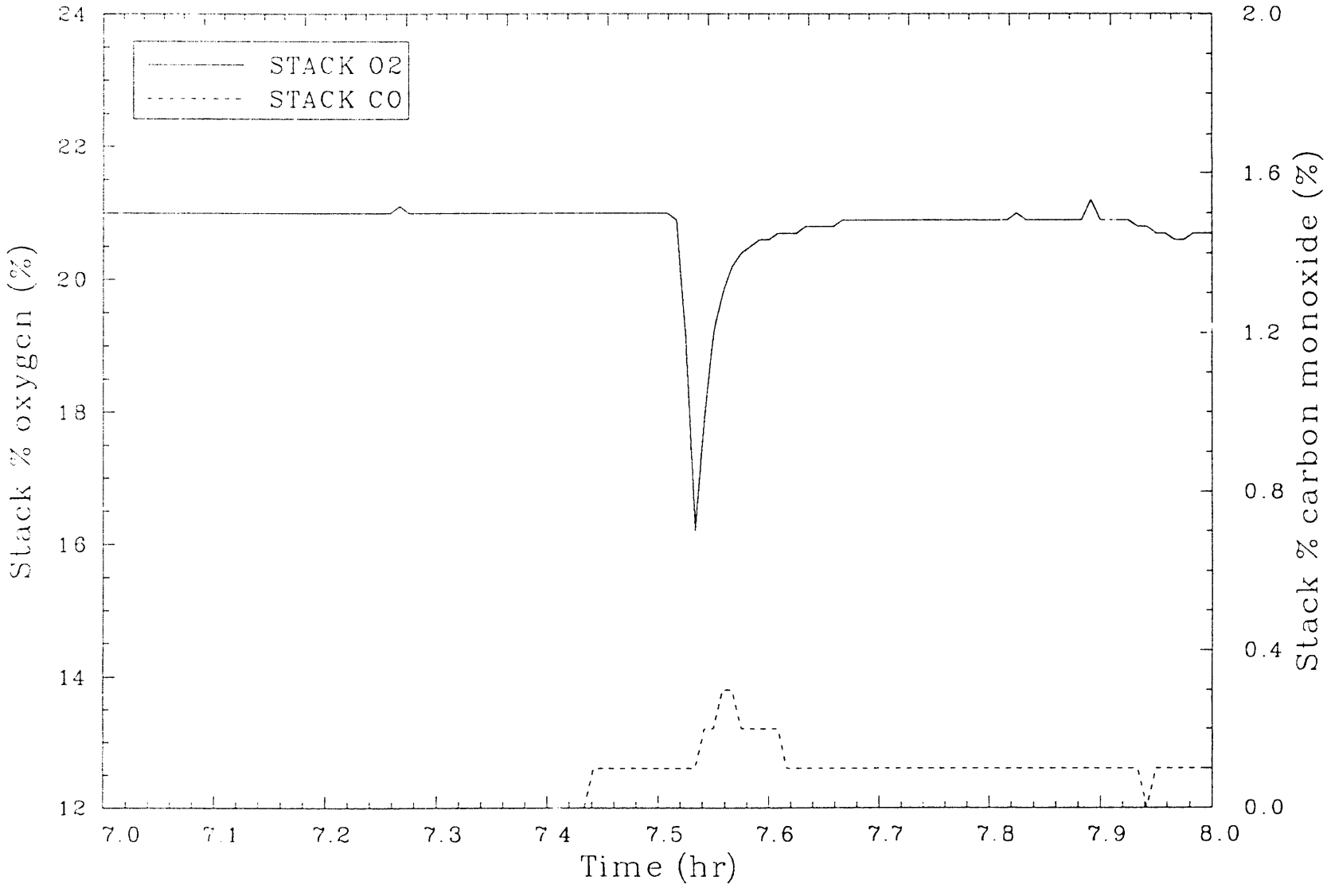

Figure 48. Stack oxygen and carbon monoxide concentrations for the third event in Test 1.

slowly than loosely packed paper or cloth. At approximately 11.3 hours, two operators observed what appeared to be a piece of charred wood floating on the melt.

3.3.6 Electrical Instabilities

As indicated in Section 3.3.2, one of the key problems associated with the test involved the use of the electrode coating used to limit oxidation of the graphite. This coating caused the electrodes to stick to the cold cap and ultimately contributed to the termination of the test shortly after achieving an approximate 2.4 m (8 ft) depth. The process suffered from electrical imbalances due to the inability to adjust the electrode positions. The imbalances created excessive heat in the transformer and caused saturable core reactor fuse and thyristor switch failures. The total power supplied to the melt at 22 hours into the test was 54 kW on phase A and 5 kW on phase B. It was evident that a phase B electrode was not sufficiently contacting the conductive portion of the melt because phase B amperes were only 15% of the phase A amperes. As shown in Figure 49, at 23 hours into the test, phase A resistance equaled 8 ohms while phase B resistance equaled approximately 40 ohms. Over the next 6 hours, phase B resistance gradually increased to over 100 ohms while phase A resistance remained relatively constant at less than 6 ohms. Phase A resistance had decreased from 8 to 6 ohms due to heat being introduced by the phase A electrodes following the extended period of nonpowered operation to replace failed fuses and thyristor switches.

Attempts to replenish the heat to the melt via electrode power through phase A was futile and resulted in localized heating between the phase A electrodes. Phase A resistance gradually increased to 170 ohms, and the glass pool being heated by the phase A electrodes ultimately melted away from the four stuck electrodes. The test was terminated when phase A amperage began to wildly fluctuate while the phase A voltage correspondingly spiked to full-scale. This indicated the advancing melt had finally melted away from at least one of the phase A electrodes. At this point, because the electrodes were frozen in place and no longer in contact with molten glass, electrode power was terminated and preparations for process equipment shutdown were initiated.

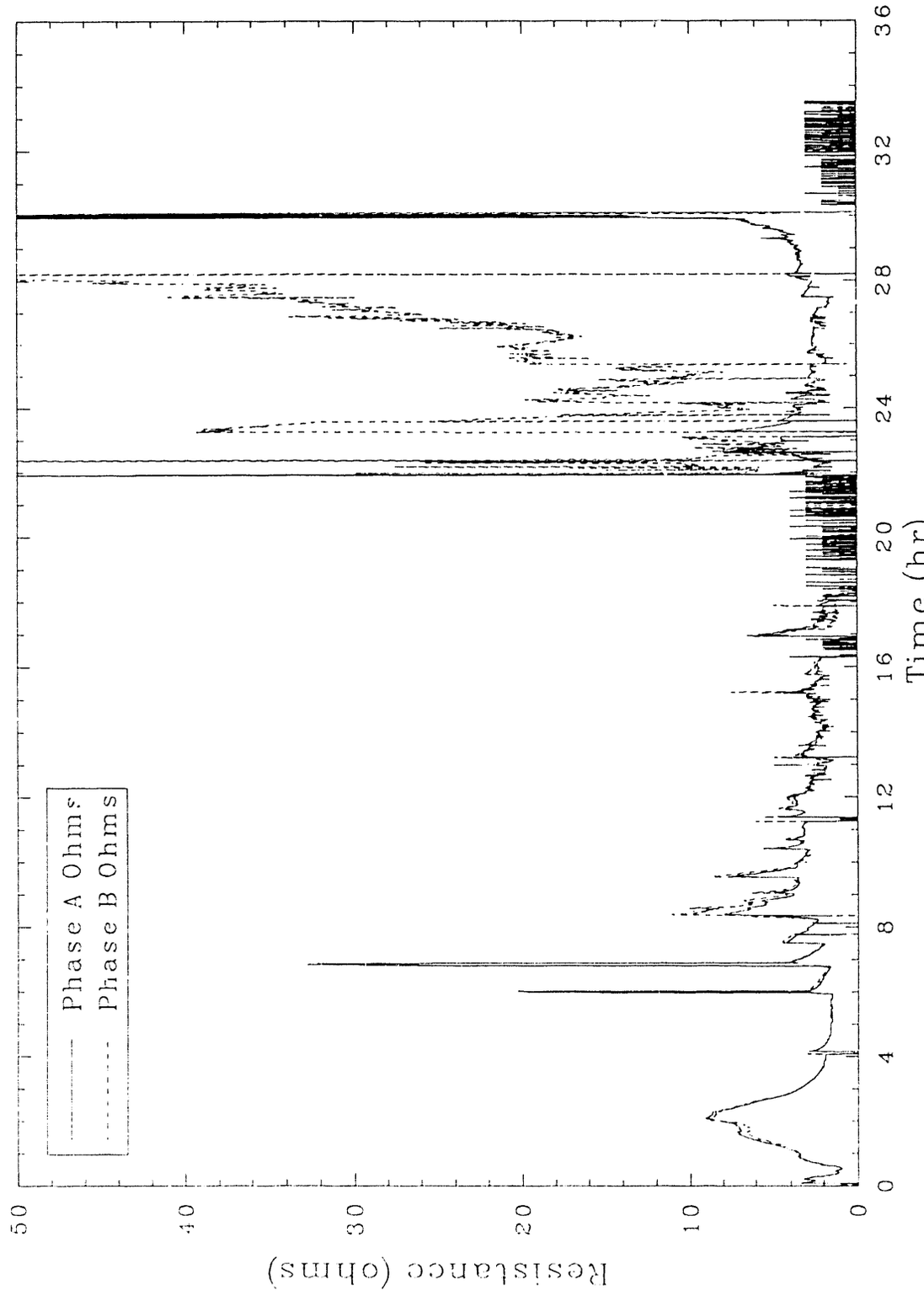

Figure 49. Phases A and B resistance for Test 1.

4. INTERMEDIATE FIELD TEST 2

This section presents information of INEL ISV Intermediate Field Test 2 and includes the specific objectives of the test, construction of the test pit, description and assessment of the data collected during process operations. Product durability data are presented in Section 5. Results of the test tracer study are presented in Section 6. And information from analytical modeling based on off-gassing is presented in Section 7.

4.1 Test 2 Objectives and Test Pit Overview

Test 2 was designed to test the ISV process under two conditions: stacked waste and high metal content waste. Stacked waste presents a potential challenge for the ISV process in that such a region may contain a reduced amount of soil relative to the waste fraction. Additionally, a stacked waste region could challenge the capability of the off-gas processing system if several containers are breached at about the same time.

High metal content waste may result in a challenge to the process because ISV is based on resistance heating, and metal shorting could interfere with this process. Previous testing indicated limitations on allowable metal content; however, this testing was conducted with fixed electrodes. The use of the EFS provides a potential method to allow processing of high metal waste because the electrode can be inserted or retracted from the melt based on changing melt electrical characteristics.

Several aspects of Test Pit 2 design should be noted. First, the particular configuration of the pit (stacked drums located over stacked boxes) does not represent a disposal practice that is known to have been used at the SDA. The test was designed to represent the two situations independently, first the stacked waste and then the high metal waste. Second, the high metal content was represented as a stacked box region in which scrap metal and fill dirt was placed in the boxes. The use of fill dirt in the boxes did not occur

as a disposal practice at the SDA. It is possible that some filling-in of void spaces may have occurred in SDA waste containers as containers deteriorated with time. This is supported by documented occurrences of subsidence (particularly in springtime) of the SDA overburden soil. For the purposes of the ISV Test Pit 2, the soil was added to the boxes to provide sufficient soil so that the effect of high metal content on process performance could be assessed.

4.2 Test Pit 2 Construction Details

Test Pit 2 consisted of approximately 0.9 m (3 ft) of soil underburden, 0.91 m (3 ft) of a stacked box region, 0.6 m (2 ft) of a three layered stacked can region, and 1.2 m (4 ft) of soil overburden. Test Pit 2 was originally constructed with 0.6 m (2 ft) of overburden; however, an additional 0.6 m (2 ft) of soil was added after the completion of Test 1. This additional soil was added to ensure an amount of molten glass was formed prior to encountering the stacked can waste region and be sufficient to maintain conductance between the electrodes. During the placement of the additional overburden, a single instrumented can was placed at an approximate 0.6 m (2 ft) depth. Figure 50 shows a schematic of the contents of Test Pit 2 with the hood in place. The number of cans of each waste type in each of the three can layers is presented in Table 9. Tables 10 and 11 provide summary information on pit waste material contents.

Test Pit 2 was constructed by laying the soil underburden, then placing the stacked boxes into the pit. The stacked cans were then placed and the overburden put on top. The stacked boxes containing scrap metal with added fill dirt were loaded onto pallets and lowered by crane into the pit. Each pallet supported 12 boxes. Figure 51 shows the placement of the stacked boxes into the pit. After the boxes had been placed approximately 2.5 to 5.1 cm (1 to 2 in.) of dirt was placed on top to cover the boxes prior to laying three layers of stacked cans. Figure 52 shows the completed bottom layer of cans. The cans containing the dysprosium oxide tracer were placed near the center of this layer.

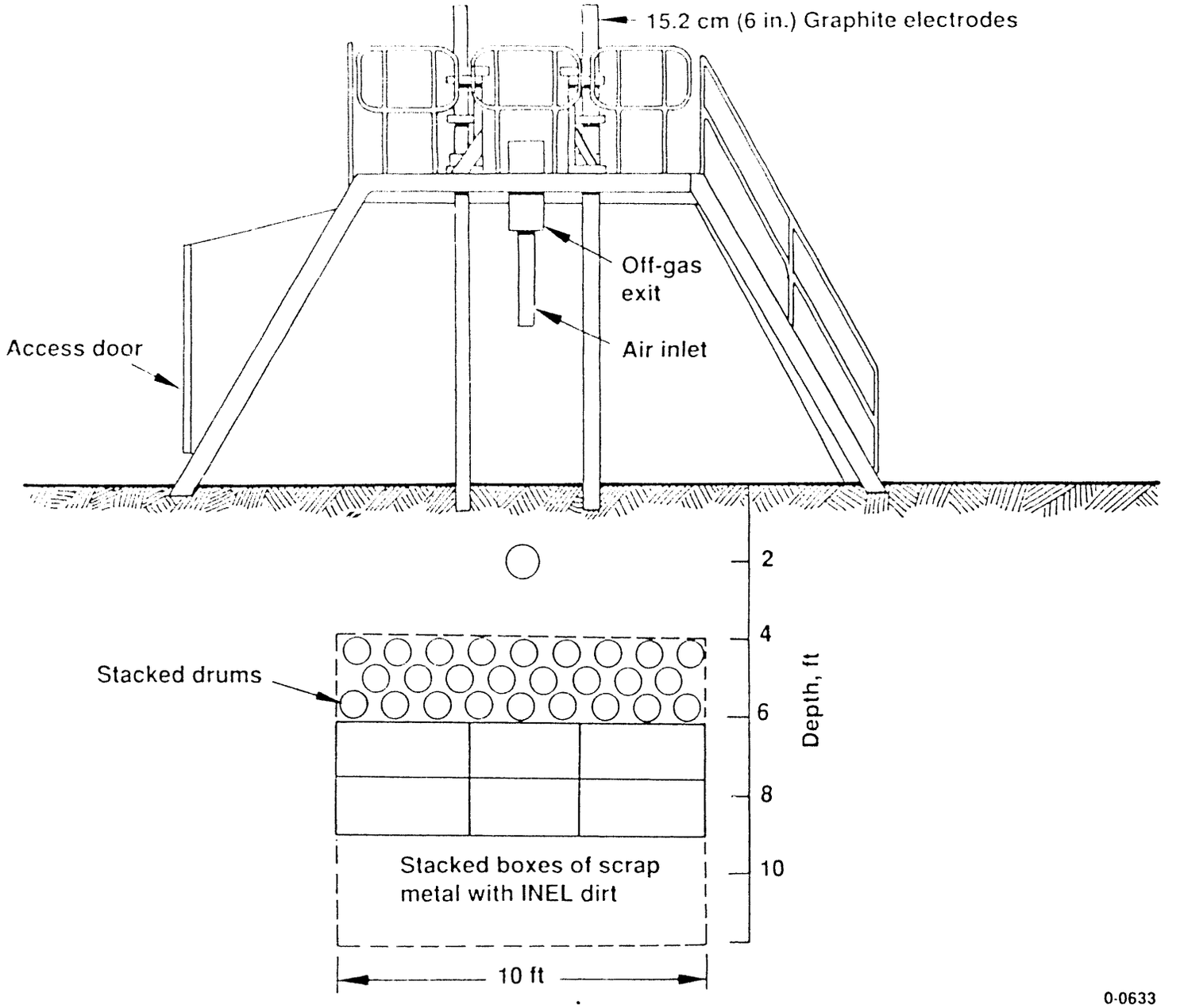

Figure 50. Schematic of Test Pit 2.

Table 9. Depth view of Test Pit 2[a]

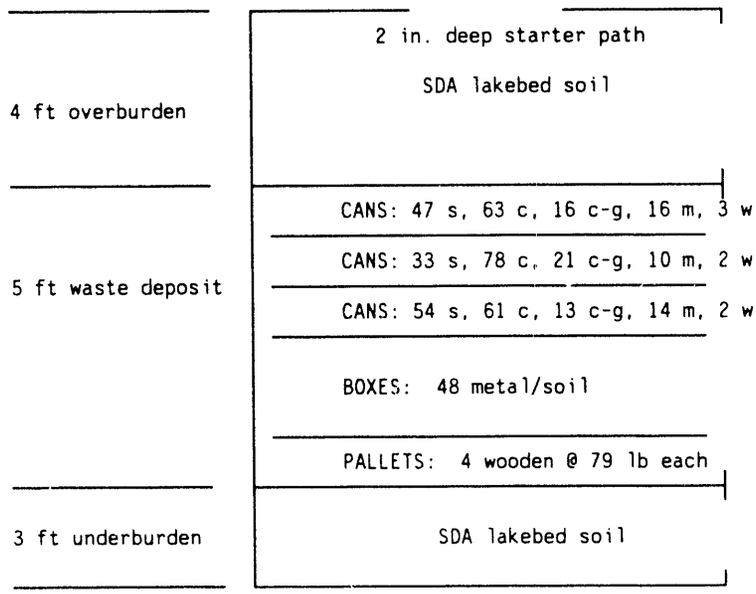

surface area is 10 x 10 ft

Where,
s is sludge cans
c is combustible cans
c-g is concrete/glass cans
m is metal cans
w is wood cans.

These cans contained the following, approximate amounts of material:

Sludge can (s) - 10.72 lb
(7.72 - H2O, 0.70 - FLOOR DRI, 2.307 - MICRO-CEL E)
Combustible can (c) - 3.96 lb (1.901 - Cloth, 2.059 - Paper)
Concrete/glass can (c-g) - 16.73 lb (12.0 - concrete, 4.73 - glass)
Metal can (m) - 6.58 lb (3.29 - carbon steel, 3.29 stainless steel)
Wood can (w) - 3.14 lb
Pallet - 79.0 lb of wood

Boxes contained the following, approximate amounts of material:
Metal/soil - 119.521 lb (50% carbon steel)
244.021 lb soil

a. Engineering Design File, EDF-ISV-034

Table 10. Test Pit 2 waste deposit material composition in pounds[a]

MATERIALS	TOTAL		ITEM WEIGHT	WASTE DEPOSIT LAYERS TOP CAN	MID CAN	BOT CAN	BOXES	PALLETS
COMBUSTIBLES:	1,513.5							
Cans:		813.5						
Paper			411.50	128.24	159.13	124.13		
Cloth			380.00	118.43	146.94	114.63		
Wood			22.00	9.42	6.29	6.29		
Boxes:		700.0						
Cardboard			384.00				384.00	
Pallet (wood)			316.00					316.00
SLUDGE: (cans only)	1,436.5							
Water		1,034.5	1,034.50	362.85	254.77	416.88		
Floor Dri		93.8	93.80	32.90	23.10	37.80		
Micro-Cel		308.2	308.20	108.10	75.90	124.20		
METALS:	6,757.95							
Cans:		1,020.95						
Stainless			131.60	52.64	32.90	46.06		
Carbon Steel			889.35	306.39	284.90	298.06		
Boxes:		5,737.0						
Stainless			2,868.50				2,868.50	
Carbon Steel			2,868.50				2,868.50	
CONCRETE/GLASS:	12,549.50							
Cans:		836.50						
Concrete			600.00	192.00	252.00	156.00		
Glass			236.50	75.68	99.33	61.49		
Boxes:								
Soil		11,713.00	11,713.00				11,713.00	
TOTALS OF COLUMNS	22,257.45		22,257.45	1,386.65	1,335.26	1,385.54	17,834.00	316.00

a. Engineering Design File, EDF-ISV-034

Table 11. Test Pit 2 waste inventory

Material	Mass (lb)	% of Total Mass
Combustible	1514	2.5
Sludge		
Water	1035	1.7
FLOOR-DRI	94	0.2
MICRO-CELL E	308	0.5
Metal	6758	11.2
Glass	237	0.4
Concrete	600	1.0
Soil (excluding underburden)	49,963	82.6
Total	60,509	

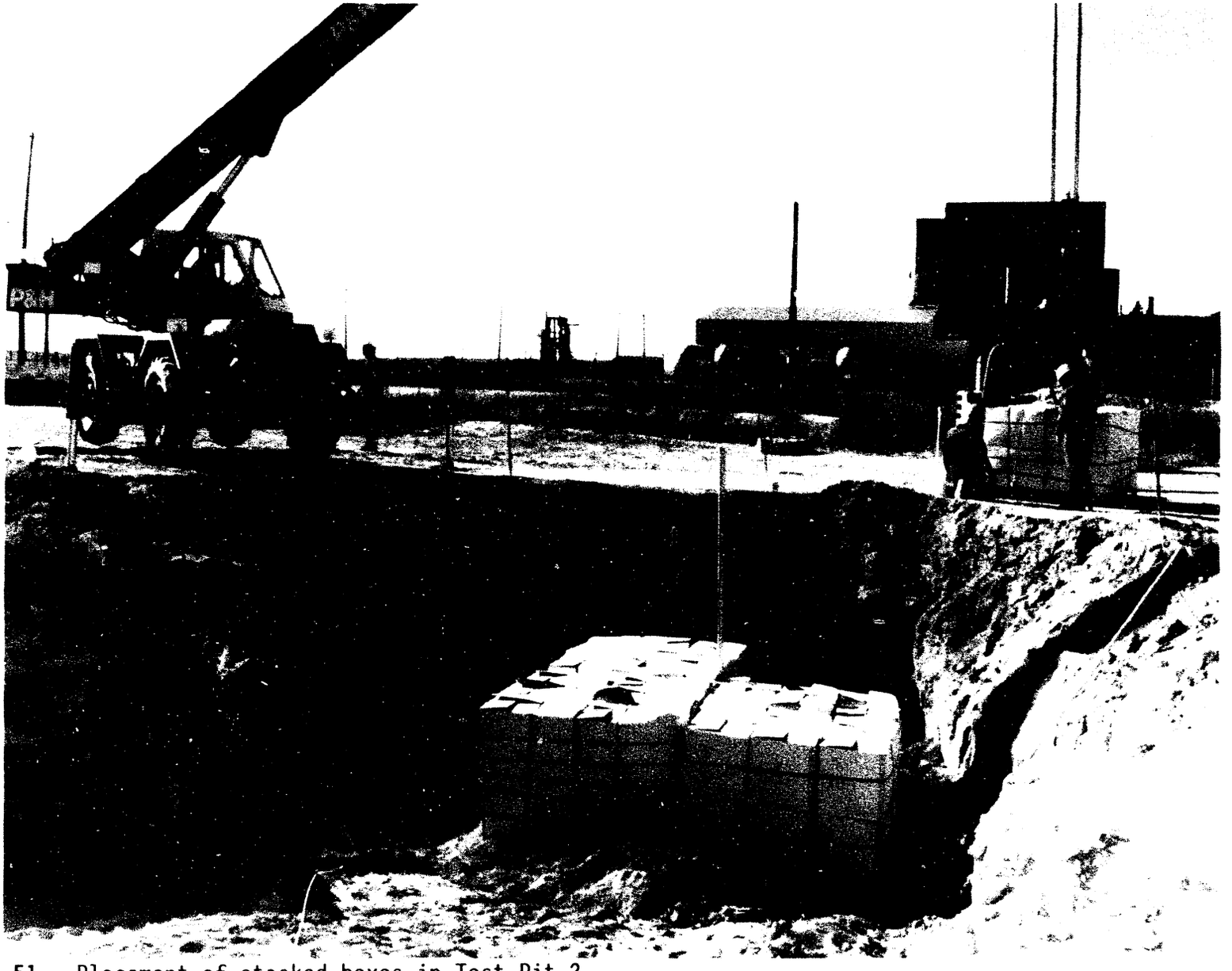

Figure 51. Placement of stacked boxes in Test Pit 2.

Figure 52. Bottom layer of cans in Test Pit 2.

During placement of the can layers, fill dirt was added to fill in the interstitial space between each layer, as shown in Figure 53. This figure also shows the placement of the horizontal array of thermocouples between the bottom and middle layers of cans. The middle layer of cans is shown in Figure 54. The dirt placed between the middle and top layers of cans is shown in Figure 55. Figure 56 shows the top layer of cans, and the final backfill is shown on Figure 57.

As indicated above, an additional 0.6 m (2 ft) of soil overburden was added to Test Pit 2 prior to conducting the second test. A single can containing approximately 1.8 kg (4 lb) of paper was added at the original ground surface layer [approximate 0.6 m (2 ft) depth after the additional overburden was added]. This can was instrumented with a type K thermocouple and a pressure transducer and was placed in order to gather pressure and temperature data from a single representative can during processing.

Two additional arrays of type K thermocouples were placed in Test Pit 2. A vertical array of 16 thermocouples was placed starting at approximately 15 cm (6 in.) from original ground level, with thermocouples spaced every 15 cm (6 in.) apart. After the addition of the extra 0.6 m (2 ft) of soil overburden, the first thermocouple was at approximately 0.76 m (2.5 ft) depth. The horizontal array of nine thermocouples was placed between the second and third layer of stacked cans as measured from the top of the test pit. These thermocouple arrays were placed using the same type of connecting wire as was used in Test Pit 1. However, after the failure of the Test Pit 1 thermocouples, it was decided to replace the connecting wire for the Test Pit 2 arrays. A trench was excavated to the point of connection and the wire replaced.

4.3 Operational Changes for Test 2

Following an evaluation of Test 1, several equipment and operational changes were initiated for Test 2. These changes were designed to gain additional data from the test and to remedy the key operational difficulties identified in Test 1; the changes implemented for the Test 2 are listed below.

Figure 53. Placement of fill dirt between can layers in Test Pit 2.

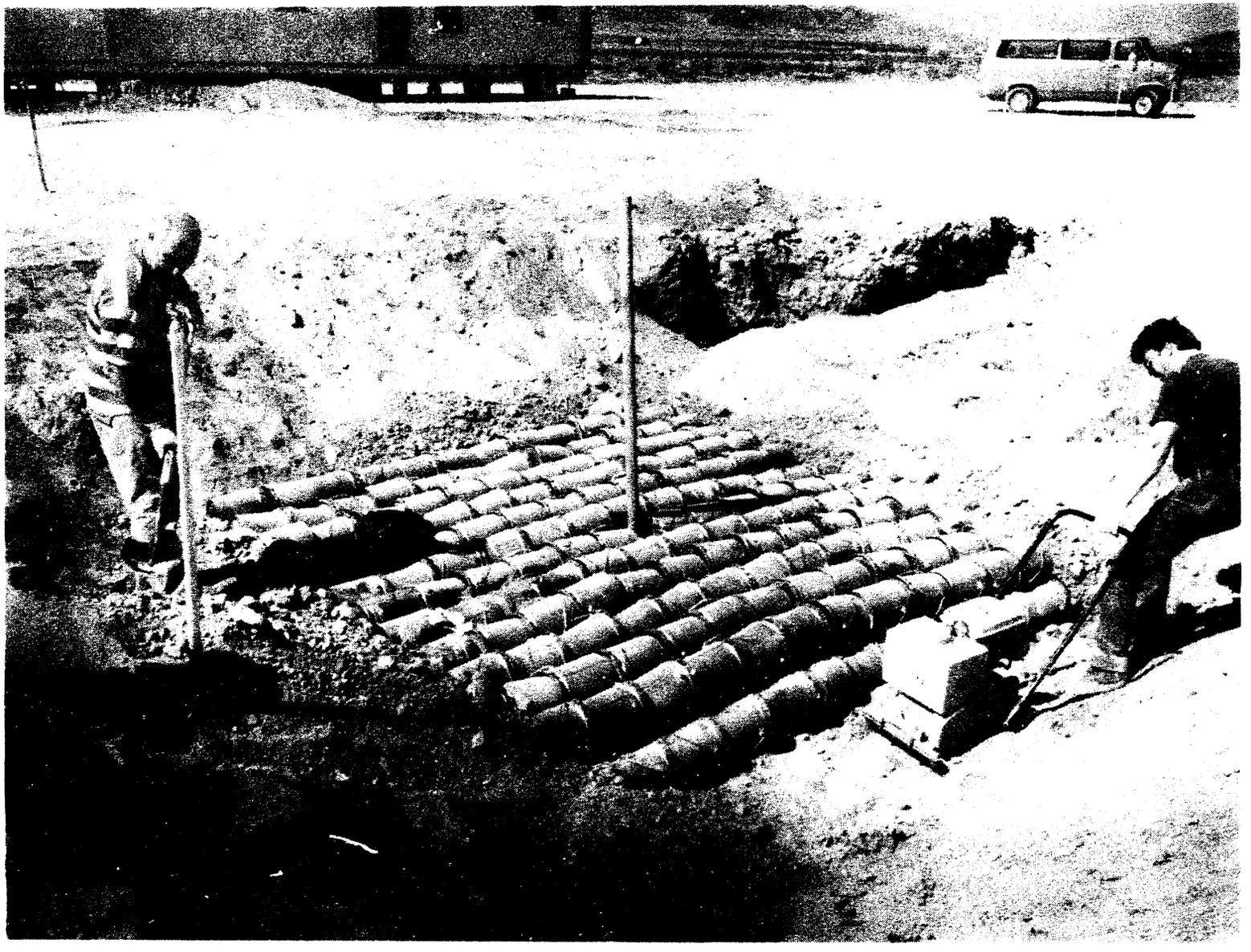

Figure 54. Placement of middle layer of cans in Test Pit 2.

Figure 55. Dirt placed between middle and top layers of cans in Test Pit 2.

Figure 56. Placement of top layer of cans in Test Pit 2

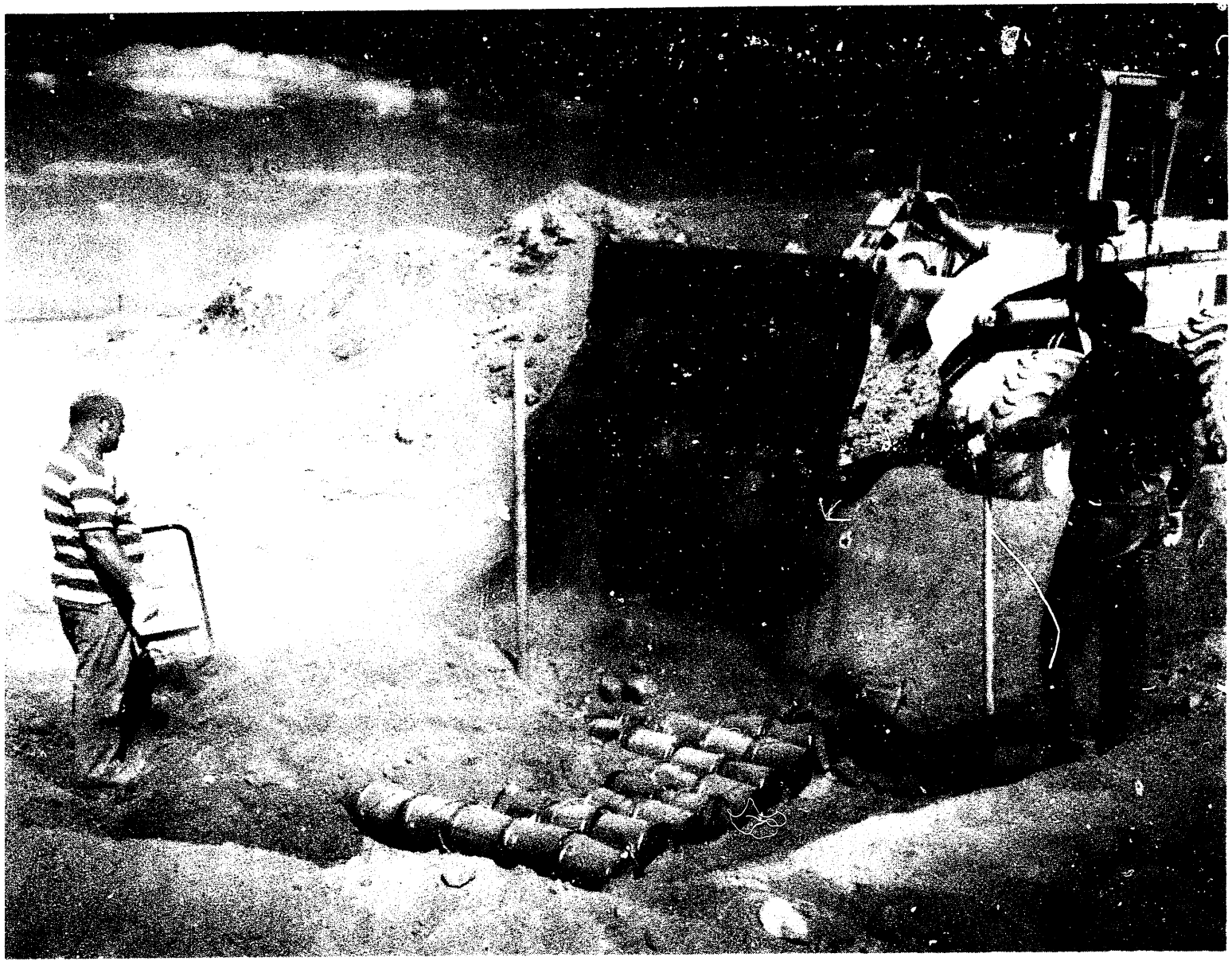

Figure 57. Final backfill for Test Pit 2.

- The electrodes were not coated with the silica-based coating as in Test 1. This change was based on the assumption the electrode coating was the cause of the sticking and allowed determination of the rate of graphite oxidation without such a coating.

- An additional 0.6 m (2 ft) of soil was added above the grade level to provide a total of 1.2 m (4 ft) of overburden above the simulated waste containers. The addition of the overburden was designed to evaluate the effectiveness of overburden in reducing or buffering the effects of the transient gas releases related to vacuum fluctuations.

- An instrumented can identical to that used in Test 1 was installed at the original grade level for an effective burial depth of 0.6 m (2 ft). The can was oriented horizontally (on its side). The can contained 1.8 kg (4 lb) of paper and was instrumented with a pressure transducer and two types of thermocouples. Both thermocouples were inside the can and were located approximately 1 cm from the upper or lower sides. The purpose of the instrumented can was to obtain the temperature and pressure data from the can at the point of gas release and to help define the conditions observed in Test 1.

- The total off-gas flow sensor, the gas sampling port for carbon monoxide and oxygen, and the downstream pressure sensor used to determine the differential pressure for HEPA filter 2 were moved to a point upstream from the blower surge protection inlet. Repositioning the sensor and sampling ports resulted in more accurate measurements due to the surge protection inlet not having a diluting effect.

- Additional instrumentation was added to monitor the incoming three phase power to the transformer to better track imbalances in the transformer. The failed fuses and thyristor switches were on the primary side of the transformer; therefore, the imbalances measured on the secondary side of the transformer were not an adequate measure of the imbalance on the primary side.

- A backup blower was added to the surge pot assembly on the hood so that the magnitude of any hood pressurization would be diminished. The blower was configured to automatically energize itself when the hood pressurized to 1.5 in. of water positive pressure. Although the backup blower could have been configured to energize when the hood vacuum was initially trending toward positive pressure, it was determined that the initial slope of the pressure curve would be best unaltered to allow comparison with Test 1 data.

- Less soil was piled around the base of the hood compared to Test 1. This change was introduced to allow less restriction of off-gas outflow around the base of the hood in the event of a significant hood pressurization as in Test 1. This allowed more air in-leakage during periods of normal operation and resulted in a lower average vacuum in the hood relative to Test 1.

4.4 Test 2 Process Data Description

In Test 2 a stacked can layer was placed above the stacked box region and resulted in a notable difference in operations when compared to Test 1. Test 2 was much less dynamic; there were fewer transient conditions in the hood. Electrical imbalances did occur when melting through the stacked can region; however, an improved understanding of this phenomenon, combined with uncoated electrodes, resulted in smoother electrical operations.

Test 2 was initiated at 1540 hours on July 11, 1990. Power to the electrodes was initially brought up to 10 kW, in accordance with the planned graduated power buildup. Over the next 8 hours, power was gradually increased to approximately 400 kW, as shown in Figure 58. Resistance followed the expected curve, peaking at 14 and 13.8 ohms for phases A and B respectively, as shown in Figure 59. This resistance plot shows the gradual transition of

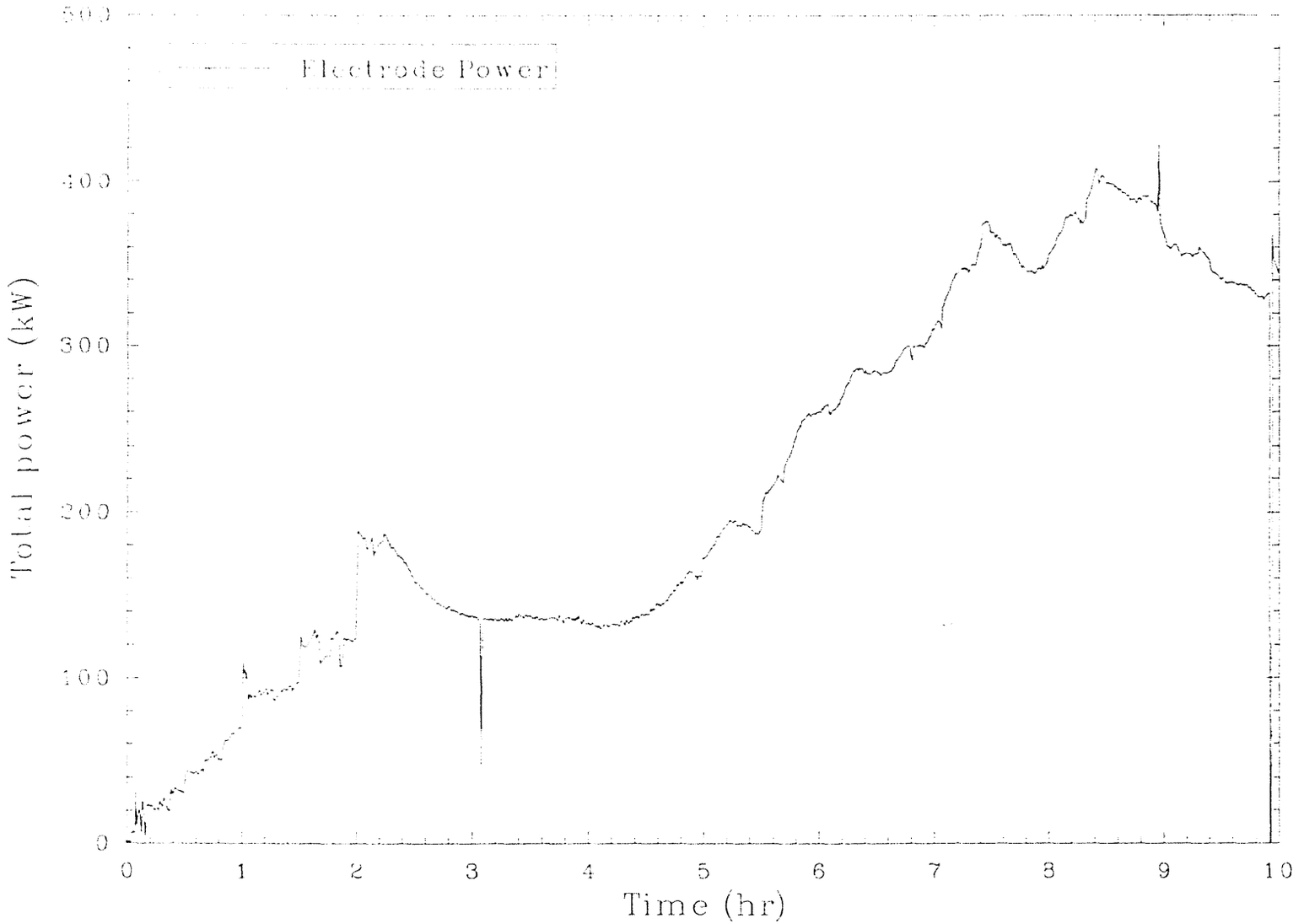

Figure 58. Total electrode power showing gradual increase during startup for Test 2.

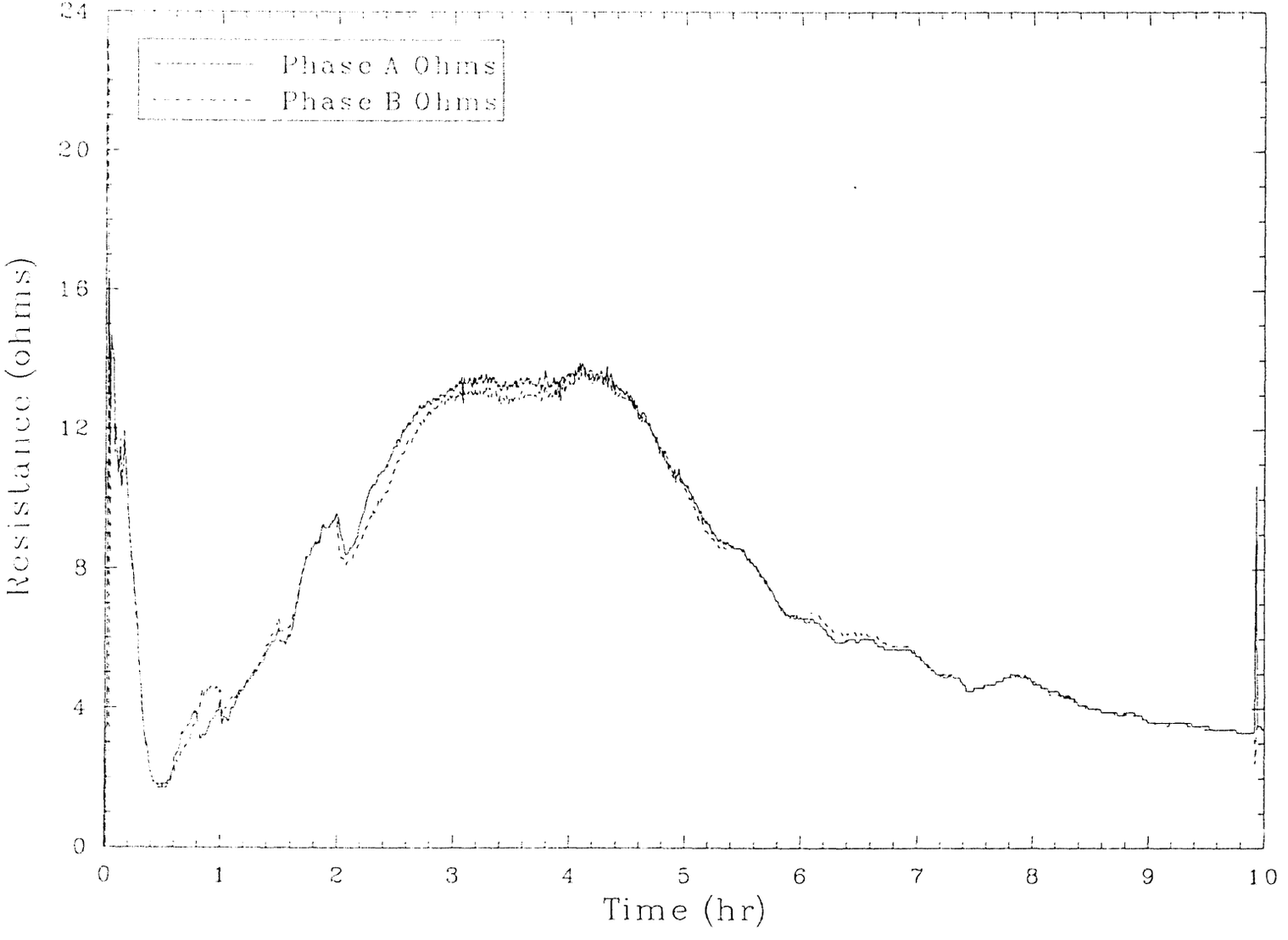

Figure 59. Phases A and B resistance during startup for Test 2.

the current path from the starter path to the adjacent molten soil as the path was consumed. At the peak of the resistance, the starter path was totally consumed, and the current pathway existed through the molten soil. The resistance gradually decreased as the molten soil mass increased in depth.

The test duration was 69.5 hours. The total power applied to the melt was 21,300 kWh. The average plenum temperature in the hood was approximately 300°C, although there were two periods of operation above 400°C. The achieved melt depth was 3.9 m (129 in.) as measured in the center of the melt using a steel pipe. The average melt rate was 1.8 in./h. Figure 60 shows melt depth as a function of time. Electrical imbalances encountered in melting through the stacked can region resulted in decreasing the overall melt rate. A summary of the test events is provided in Table 12.

Overall, there were three distinct phases during Test 2 that were well-suited to analyses. Test 2 will be analyzed according to each of the distinct phases, rather than through the analysis of the individual events as was done for Test 1. The three distinct phases involved the following items.

- The instrumented can at the 0.6 m (2 ft) depth
- The layer of stacked cans
- The layer of stacked boxes.

In addition to the analyses of the three test phases, equipment performance including the hood, electrodes, and off-gas treatment system was analyzed in a manner similar to Test 1.

4.4.1 Instrumented Can

The instrumented can, identical to that used in Test 1, was installed at the original grade level for an effective burial depth of 0.6 m (2 ft). The can was oriented horizontally (on its side). The can contained 1.8 kg (4 lb)

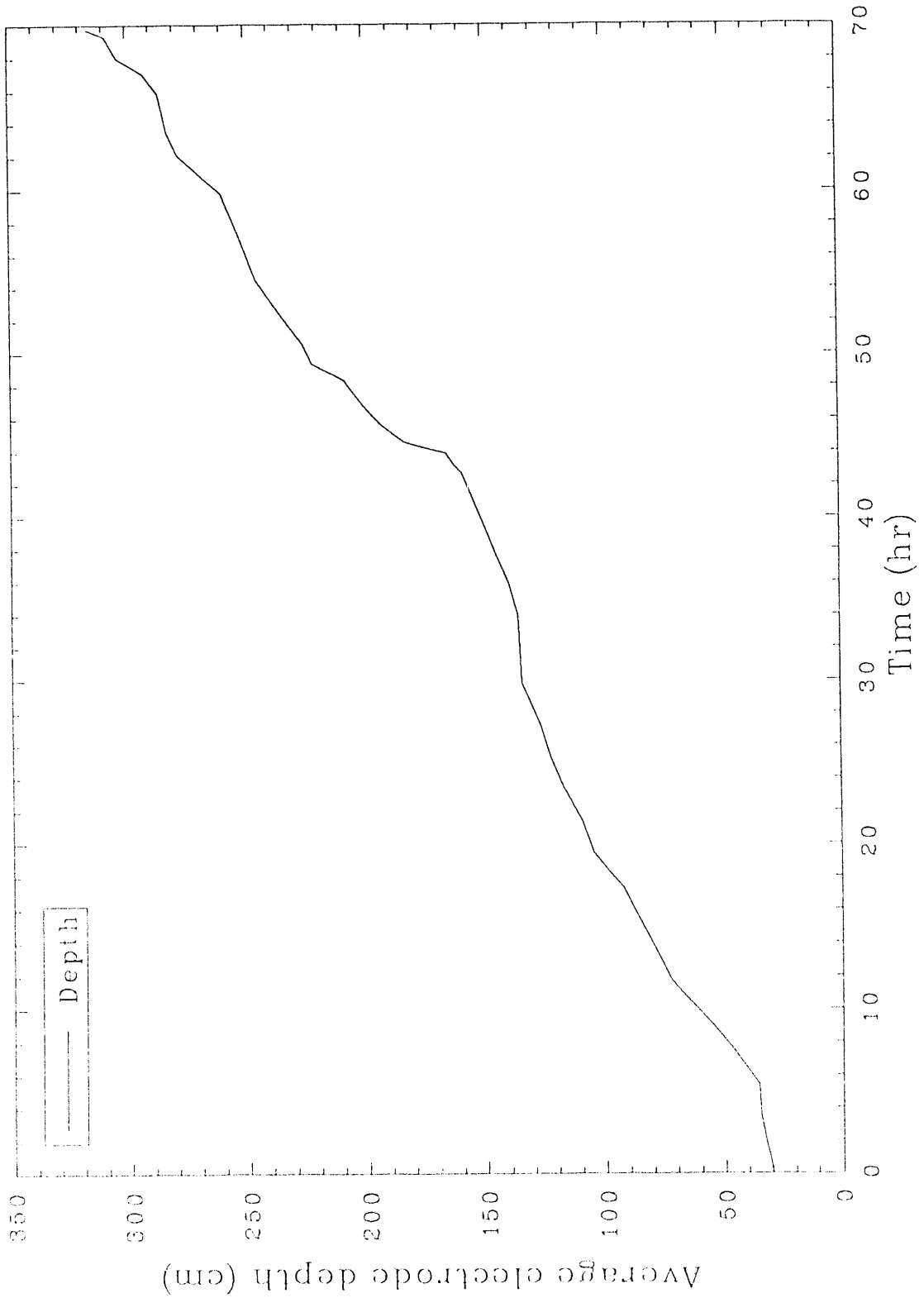

Figure 60. Average electrode depth for Test 2.

Table 12. Test 2 - summary of events

Date	Time	Elapsed Time (hour)	Event
7/11/90	1540	0.0	Power to the electrodes.
	1932	3.70	Melt observation indicates entire surface is molten.
	2314	7.57	Melt observation indicates active surface, about 15 cm (6 in.) of subsidence.
	0100	9.33	Average electrode depth 23 in.
7/12/90	0150	10.16	Hood pressurization event to approximately 2.9 in. of water. Instrumented can temperatures were less than 100°C prior to event.
	0324	11.73	Average electrode depth 29 in.
	0410	12.50	Several tap changes between the 1000 V and 650 V taps between 0235 and 410 hours.
	0627	14.78	Power temporarily off to fix loose air hose. At ~16 hours can region begins to be thermally influenced by the melt.
	0900	17.33	Average electrode depth 37 in.
	1357	24.28	Power off for 10 min due to transformer thermal trip. Power reduced slightly.
	1655	25.25	Average electrode depth 48 in.
	1749	26.15	Transformer thermal trip.
	1808	26.47	Power restored to electrodes.
	2030	28.83	Hissing sound from within hood. Flare, estimated 91 - 107 cm (36-42 in.), observed.
	2153	30.22	Tap change from 650 V to 430 V. Some fluctuations in amperage subsequently observed. Power was therefore reduced somewhat.

Table 12. (continued)

Date	Time	Elapsed Time (hour)	Event
	2315	31.58	Two saturable core reactor fuses blown. Power off.
	2345	32.08	Power back on. Power is controlled up and down over the next 15-20 min during attempts to establish an electrical balance.
7/13/90	0050	33.17	Power balance recovery noted. Phase A = 62.4 kW; phase B = 87.6 kW.
	0140	34.00	Average electrode depth 54 in.
	0150	34.17	Tap change from 650 V to 430 V.
	0345	36.08	Two transformer saturable core reactor fuses blown.
	0705	39.42	Average electrode depth 48 in.
	0840	41.00	Three pops were heard coming from within the hood. Off-gas temperature rises to 300°C. Dust observed rising from around base of hood.
	0945	42.08	A single pop heard from within the hood. Hood pressure increases to +1.9 in. of water and backup blower started momentarily.
	1233	44.88	Breaker trip.
	1240	45.00	Power back on.
	1300	45.33	Melt front at the beginning of the stacked box region. Electrodes average depth is 191 cm (75 in.).
	1540	48.00	Breaker trip.
	1545	48.08	Power back on.
	1700	49.33	Average electrode depth 88 in.
	1900	51.33	Melt observation indicates estimated 1.5 m (5 ft) subsidence.

Table 12. (continued)

Date	Time	Elapsed Time (hour)	Event
7/14/90	0552	62.2	All electrodes at approximate equal depth 2.7-2.8 m (9.0 to 9.3 ft). Power balanced.
	0601	62.35	Power off momentarily to drop electrodes.
	1010	66.50	Stack CO observed to be up slightly; assumed due to wooden pallets at bottom of boxes burning.
	1140	68.00	Average electrode depth 120 in.
	1200	68.20	Power off momentarily to drop electrodes.
	1309	69.48	Power off - test completed.
	1552	72.20	Data Acquisition System turned off.

of paper and was instrumented with a pressure transducer and two Type K thermocouples. Both thermocouples were inside the can and located approximately 1 cm from the upper or lower side surfaces of the can.

At approximately 8.5 hours, the melt started to thermally influence the can. At 8.9 hours, the can reached a maximum pressure of 4.5 psig with the upper thermocouple at 94°C and the lower thermocouple at 88°C (see Figure 61). At approximately 10.2 hours, an apparent gas release from the can caused the hood plenum temperature to spike to approximately 630°C (see Figure 62) and the hood to pressurize to 2.9 in. W.C. (see Figure 63). Immediately after the hood pressurization, an operator noted that the interior surfaces in the hood were covered with what appeared to be soil. A review of the pressure and temperature measurements of the can (see Figure 61) revealed that the can had not depressurized and was maintaining an internal pressure of 4 psig at 94°C for the upper thermocouple. Immediately after the event, the internal can temperature climbed steadily to just over 100°C. Since the can pressure was relatively steady, the temperature increase in the can is suspected to be due

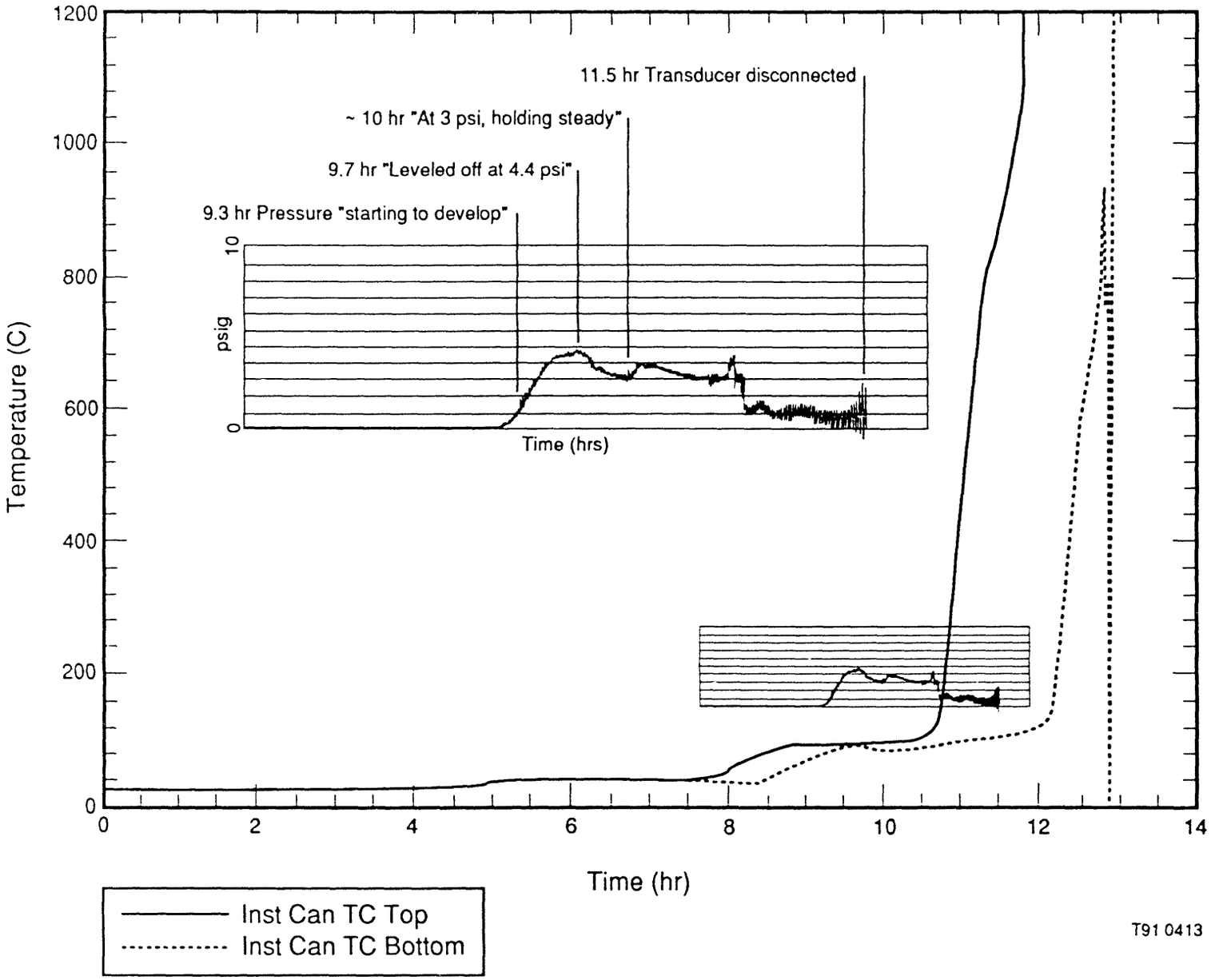

Figure 61. Instrumented can temperatures and can pressure for Test 2.

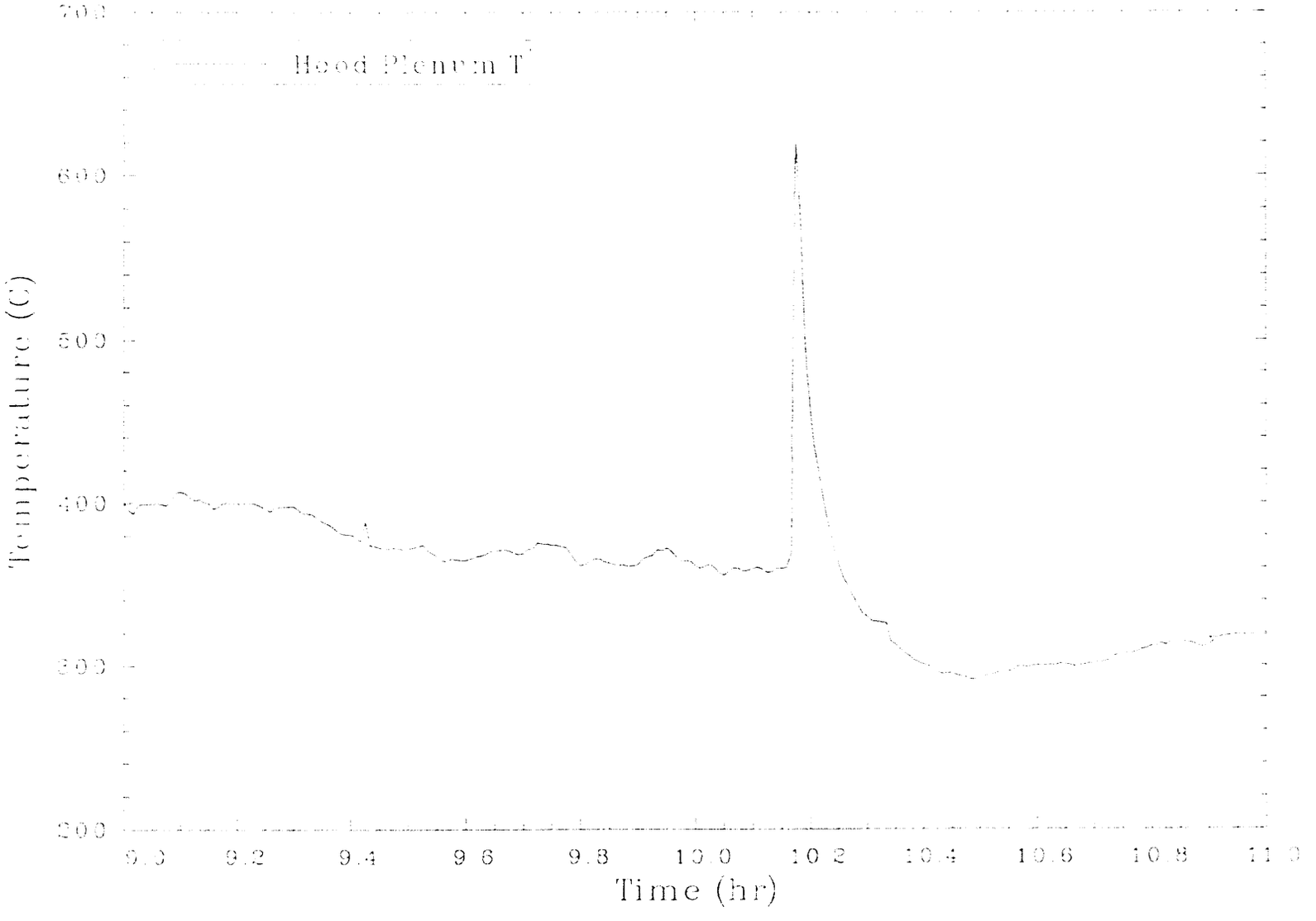

Figure 62. Hood plenum temperatures during processing of the instrumented can for Test 2.

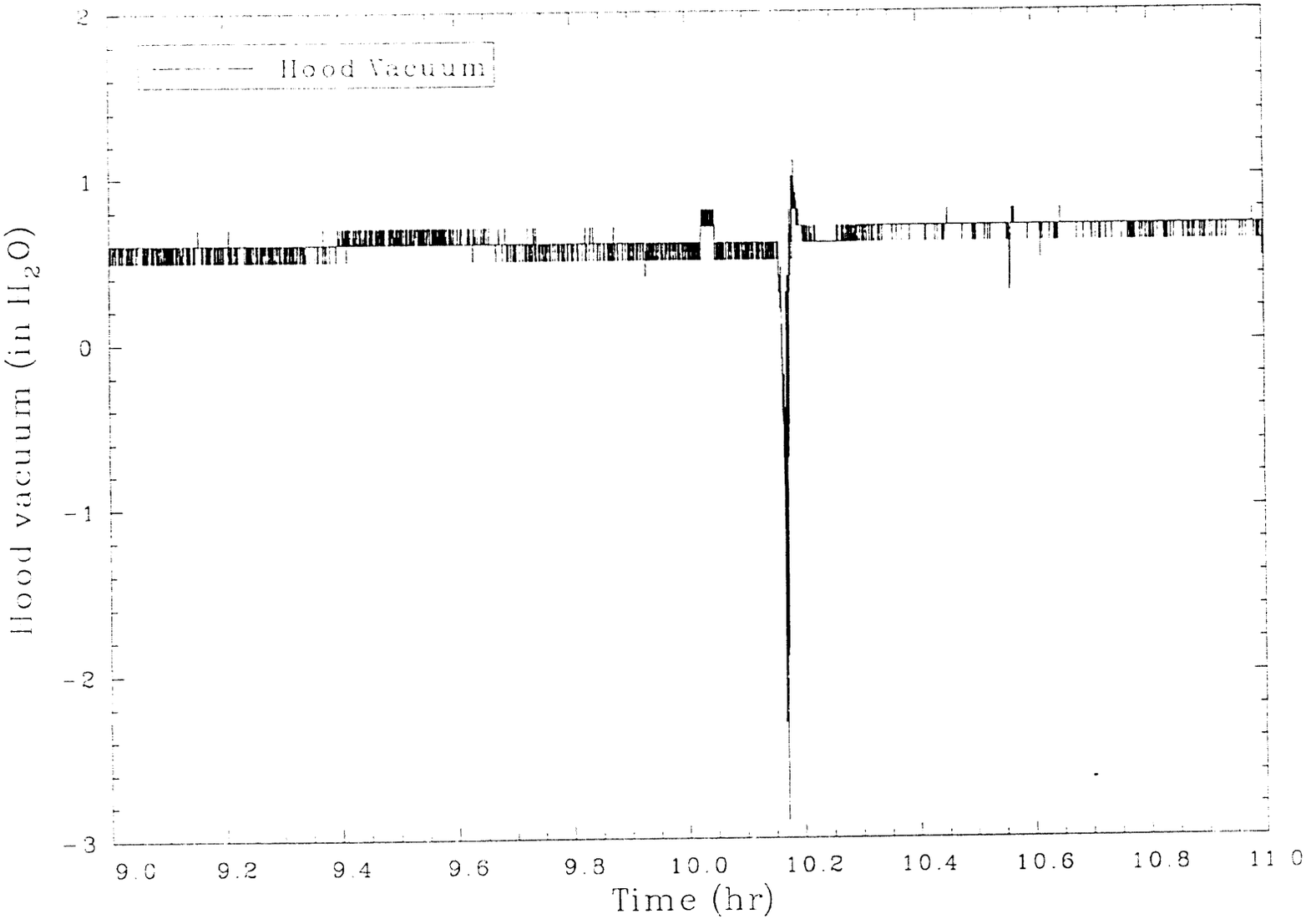

Figure 63. Hood vacuum during processing of the instrumented can for Test 2.

to an increased rate of heating of the adjacent soil once the water vapor in the adjacent soil was released.

Since the can did not appear to be responsible for the hood pressurization, the gas release must have been initiated by water vapor from the soil column. It is possible that sudden gas releases can occur from the soil column if the rate of gas or vapor generation exceed the capability of the soil column to dissipate the gas. This condition is dependent upon the gas generation rate (a function of the melt rate and soil moisture), the permeability of the soil column, and the pressure required to release gas through the melt. Gas can release through the melt if the pressure beneath the melt exceeds the sum of the head pressure of the melt and the additional pressure increment required to force gas through the less permeable sintered layer (the incremental zone of soil undergoing the fusing melting process). If pressures are not sufficient to overcome the glass head and to breach the sintered layer, it is likely that the gas will release through the adjacent soil column.

In this event, it is suspected the vapor was released through the melt and, in doing so, entrained a considerable amount of soil. With no heat of combustion, the increased heat measured in the hood must have been due to the addition of superheated water vapor mixing with the gas originally present at nominal conditions with additional radiant heat contribution to the hood shell, thermocouples, and suspended particulate (soil) once the cold cap was disrupted. Since the entire inner surface of the hood and electrodes were covered with soil, it is suspected that extremely heavy loadings of particulate were present in the hood plenum. The temperatures in the hood spiked from 360 to 630°C (270°C increase). The temperature measured at the inlet to the venturi-ejector which would provide a true gas temperature unbiased by thermal radiation inside the hood spiked from 280 to 420°C (140°C increase). A gas release adjacent to the melt would not likely super-heat the gas to this extent; therefore, it is probable that the gas passed through the melt. Additionally, a gas release adjacent to the melt would not likely disrupt the cold cap exposing the significant thermal radiation source of the melt.

Phases A and B resistance values both increased slightly during the event at 10.2 hours, indicating the likelihood that gas had indeed passed through the melt, increasing its electrical resistance. The increased resistance diminished over approximately 12 minutes. The increased resistance was likely due to a cooling action of the melt by the gas, the disruption of the insulating cold cap, and the introduction of some of the entrained soil. Figure 64 shows a plot of A and B phase resistance as a function of time. The total power lost as a result of the event equaled 60 kW.

At approximately 11 hours, the temperatures in the can began to increase dramatically as shown in Figure 61. The can pressure wavered around 4.1 psig before the can suddenly depressurized, causing the hood vacuum to decline from approximately 0.8 to 0.25 in. W.C. At this point, the temperature in the hood increased gradually from approximately 300 to 380°C over a 15 minute period. The internal can temperatures at the time of the release were approximately 510°C for the upper thermocouple and only 98°C for the lower thermocouple. Since the can had a rubber gasket, it is suspected that the release mechanism was a temperature-induced failure of the rubber gasket rather than a structural failure of the metallic sidewall. It is evident that the can was adequately sealed since the pressures in the can were maintained between 4 and 5 psig for several hours prior to the release. If the can was not sealed, it is probable that any water vapor and heated air would have gradually been released over several hours prior to the hood pressurization. The majority of the time the can was at pressure, the temperature in the can was insufficient to produce any other gases, such as decomposition gases, from the pyrolysis of paper.

Later, at 14 hours, the plenum temperature increased again approximately 50°C over a 15 minute period. It is unknown if the can still contained some residual paper that was further pyrolyzed and released at this point since the initial breach of the can occurred 2 hours earlier. Additionally, the collection of pressure data from the can was discontinued shortly after the

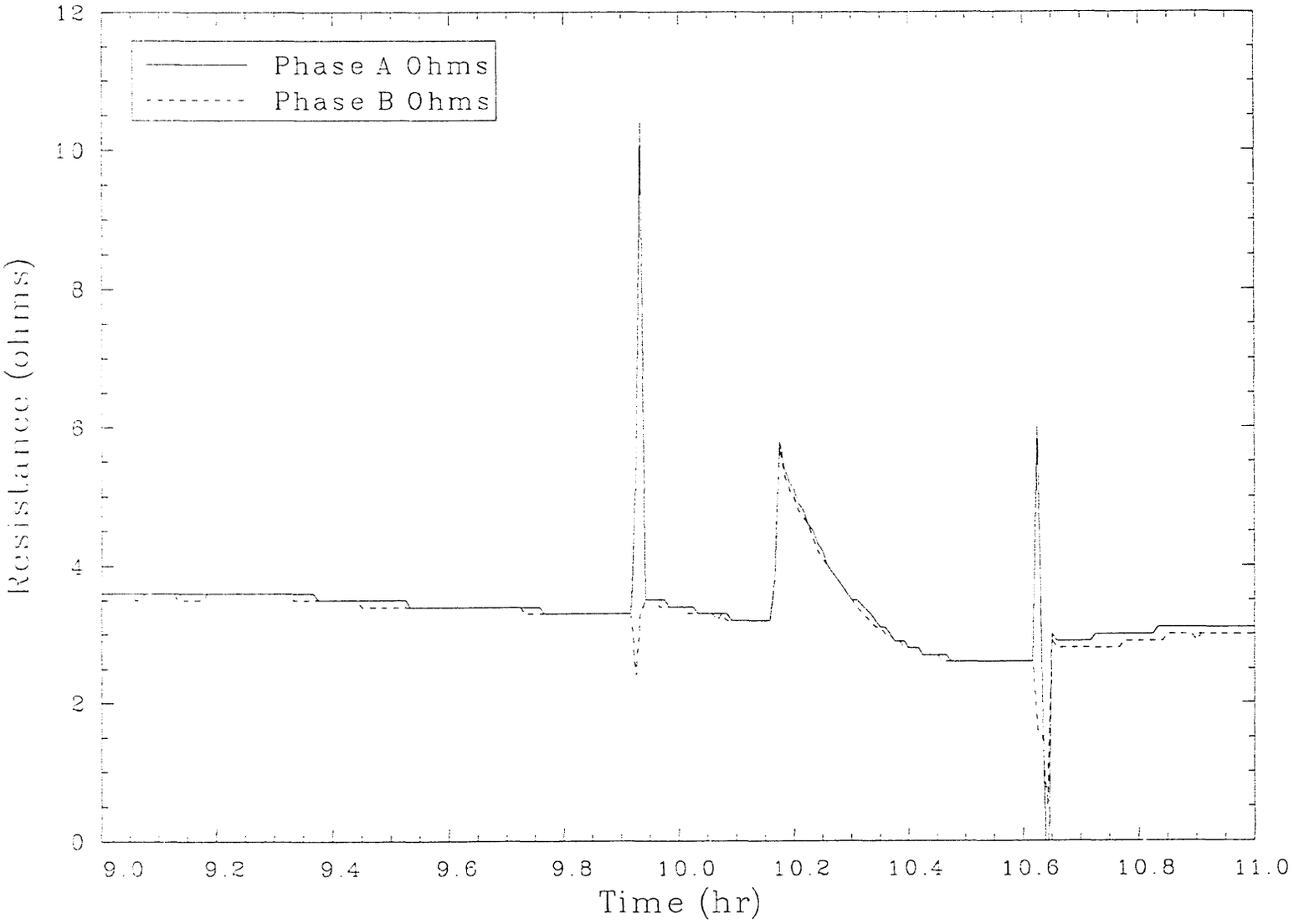

Figure 64. Phases A and B resistance during processing of the instrumented can in Test 2.

initial breach since the readings were erratic, indicating transducer failure. It is possible that paper remnants were still present in the can and the can had not fully filled with glass upon initial breach. Previous studies involving sealed containers have shown that glass may flow into cans and temporarily freeze until thermal momentum reetablishes flow to fill the remainder of the can.[8] This explanation would support the increased hood temperatures over the 15 minute period since there were no other known sources of heat generating materials in the vicinity of the melt front. This event did not appear to affect the hood vacuum as the vacuum was relatively steady at 0.8 in. W.C.

It is unknown what created the slight vacuum spike, at 14.5 hours, from 0.8 to 0.25 in. W.C. There was no significant fluctuation in the hood temperature that correlated to the event; however, it is possible that this event was associated with a concluding release from the can.

4.4.2 Stacked Can Region

The stacked can region resulted in a slowdown of the downward melting rate and fewer pressure spikes in the hood than experienced in Test 1. The can region appeared to act as a heat sink causing the downward melt progression to slow dramatically, as shown in Figure 65. For approximately 14 hours, the melt front remained at the same depth until all thermocouples in the stacked can region indicated a temperature of at least 100°C. The melt depth, as measured by the depth of the electrode inserted into the melt, did not progress into the can region until the entire can region reached 100°C. A positive consequence of this situation is that most, if not all, water in any of the sludge cans vaporized and escaped from the cans into the surrounding soil well ahead of the approaching melt front. Additionally, the cans released any pressure generated, due to the simple heat expansion of air, well ahead of the approaching melt front. These factors, combined with the additional 0.6 m (2 ft) of soil overburden, effectively prevented the dramatic pressure spikes that were characteristic of Test 1.

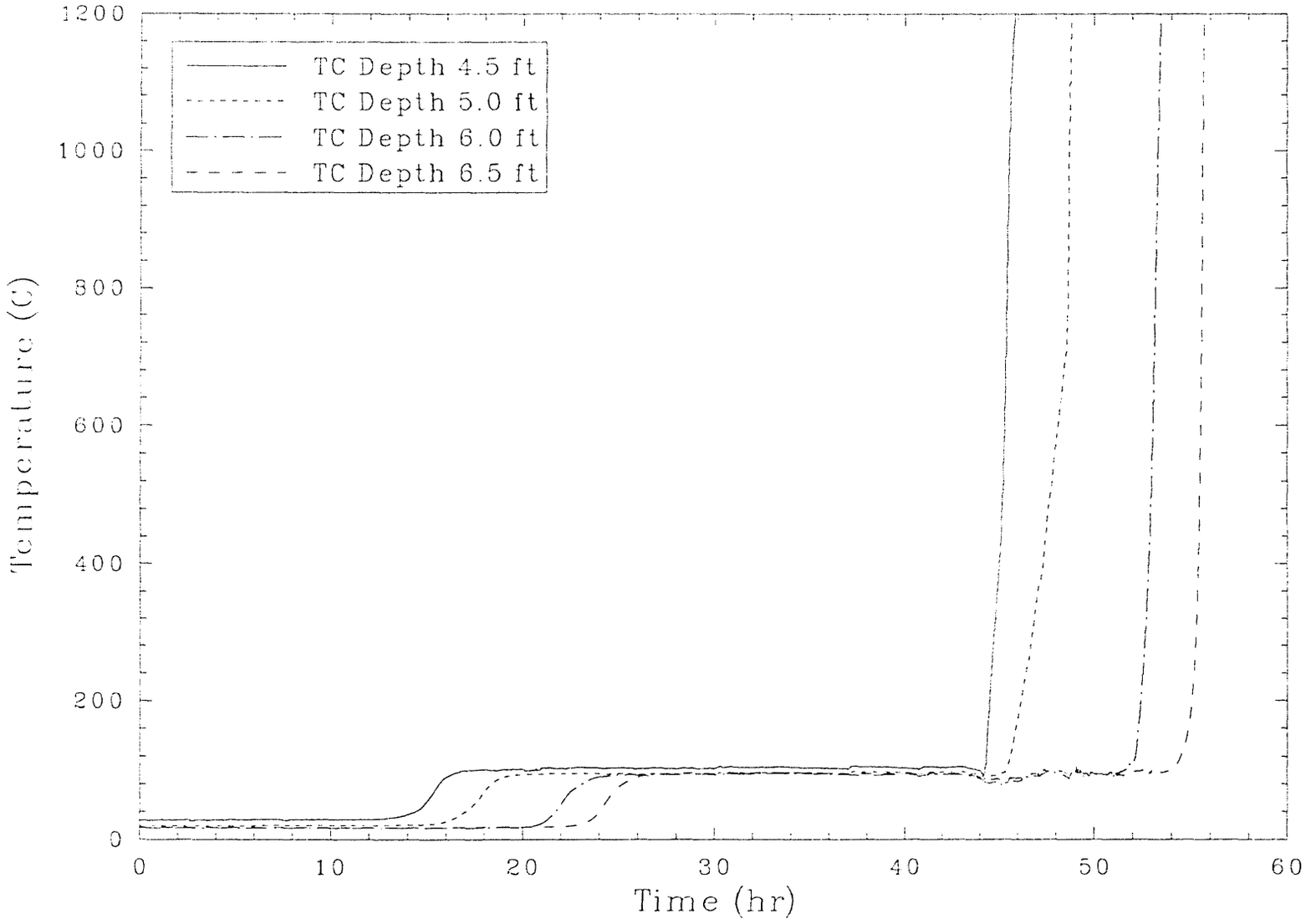

Figure 65. Thermocouple temperatures in the stacked can region for Test 2.

As the melt progressed into the can region, power imbalances hampered operations of the transformer. The positive aspect of the situation was that the electrodes were free to be adjusted to compensate and control the electrical imbalances. At several points during the processing of this region, electrode power was significantly reduced or turned off during attempts to adjust the position of the electrodes and to regain a power balance between phases A and B. Based on current large-scale transformer designs utilizing independent secondary control, the imbalances could have been more effectively controlled with secondary control and adjustment of the electrode positions. Because it has a single controller for both secondary phases, the intermediate-scale system design limits the operator's control options to electrode movement. Figure 66 illustrates the power disruptions associated with this region. From approximately 20 to 40 hours, total power levels averaged less than 200 kW as compared to an overall test average of 300 kW. Figures 67 and 68 illustrate the imbalances between the secondary phases, with Figure 67 plotting phases A and B voltage and Figure 68 plotting amperes for both phases. At 31.5 hours and again at 32 hours into the test, the most significant imbalances measured on the primary side of the transformer were observed. These are listed in Table 13. A general operating guideline is to maintain balance on the primary side within 20%. At greater imbalances for periods exceeding 20 to 30 minutes, the saturable core reactor fuses tend to fail due to excessive heat. This type of fuse failure is precisely what occurred at 31.6 hours. Two of six saturable core reactor fuses failed due to the 25 to 33% (100 A) imbalance in the transformer. A large-scale transformer designed with independent control of the secondary phases would be capable of accommodating these imbalances without significant difficulty.

There are several causes for the imbalances.

- As the melt contacted and melted through the can region, cans randomly failed and were filled with glass. This continuing process resulted in the bottom surface of the melt to be irregularly shaped, resulting in partially melted containers that disrupted the current pathway between the opposing electrodes.

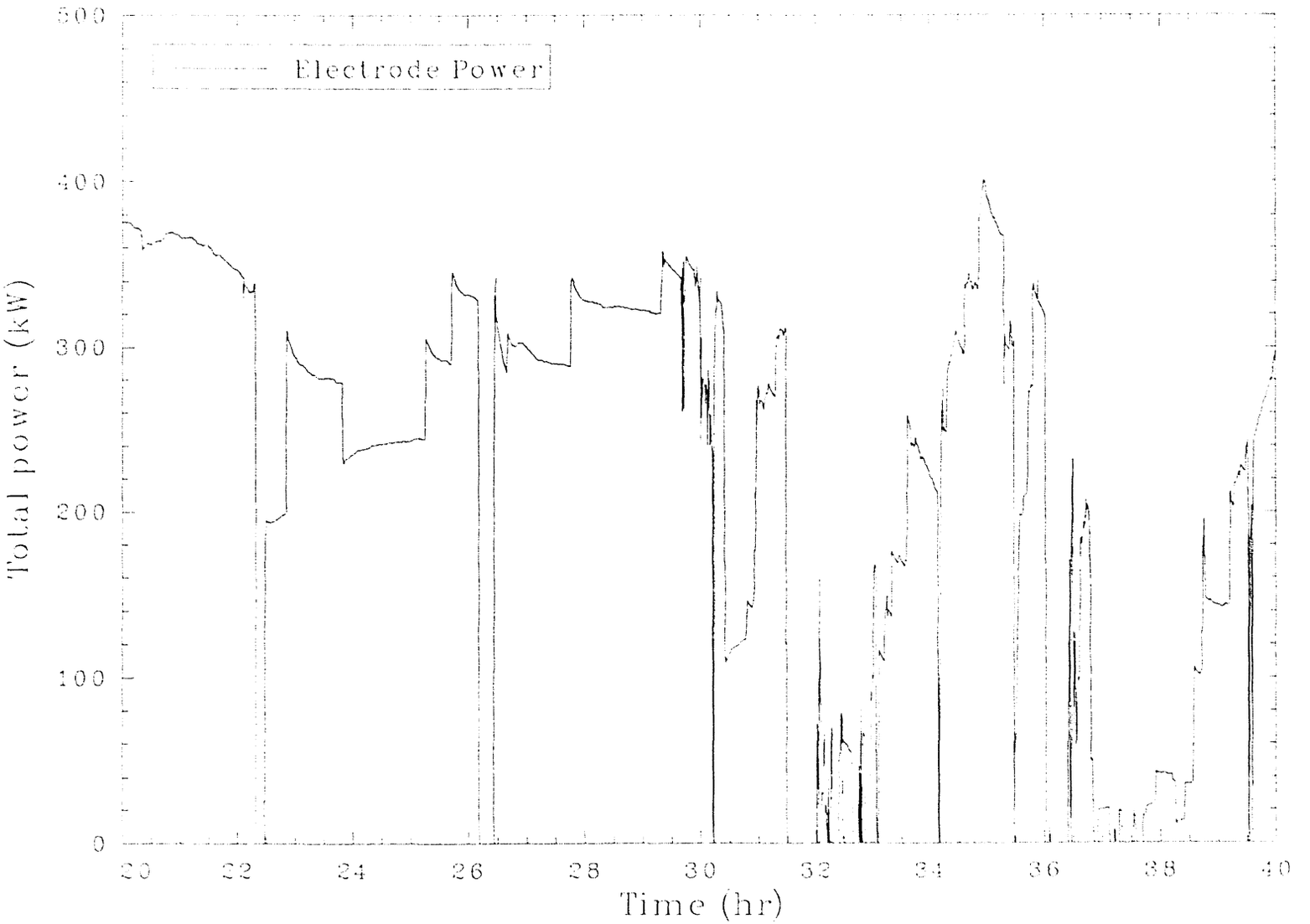

Figure 66. Total electrode power during processing of the stacked can region on Test 2.

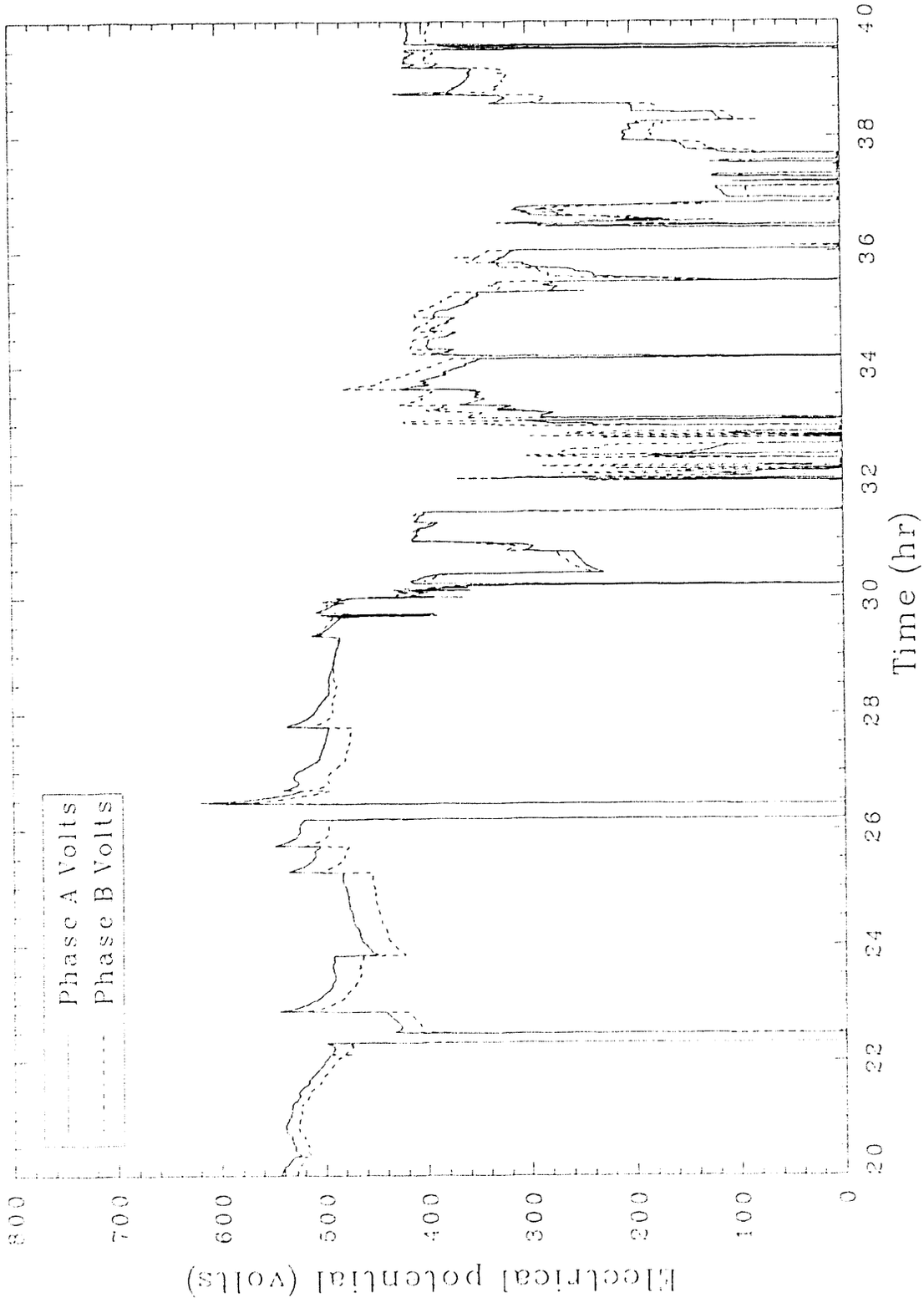

Figure 67. Phases A and B voltage during processing of the stacked can region for Test 2.

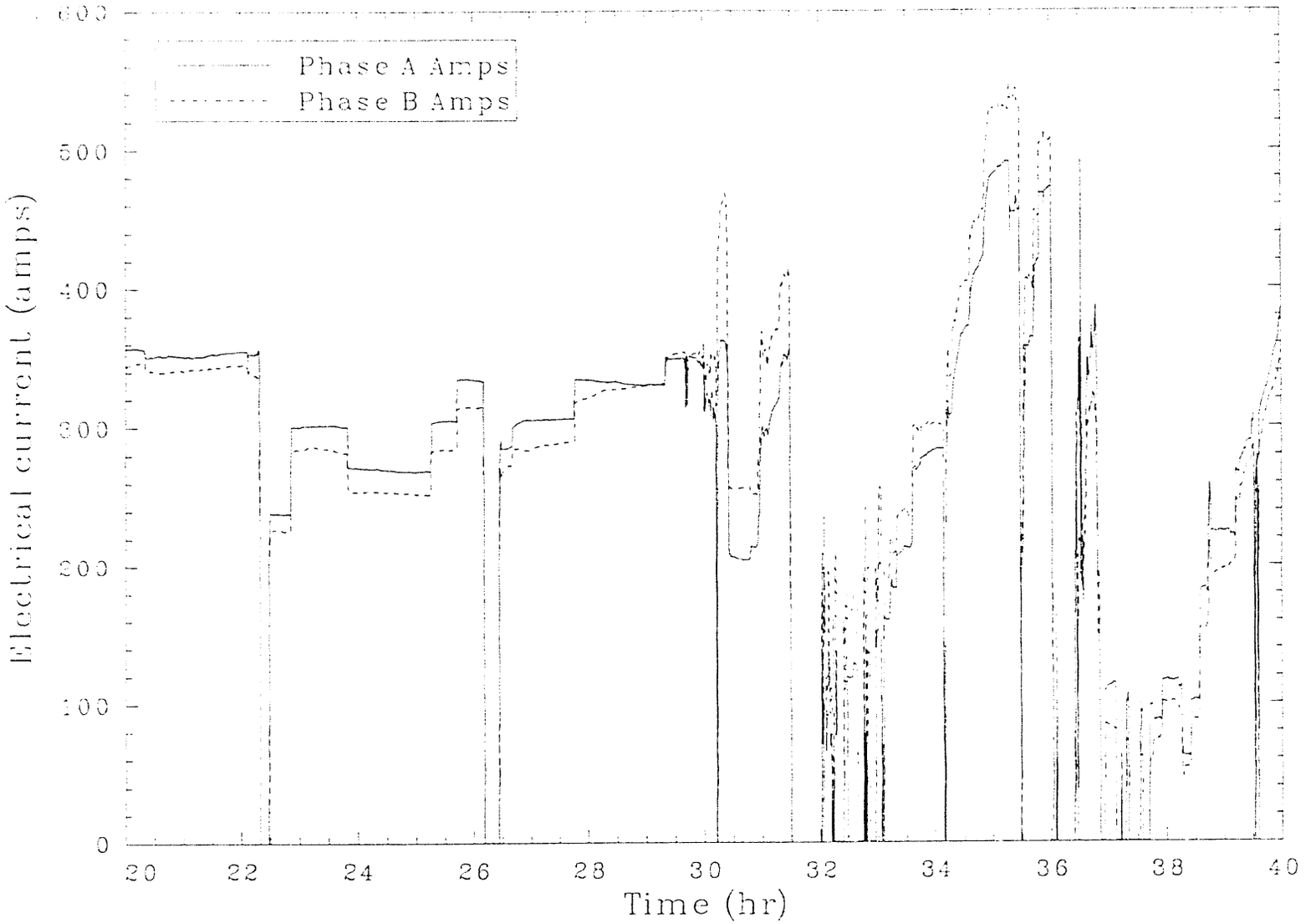

Figure 68. Phases A and B amperage during processing of the stacked can region for Test 2.

Table 13. Primary amperage

Run Time (hours)	A Phase	B Phase	C Phase
31.5	285	196	291
32.0	385	295	392

- As a result of Test 1 operations and the fact that Test 2 contained a higher percentage of metal, new electrode control measures were implemented. To help eliminate the possibility of encountering a direct electrical short of two opposing electrodes contacting a single molten metal pool, opposing electrodes were slightly staggered relative to the insertion depth. This operating philosophy resulted in some imbalance because the primary firing pattern between opposing electrodes was partially disrupted, creating an unequal electrode surface area available in the melt for conduction. Because imbalances were occurring, operational modifications were made to equally insert electrodes.

- After operational modifications, some imbalances persisted. Electrodes resting on the bottom surface of the melt in the can region contacted metal cans and created a highly conductive current pathway through the upper layer of partially melted cans to the opposing electrodes. Therefore, an additional operational modification was made to grip and hold the electrodes a few centimeters above the bottom surfaces of the melt, above any molten metal. This change resulted in a more balanced electrical operation.

The total glass depth at the time of the imbalances was less than 0.6 m (2 ft) based on a final glass depth of less than 1.2 m (4 ft) at the conclusion of the test. This minimal glass depth tends to exaggerate the consequences of an imbalanced situation. Once all electrodes were retracted to an equal insertion depth of several centimeters above the bottom of the melt surface and after inclusions contributing to the initial imbalanced situation finally melted to create a relatively unrestricted, electrically conductive pathway

through the molten glass, a balance between the phase A and B power input was achieved and maintained at approximately 50 hours.

The only notable gas releases from cans in the region occurred at 30.0, 41.1, 41.8, and 42.1 hours. An operator observed at approximately 30 hours flares estimated to be 1 m (3.3 ft) in height. At that point during the test, the plenum temperature data revealed a minor rise of approximately 15°C. Hood vacuum was essentially unchanged at 0.9 in. of water. This data is provided in Figure 69. The carbon monoxide concentration at 30 hours was stable at 0.1% and did not indicate any increase. No changes in electrical power or resistance were observed at that specific time during the test. The second gas release, at approximately 41.1 hours, was audible and was described by operators as a series of three pops emanating from the hood at approximate 1 second intervals. Hood vacuum fluctuated from 0.8 in. of water vacuum to 4.0 in. of water pressure over a 16 second period, then spiked 6 seconds later from 0.75 to 0.1 in. of water vacuum. The hood plenum temperature spiked from 230 to 295°C. The third event occurred at 42.1 hours. In the third event, hood vacuum spiked from 0.75 in. of water vacuum to 2.25 in. of water positive pressure over a 29 second period. The hood plenum temperature increased from 240 to 340°C. This series of events is depicted in Figure 70.

Because the gas releases at 41.1 hours were accompanied by three audible "pops", it follows that the gas was released from containers at or slightly above the glass surface along a side wall because the molten glass would tend to muffle the sound of any release. In addition, the magnitude of the pressure spikes were greatly diminished in Test 2 relative to Test 1 primarily because of the additional glass volume created by increased soil overburden. Because the first gas release lasted over 16 seconds, it is likely the last two of the three audible gas releases at 41.1 hours occurred during the initial 16 second period.

Phase A and B resistance did not fluctuate during this series of events, as shown in Figure 71. The spikes shown at 42.6 hours in this figure are not

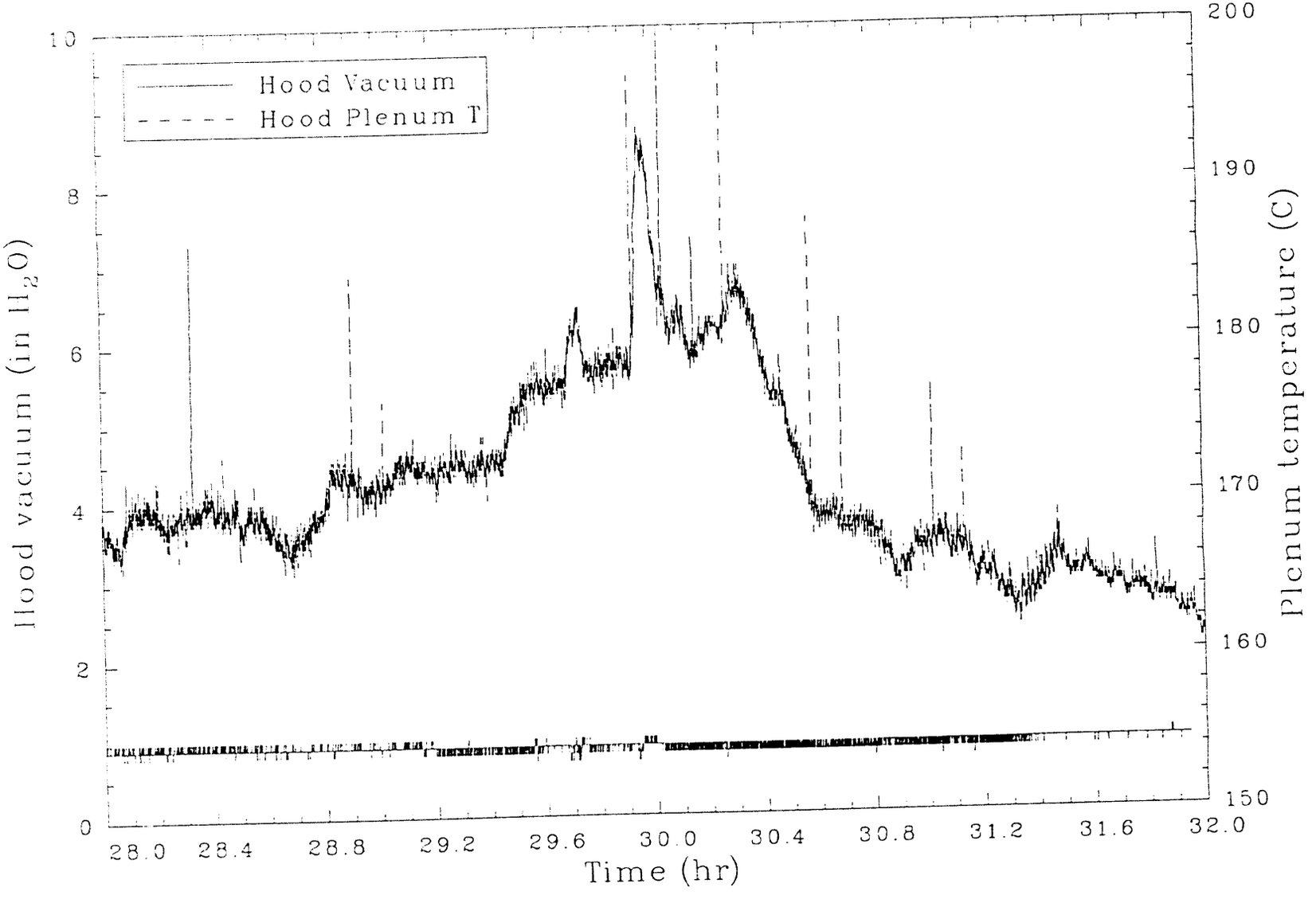

Figure 69. Hood plenum temperature and hood vacuum at approximately 30 hours, Test 2.

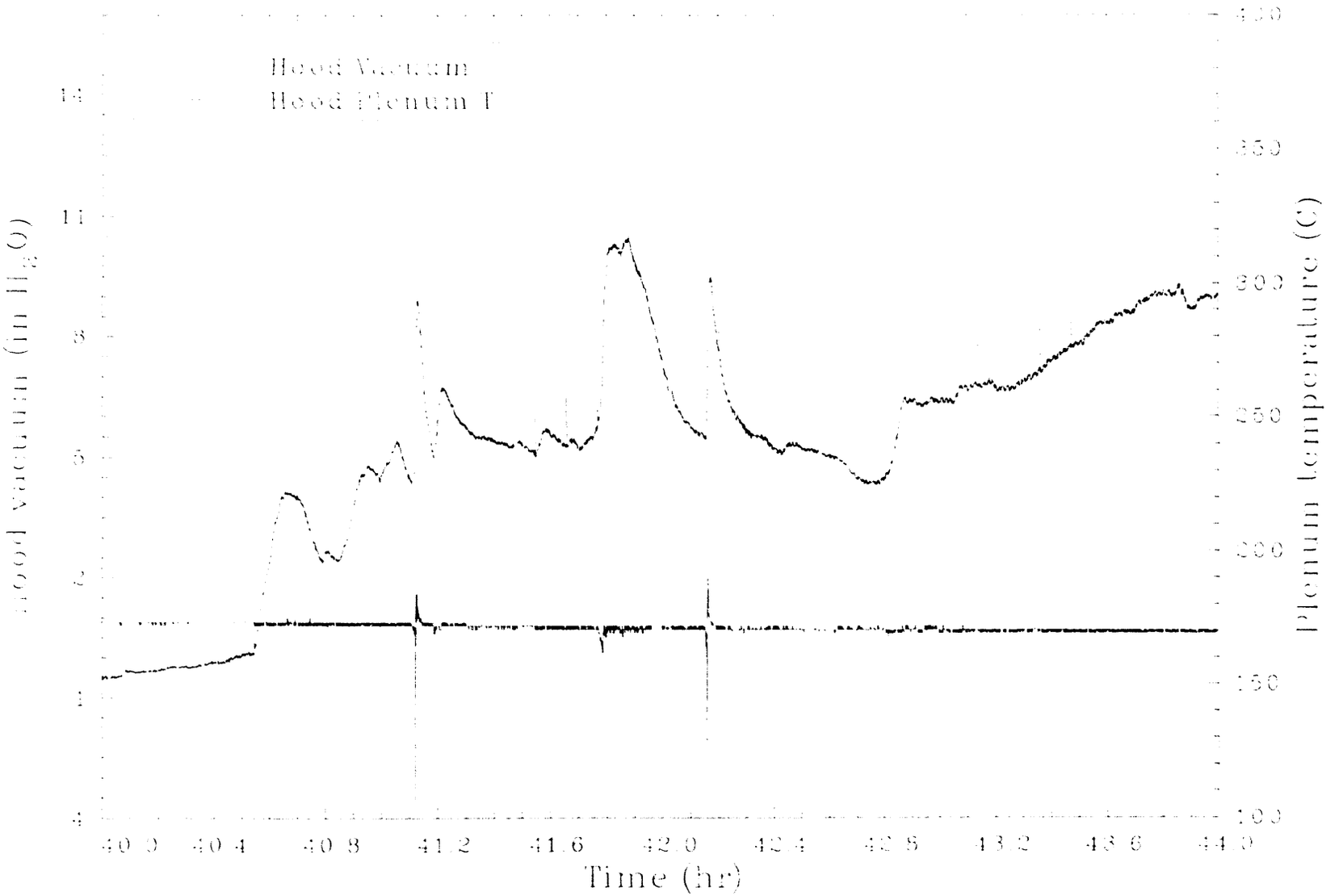

Figure 70. Hood plenum temperature and hood vacuum for several gas release events during processing of the stacked can region in Test 2.

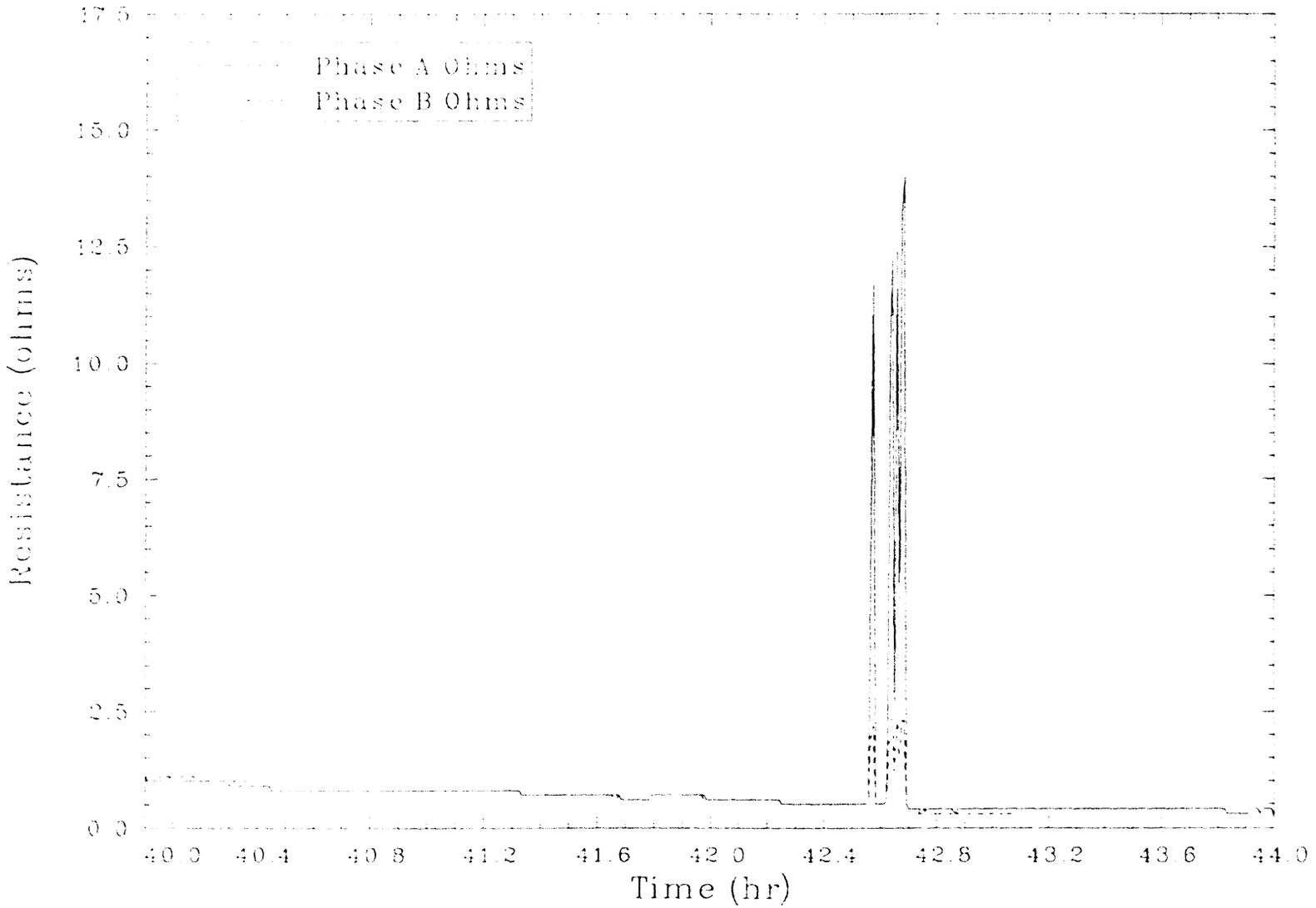

Figure 71. Phases A and B resistance for several gas release events during processing of the stacked can region in Test 2.

correlated with the gas releases. Total power levels, as well as amperage or voltage, did not fluctuate to any significant degree due to the gas releases. This indicates the gas releases were not complicated by disruptive inclusions in the melt or by other mechanisms such as melt cooling, which would increase the resistance of the melt and decrease the power input levels.

4.4.3 Stacked Box Region

The stacked box region, consisting of high metal content waste intermixed with soil, resulted in an entirely different operational behavior compared to the stacked can region. The stacked box region was encountered at approximately 1300 hours on July 13 at a run time of approximately 45 hours. At the time the stacked box layer was encountered, hood plenum temperatures had increased to 300°C, following the imbalanced period of operation between 30 and 40 hours, as shown in Figure 72. Since approximately 40 hours run time, the hood vacuum had been declining gradually and at 40 hours had reached a relatively steady state level of 0.5 in. of water, from an original level of 1.9 in. of water. This decrease in vacuum is due to an increased generation rate of off-gas from the melt. The hood plenum temperature spiked from 360 up to 490°C at 48 hours and again from 400 up to 440°C, as shown in Figure 73. In each case, increased temperatures did not immediately decline as in previous temperature spikes but remained elevated at the peak values for several minutes. These temperatures represented the highest sustained temperatures observed during the test and are due to extensive and continued pyrolysis and combustion of the top layer of boxes. Due to the extensive combustion occurring in the hood, the hood vacuum spiked downward at this same point during the test--from an initial level of 1.0 down to 0.1 in. of water vacuum. The vacuum level decreased, but, unlike previous vacuum spikes, this event had more of a gradual downward trend and was sustained at 0.1 in. of water for several minutes, as shown in Figure 74. There is a gap in data at approximately 47 hours; however, the second pressure transducer indicated a gradual decrease of vacuum to the 0.1 in. of water during that time period.

During the processing of the stacked box region, power levels averaged 300 to 350 kW, as shown in Figure 75. The high metal content of this region

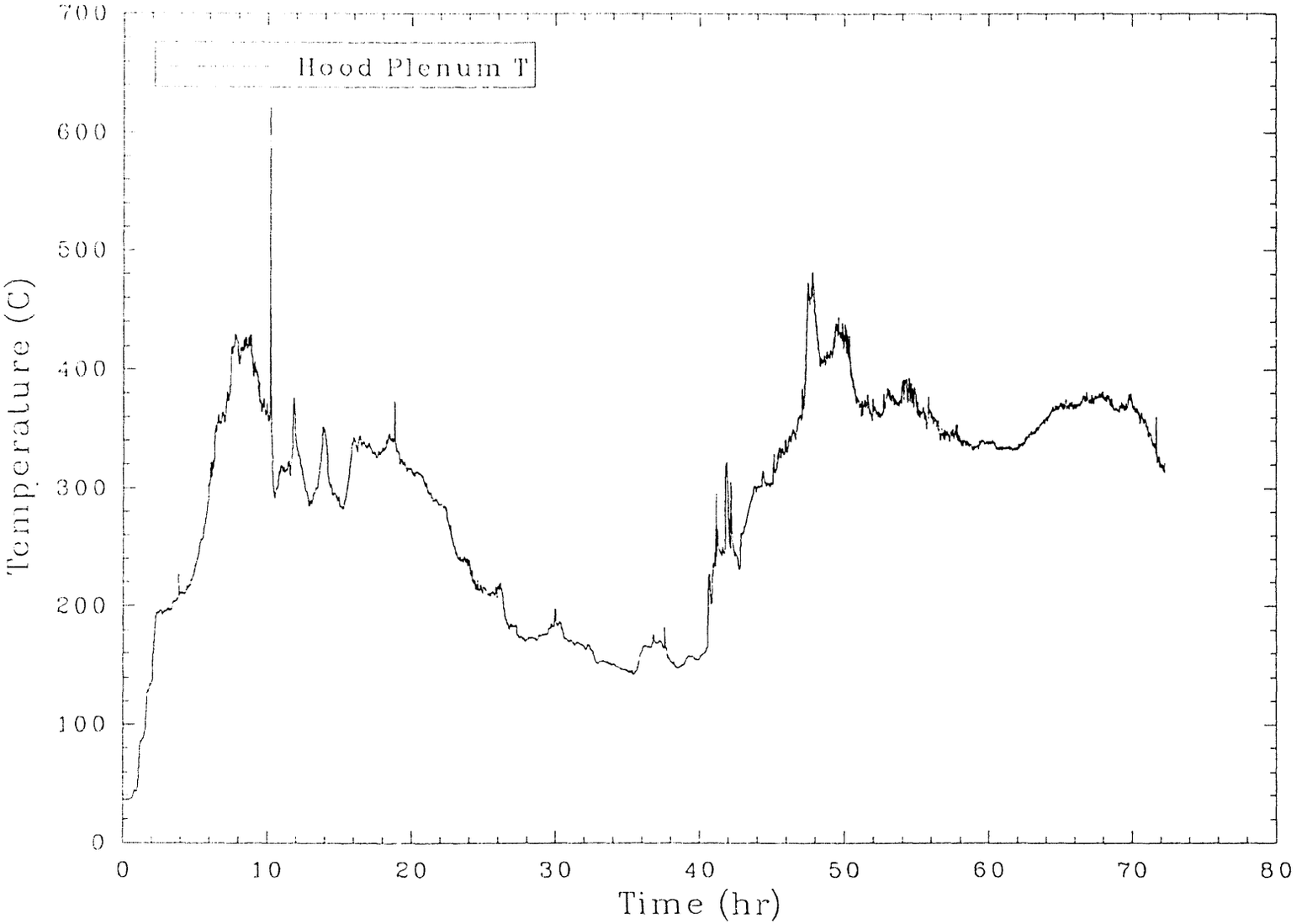

Figure 72. Hood plenum temperatures showing gradual increase prior to encountering the stacked box region in Test 2.

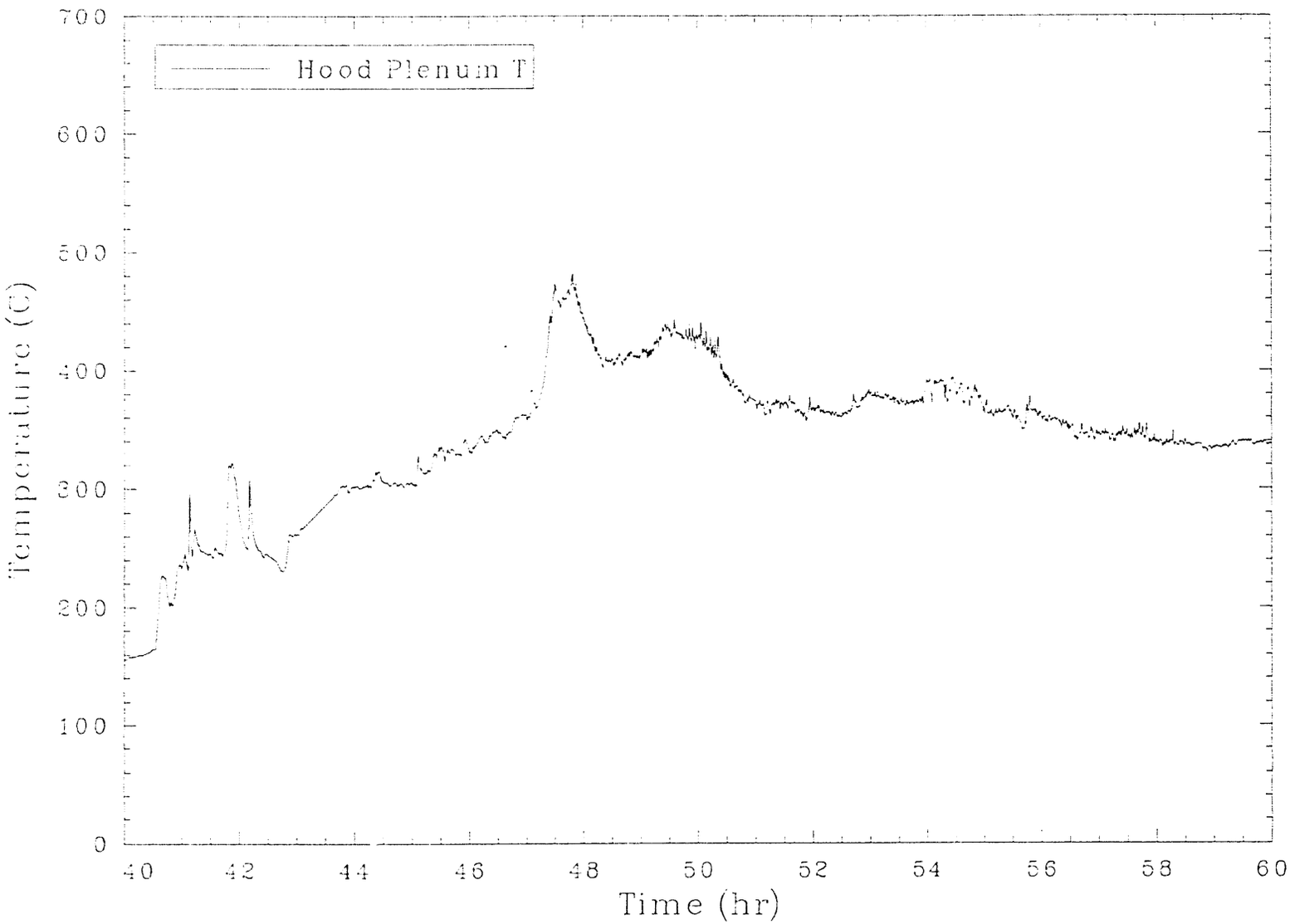

Figure 73. Hood plenum temperature showing temperature increases at 48 to 50 hours during processing of stacked box region, Test 2.

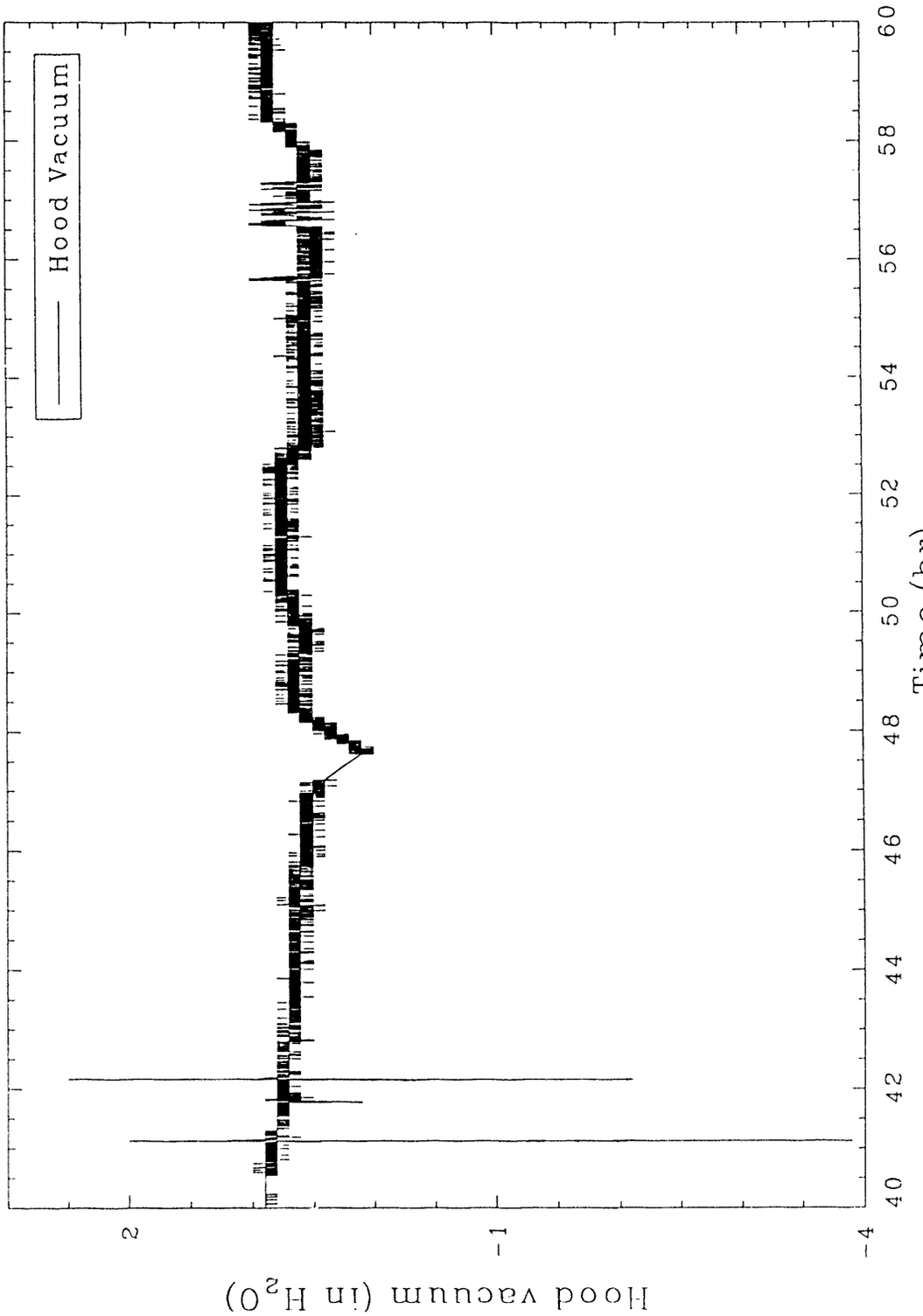

Figure 74. Hood vacuum showing mild decrease during processing of the top layer of stacked boxes for Test 2.

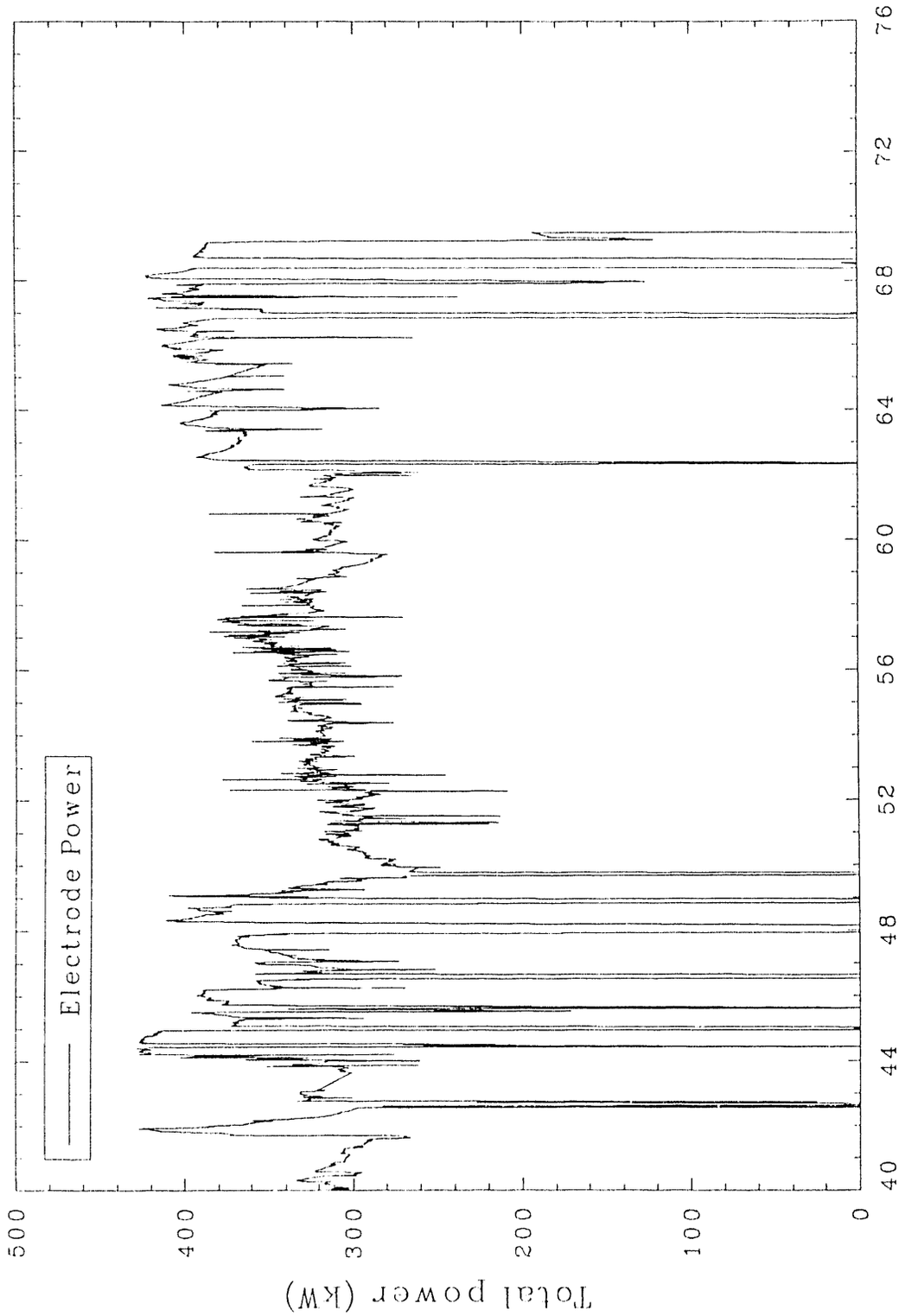

Figure 75. Total electrode power during processing of the stacked box region for Test 2.

combined with the molten metal from the stacked can region did not hamper electrical operations of the transformer. The reasons for the smooth electrical operations relative to Test 1 include (a) the electrodes were free, allowing their insertion depths to be adjusted as needed, (b) the electrodes were continually suspended above the molten metal at the bottom of the melt, and (c) the mass of the melt was increased relative to Test 1 due to increased overburden. No significant fluctuations in resistance were observed, and resistance averaged less than 1 ohm for both phases. From 48 hours through the remainder of the test, voltage consistently averaged 220 for both phases A and B.

Both secondary phases averaged 800 A over the final 22 hours of the test, as shown in Figure 76. At approximately 68 hours, power to the electrodes were deenergized and the electrodes allowed to rest on the bottom surface of the melt to confirm the depth of the melt. Melt depth was confirmed at an average electrode depth of 3.1 m (122 in.).

4.4.4 Equipment Performance for Test 2

The off-gas hood performed exceptionally well during Test 2. The temperatures observed in the hood represented the highest sustained temperatures ever recorded in the hood. No thermal degradation of the hood, RTV-106 sealant, or electrode seals resulted from the test.

Like Test 1, the off-gas treatment system performed well with respect to cooling the off-gas stream. This is illustrated by Figure 77, which provides the inlet and exit temperatures of the Venturi-Ejector and shows that the heat was effectively removed from the off-gas stream by the Venturi-Ejector.

The off-gas treatment system effectively removed particulate from the off-gas stream. Figure 78 illustrates that the efficient scrubbing action did not result in a gradual plugging of the filters due to particulate buildup. The sudden decrease in pressure at 48 hours reflected the increased rate of off-gassing from the melt and the corresponding decrease in hood vacuum. The

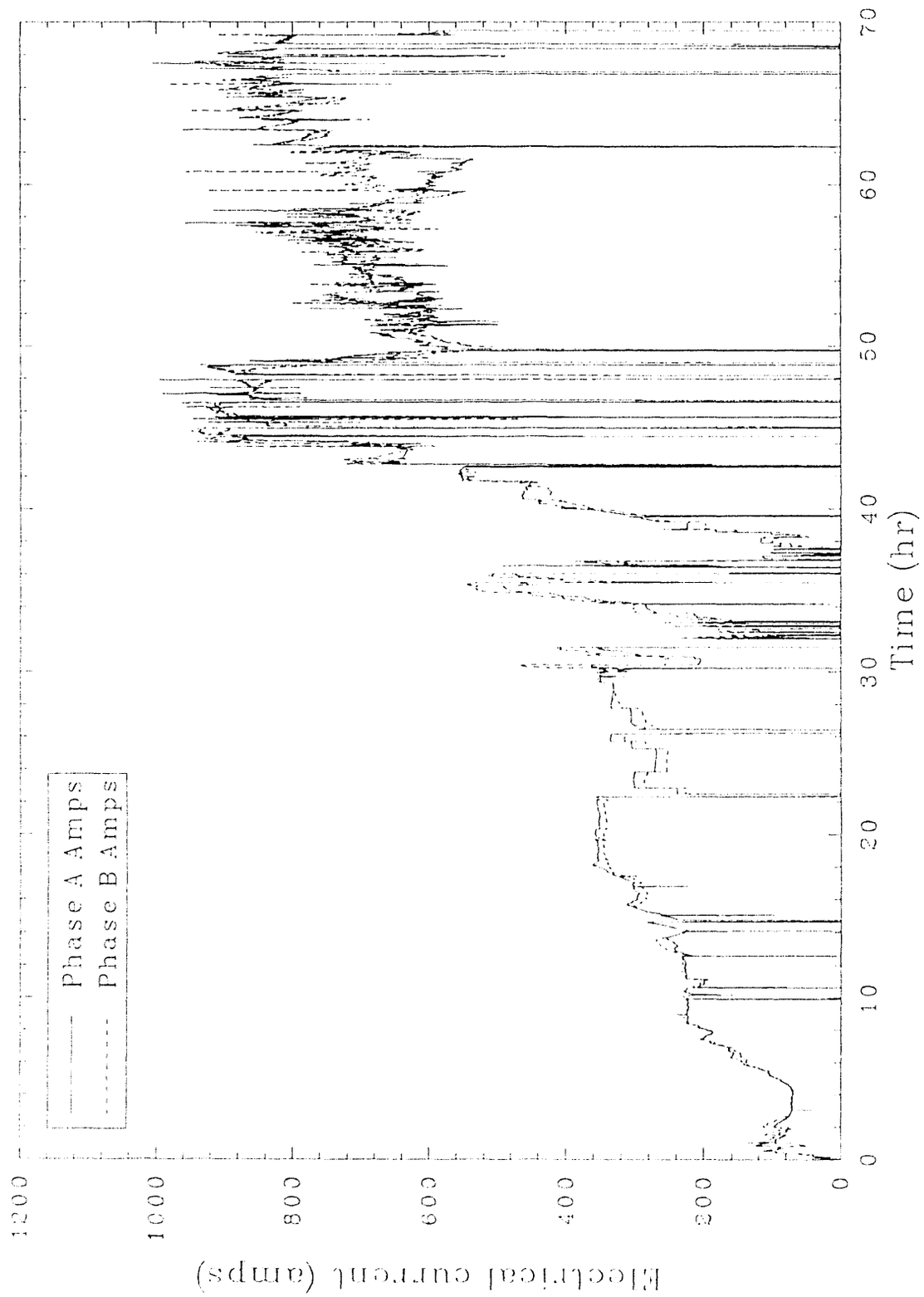

Figure 76. Phase A and B amperage for Test 2.

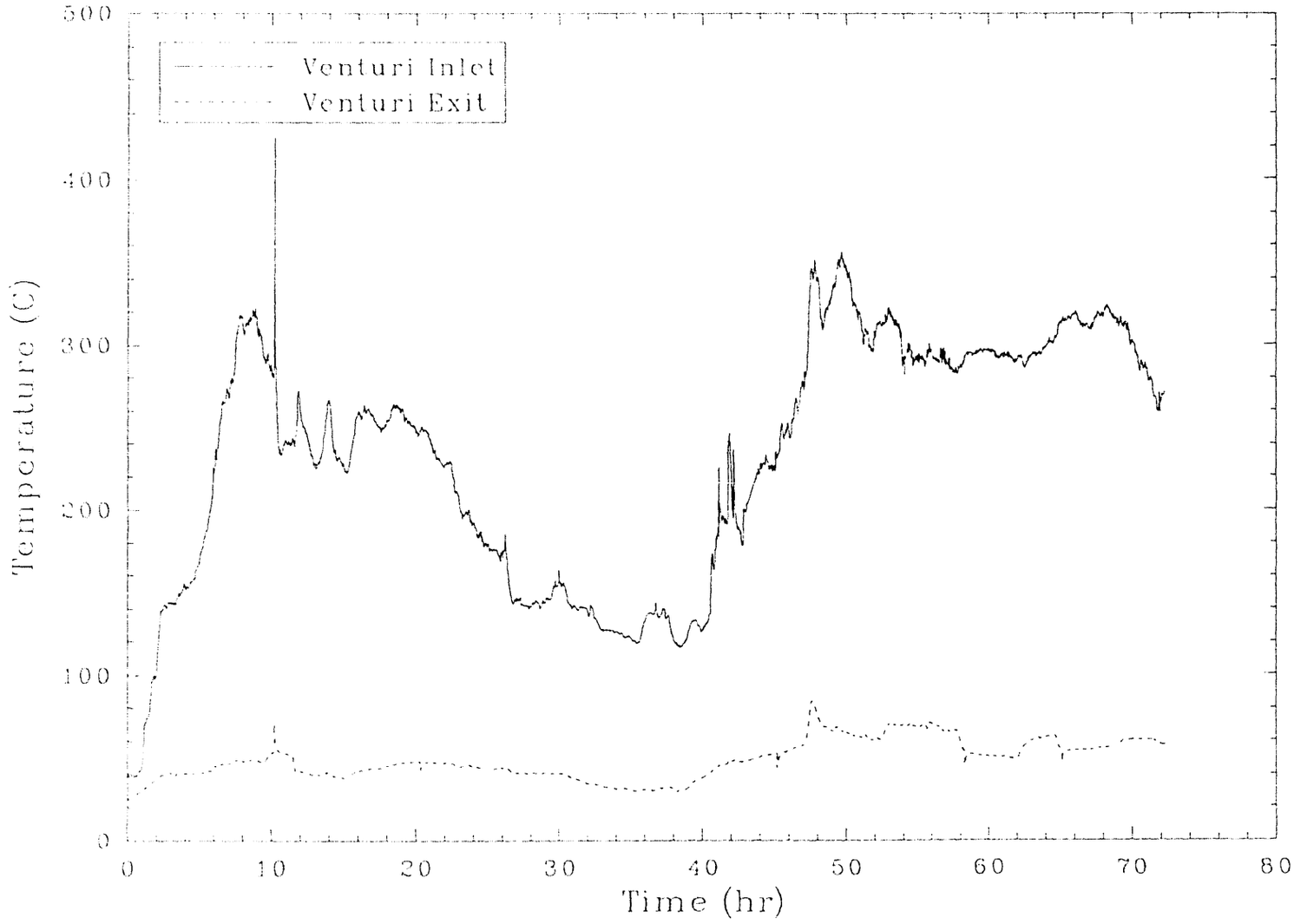

Figure 77. Venturi-Ejector inlet and exit temperatures for Test 2.

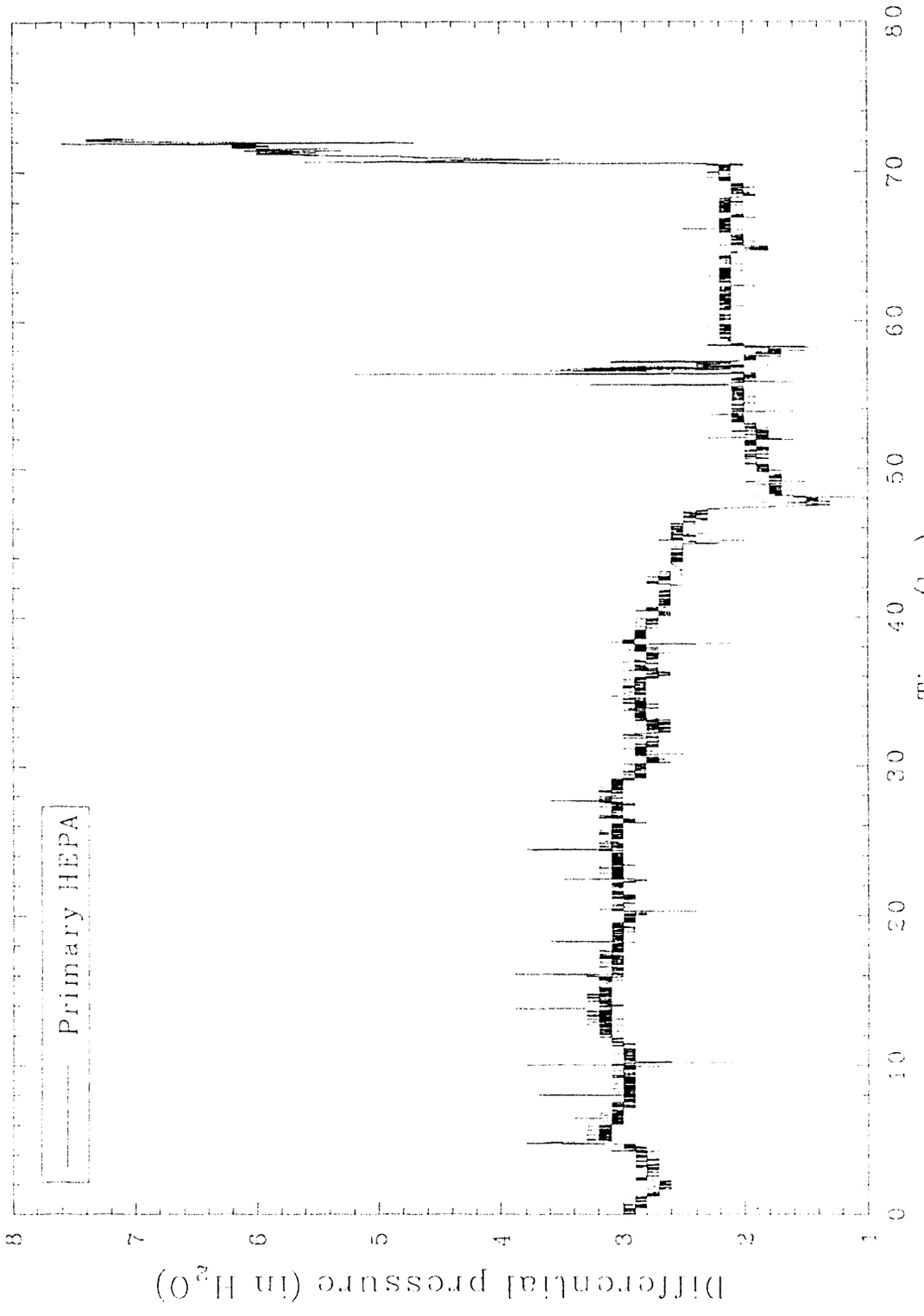

Figure 78. Primary HEPA filter differential pressure for Test 2.

spikes at 57 and 71 hours represented a sudden increased differential pressure due to a wet HEPA filter caused by the flooding of scrub solution tank 2. The depth level indicator for tank 2 failed due to the plugging of the small diameter tubing associated with the differential-pressure depth indicating system. The tubing became plugged due to the heavy particulate loading in the off-gas stream and created an inability to ascertain the level of the scrubbing liquid in tank 2. The first wet HEPA was dried by increasing the temperature on the gas heater upstream of the filter. The second wet HEPA occurred at a time immediately prior to the termination of the test, well after electrode power had been terminated.

The plugging of the small diameter tank-level indicator tubing illustrates a larger problem with particulate generation from the test. Relative to a contaminated soil site, the vitrification of a simulated buried waste site apparently results in a greater amount of particulate generation from the melt. The increased levels of particulate generation will require design considerations for a large-scale buried waste ISV machine. The increased amount of particulate in the off-gas stream created two key problems in addition to the small diameter tubing problem mentioned above.

- Solids deposited at the inlet to the Venturi-Ejector resulted in an increased differential pressure across the Venturi-Ejector. This increase in differential pressure is illustrated in Figure 79. The first indication of solids buildup occurred between 30 to 35 hours. Because the differential returned to previous levels, the solids deposit dislodged. Later, at approximately 45 hours, the differential trended more negative, indicating additional solids were depositing at the Venturi-Ejector inlet. The solids deposit created a restricted orifice that reduced total off-gas flow through the system. Upon removal and disassembly of the off-gas line following the test, a large barnacle-like deposit of solids was discovered at the inlet of the Venturi-Ejector.

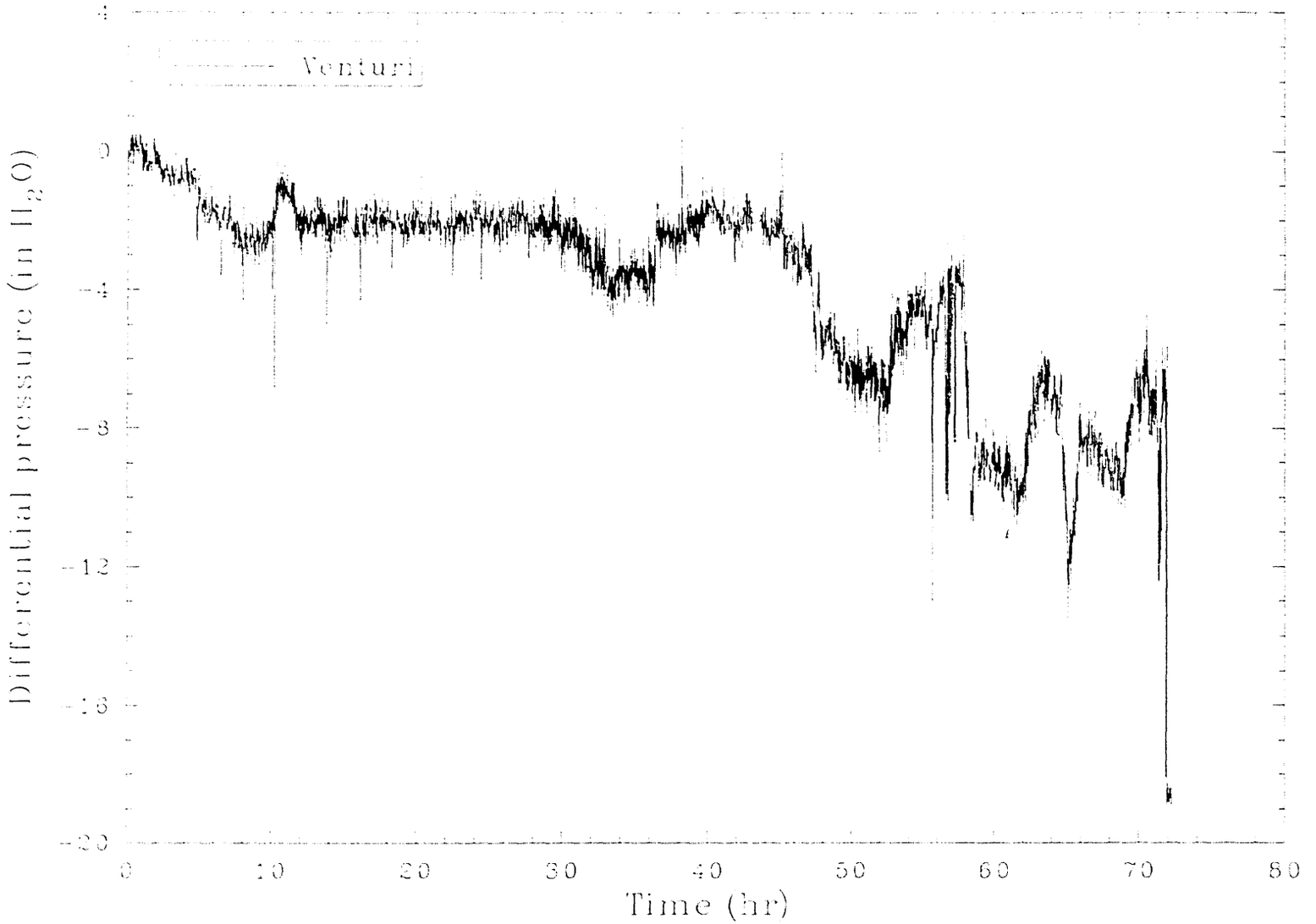

Figure 79. Venturi-Ejector differential pressure for Test 2.

- Spray nozzles in the Hydro-Sonic scrubber became partially plugged due to solids in the scrubbing solution. Approximately 50% of all nozzles in each of the two scrubber stages were found to be plugged once equipment was disassembled for inspection following the test. This plugging resulted in an increased pump 2 pressure and a decreased differential pressure across the Hydro-Sonic scrubber, as shown in Figure 80. However, the differential pressure was sustained above 50 in. of water for the test duration except for two short periods at approximately 56 and 58 hours. The average differential would have resulted in an adequate scrubbing efficiency to prevent particulate carryover to the HEPA filters.

Note that because the scrub solution used for Test 2 was the same for Test 1, the solids accumulation in the scrub tanks, nozzles, and small diameter tubing represented the contribution of particulate from two tests. However, the solids accumulation from these tests of simulated buried waste sites is still considered to be excessive based on numerous contaminated soil tests.

The off-gas flow rate averaged 15 m^3/min and was more consistent compared to the flow rate in Test 1, shown in Figure 81. The more consistent flow rate was due to the absence of the dramatic pressure spikes that were observed in Test 1 and the new position of the flow sensor upstream of the blower surge protection inlet. Because the off-gas flow was much more consistent with fewer pressure spikes compared to Test 1, the surge protection device remained closed during the vast majority of the test.

The uncoated electrodes performed well. No sticking was observed during the test indicating the difficulties observed in Test 1 were primarily due to the silica-based coating. Oxidative losses were acceptable. One phase A electrode decreased in diameter from 15.2 to 8.9 cm (6 to 3.5 in.) and exhibited a sharp taper over a 17.8 cm (7 in.) region just above the glass level. One phase B electrode reduced in diameter from 15.2 down to 10.2 cm (6 to 4 in.) and exhibited a gradual taper over a 0.6 m (2 ft) length above the glass level. As in Test 1, Test 2 represented a difficult challenge for the

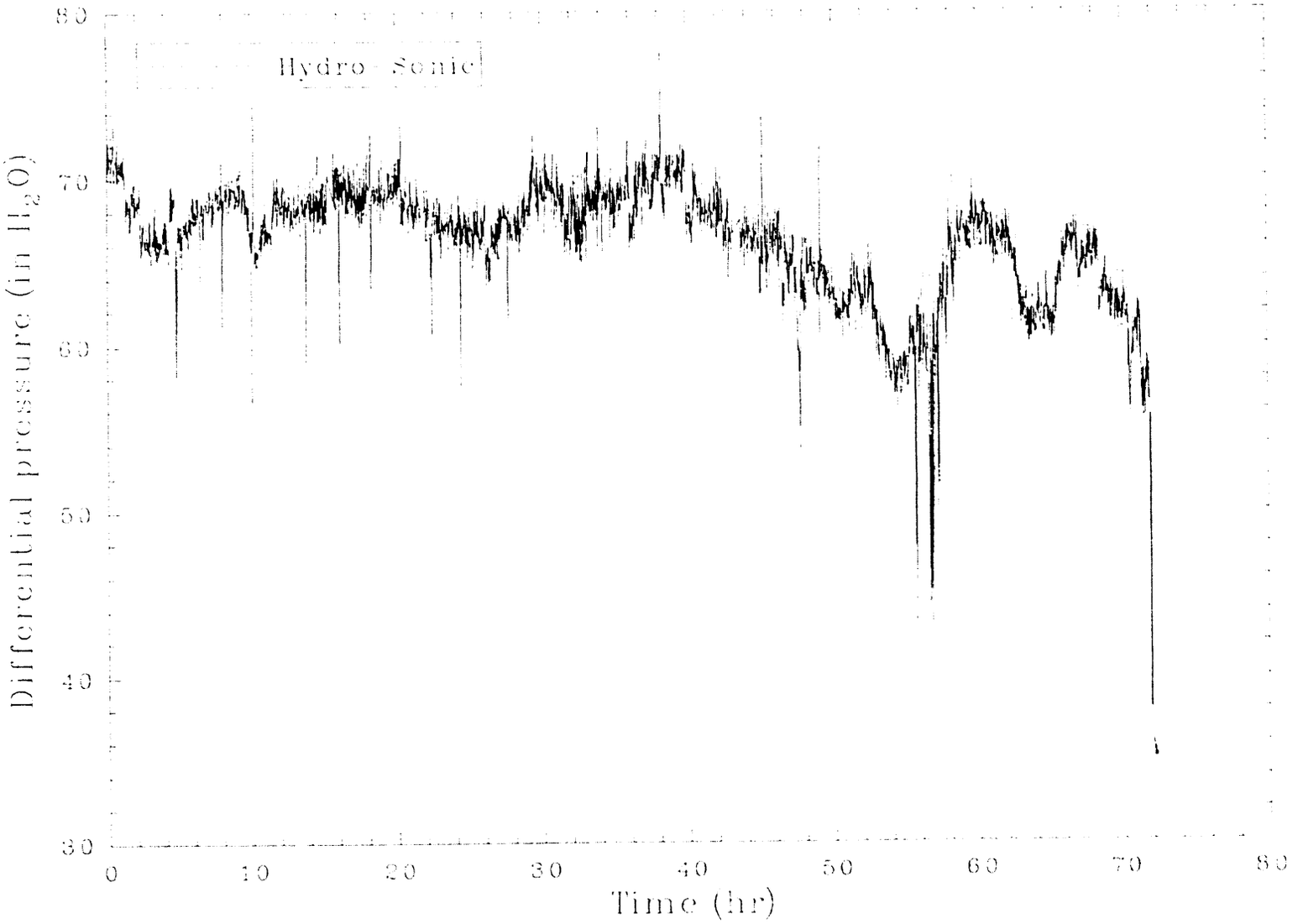

Figure 80. Hydro-Sonic differential pressure for Test 2.

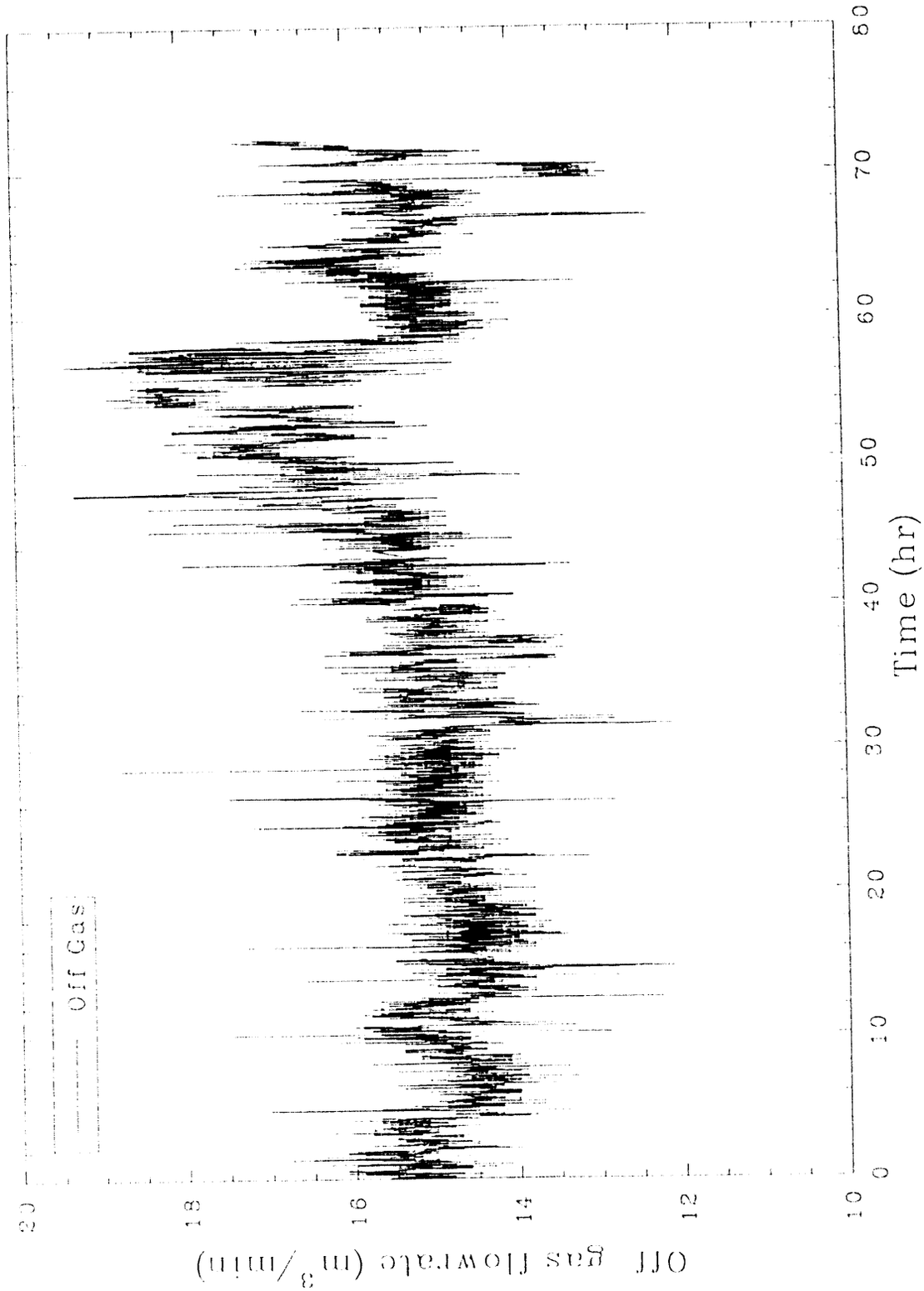

Figure 81. Off-gas flow rate for Test 2.

graphite electrodes. Due to the significant amount of subsidence in the melt [measured at 2.3 m (7.5 ft.)], the portion of the electrode at the air/glass interface remained relatively constant throughout the test. Initially, the electrodes were inserted in the soil to a 30.5 cm (12 in.) depth. Consequently, the air/glass interface location relative to the electrodes stayed fairly constant throughout the test. Final glass depth was measured at 0.9 m (36 in.).

5. PRODUCT EVALUATION

Since the primary purpose of the ISV process is to stabilize and immobilize nuclear and toxic waste components, the chemical morphology and release characteristics of ISV waste forms must be known to provide for an accurate performance assessment. Full characterization of ISV waste forms from laboratory, engineering, intermediate field, and large field tests is needed to establish the adequacy of the ISV process as a buried waste treatment option.

The properties of ISV waste forms are directly related to the composition of the waste, composition of surrounding soil, and the thermal history of materials reacted during vitrification and cooling. The application of the ISV process to buried waste and soil at the INEL presents unique conditions compared to the homogeneous soil/waste conditions previously tested at Hanford and Oak Ridge National Laboratory (ORNL). Since the INEL soil and buried waste differ from previous soil and waste of ISV tests, a detailed characterization of the INEL ISV waste forms was performed.

Evaluation of the ISV waste form was divided into three general categories: (a) sampling and bulk description, (b) chemical and physical properties, and (c) durability testing. This is outlined in detail in the ISV product evaluation strategy.[9]

The objective of the sampling and bulk description activity was to provide representative samples to generate a general description of the ISV monolith and a gross identification of the different bulk phases. This megascopic description of the monolith was necessary before other characterization techniques could be detailed.

The purpose of the chemical and physical evaluation was to determine the elemental composition of the waste form. Because of the many elemental components in an ISV waste form, the slow thermal diffusion of the glass, and the long cooling times of the monolith, some glass will devitrify to crystalline material. The structure and elemental composition of each

crystalline phase will reveal if any waste components have segregated into a less durable phase.

Durability testing is divided into three types of leaching tests. The first, the Environment Protection Agency's Toxicity Characteristic Leach Procedure (TCLP),[10,11] meets the minimum regulatory testing requirements established for landfill disposal. However, the TCLP does not address radioactive waste components, provide a technical basis for assessing long-term durability, provide a basis for a comparison to highly durable waste forms or natural analogs, or provide an assessment of the source term release of the waste component for risk assessment models. To provide this information, additional durability tests must be conducted. These additional tests fall into two categories: comparative testing (comparing ISV waste forms to similar waste forms and natural analogs) and testing to determine the intrinsic rate (fastest) of waste form dissolution (k_+).

5.1 Excavation, Sampling, and Bulk Description

The two ISV blocks were allowed to cool prior to excavation. Although no cooldown data on the blocks were recorded, it appeared that both blocks had cooled to ambient conditions at the time of excavation, which began on September 10, 1990.

A careful and systematic excavation of the ISV processed pits was conducted in order to obtain physical descriptions of the waste pit morphology, the processed waste, and the vitrified product. Additionally, samples were collected for chemical and physical analysis. Direct observation of the product, achievable only through excavation, provided data directly applicable to such issues as the probability of underground fires due to ISV processing, thermal gradients adjacent to the melt front, correlation of ISV processing events with features exhibited by waste pit morphology, physical and chemical properties of the product, as well as other features that would provide insight into the dynamics of the ISV process. The materials

collected during the excavation of the test pits were analyzed to determine the bulk composition, the mineralogy, the tracer rare-earth element distribution, the density, the chemical and mechanical durability, and the micro-structure of the vitrified product. The chemical and physical characterization provided information about melt properties during the ISV processing and subsequent cool-down period, melt mixing and homogeneity, and the representativeness of "melt samples" taken from the molten waste form.

It should be noted that much of the following description involves unvitrified or partially vitrified waste at the edge of the vitrified block. Although much useful information is derived from these observations, it should be emphasized that these edge effects are inherent to single melts such as these test melts. For production-scale application of ISV to a large buried waste site, the edges would be fused together in larger contiguous blocks in multiple melts. Further testing will provide insight into operational and engineering considerations for processing adjacent areas.

5.1.1 Excavation/Sampling Methods

Many tools and techniques were used during the excavation process. A front loader and backhoe were used for major excavation activities. The backhoe was the primary excavation tool and was used to trench each side of the pit areas to a depth of about 0.91 m (3 ft). The front loader was not generally useful for direct excavation of the test pits because the force required for scooping dirt severely disturbed the pit and fractured the waste form. When necessary to preserve delicate features, the walls of the trench were then carefully collapsed by hand using shovels and a 5 in. masonry trowel. Dislodged soil and fused product, as well as unaffected simulated waste, were described, photographed, and then removed from the trench with the backhoe as the trench wall removal progressed. The trenching/caving process was repeated as necessary until the product had been completely exposed and/or

removed. Figure 82 shows Test Pit 1 excavated to a depth of approximately 1.2 m (4 ft) and illustrates the general shape of the pit area during the excavation process. All features of interest were described in the field notebook and photographed using a 35 mm single-lens reflex camera equipped with a 55 mm, 2.5f, macro lens.

Each film roll was identified by photographing a page from the field notebook showing the roll number, date, film type, camera and lens used, and other information. The film roll identifying frame was usually the first frame in the roll. Additional photographs were taken by personnel from the EG&G Idaho photography laboratory; however, detailed records were not maintained for these photographs in the field notebook. Direction, distance, and depth measurements were made with a transit, measuring tape, and 12-ft stadia rod. Each day the transit was set up in the same position by locating the transit over a steel rod driven permanently into the ground for reference. The location of the transit was verified by measuring the height and bearing of two to three reference points in the area. Samples were taken as appropriate and included soil, crystalline and vitrified product, and simulated waste in several stages of thermal alteration. Samples were placed in appropriate containers (e.g., new heavy-duty polyethylene trash bags for coherent materials and new 400 mL plastic bottles with tight screw lids for loose soils). Samples were labeled, and sampling information was recorded in the sample logbook.

Cores were drilled into the glassy waste form, or monolith, that pooled in the bottom of each pit. The drilling was carried out using a trailer-mounted rig with an air-cooled 10.2 cm (4 in.) diamond drill bit having a Hastalloy matrix. A 1.8-m (6-ft) steel "clam shell" type core-barrel was used. Four cores were drilled into the Test Pit 2 monolith and two cores were taken from the Test Pit 1 monolith. The cores were stored in 10.2-cm (4-in.) diameter Lexan tubes and were described in the sample notebook, bagged, and labeled, as were all the other coherent samples. Most cores were broken into

Figure 82. Test Pit 1 partially excavated.

small (approximately 5.1 to 10.2 cm [2 to 4 in.] on a side) fragments during the drilling process; therefore, the original location of each piece is probably known within a precision of ± 5 cm (2 in.).

5.1.2 Bulk Description

5.1.2.1 Processed Waste Test Pit 1. The general shape of Test Pit 1 after ISV processing was a square shaft with rounded corners, as shown in Figure 83. The depth from ground surface to the uppermost glassy material in the pit bottom, as measured directly from ground level, was about 1.5 m (5 ft). Depth from ground surface to the monolith (i.e., dense, well-defined glassy material in a contiguous mass), centered among the four electrodes, was approximately 1.9 m (6.1 ft) when measured during excavation. The monolith was approximately oval and about 1.5 x 1.8 m (5 x 6 ft) with the long axis under diagonal electrodes (SW to NE). The thickness of the monolith was about 0.55 to 0.61 m (1.8 to 2.0 ft) and was measured as the length of each of the cores taken from Test Pit 1. Figure 84 shows a schematic cross section of Test Pit 1 after ISV processing. Significant amounts of glassy material were found outside the cylindrical pit walls but within the simulated waste. This material was in the form of glassy fillings in cardboard boxes. The original shape of the boxes was preserved. A typical example of a "glassy box" is shown in Figure 85. In some cases, the boxes were completely filled with a mixture of glass and scrap metal. In other cases, the glassy boxes were empty and had a wall thickness as small as 0.64 cm (0.25 in.). Scrap metal was the only waste material found in the glassy boxes. An explanation for the "empty" glassy boxes suggests that the boxes originally contained nonmetal substances such as concrete and scrap glass. This material probably dissolved into the melt and/or was carried out of the box as the melt level in the pit dropped below the level of the box and as the molten material in the box drained back into the pit. Both glassy boxes and unaffected boxes were found at all levels in the pit. Glassy boxes were laterally distributed the full width, 3.05 m (10 ft), of the test pit. The total amount of processed waste recovered was 8267 kg (18,225 lb).

Figure 83. Test Pit 1 after ISV processing.

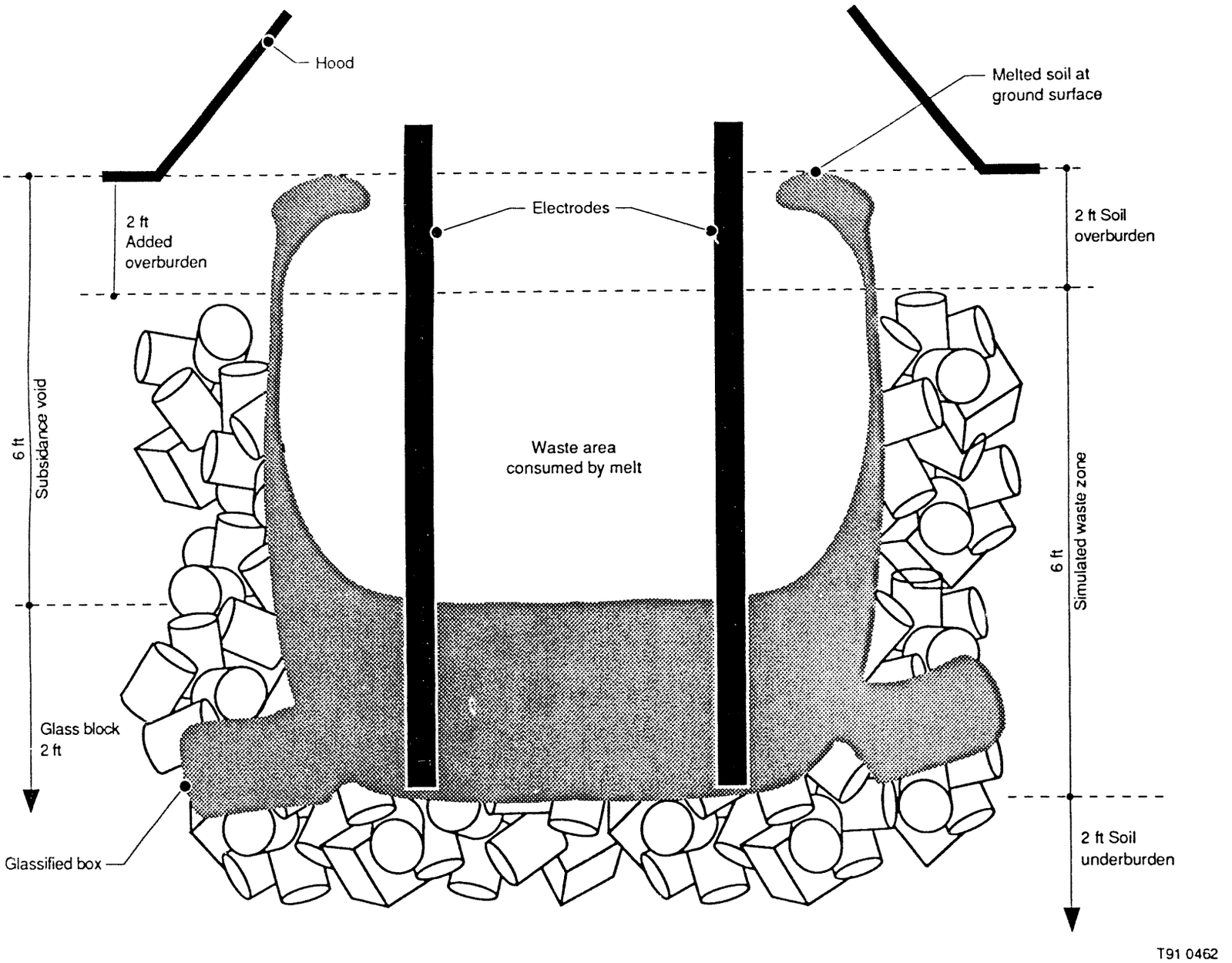

Figure 84. Schematic cross section of Test Pit 1 after ISV processing.

Figure 85. Test Pit 1 "glassy box."

5.1.2.2 Processed Waste Test Pit 2. The general shape of Test Pit 2 resembled a funnel on a box and is shown in cross section in Figure 86. The shaded cans shown in this figure are depicted for illustrative purposes; these cans were processed and incorporated into the melt. At the end of the test, a subsidence hole existed down to the top of the melt. Depth from ground surface to the monolith upper surface ranged from about 2.2 to about 2.3 m (7.2 to about 7.5 ft), with the monolith being about 0.98 m (3.2 ft) in thickness. (Note that "ground surface" was 0.6 m [2 ft] higher than Test Pit 1 and that the maximum thickness of the monolith was 1.14 m [3.75 ft] along the south edge of the block to 2.75 ft along the north side.) The maximum diameter of the funnel was 3.35 m (11 ft) at a depth about 0.46 m (1.5 ft) below ground surface. The funnel pinched inward to a diameter of about 1.5 m (5 ft) near the monolith upper surface. The funnel walls are shown in Figure 87. The thickness of the funnel wall was about 10.2 cm (4 in.).

The upper lip of the funnel was a rim of glass, roughly oval in cross section, at ground level with a diameter of 0.46 to 0.61 m (1.5 to 2 ft). The shape of the monolith was a rough rectangle with rounded corners. The maximum dimension was 3.35 m (11 ft) (N-S) and minimum was 2.90 m (9.5 ft) (E-W) measured from exposed coherent glass to exposed coherent glass on opposite sides of the monolith. Figure 88 shows the shape of the monolith together with the exposed scrap metal on the unlithified corners of the monolith. The simulated waste in Test Pit 2 was arranged with layers of cans on cardboard boxes. The melt filled and obliterated virtually all of the boxes, which measured 3.05 x 3.05 m (10 x 10 ft) total, except at the pit corners and, in a few cases, the very outermost surfaces of the boxes. The three sets of outermost cans, directly above the boxes, were affected much less extensively and are shown in Figure 89. Note that the cans in the third set were in contact with the glass of the funnel wall directly above the monolith. The weight of the monolith was 13,109 kg (28,900 lb), and the total amount of vitrified waste recovered from Test Pit 2 was 17,430 kg (38,425 lb).

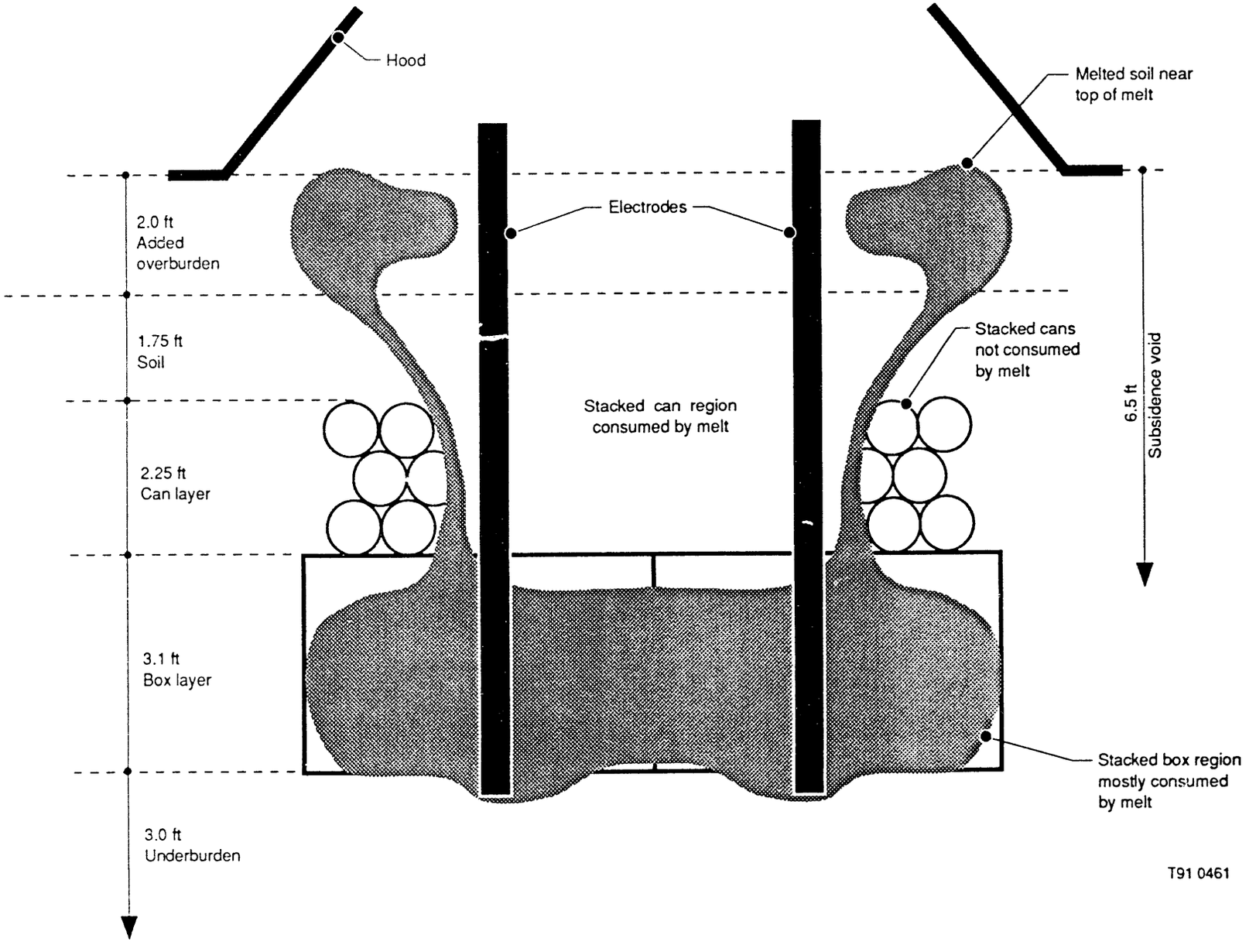

Figure 86. Schematic cross section of Test Pit 2 after ISV processing.

Figure 87. Test Pit 2 funnel walls.

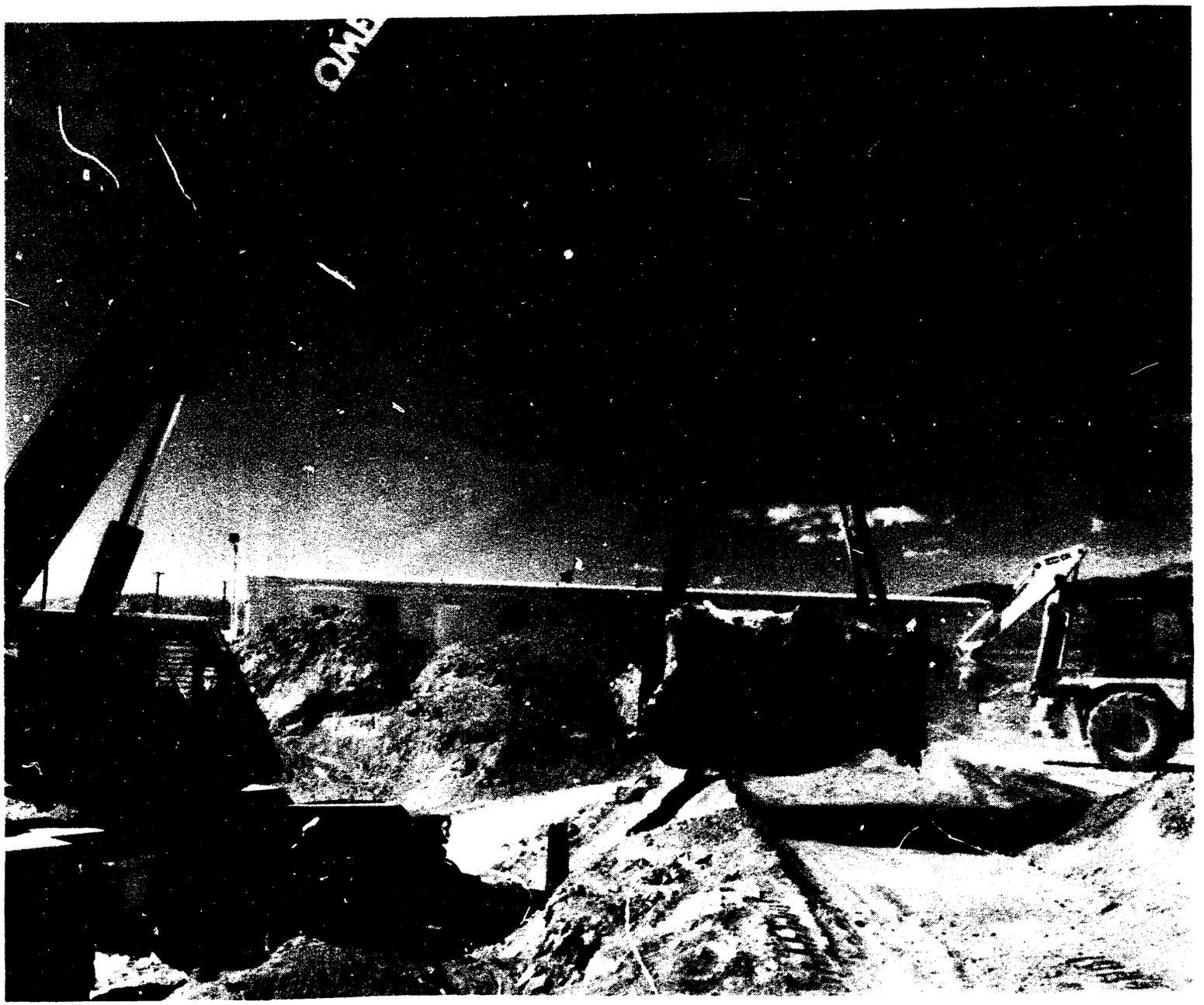

Figure 88. Test Pit 2 monolith.

Figure 89. Edge effects on cans in Test Pit 2.

5.2 Chemical and Physical Properties

5.2.1 Methods

Nearly one hundred samples were taken as appropriate and included soil, crystalized and vitrified product, and simulated waste in several stages of thermal alteration. Samples were placed in appropriate containers (e.g., new heavy-duty polyethylene trash bags for coherent materials and new 400 mL plastic bottles with tight screw lids for loose soils). Samples were labeled, and sampling information was recorded in the sample logbook. Cores were obtained as described alone in Section 5.1.1.

Twenty eight samples, including cores, from both test pits were selected for detailed study. In general, samples were taken systematically from each core at about 30 cm intervals and included both glassy and metallic materials. Additional core samples were collected so that all megascopically observable variations of the material were represented in the sample collection. Similarly, the remainder of the samples were selected so that representatives of all megascopically observable variants in the vitrified product were present in the data set. Sample descriptions are given in Tables 14 and 15 and sample locations within the test pits are shown on Figures 90 and 91. All samples were submitted for analysis under chain of custody. No special preservation or storage of the samples was required.

The major element bulk chemical analyses reported were carried out at three laboratories using two different analytical methods. The Separations and Analysis Unit of EG&G Idaho performed bulk chemical analysis by inductively coupled plasma atomic emissions spectroscopy (ICP-AES) using an ARL 3410 instrument. The preparation of glass samples involved first crushing, then dissolution using HF and nanopure water, followed by additions of HNO_3 and nanopure water. The metallic samples were prepared using the described HF dissolution on metal shavings. The ICP analyses were carried out using standard techniques. A multipoint calibration with replicate standards

Table 14. Sample descriptions Test Pit 1

Sample	Block Location	Description
IC013C90IW	1	Green glass, top of pit rim and edge, which contains ≈50% gas bubbles (diameter up to ≈1.3 cm) and traces of brown inclusions which are probably soil
IC044B90IW	2	Green glass from the top the central core (#5) The glass contains up to 20% bubbles (diameter up to 15 mm)
IC044D90IW	3	Dark green glass with 20% grey spherulites (≈2 mm diameter) trace of gas bubbles, core (#5) center 28 cm below IC044B90IW
IC044H90IW	4	Dark greer glass with 2% grey spherulites (≈2 mm diameter) core (#5) bottom, 56 cm below IC044B90IW
IC048B90IW	5	Dark green glass, top of core#6, 76 cm NNW of core #5 (IC044B90IW), ≈30% gas bubbles ≈1 cm diameter
IC048C90IW	6	Dark green glass with 50% grey spherulites ≈1 mm in diameter and trace of gas bubbles, core #6, 30 cm below IC048B90IW
IC048H90IW	7	Dark green glass with about 60% spherulites ≈1 mm diameter and trace of gas bubbles, core bottom, 56 cm below IC048B90IW
IH061D90IW	8	Nodular aggregate of grey metal pooled beneath center of Test Pit 1 monolith, contains trace amounts of green glass

Table 15. Sample descriptions Test Pit 2

Sample	Block location	Description
IC006C90IE	1	Dark green glass with up to 30% gas bubbles, located ≈46 cm from pit top on the interior of the pit
IC007C90IE	2	Dark green glass with trace amounts of very small bubbles, collected from the lower "funnel" ≈1.5 m below ground surface
IC026D90IE	3	Green glass with a blue-grey cast, contains 25% gas bubbles and about 5% grey spherulites, top of central monolith core (#1)
IC026F90IE	4	Grey porcelinous material with ≈7% gas bubbles (diameter < 7 mm), 6.3 cm below IC026D90IE core #1
IC026I90IE	5	Aphanitic and spherulitic material (diameter up to 8 mm) with traces of gas bubbles, located ≈28 cm below IC026D90IE, core #1
IC026M90IE	6	Green glass and grey spherulitic material (diameter up to 7 mm) ≈54 cm below IC026D90IE, core #1
IC027D90IE	7	Green glass with 7% gas bubbles (diameter up to 7 mm), top of core #2, 43 cm due south of core #1 (IC026D90IE)
IC027B90IE	8	Aphanitic and 3 to 5 mm diameter spherulitic material, located 27 cm below IC027D90IE, core #2
IC037D90IE	9	Grey spherulitic material (3 to 5 mm in diameter) with traces of gas bubbles, core #2, ≈38 cm below IC027D90IE
IC037F90IE	10	Grey devitrified glass, core #2, 27 cm below IC037D90IE

Table 15. (continued)

Sample	Block Location	Description
IH037J90IE	11	Massive metal and traces of glass 10 cm thick located at the bottom of core #2,
IC038B90IE	12	Dark green glass with bubbles, top core #3, 46 cm NE of core #1
IC038C90IE	13	Grey green devitrified glass with traces of grey spherulites up to about 2 mm in diameter, located ≈7 cm below IC038C90IE, core #3
IC038D90IE	14	Green glass and grey spherulites up to 1 cm in diameter, located 46 cm below IC038B90IE, core #3
IC043D90IE	15	Dark green glass with 60% gas bubbles up to 2 cm in diameter, top of core #4, 1.3 m NE core #1, inline with cores #1 & 3
IC043F90IE	16	Green glass, grey devitrified material and grey spherulites ≈3 mm in diameter, core #4, located 34 cm below IC043D90IE
IC043J90IE	17	Aphanitic grey material with traces of spherulites (1 mm diameter) and gas bubbles, located at the bottom of core #4, ≈63 cm below top of core
IH074D90IE	18	Grey nodular metal from the bottom of Pit 2 monolith, 1 m toward monolith center from the NE corner
IC086C90IE	--	Dark green glass with traces of gas bubbles, sample of melt taken while ISV waste form was molten

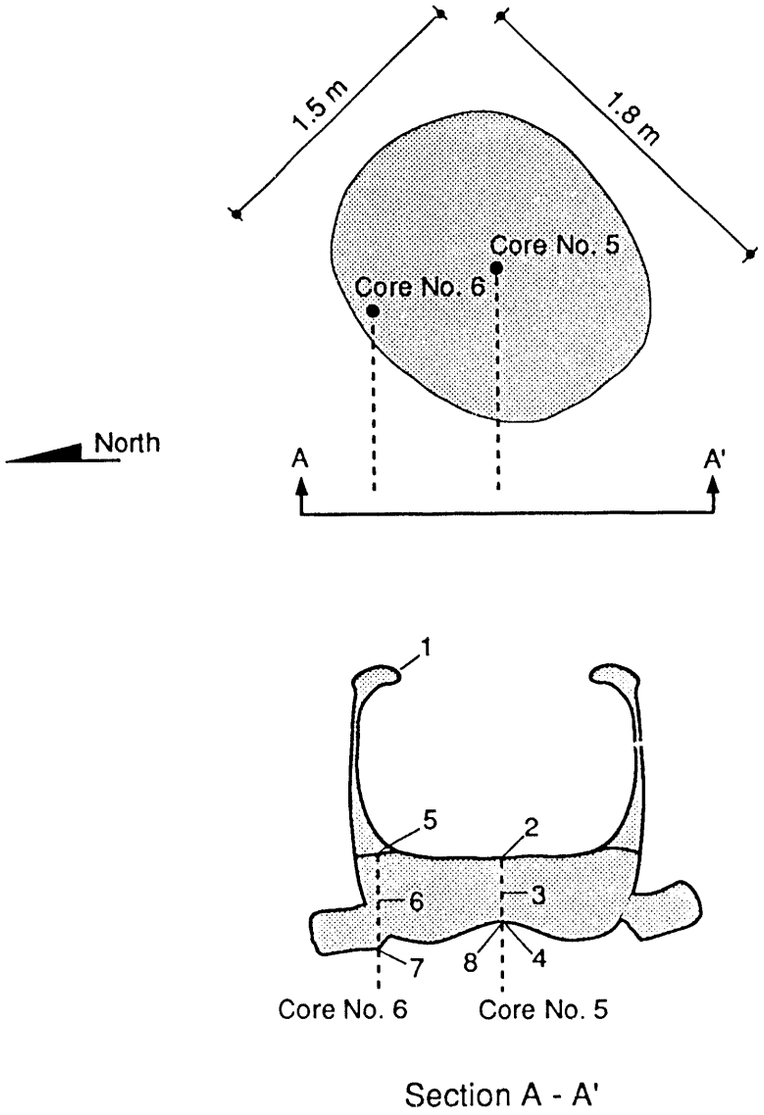

Figure 90. Product sample locations for Test Pit 1.

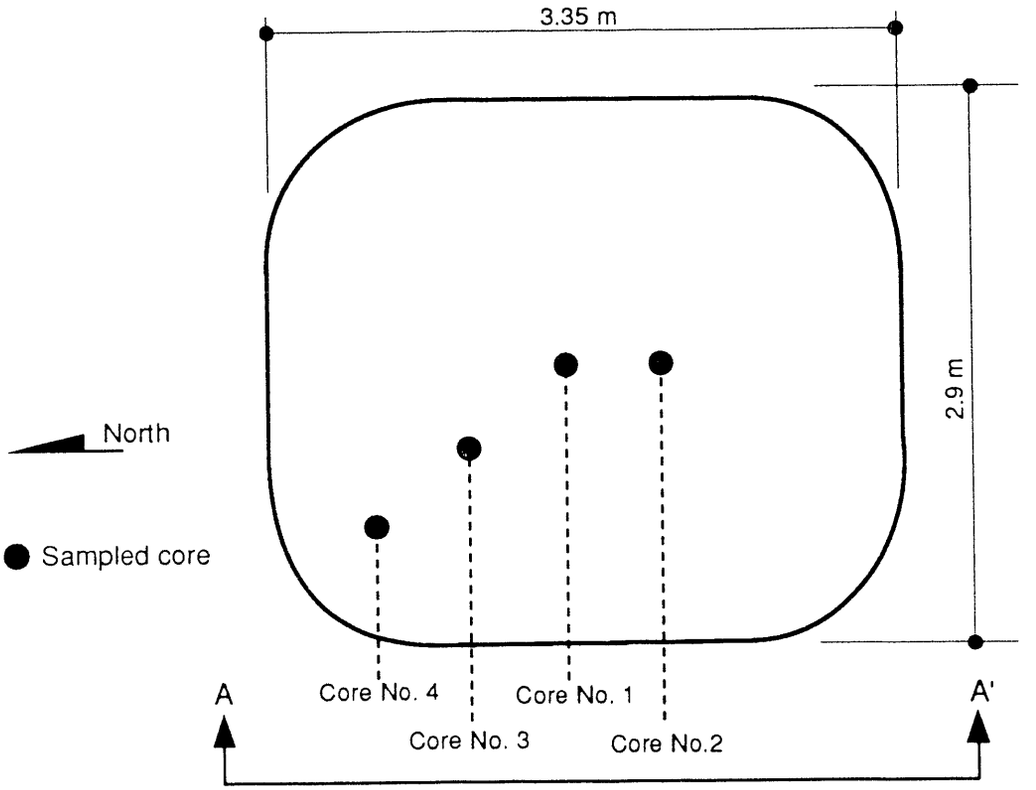

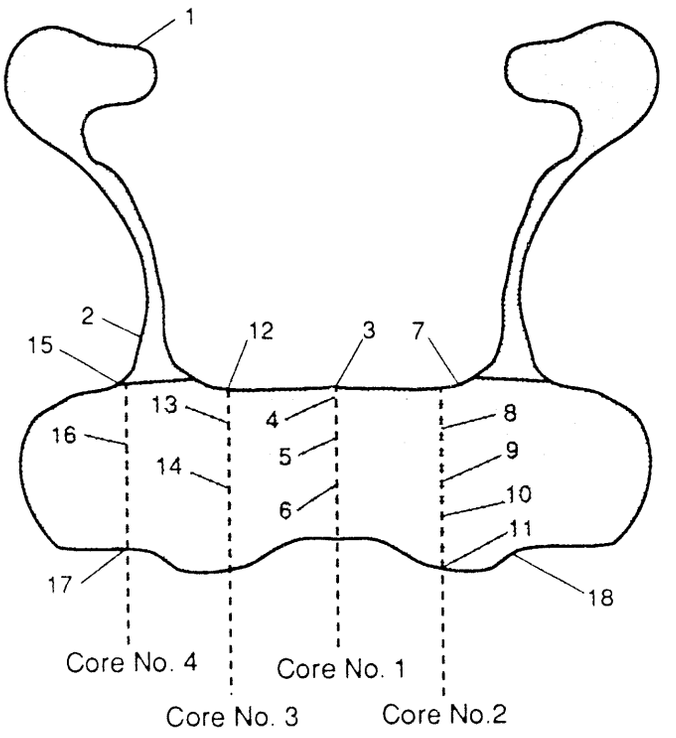

Section A - A'

T91 0477

Figure 91. Product sample locations for Test Pit 2.

determinations was performed over a suitable concentration range. The quality control associated with the glass analysis included two internal standards, matrix blanks, duplicate samples, sample spikes and blank spikes. The quality control associated with the metal samples consisted of matrix blanks, sample spikes, and blank spikes. The quality control procedures and data were reviewed for compliance with acceptable limits. About one-third of the data were found to be suspect for many reasons. The suspect data are not included here. The reported mean percent spike recovery and the relative standard deviation of the duplicate samples are shown in Table 16. An additional test of the reliability of the data is that the sum of the major elements oxides of an acceptable analysis will be 100 ±5 weight percent. Many of the analyses do not meet this requirement.

Table 16. Reported QA/QC summary of ICP-AES analysis by the separations and analysis unit

	Si	Fe	Mg	Ca	Al	Na	K
Mean%Spike Recovery	74.6	101.6	96.1	N/A	91.2	N/A	103.3
Relative Standard Deviation on Duplicate Samples	3.3	0.4	1.2	0.9	2.2	3.8	6.3

Some of the major element bulk chemical data reported here, as well as all of the microchemical analysis, were carried out at the Idaho Geologic Survey/Comer Laboratories electron microprobe laboratory at the University of Idaho using an ARL-EMX electron microprobe operated at 15KV and 0.1 microamp beam current. Standard operating procedures and five well-characterized mineral standards were used. Polished thin-sections were used for both bulk analysis and also the microchemical observations and measurements. Each bulk analysis datum is the mean of about twenty individual measurements. The reported standard deviation of each oxide value ranges from a worst case 27% (Na_2O) to 1.5% (SiO_2) of the amount present. The reported sum of the major element oxides varies from 97.3 to 100.3 weight percent. In addition, a blind analysis of three National Institute of Standards and Technology (NIST) glass

standards was carried out. The agreement between the oxide values measured and the published values is excellent.

The Pacific Northwest Laboratory also carried out bulk chemical analysis of some of the samples described here as part of a study of the durability properties of the Intermediate Field test (IFT) waste form. Preparation of the samples was performed by $NaOH/Na_2O_2$ and KOH/KNO_3 fusions of samples ground to -200 mesh. The fusions were dissolved in deionized waster and analyzed by ICP-AES using standard procedures. The reported sum of the major element oxide data varied from 98 to 100.5 weight percent with the exception of sample IC048C90IW which had an 88 weight percent oxide sum.

Interlaboratory agreement of the data was checked by having duplicated samples analyzed by all of the laboratories. The agreement between the measurements made at the University of Idaho and PNL is excellent. Agreement between the data of the Separations and Analysis unit and both the other laboratories was not close in many cases. Since the PNL and University of Idaho data are in agreement, their oxide weight percent sums are close to 100%, and the University of Idaho methods were tested by blind analysis of three NIST glass standards, the data produced by these two laboratories are reported here except where noted.

X-ray powder diffraction analysis was carried out using an automated diffractometer equipped with a monochrometer and using Cu K_∂ radiation. The goniometer was used in step scan mode with 0.015 degree two theta per step and held one second per step. The goniometer scanned from 15 to 70 degrees two theta. CaF_2 was mixed with the powdered sample (< 100 mesh) and used as an internal standard. The data were automatically compared to the Powder Diffraction Files by computer match to obtain the identification of the crystalline compounds present in the sample. The compound identity selected by computer must be used with caution because compounds found in the ISV waste form are not necessarily those found in the computer file. The x-ray diffraction measurements were made by personnel in the Metals and Ceramic Unit, EG&G Idaho. Samples were also analyzed at the Idaho Geologic Survey/ Comer Laboratory and at PNL as part of the sample durability measurements.

Agreement among the three laboratories is excellent. Final interpretation of the data and compound identification was done by Jerry R. Weidner of the Waste Technology Development Department (WTDD) of EG&G Idaho using both the x-ray diffraction data and the microchemical data.

Apparent bulk density measurements of selected samples were performed by the Metals and Ceramics Unit, EG&G Idaho, using a standard procedure slightly modified from ASTM C-93-84 (the archimedean method). The procedure was tested using NBS 710 standard glass and achieved excellent agreement with the published values for this standard.

5.2.2 Results and Discussion

The products from Test Pits 1 and 2 are virtually identical and include several types of material. The outermost surface of the product was a grey-white, pebbly, and friable material, 1.27 to 1.91 cm (1/2 to 3/4 in.) thick, and was similar in both pits. This material is referred to as "rind," and is in direct contact with dark green-black glass on its inner surface (toward the test pit center) and loose soil on its outer surface. It is the calcined and sintered soil immediately adjacent to and in contact with the former melt. In general, the product from both pits consisted of a black (with green tints) glassy material containing variable amounts of bubbles and crystalline material. The amount of bubbles varied with position in the pits. Glass from the bottom of the pit generally contains less than 1 vol% bubbles, whereas glass from the upper regions of the pit near ground surface often contain greater than 90 vol% bubbles. Bubble diameter ranges from microscopic to several centimeters and the larger bubbles tend to occur within the glass areas having the largest portion of bubbles. Glass from the pit walls and top is generally dense and without voids adjacent to the rind, but becomes progressively more vesiculated toward the central cavity of the test pit. Some glass on the inner walls near the top of the pit are very vesicular (about 60 to 90 vol% vesicles as estimated by eye) and contain vesicles up to about 4 cm in diameter. The upper surface of the monolith, i.e., that surface in contact with gas in the bottom of the test pit central cavity, is similarly coarsely vesiculated (bubbly). In contrast, glass from the "glassy

boxes" (Test Pit 1) was generally without voids. Although the crystalline materials found in the products from the two test pits were very similar, the megascopic appearance of the materials was somewhat different. Glass was the principle phase found within the monolith. The outermost portion of the monolith, the most quickly cooled portion next to the "rind," was virtually pure glass (containing ≤2 vol% vesicles and opaque inclusions as estimated by eye). Grey spots, first appearing at about 10 cm from the monolith surface, increased in abundance (to about 60 vol% as estimated by eye) toward the interior of the monolith. The grey spots had a maximum diameter of about 3 mm. Examination of the spots using the scanning electron microscope, the petrographic microscope, and X-ray powder diffraction indicated that they were dendrites of crystalline material having a spherulitic structure and that small (<10μm) spherical metallic inclusions or bubbles often acted as nucleation sites.

Most of the material in the Test Pit 2 monolith was quite different in appearance from the black glass in the remainder of Test Pit 2 and all of the material in Test Pit 1. The Test Pit 2 monolith consisted of an outermost zone of black glass about 5.1 cm (2 in.) thick followed by an aphanitic white to beige zone and an aphanitic faint lavender porcelainous region 5.1 to 10.2 cm (2 to 4 in.) thick that graded into a phaneritic-appearing material. Examination using the transmitted light microscope and the scanning electron microscope indicated that the aphanitic materials were made of dendritic crystals (< 10μm) and glass. The phaneritic material constituted the bulk of the monolith. The phaneritic material had a green-black glassy matrix covered with up to 60% white spots that ranged in diameter from about 0.32 to 0.64 cm (1/8 to 1/4 in.). Figure 92 shows the texture of the Test Pit 2 monolith material. The spots are spherulites (i.e., 3-dimensional feather-like dendrites radiating from a common center) of dendritic crystals. A photomicrograph illustrating the typical dendritic microstructure is shown

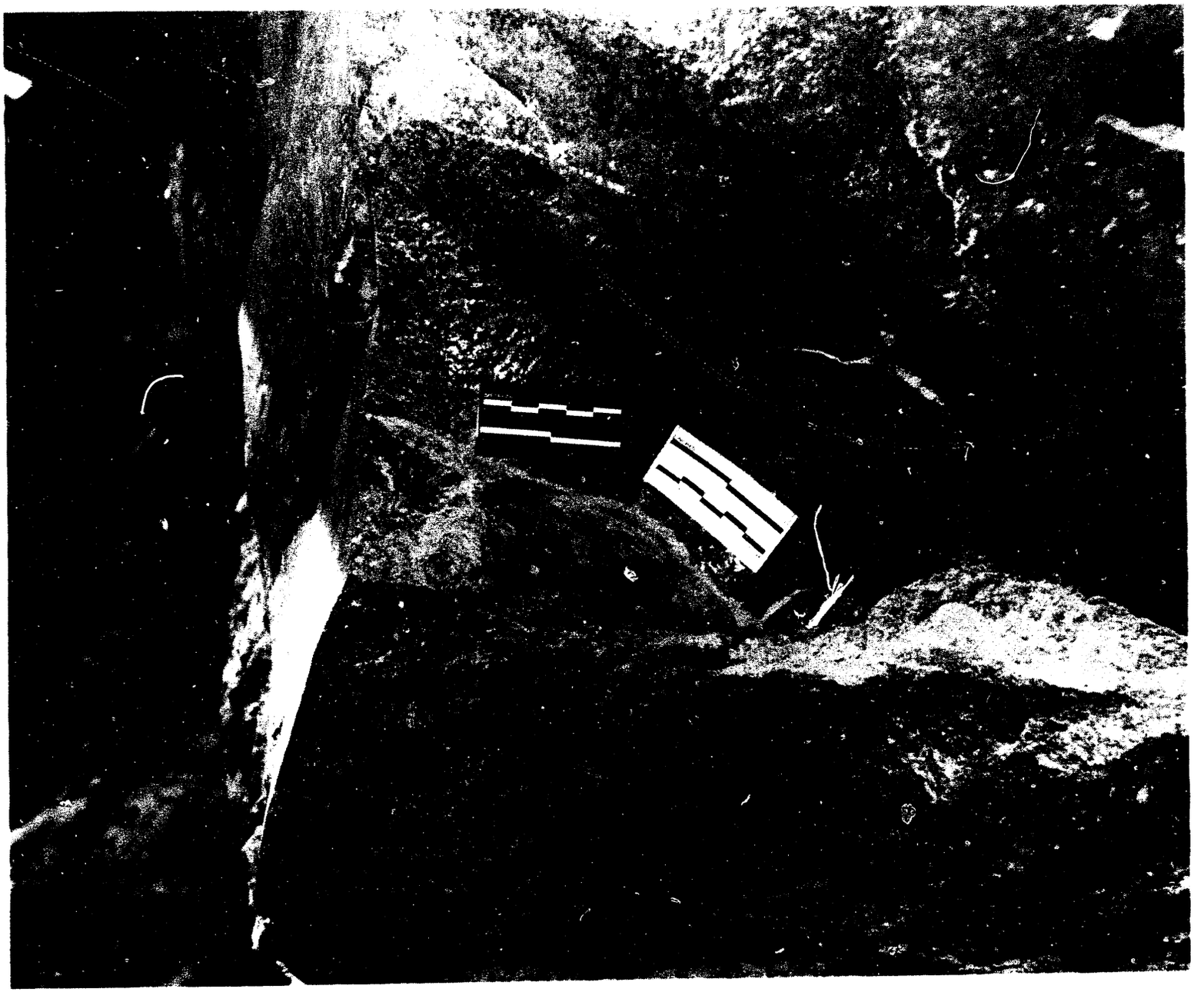

Figure 92. Test Pit 2 texture of vitrified monolith material.

in Figure 93. X-ray powder diffraction and microchemical analysis indicated that all of the dendritic materials found in both pits, indeed the only silicate mineral, was the mineral augite, a variety of clinopyroxene. Although quantitative analysis could not be made on individual crystals because the crystals were too small (<5μm) the data indicated that the crystals were chemically heterogeneous and zoned. Augite is a calcium-magnesium-iron rich silicate. The crystallization of this mineral caused the coexisting liquid to be enriched in sodium, potassium, aluminum, and silicon and depleted in calcium, iron, and magnesium. An example of magnesium depletion is illustrated by the x-ray photomicrograph Figure 94. Augite is a common, naturally occurring pyroxene found in volcanic rocks, such as the basaltic rocks found at the INEL, which have compositions and cooling histories similar to the vitrified material in the Intermediate Field tests reported here. The textural variations found between the test pits and within each pit are probably due to differences in cooling rate. Glass materials are the most quickly cooled and the phaneritic materials are the most slowly cooled. The heterogeneous nature of the crystals arises from the high rate of cooling of the test pit materials compared to the cooling rate required for equilibrium crystallization.

Twenty-three glassy samples were selected for bulk chemical analysis. Seven representative samples were selected from Test Pit 1; the remainder are from Test Pit 2. The data indicate that the bulk composition of all samples was virtually identical (within analytical uncertainty) and that the test materials were chemically homogeneous. The analyses are shown in Tables 17 and 18 with the analysis of a grab sample of INEL soil (<1 mm size fraction) from the Lost River Settling Area "A", which is just outside the boundary of the SDA, for comparison. Soil for the IFT test pits came from the Lost River Settling Area.

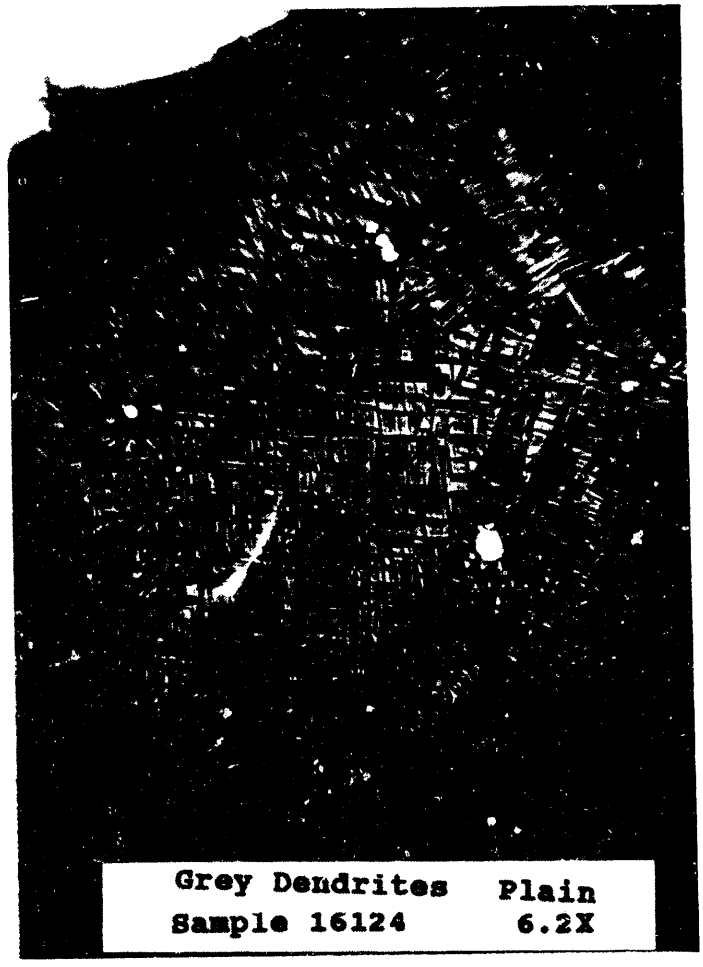

Figure 93. Typical dendritic microstructure showing glass (white) and needle-like augite crystals (photomicrograph white light, 6.2X), sample IC026I90I, Core #1 center of Pit 2 monolith, 28 cm below core top.

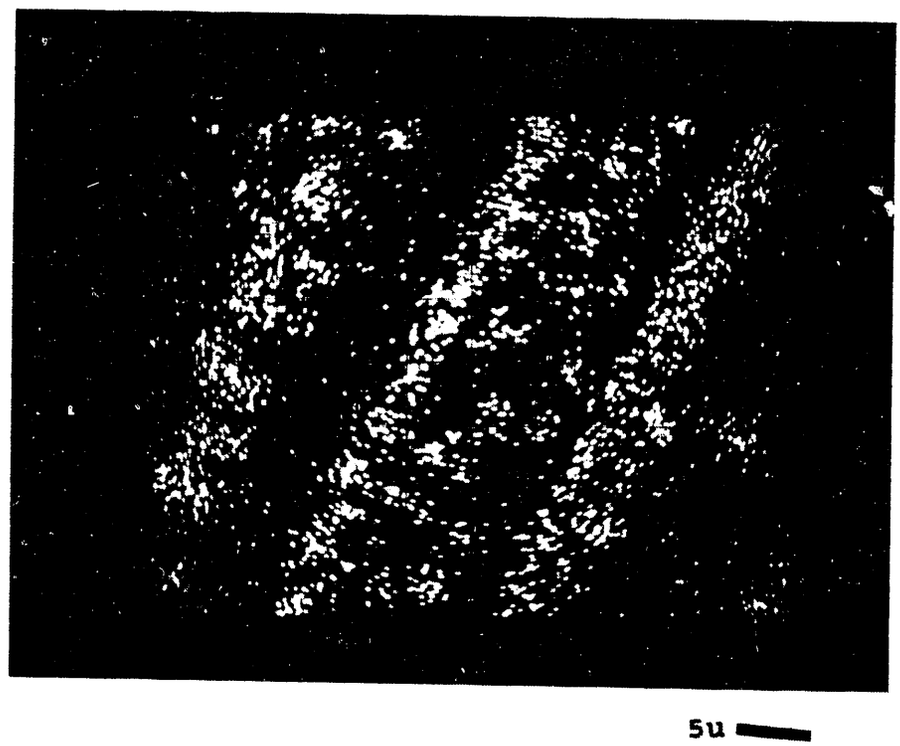

Figure 94. X-ray fluorescence photomicrograph (200X) showing magnesium concentration in dendrite crystals and depletion in glass matrix, sample IC026I90IE. Light areas show increased magnesium concentrations.

Table 17. Bulk composition of Intermediate Field Test Pit 1 Glass

Sample	Block Location	Oxide Weight Percent (SD) SiO_2	FeO	MgO	CaO	Al_2O_3	Na_2O	K_2O	Remarks
IC013C90IW	1	--	4.0	2.4	8.1	13.1	---	3.6	Glass, top of pit rim and edge
IC044B90IW[a]	2	63.6 (1.1)	4.7 (0.2)	2.8 (0.1)	8.6 (0.4)	13.4 (0.2)	1.2 (0.3)	2.8 (0.1)	Glass, top, central core (#5)
IC044D90IW[a]	3	66.6 (1.1)	4.8 (0.8)	2.7 (0.1)	9.0 (0.3)	12.9 (0.3)	1.2 (0.2)	2.8 (0.1)	Glass, dendrites core center
IC044H90IW	4	--	5.1	2.8	9.5	13.6	---	---	Glass, trace dendrite, core (#5) bottom
IC048B90IW[b]	5	65.6	4.4	2.6	8.8	12.5	2.0	3.1	Glass, top core #6
IC048C90IW[b]	6	65.3	4.2	2.7	8.5	12.5	2.7	3.2	Glass, dendrites, core #6, 30 cm below top
IC048H90IW	7	61.2	4.7	2.8	9.3	13.6	---	---	Glass,dendrites, core #6 bottom
Average		64.3	4.6	2.7	8.8	13.1	1.8	3.1	
INEL Soil[c]		71.0	4.3	2.3	7.5	12.2	0.3	2.5	

a. Electron-microprobe, University of Idaho, C. Knowles, analyst.

b. ICP-AES, Battelle North West, PNL.

c. Soil (<1 mm size fraction) from INEL Lost River Settling Area (EGG-WTD-9794) analysis.

analysis ---ICP-AES, Idaho Research Center, INEL, K. Messic, analyst.

Table 18. Chemical composition of Intermediate Field Test 2 Glass

Sample	Block Location	SiO_2	FeO	MgO	CaO	Al_2O_3	Na_2O	K_2O	Remarks
IC006C90IE	1	---	4.2	2.9	12.3	12.4	---	---	glass
IC007C90IE[a]	2	62.2	3.7	2.7	11.5	11.3	2.2	2.9	glass
IC026D90IE[b]	3	65.7 (0.5)	3.9 (0.1)	2.5 (0.3)	10.7 (0.4)	12.6 (0.5)	1.3 (0.3)	3.0 (0.05)	glass
IC026F90IE[b]	4	64.9 (1.8)	3.3 (0.9)	2.9 (0.9)	11.1 (0.8)	12.9 (0.1)	1.1 (0.1)	2.7 (0.2)	grey porcelain material
IC026I90IE[b]	5	64.6 (1.2)	3.9 (1.3)	2.0 (1.4)	11.1 (0.8)	12.8 (0.4)	1.2 (0.1)	2.8 (0.1)	aphanitic and spherulitic material
IC026M90IE65	6	7.7	4.1	2.6	10.7	11.8	1.5	2.5	glass and devitrifies material
IC027D90IE7	7	59.0	---	---	10.5	11.6	---	2.4	glass, top core #2
IC037B90IE[a]	8	64.3	3.9	2.6	10.7	12.2	2.3	3.2	asphanitic and devitrified material
IC037D90IE	9	56.5	---	---	11.4	13.3	---	2.5	devitrified glass
IC037F90IE	10	58.8	---	2.7	11.2	11.9	1.5	2.7	devitrified glass, core #2, 27 cm below IC037D90IE
IC038B90IE[a]	12	63.6	3.4	2.7	10.9	12.0	2.4	3.1	glass, top core #3, 46 cm NE core #1
IC038C90IE[a]	13	64.4	4.0	2.7	10.5	12.0	2.7	2.9	devitrified glass, ≈7 cm below IC038C90IE
IC038D90IE[a]	14	63.1	3.9	2.6	10.7	11.9	2.0	3.0	glass and spherulites, 46 cm below IC038B90IE

Table 18. (continued)

Sample	Block Location	SiO_2	FeO	MgO	CaO	Al_2O_3	Na_2O	K_2O	Remarks
IC043D90IE	15	60.3	---	2.7	11.2	12.1	1.5	2.7	glass, top core #4, 1.3 m NE core #1 inline with cores #1 & 2
IC043F90IE	16	---	4.2	2.6	10.7	11.7	2.6	2.6	glass dendrites core #4, 34 cm below IC043D90IE
IC043J90IE	17	58.2	---	2.8	---	14.4	---	2.6	grey, asphanitic material, bottom core #4, ≈63 cm below top
IC086C90IE[b]		62.9 (1.5)	3.8 (0.2)	2.6 (0.1)	1.3 (0.4)	12.6 (0.5)	1.1 (0.3)	2.6 (0.1)	melt sample
Average		62.0	3.9	2.6	11.0	12.2	1.8	2.8	
INEL Soil[c]		71.0	4.3	2.3	7.5	12.2	0.3	2.5	

a. ICP-AES, Battelle North West, PNL.

b. Electron-microprobe, University of Idaho, C.Knowles, analyst.

c. Soil (<1 mm size fraction) INEL Lost River Settling Area (EGG-WTD-9794); normalized volatile-free analysis-ICP-AES, Idaho Research Center, INEL, K. Messic analyst.

The data indicate that the ISV test product is identical to the INEL soil except for the greater quantity of silica and lesser amount of sodium in the soil grab sample, presumably indicating that the grab sample contains slightly more quartz and less feldspar. Note also that the composition of the "melt sample," IC086C90IE, is virtually identical to the average value. The "melt sample" was collected by pushing a 2.4 cm (1 in.) steel rod directly into and then withdrawing it from the still molten silicate material immediately following the termination of Pit 2 processing. The sample was taken from the material adhering to the rod. The close agreement between the average values and the "melt sample "values indicates that such melt sampling and subsequent rapid chemical analysis provides an excellent first-look data set for predicting the composition and, therefore, the properties of the monolith before it has cooled. This suggests that the composition analysis of a full-scale melt could be taken, analyzed, and modifications could be made to the melt by additives during processing.

The bulk density values of seven glassy samples from both pits (see Table 19) are also nearly identical and also show that the test pit materials are homogeneous. The minor density variations are probably due to the variation in the number of bubbles and metallic inclusions in the samples.

Three distinguishable classes of metallic materials are found in both pits. One category is the metal found with the shape of the original scrap, i.e., cans, bars, plates, sheets, turnings, and various artifacts of mild steel, carbon steel, and stainless steel. This class of metals was not melted during ISV processing, otherwise the original morphology would have been destroyed. In general, cans, turnings, and sheet stock (thinner than about 1 mm) were not observed within the monolith and probably were dissolved/melted when incorporated into the melt. The unmelted metal within the lithified (previously melted) regions appeared to be only the massive pieces of scrap metal such as machine parts or thick plates. The massive metal scrap is concentrated into the lower one-quarter of the monoliths, suggesting that some of the metal settled toward the bottom of the silicate melt pool. The second class of metal occurs as megascopically observable spherical particles to nodular lumps. This morphology indicates that these materials have undergone some transformation, most likely melting, during the ISV processing. Because

Table 19. Intermediate Field Test glass density

Sample	Block Location	MEAN DENSITY (sd) gr/cm^3	Remarks
IC026M90IE (Pit 2)	6	2.619 (±0.002)	glass and dendritic material, core #1, Pit 2, ≈54 cm below top
IC027D90IE	7 (Pit 2)	2.550 (±0.001)	glass, top of monolith core #2, 43 cm south of core #1, Pit 2
IC037D90IE	9 (Pit 2)	2.624 (±0.003)	devitrified glass, core #2, ≈38 cm below top
IC044F90IW	3 (Pit 1)	2.538 (±0.001)	glass and dendritic material core #5 center of Pit 1 monolith, 28 cm below top
IC044H90IW	4 (Pit 1)	2.526 (±0.001)	glass and dendritic material core #5, Pit 1,≈56 cm below top
IC048D90IW	5 (Pit 1)	2.520 (±0.002)	glass, top of core #6, 76 cm NNW of Pit 1 central core
IC087A90IE	--	2.539 (±0.004)	glass, melt sample, Pit 2

the megascopically observable metal was found associated with unmelted and partially melted scrap metal, for example in the glassy boxes, some of it was apparently produced by melting the scrap metal. This interpretation is also indicated by the chemical analysis (see Table 20) which shows that some of the metal contains chrome and nickel, an indication of melted stainless steel scrap. Nodular lumps of metal are concentrated at the base of the monolith below the electrodes. The nodular lumps are aggregates of spheres and are predominantly iron with minor amounts of chromium, nickel, and non-metallic inclusions. Chemical analysis of this material is included in Table 20. The spacial association of the metal lumps with the electrodes suggests that the high temperature and reducing nature of the graphite electrodes reduced ferrous iron dissolved in the silicate melt to the metallic state in a manner analogous to the industrial production of steel using the electric furnace. The density contrast between iron and silicate probably caused the molten metallic iron to settle to the bottom of the silicate melt pool. Figure 95 shows an example of the metallic balls formed below electrodes. The third class of metallic materials includes the microscopic (<10 μm) spheres of opaque metallic material, mostly metals, found in all samples that were examined in detail. Usually the amount of opaque material is one volume percent or less (as observed in thin-section using the petrographic microscope and estimated by eye). Microchemical analysis indicates that the composition of the opaque particles is often complex (see Table 20). The most common opaque particles include (a) virtually pure metallic iron, (b) iron phosphide, probably Fe_3P, (c) complex spheres having an iron core and an iron phosphide rim, and (d) iron alloys containing small amounts of chromium and nickel, probably derived from stainless steel in the scrap metal.

5.3 Product Durability

There are currently no specific durability specifications established for ISV waste forms. The minimum expected testing requirements will be those currently established for RCRA hazardous materials landfill disposal, the Toxicity Characterization Leach Procedure (TCLP). Passing the appropriate

Table 20. Composition of Intermediate Field Test metals

Sample	Block Location	Weight Percent Fe	Al	Cr	P	Ni	Remarks
IH037J90IE	11 (Pit 2)	80.3	7.21	3.8	0.5	6.3	massive metal and traces of glass, bottom of core #2, Pit 2 monolith
IH061D90IW	8 (Pit 1)	96.9	3.5	1.5	0.2	0.9	nodular metal from the bottom center of Pit 1 monolith
IH074D90IE	18 (Pit 2)	96.1	6.1	0.4	0.2	0.8	nodular metal from the bottom of Pit 2 monolith, 1m. toward monolith center from the NE corner
IC007D90IE[a]	2 (Pit 2)	100	ND	ND	1.2	ND	opaque inclusion in glass, lower "funnel"≈1.5m. below ground surface Pit 2
IC026D90IE[a]	3 (Pit 2)	94.1 77.0	ND ND	ND ND	1.3 25.2	ND ND	opaque inclusions in glass, top of center monolith core #1 Pit 2 monolith
IC086C90IE[a]	--	90.5	ND	ND	21.3	ND	opaque inclusion in glass, melt sample, Pit 2

a. Electron-microprobe, University of Idaho, C. Knowles, analyst

ND not detected
analysis---ICP-AES, Idaho Research Center,INEL, K.Messic, analyst

Figure 95. Metallic balls in Test Pit 2.

test only classifies the waste form as RCRA-regulated for TCLP characteristics. However, the TCLP does not: (a) address radioactive waste components, (b) provide a technical basis for assessing long-term durability, (c) provide a basis for a comparison to highly durable waste forms or natural analogs, or (d) provide an assessment of the source term release rate of the waste component for risk assessment models. To provide this information, additional durability tests must be conducted. These additional tests fall into two categories: comparative testing (comparing ISV waste forms to similar waste forms and natural analogs) and testing to determine the forward rate of waste form dissolution (k_+). Each category of durability testing is discussed in detail in the following subsections. A detailed account of the method development, procedures, results, and calculations is presented else where.[12]

For each type of durability testing, all major phases within the ISV monolith were tested, if possible. Where multiple phases could not be separated, such as when devitrification produces an intimate mixture of different small grain crystalline phases, these phase mixtures were tested as a single phase.

5.3.1 Toxicity Characteristic Leach Procedure (TCLP)

The required regulatory testing for retention of waste components is the TCLP test. Waste is hazardous by definition if it displays the characteristics of ignitability, reactivity, corrosiveness, and/or TCLP toxicity. After being formed at temperatures greater than 1300°C, the ISV waste forms are neither ignitable, reactive, nor corrosive. The TCLP test is designed to simulate the rainwater leaching process a waste would undergo if disposed of in a sanitary landfill.

The TCLP is designed to simulate rainwater leaching of certain metals from landfill wastes. The testing consists of extracting 100 g of crushed waste form with 1600 g of deionized water (DIW). One of two acetic acid

Table 21. Maximum concentrations allowed for TCLP and testing results.

	SAMPLE IDENTIFICATION NUMBER						
Element	IH064B90IE	IC066B90IE	IC068B90IE	IC069B90IE	IC052B90IW	IH053A90IW	Max. Conc. (µg/L)
Arsenic	<250	<250	<250	<250	<250	<250	5000
Barium	44.0	64.7	77.8	57.0	50.7	76.8	100000
Cadmium	26.0	<5.0	<5.0	5.9	7.3	34.1	1000
Chromium	1960	8.4	<5.0	8.2	11.1	532	5000
Lead	<150	<150	<150	<150	<150	<150	5000
Mercury	0.08	0.31	0.56	0.32	0.21	0.15	200
Selenium	<300	<300	<300	<300	<300	<300	1000
Silver	<10.0	<10.0	<10.0	<10.0	<10.0	<10.0	5000

extraction fluids (pH 2.88 ± 0.05 or pH 4.93 ± 0.05) are used and the temperature is maintained between 20 and 40°C. The duration of the TCLP is 24 hours. The extract is then analyzed by ICP or Atomic Absorption Spectrometry (AA) (Hg and Cs). The maximum concentrations allowed for inorganic elements are listed in Table 21 with the results from the samples from the two pits. No organic will be present in the glass due to the high ISV processing temperatures; therefore, the organic analysis portion of TCLP is not required.

Samples of both glass/crystalline and metal phases were taken from various parts of the waste forms. A description of these samples is presented in Table 22. There was no hazardous materials placed in the pits. However, some of the materials placed in the pits and the soil have small amounts of TCLP metals in them (i.e., barium in the soil and chromium in the stainless steels). TCLP testing was conducted to document that the ISV waste form could be disposed of in a landfill. The data summarized in Table 21 demonstrate that the samples do not exhibit hazardous characteristics of TCLP toxicity. In most cases, the TCLP results are below detection limits or 10 to 100 times lower than the maximum acceptable concentrations. The two metal samples, IH064B90IE and IH053B90IW, have concentrations 10 to 40% of the maximum acceptable concentration for chromium. This is thought to be due to the stainless steel in the samples.

5.3.2 MCC-1 and MCC-3 Testing

To provide a scientific basis for evaluating the short- and long-term durability of ISV waste forms, additional testing will be required. While the TCLP test satisfies compliance with EPA requirements for hazardous waste disposal, this test has little value in quantifying the release characteristics of the ISV waste form. The waste form produced from the ISV process is similar to a number of natural analogs, and also the waste forms evaluated for high-level nuclear waste. By comparing test results for ISV waste forms to other well documented waste forms and to natural analogs, a baseline can be established for assessing the durability of the ISV waste forms.

Table 22. Description of samples used in TCLP testing

Sample Number	Description
IH064B90IE	Metal sample taken from Pit 2 from approximately 3 feet into monolith on north side and bottom. Large magnetic metal chuck of molten metal with glass adhered to the metal in crevasses glass covers 20% of the surface.
IC066B90IE	Crystalline, aphanitic, very pale purple, porcelain-like material from Pit 2, bottom level, east side.
IC068B90IE	Bottom of Pit 2, east side of melt, darker green glass (with less than 1% of the total sample consisting of small white phase). Small gas bubbles the glass, grayish glass interfacing with green glass, also glass looks like it was next to some metal and has very small amount of rust-colored flecks.
IC069B90IE	Course texture of approximately 1/8 in. crystals that are green, gray and greenish gray in color, with irregular grain pattern. Taken from Pit 2 east side of pit at bottom of melt.
IC052B90IW	Random glass sample taken from storage boxes from Pit 1.
IH053A90IW	Random metal sample from Pit 1 pulled from storage box. Metal was molten at one time during the test. Sample was magnetic and has some glass fixed to them. They are dull, metallic-gray in color.

To allow for direct comparison of waste forms, the test method, leachate, temperature, and surface area/volume (S/V) used in testing the ISV waste form should be the same as those used in testing glass waste forms chosen for high-level nuclear waste. The differences in application (repository conditions such as groundwater saturation and temperature) and the nature of the waste form (multiphase ceramic-glass versus single-phase glass) make such comparisons difficult. Most high-level nuclear waste glasses have been tested at 90°C. The MCC-1 and MCC-3 test methods were originally developed, and the current procedures written, for application to high-level waste repositories in deep geological environments. The primary applications of the MCC tests will be to compare ISV waste forms and will have limited utility for mass transport analysis. By conducting the MCC-1 and MCC-3 leach testing at 90°C, the results can be compared to the existing large data base of leaching data on the high-level glasses. The MCC tests will be used because of the large data base of data glassy materials.

To allow comparison of leach tests results from waste forms with different compositions, results are given in terms of normalized elemental mass release for the MCC-1 and MCC-3 tests and normalized concentration for the modified MCC-3 test.

The MCC-1 static leach test[13] measures the elemental mass loss of a glass sample as a function of time. For this test, a glass monolith is suspended within a sealed Teflon™ container. The surface-area-to-volume ratio (surface area of sample/volume of leachant, S/V) of 10 m^{-1} was used. The leachant was deionized water (DIW). The sealed containers were maintained at 90°C for 7, 14, 28, and/or 90 days. The test results are based on leachate elemental analysis from which the total concentrations of materials leached from the sample are determined. The most commonly used test parameters are an S/V of 10 m^{-1} in DIW at 90°C for 28 days. These were used for ISV testing to allow for comparison with the largest amount of data. One drawback to this type of test is that the MCC-1 procedure requires a small monolith of sample. Inhomogeneities in the test samples, such as varying amounts of exposed crystalline phases or metals, may result in inconsistent results.

5.3.3 MCC-3

The MCC-3 agitated powder leach test[14] is similar to the MCC-1 test procedure, with two exceptions: the glass is in a powdered form, and glass powder and leachant are agitated by rotating the Teflon container in which the sample is placed. The elemental leachate concentrations from MCC-3 tests are estimated to be representative of longer-term (more saturated leachates) extrapolation of MCC-1 test results. This objective is achieved more rapidly in the MCC-3 test because higher S/V ratios are used than those used for the MCC-1 tests. For evaluation of ISV waste forms, tests were conducted with an S/V of 1000 m^{-1} in DIW at 90°C for 28 days (a large amount of 7 to 90 day data also exist). Because of the higher S/V used in the MCC-3 testing compared to that used for MCC-1 testing (2000 m^{-1} and 10 m^{-1}, respectively), the leachants in the MCC-3 tests became saturated much sooner than the leachants in the MCC-1 tests. This saturation slows the dissolution process. Therefore, direct comparison of normalized release values from the MCC-1 and MCC-3 tests is not appropriate. Because a powdered sample is used for the MCC-3 tests, combinations of glass and devitrified phases may be tested together. At this time, a modified MCC-3 test called the Product Consistency test (PCT)[15] is now the standard test MCC-3 method being used.

Previous testing of samples from the ISV laboratory scale test ES-4 had shown that allowing leachates to cool to room temperature prior to filtering and acidification may result in the precipitation of secondary phases in the leachates. To prevent this, the IFT samples were treated in a different manner as follows: the container was removed from the leaching oven and weighed, then placed in a pre-heated metal block machined to fit the knurled leach containers. Immediately, 10 mL of leachate (each) was filtered, using a 0.45 μm filter, and placed in three polyethylene vials. The pH was then measured of the remaining leachate in the container. The temperature was measured immediately after pH measurement and the temperature was found to be 75 ±5°C. The pH was also remeasured at room temperature. As before, two of the leachates were acidified, one for inductively coupled plasma atomic emission spectroscopy (ICP-AES) analysis and another for storage. The unacidified sample was analyzed by ion chromatography (IC).

5.3.4 MCC-1 and MCC-3 test Matrix

A series of closed-system, isothermal experiments were designed to elucidate the dissolution behavior, alteration phase formation, and elemental solubilities for the INEL ISV glasses. The test matrix is given in Table 23. Three different surface area-to-volume (S/V) ratios were investigated with overlapping (S/V)·time as illustrated in Figure 96. This range was selected so that sufficient glass reaction occurs to saturate the leachate with respect to the major elements of concern. The 10 m^{-1} experiments were performed with the MCC-1 method and the higher S/V tests used the modified MCC-3 test, PCT. The test matrix shown in Table 23 was performed in its entirety for samples IC007C90IE, IC027B90IE, IC038C90IE, and IC048B90IW. Samples IC038B90IE, IC038D90IE, and IC048C90IW were tested in triplicate for 28-day duration using both MCC-1 and PCT test methods. A short description of each of these samples is found in Table 24. The elemental and $Fe^{+2}/\Sigma Fe$ for these samples (as analyzed at PNL) are reported in Table 25.

At the present time, only experiments at 90°C in deionized water have been conducted. Although 90°C is far above the expected temperature range where the ISV waste form may be contacted by water, the elevated temperature permits the more rapid formation of crystalline alteration products that may be identified by surface analysis techniques and gives a greater extent of alteration in a short period of time. Both of these factors simplify comparison of the experimental results and model with model predictions. It has also been recently demonstrated that the basic mechanism of the reaction of a complex waste glass with water does not change up to 200°C.[16] Also, 90°C has been a *de facto* standard for the majority of dissolution experiments that have been conducted with nuclear waste glasses. Comparisons of the performance of INEL ISV glasses with this extensive database are facilitated by using the same conditions. However, low temperature experiments should be planned in future work to validate the model at lower temperatures.

The results from both MCC-1 and PCT tests with the IFT samples are shown in Figures 97 and 98. Only results from 7 & 28 day duration experiments are available at this time. However, the data do show differences

Table 23. Static testing for ISV product evaluation

				No. tests				
Material	test	S/V, m^{-1}	Temperature	7d	14d	28d	56d	91d
ISV Glass	MCC-1	10	90°C	1	3	1	1	3
Blank				1	1	1	1	1
ISV Glass	PCT	100	90°C	3	1	3	1	3
	PCT	1000	90°C	3	1	3	1	3
Blank				1	1	1	1	1

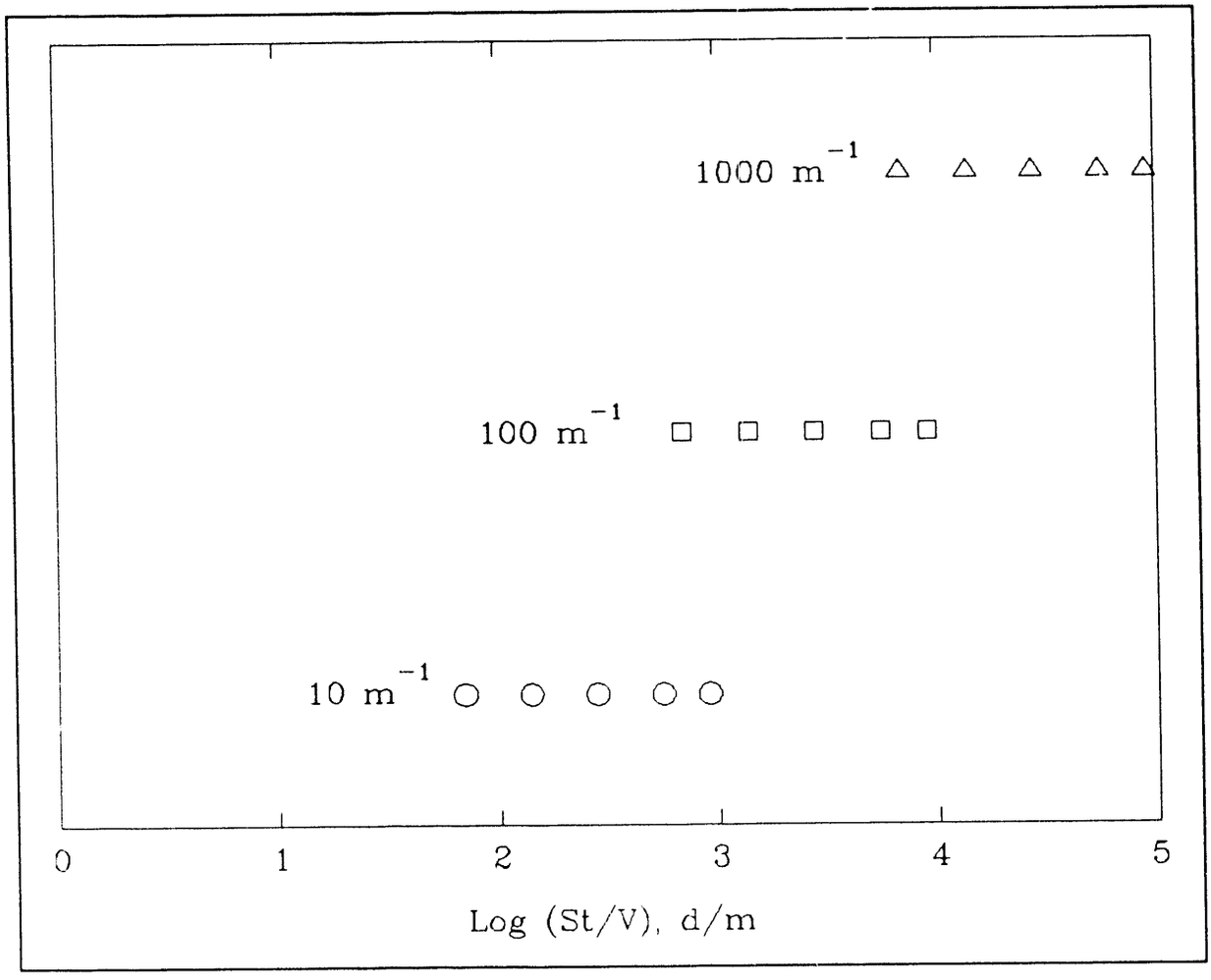

Figure 96. Range of glass surface area/leachate volume times time (ST/V) values used to investigate the static dissolution behavior of INEL ISV glasses.

Table 24. Description of samples used in durability testing

Sample Number	Description
IC007C90IE	ISV Pit 2 Glass sample from lower "funnel" taken from east side. Very dark green glass with 3% of volume being gas bubbles <2 mm. The glass interfaces with two different substances (a) a light gray hard substance resembling dirt and (b) small undissolved pieces of rocks.
IC027B90IE	Core Pit 2, hole two taken from a larger piece of core material located at bottom of core. Neutral gray glass that is not see-through, makes up 50% of the composition. Large crystals are mixed in with the neutral gray glass. Crystals are 3 mm to 5 mm in width; they are slightly darker gray/green glass covering 50% of the surface area.
IC038B90IE	Pit 2, third hole, 18" NE of hole 1, drilled to 2'-3 1/4", 5 cm to 13.5 cm down from top of core. The top is dark-green shinny glass with gas bubbles of different sizes and shapes. Top of green glass is where gas bubbles have come to the surface. A 90% gas interface with bubbles. Bottom of sample has gas bubbles 1 cm x 1.5 cm and smaller covering 5% of the surface area. Medium gray crystals mixed in with the green glass, covers approximately 2% of the surface, ranges in size from 1 cm to 1.5 cm. The bottom of the sample is optic & medium-grayish green.
IC038C90IE	Pit 2, third hole, 18" NE of hole one; top of sample is optic grayish-green glass. Medium gray crystals are mixed with the green glass (approx 2% of the surface, ranging in size from 1 cm to 1.5 cm). Gas bubbles are 1.3 cm x 2 cm in diameter and make up 25% of surface. Three metal beads are located near the center; they are magnetic and are <1 mm in diameter.
IC038D90IE	Pit 2, third hole, 18" NE of hole one, 1'-6" from top of core. Neutral gray, medium gray, and green crystals, 5 mm to 1 cm in size. Gas bubbles make up <1% of surface, size <1 mm.
IC048B90IW	Pit 1 core 6, depth 1'-10" (core depth), 1'- 4" recovered. North-northwest of center core #5. Glassy phase, gas bubbles cover 30% with size of 1 cm x 2 cm to 1 mm. Medium gray crystals mixed in with the glass (approximately 25% of the surface, <1 mm in diameter).
IC048C90IW	Pit 1 core 6, 12" from top of core. Glassy phase with gray crystals 1 mm in diameter cover 50% of the surface area. Gas bubbles are <1 mm in diameter and make up <1% of the surface mass.

Table 25. Bulk chemical analysis of IFT samples

Oxide	IC007C90IE	IC027B90IE	IC038B90IE	IC038C90IE	IC038D90IE	IC048B90IW	IC048C90IW
Ag_2O	0.00	0.00	0.00	0.00	0.00	0.00	0.00
Al_2O_3	11.30	12.20	12.00	12.00	11.90	12.50	12.50
BaO	0.40	0.09	0.09	0.09	0.09	0.09	0.09
CaO	11.50	10.70	10.90	10.50	10.70	8.77	8.48
Cr_2O_3	0.00	0.26	0.27	0.26	0.26	0.13	0.14
FeO	3.68	3.94	3.36	3.96	3.90	4.42	4.21
Fe_2O_3	0.47	0.17	0.79	0.22	0.24	0.19	0.39
K_2O	2.90	3.20	3.10	2.90	3.00	3.10	3.20
MgO	2.70	2.60	2.70	2.70	2.60	2.60	2.70
MnO	0.08	0.19	0.19	0.19	0.19	0.13	0.13
Na_2O	2.15	2.30	2.40	2.70	3.18	2.00	2.70
SeO_2	0.00	0.00	0.00	0.00	0.00	0.00	0.00
SiO_2	62.20	64.30	63.60	64.40	63.10	65.60	65.30
SrO	0.03	0.03	0.03	0.03	0.03	0.03	0.03
TiO_2	0.54	0.58	0.58	0.57	0.58	0.61	0.62
TOTAL	97.95	100.56	100.01	100.52	99.77	100.17	87.99
Fe^{2+}/Fe	0.897	0.963	0.827	0.952	0.947	0.963	0.924

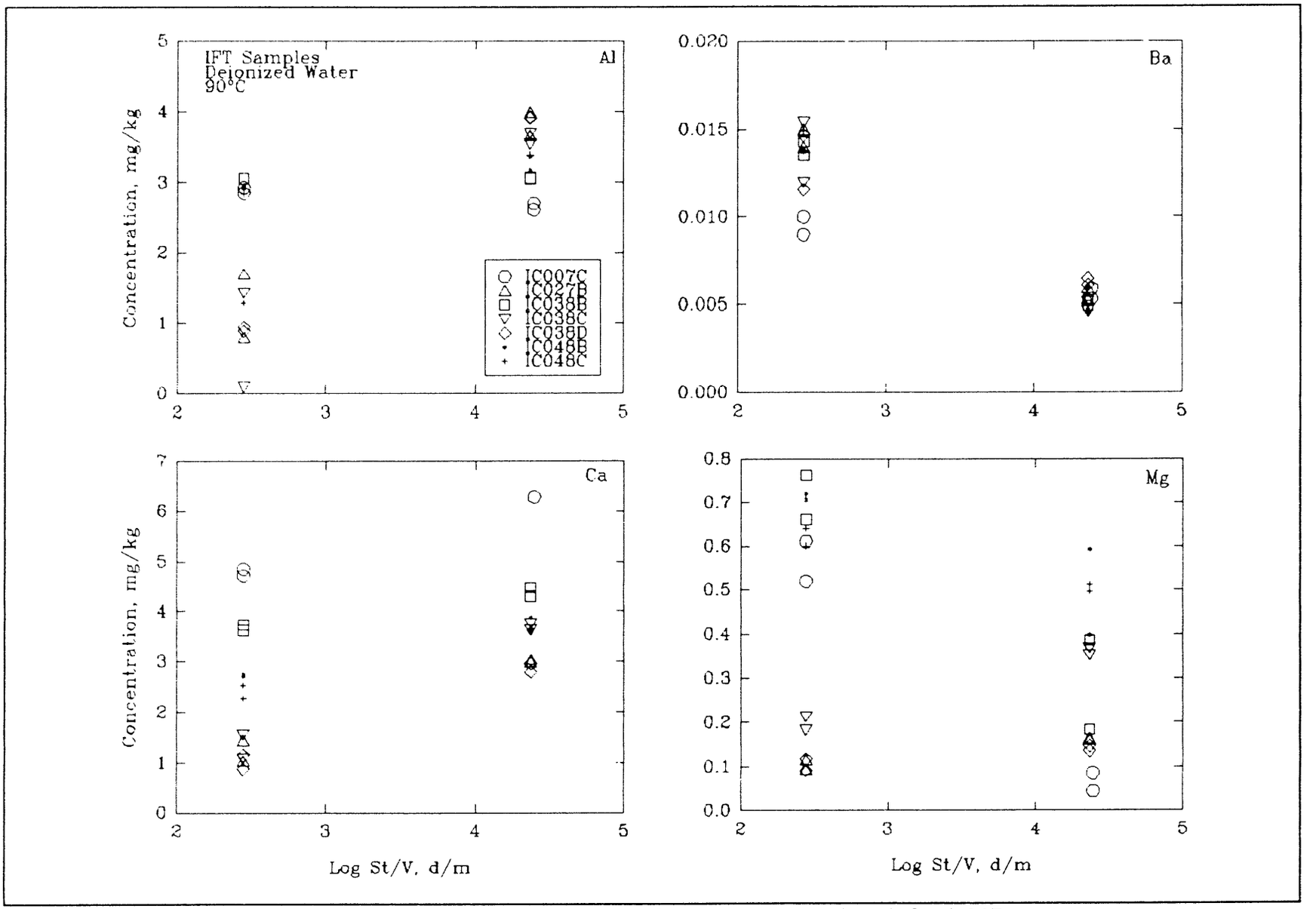

Figure 97. Release of selected elements from IFT samples in MCC-1 and modified PCT tests.

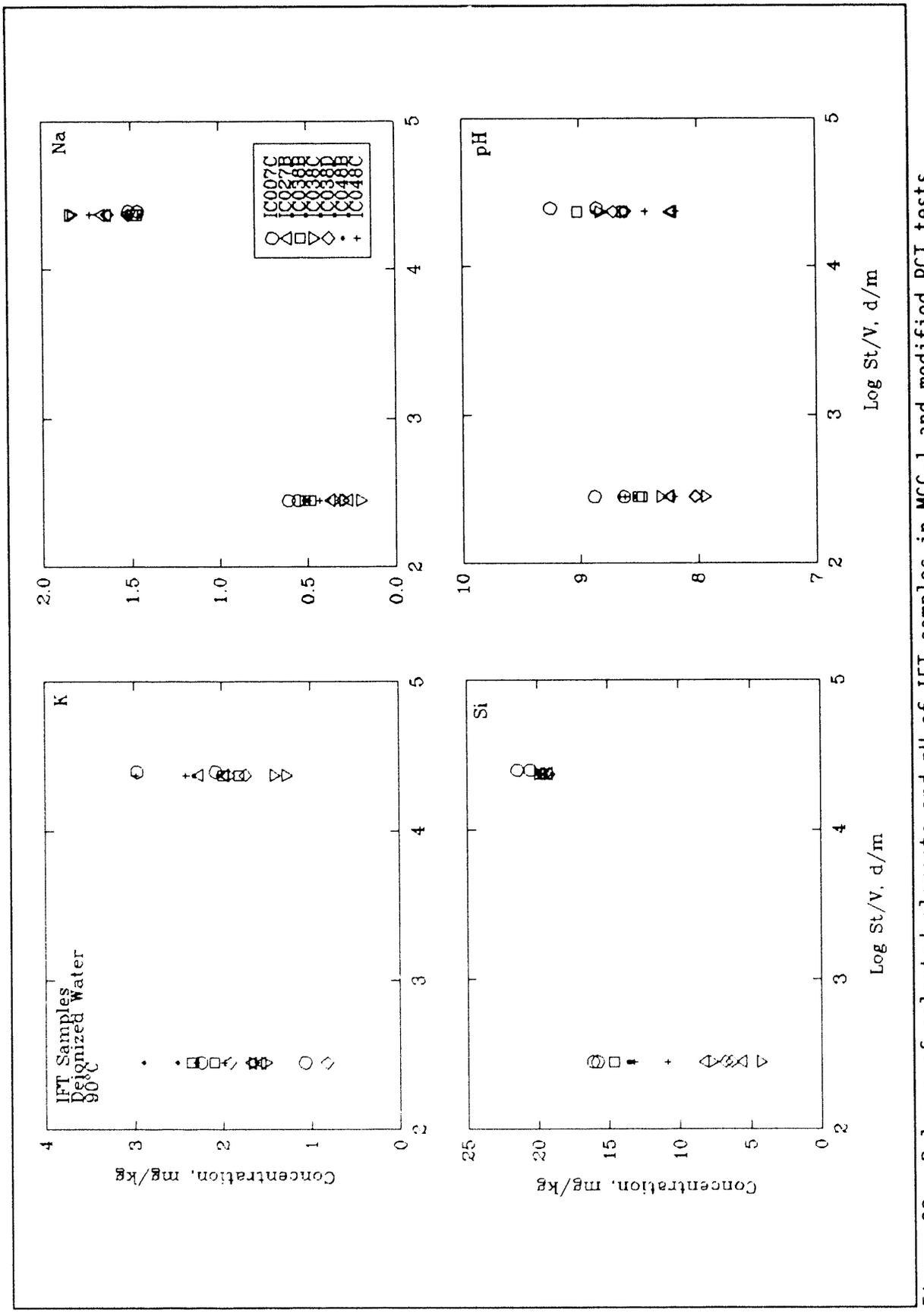

Figure 98. Release of selected elements and pH of IFT samples in MCC-1 and modified PCT tests.

among the field samples that appear to correspond to the degree of crystallinity in the samples. While not statistically differential, the trend appears to be consistent. Sample IC038C90IE appeared to the eye to be completely devitrified and this sample shows consistently lower releases for Ca, Mg, Al, and Si compared with sample IC007C90IE that analyzed X-ray amorphous. The releases of Ca and Mg are as much as 2 to 3 times smaller for the other devitrified samples. Because most of the ISV monolith is devitrified, these lower release rates for the devitrified phase of the ISV waste form may result in a lower source term for heath-based risk assessments.

Table 26 and Figure 99 compare MCC-1 and MCC-3 results for the IFT ISV waste form with typical high-level nuclear waste glasses and natural analogs. The IFT waste form is comparable to obsidian and granite, and 4 to 10 times more durable (based on MCC-1 testing) than typical high-level nuclear waste glasses.

Table 26. Comparison of MCC-1 data for IFT, other waste forms and Natural Analogs

SAMPLE	Normalized Concentration g/m^2
IC07C90IE	5.50
IC027B90IE	2.33
IC038B90IE	4.93
IC038C90IE	1.97
IC038D90IE	2.22
IC048B90IW	4.43
IC048C90IW	3.95
IFT AVERAGE	3.62
High Level Waste Class	16
ISV Hanford Soil	4
Pyrex	1.3
Obsidian	1.2
Granite	0.98

5.3.5 Intrinsic Rates of Dissolution

The fastest rate at which a glass/ceramic will dissolve is the forward rate of dissolution (k_+). This glass parameter has the most technical

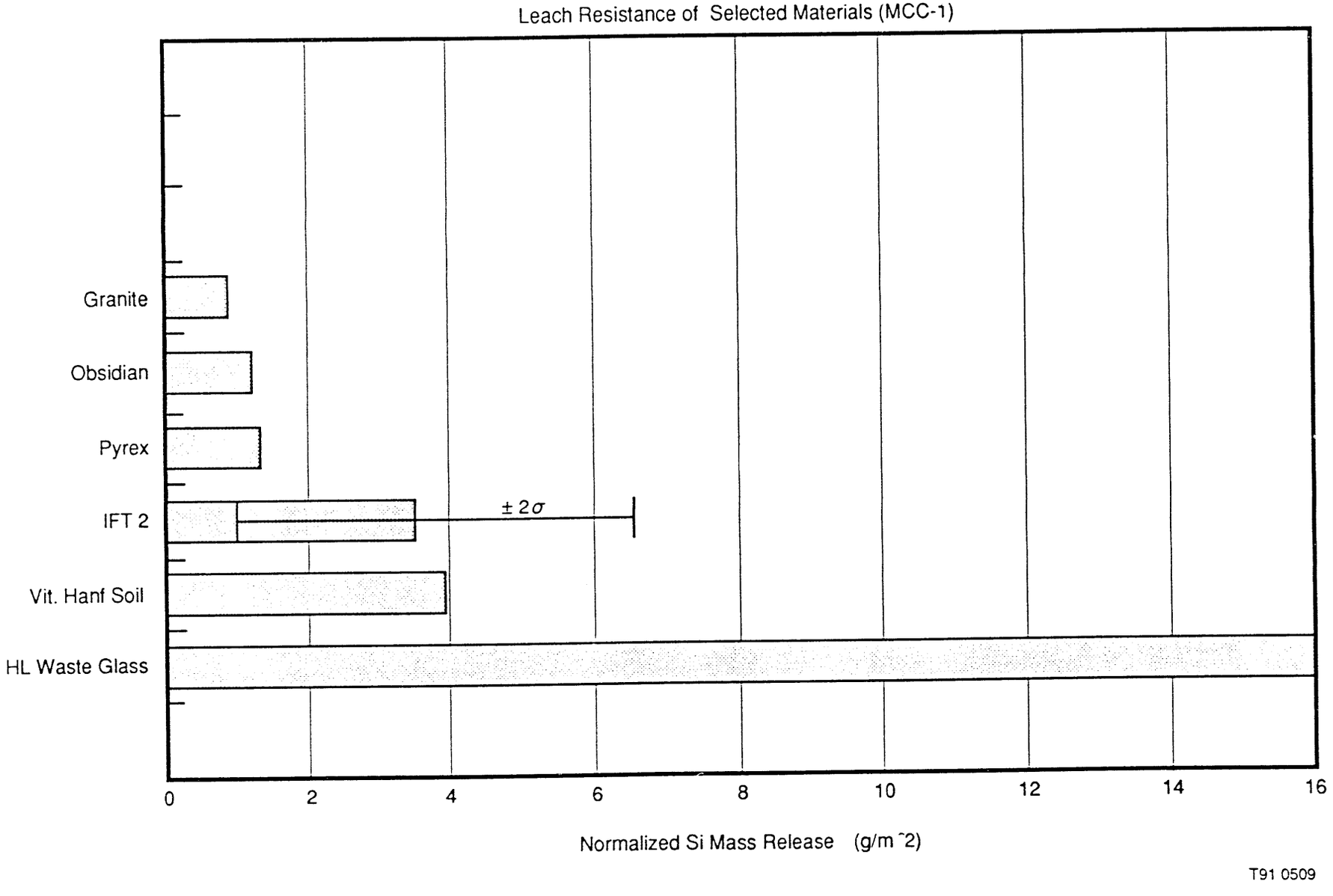

Figure 99. Comparison of durability of ISV samples based on MCC-1.[17]

relevance when evaluating and predicting the dissolution (durability) behavior of the glass (see Reference 9).

To understand the forward rate, it is beneficial to discuss the three different regimes typically observed in glass dissolution: (a) the period in which the glass first contacts a leachate and the glass dissolution rate is uninhibited by any solubility effects, (b) a transient regime where the increasing concentrations of dissolved glass components in the leachate slows the dissolution rate through solubility effects, and (c) a steady-state regime in which the dissolution rate is constant because alteration processes (saturation) have reached a steady-state. Typical release data can be plotted as the elemental concentration in the leachate versus (S/V) · time, which shows these different regimes. This behavior can be understood by considering what happens at the beginning of glass dissolution (no saturation effects) and under conditions where the leachate has high concentrations (near saturation) of dissolved glass or groundwater components.

At both ends of the dissolution curve, there are linear portions at which the dissolution rate is linear. At early times, the glass matrix dissolves with the forward dissolution rate (k_+) because there is nothing in solution or on the surface of the glass to impede the dissolution process. The forward dissolution rate is the slope of the linear portion of the curve at low saturation smaller values of (S/V) · t. As the leachate becomes saturated, the dissolution rate of the glass decreases. These are the slower rates observed in a static test, such as MCC-1 and MCC-3.

Low values of (S/V) · t (and the resulting solution concentrations) are analogous to the ambient (low solution saturation) conditions expected for the ISV waste form as unsaturated surface water percolates past the waste form. Data obtained over this range of (S/V) · t products can be used to compare the relative chemical durability behavior of glasses in a way that is more relevant than a single static test condition which may be in the transient regime. Because the ISV waste form will be in a near-surface environment where water flow rates could be postulated to a relatively high, saturation of the water may not occur and the forward rate of dissolution will limit the

release rate. In addition, because k_+ represents the absolute maximum dissolution rate, a conservative source term can be derived from an accurate determination of this parameter of the ISV products. This source term can be used in health-based risk assessment modeling. The k_+ is also required for predictive modeling of waste form dissolution as a function of waste form composition and solution chemistry.[18,19]

Reaction rates, such as the forward rate, are known to have strong temperature dependence. Because of the high durability of waste forms, such as those produced from ISV, it may not be possible to conduct leach testing at ambient ground temperatures ($\leq$ 20°C) and have concentrations in the leachate above analytical detection limits. Conducting leach testing at higher temperatures ($\approx$40 to 90°C) will provide adequate leachate concentrations. If conducted at three or more temperatures, the forward rate's Arrhenius activation energy can be determined, which will allow the temperature dependence to be established. Using this temperature dependence, the forward rate at ambient storage conditions can be calculated.

The forward rate of dissolution has been measured using a number of techniques.[20,21,22] One technique that is promising for k_+ measurements is the pH stat method. This method has significant advantages over other techniques such as Soxhlet extraction, MCC-1 tests, or MCC-3 tests because the solution pH is held constant over the course of the test and a large quantity of data is generated in a short time.

Extensive Soxhlet extraction data have been obtained on nuclear waste glasses at temperatures ranging from 50 to 200°C.[23,24] Because the Soxhlet extractor provides a continuous flux of distilled water over the sample, dilute conditions are maintained throughout the duration of the test as required to accurately measure k_+. The primary disadvantage of the Soxhlet device is the difficulty in applying reduced pressures to run at temperatures lower than 100°C and the difficulty in measuring and controlling the pH of the distillate.

A modified Soxhlet extraction apparatus was developed for these measurements. All wetted parts of the reactor were made from Teflon® PTFE to minimize Si or Na contamination of the extract. Approximately 1 g of -100 +200 mesh glass was placed in the overflow cell and the Soxhlet extractor assembled. A 5 mL sample of the extract was obtained approximately every 24 hours using a syringe. The sample was immediately acidified to 1% HNO_3. The 5 mL sample was replaced with 5 mL deionized water to maintain a constant volume of water. For the current series of tests, run durations were limited to 7 days.

The pH stat method[25] has significant advantages over other dissolution rate measurement methods because the solution pH is held constant over the course of the test automatically by adding small quantities of a strong acid or base to the solution. A high density of data is thereby generated in a short time. For simple alkali silicate glasses, the rate of glass reaction can be precisely determined from pH stat alone by relating the one-to-one correspondence between alkali and hydronium ion exchange to the reaction rate. Unfortunately, the utility of pH stat is limited with more complex glasses because precipitation of highly insoluble secondary phases (such as gibbsite and ferrihydrite) may consume or release OH, making interpretation of the pH stat data extremely difficult, if not impossible. In addition, the measurements are restricted to near-neutral pH where the sensitivity to changes in solution pH from glass dissolution are maximized.

To overcome these limitations with the pH stat technique, the method was modified. The time rate-of-change in the concentration of a soluble glass component, such as Na, was monitored along with the H_3O^+ consumption, and an ion-selective electrode was used to monitor the selected cation concentration. Commercially available electrodes are capable of measuring M^+ concentrations as low as 10^{-6} M and will tolerate prolonged exposure to temperatures between 70 and 80°C.

Figure 100 shows typical results from the Soxhlet tests for IC007C90IE IFT glasses. Because of the scatter in the results for several elements and the lack of clear trends for other elements (such as K), dissolution rates for the samples were calculated from least squares fits to Na and Si only. The results from these fits for all of the INEL ISV glasses tested to date are given in Table 27. Note that these are the dissolution rates at 100°C.

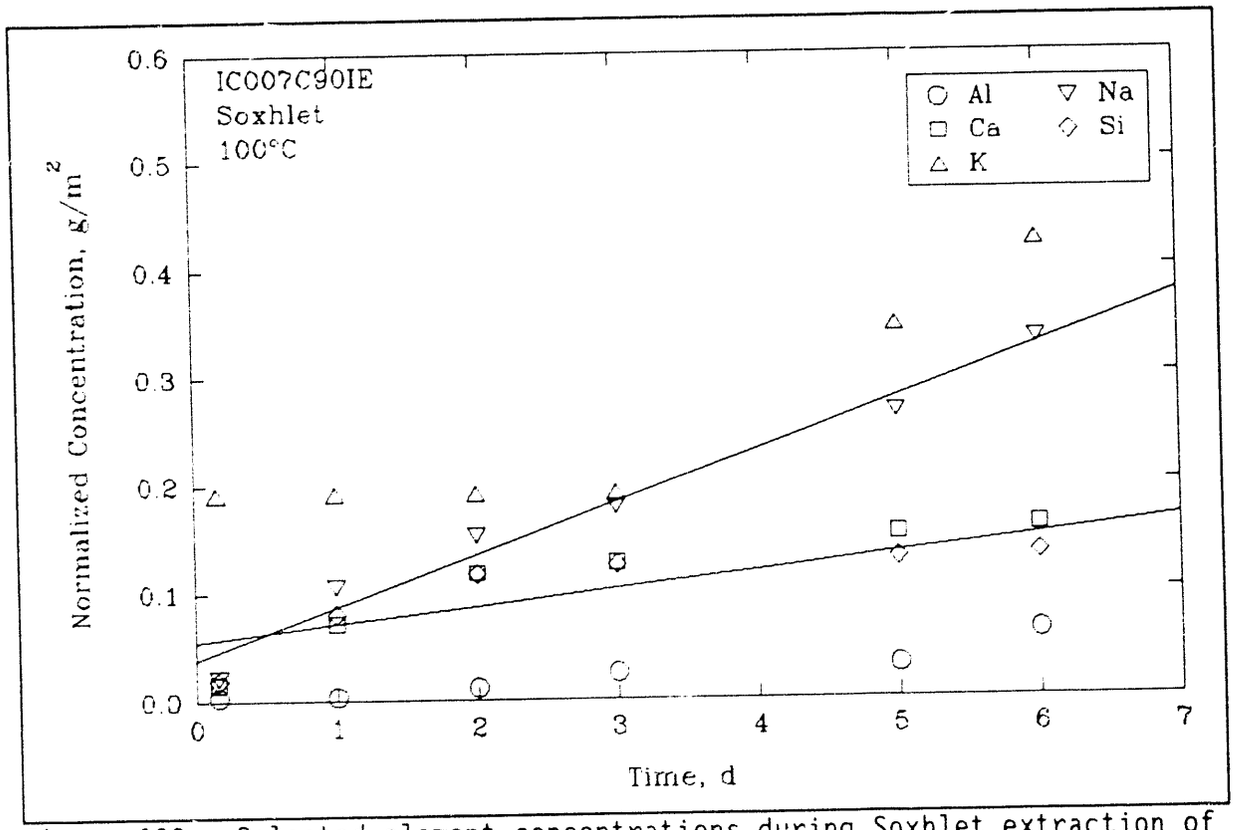

Figure 100. Selected element concentrations during Soxhlet extraction of IFT sample IC007C90IE at 100°C.

Figure 101 summarizes the results from pH stat/ISE experiments conducted with IFT sample IC007C90IE. The dissolution rates are for the ISV glasses are approximately one tenth compared to the reference waste glass at 80°C. Because of the small dissolution rate and low Na content of the ISV glasses, absolute concentrations of Na were nearly two orders of magnitude smaller than for the waste glass and near the detection limit for the ISE. This results in a small signal to noise ratio as is evident in the data in Figure 101. Accuracy and reproducibility are also poor because at Na^+ concentrations near 10^{-3} M, the response of the ISE is poor and non-linear with respect to Na^+

Table 27. Dissolution rates measured for INEL ISV glass samples by Soxhlet extraction at 100°C

Sample ID	Dissolution rate [g/(m^2·d)]	
	Na	Si
IC007C90IE	0.048 ± 0.004	0.016 ± 0.006
IC038B90IE	0.024 ± 0.002	0.004 ± 0.003
IC038C90IE	0.027 ± 0.001	0.014 ± 0.004
IC048B90IW	0.035 ± 0.002	0.002 ± 0.001

concentration. Although several attempts were made to adjust S/V ratios and reduce interferences from competing cations (such as NH_4^+ leakage from the pH and ion-selective electrodes), consistently satisfactory results could not be obtained with the technique. Consequently, we conclude that an alternate experimental method, such as a single-pass flow-through cell is needed to accurately measure k_+ for the INEL ISV glasses. Design and construction of such an apparatus is in progress. Because the release at 80°C was near the detection limit, testing at lower temperatures was not possible and the activation energy could not be determined. Determination of k_+ down to the ambient temperature is expected for final disposal of the ISV waste form

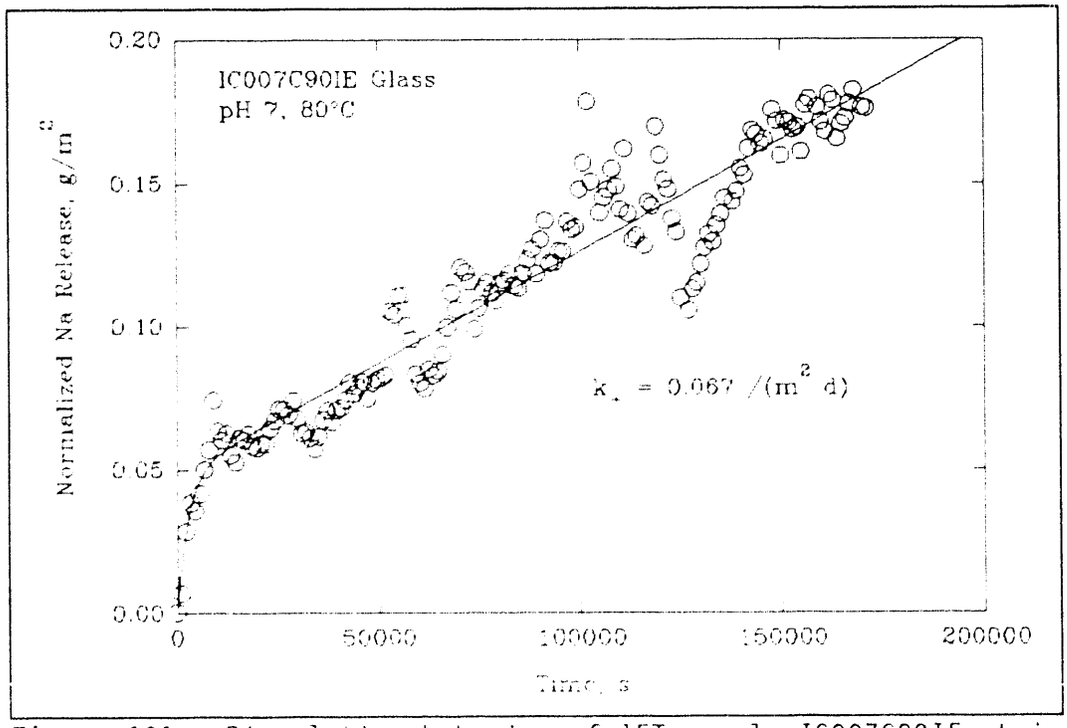

Figure 101. Dissolution behavior of IFT sample IC007C90IE at in situ pH 7 and 80°C.

(approximately 20°C). Because k_+ will decrease as the temperature decreases, the k_+ at 80°C can be used as a conservative value until the activation energy can be determined. Based on these results, a preliminary evaluation was also performed to evaluate the effects (if any) that devitrification of the IFT samples may have on the solution chemistry. Although the results are still preliminary, the static tests indicate that the devitrified samples have lower releases of several key elements including Ca, Mg, Al, and Si. This difference may be due to smaller dissolution rates for the glass matrix, the crystalline phase(s), or both. The smaller release could also be due to a smaller thermodynamic driving force for the irreversible dissolution of the crystalline phase(s) in the devitrified samples. Although dissolution rates of diopside (Ca, Mg, SiO_2) have been reported,[26,27] reliable kinetic data are not available for the pyroxene solid solution identified in the IFT samples. However, we have used the EQ3/6 code[28] to analyze the thermodynamics for the irreversible dissolution of the pure end member phases, diopside and hedenbergite. Diopside and hedenbergeite are very similar in composition, structure, and behavior to the augite found in the IFT waste forms and are suitable models. In performing this calculation, the analyzed bulk composition for sample IC038D90IE was used, assuming that the entire Mg inventory is partitioned to the end member diopside and the remaining elements (Ca, Fe, Si, and O) partition according to their stoichiometric amounts in both the diopside and hedenbergite phases. This procedure left a residual glass completely depleted in Mg and partially depleted in Ca and Fe. The data show a large driving force for the dissolution of both end-member phases at reaction progress values less than 10^{-3} mol/kg. Consequently, the smaller release rates observed in the static tests with the IFT samples cannot be attributed to smaller chemical affinities associated with the dissolution of the crystalline phases. Smaller dissolution rate constants appear to be the most likely cause for the smaller releases observed with the devitrified IFT samples.

In all of the above calculations, we have fixed the O_2 and CO_2 gas fugacities to correspond with the conditions of the dissolution experiments, i.e., essentially open to the atmosphere. Because of the oxidizing conditions and unlimited availability of carbonate, the release of many of the hazardous elements are predicted to be congruent with the dissolution rate of the glass (i.e., Se, As, Pu). However, water contacting the interior of ISV product,

where the hazardous elements are immobilized, must migrate through a series of cracks or channels that may not be open to direct contact with the atmosphere. We have used the EQ3/6 code to simulate this effect by allowing air-equilibrated deionized water to react with IFT sample IC007C90IE under closed-system conditions, i.e., mass balance constraints are allowed to determine the fO_2 and fCO_2. Under these conditions, those elements with multiple oxidation states will be reduced and, for several key elements such as Se and Pu, the calculated solubilities will be several orders of magnitude smaller. These elements would be sequestered in the alteration layers on the glass surface and, therefore, released at a rate less than the matrix dissolution rate. Accounting for the chemical interaction of the ISV product with water under closed-system conditions could provide smaller predicted release rates than by matrix dissolution alone.

In summary, a series of experiments was performed to determine the dissolution behavior of samples produced from the ISV processing of typical soils from the INEL Subsurface Disposal Area. Preliminary results from intrinsic rate constant measurements using pH stat/ISE and Soxhlet extraction methods showed that the dissolution rates of the ISV samples range from 0.01 to 0.06 $g/(m^2 \cdot d)$ at 90°C and pH 7. These values are 10 to 100 times smaller than measured for a typical borosilicate nuclear waste glass (see Reference 24). Devitrified samples from an intermediate-scale field test showed a possible trend to have slower dissolution behavior then amorphous samples of equivalent bulk composition. Additional thermodynamic and kinetic data on the clino-pyroxene minerals will be required to adequately explain the differences in the dissolution behavior of the partially-devitrified ISV products. Solids characterization of the ISV products showed that the ISV melts are reducing, resulting in Fe^{2+}/Fe ratios > 90%. Under equivalent closed-system conditions, as might occur during the slow migration of water through cracks in the solid mass, the reaction of the ISV glass with water reduces the redox potential to the lower stability limit of water. Under these conditions, several redox sensitive elements such as Se and Pu are expected to be sequestered in an alteration layer on the glass surface resulting in a smaller predicted release rate than calculated from the matrix dissolution rate alone.

5.4 Other Issues and Observations

Several observations that provide the basis for qualitative estimates of thermal gradients (edge effects) and of the probability of underground fires in the simulated waste materials in contact with the ISV melts are described below.

5.4.1 Alteration of Materials and Thermal Gradients

The simulated waste materials included wood, paper, cloth, sludge, scrap metal, and concrete/scrap glass contained within covered but unsealed steel cans. Cardboard boxes contained scrap metal or concrete/scrap glass. In general, cans containing concrete/scrap glass, simulated sludge (i.e., calcium silicate), and scrap metal showed no visible effects that could be attributed to the thermal effects of the melt. All of these materials appeared to be unaffected even when in physical contact with the melt. The cans of sludge were dry when within about 25 cm (10 in.) of glass, otherwise, the cans of sludge had minor (<25% interior area) surface rust on can interiors, presumably corrosion generated by the very basic solutions produced by wet sludge and not by thermal effects from the melt. Combustible materials included paper, cloth, cardboard, and wood.

In general, these combustible materials showed significant effects of thermal alteration. The alteration ranged from no effect to complete carbonization. Grey-white ash, indicating oxygen-rich combustion, was observed in only two cans, both within 0.76 to 0.91 m (≈2.5 to 3 ft) of a surface in contact with air. These cans also contained carbonized material, which indicates the environment became oxygen deficient before combustion was complete. The degree of alteration is directly related to distance from the melt and, thus, temperature. In general, in both pits visible alteration effects were observable up to about 46 cm (18 in.) maximum from the melt, at which distance only a very slight darkening of the combustible materials was evident. At distances progressively closer to the melt, the combustible wastes were increasingly carbonized. Black materials coated the insides and lids of the cans and the adjacent soil. The black coating on the cans and soil is presumably the carbonized remains of organic tars or similar substances driven from the combustible waste during the heating process.

Figure 102 shows typical carbonization of a paper-filled can when located within about 30 cm (12 in.) of the melt. Note the black deposits on the can lid in the figure. Often, carbonized paper and cloth are in direct contact with the glass which is indicative of an oxygen deficient environment. The effects in Test Pit 1 are similar to Test Pit 2. Alteration effects are often restricted to distances much less than the 46 cm (18 in.) noted above. For example, molten steel sheet metal was observed within about 5 cm (2 in.) of unaltered cardboard (see figure 103). Many other examples were also observed. The extent of alteration, and therefore the thermal gradient, is probably a function of both the temperature and mass of nearby melt and is highly variable from point to point around the pits. The above observations indicate the probability of underground fires is very low provided that there are no oxygen sources.

The soil adjacent (less than approximately 10 cm [4 in.]) to glass usually shows thermal alteration effects as well. Such soil within about 10 cm (4 in.) of the ground surface is salmon colored, but becomes bleached grey-hite at greater distances from ground surface. A very dark brown soil zone is found directly outside the grey-white region. Soils outside the dark brown zone appeared to be unchanged.

Figure 102. Carbonization of paper outside of vitrification zone for Test Pit 2.

Figure 103. Edge effect showing molten steel near cardboard in Test Pit 2.

6. TRACER STUDY

6.1 TRACER BACKGROUND

During preparation of the test pits, rare-earth tracer elements were added to selected waste containers. The added tracers were oxides of dysprosium, terbium, and ytterbium (Dy_2O_3, Tb_4O_7, Yb_2O_3). These tracers were added with the intent to use them as simulants of PuO_2 (see Reference 29). Rare-earth tracers (i.e., lanthanide series elements) have been previously used as simulants for Pu (an actinide).[30, 31]

The retention of elements or compounds in the glass, or alternatively the transport of materials to and within the off-gas system, is governed by a number of thermodynamic and/or transport properties. Thermodynamic properties such as boiling points, equilibrium solubilities in the various phases, and redox potentials are significant parameters which affect the retention of actinide components. Additionally there are transport mechanisms which can result in material transport from the melt and into the off-gas system; these include direct entrainment in gases released from the melt and steam transport, as well as ejection of material from the surface of the melt from collapsing bubbles.

The relative amount of retention of elements within the ISV melt is generally defined by the decontamination factor (DF). The DF of an element or compound is defined as m_i/m_e, where m_i is the initial input mass of contaminant in the control volume (soil) per unit time and m_e is the exit mass from the control volume per unit time. DFs can be presented to show what the relative retention of an element is in the melt relative to escape to the off-gas (i.e., soil-to-off-gas DF). A total DF for the ISV processing can be calculated which takes into account the additional retention of elements within the off-gas processing system.

Data from previous ISV testing have been published (see Reference 2) which indicate that Pu is primarily retained within the melt during ISV

processing. This is consistent with thermodynamic considerations, as well as previous data for Pu solubility in basaltic rock.[32] Data from a PNL pilot-scale radioactive test indicate a decontamination factor from the soil to off-gas of 4.5×10^3 (see Reference 2). An additional observation made during previous testing is the apparent greater retention of elements within the melt if they are initially buried at greater depth.

As indicated above, the retention of an element within the ISV melt is dependent on multiple factors. Transport factors such as direct entrainment of elements into melt gases, are of particular concern for ISV processing of buried waste, since these mechanisms offer the potential to increase the amount of released material in spite of equilibrium thermodynamic properties which may favor retention in the melt. The effect, if any, of these additional factors must be determined for the case of ISV buried waste processing.

The use of tracers in these Intermediate Field Tests provides some qualitative indication of potential for element release from the melt. The tracers were added to the pretest waste to simulate Pu behavior; however, a direct correlation between tracer behavior and Pu behavior remains uncertain. In addition, as discussed below, the uncertainties introduced during the sampling and analyses also act to prevent a rigorous quantification of the amounts of tracer released.

6.2 Tracer Study Objectives

The above considerations have resulted in modifications of the objectives of the tracer study as originally proposed. Despite the chemical similarities between the tracer materials and Pu, there remains no way to infer quantitative amounts of Pu retention/transport from tracer data. Despite uncertainty in the quantitative correlation between tracer behavior and Pu behavior, and the uncertainties introduced during the sampling and analyses,

essential information can be derived from the study. The modified objectives of the tracer study are as follows:

- Assess presence or absence in off-gas treatment system. Provide order of magnitude estimates of amounts.
- Determine relative amounts of tracer materials found retained within block, on hood and off-gas line surfaces, within the scrub system, and on the exit HEPA filter.
- Determine tracer release patterns over time.
- For Test 1, assess the amounts of tracer on the air inlet filter. This tracer could only be deposited as a result of positive pressure transients. The amount, if any, of tracer captured on the air inlet filter may allow evaluation of significance of direct air entrainment as an element release mechanism.
- Evaluate whether the tracers are found homogeneously within the block. This provides a measure of the amount of mixing of the block.
- Determine the partitioning of tracer material between solid phases in the final waste form.

6.3 Tracer Placement in Pit 1

Three tracers were placed in Pit 1 as shown schematically in Figure 104. The amounts of added tracer were as follows: Dy_2O_3 - 1.336 kg; Tb_4O_7 - 1.337 kg; and Yb_2O_3 - 1.331 kg. Each tracer was equally divided and placed into six paper bags. Each bag was placed into an individual can of waste materials. During placement, the contents of the bag were dumped into the can and a

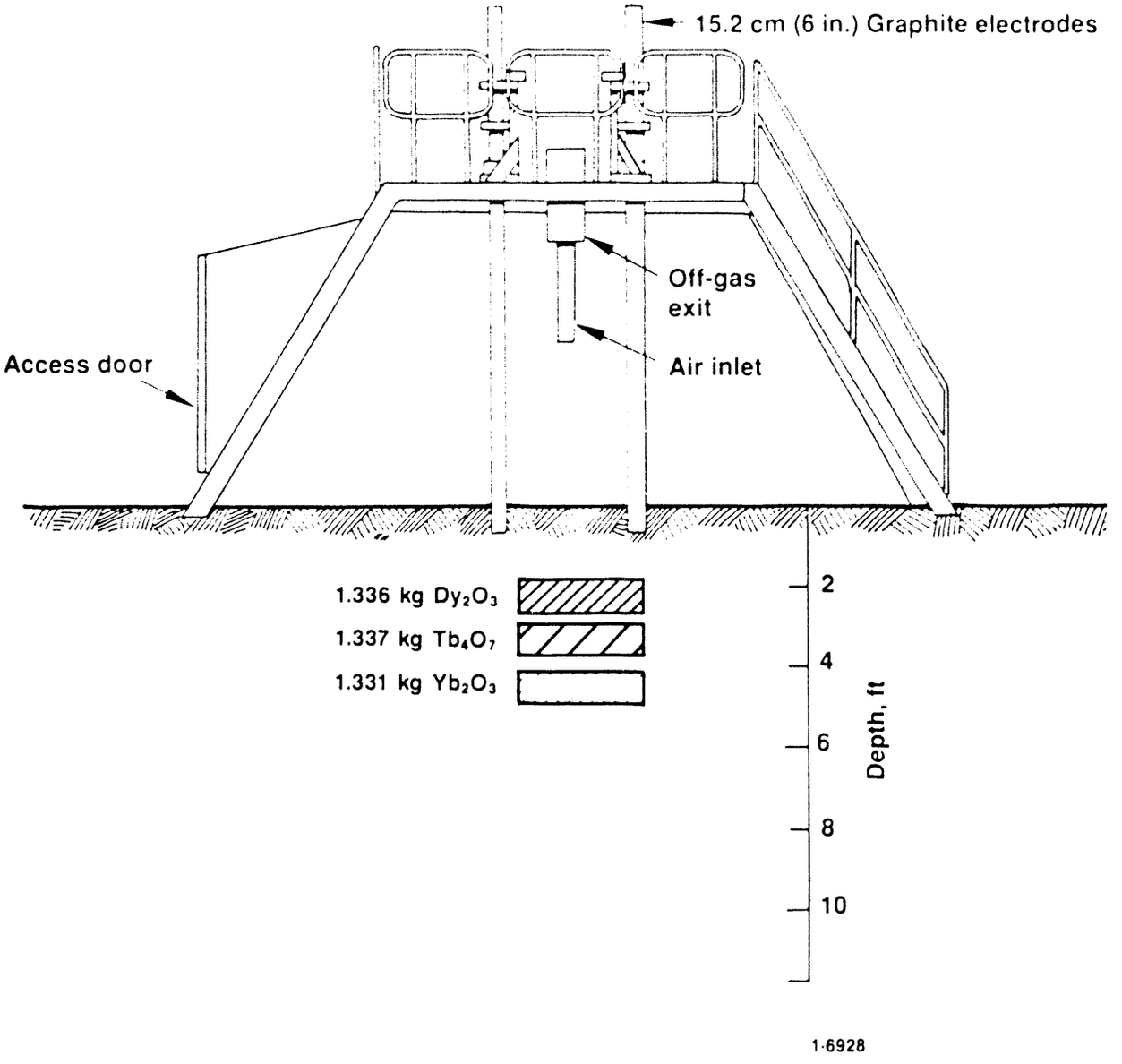

Figure 104. Tracer placement location for Test Pit 1.

limited attempt made to disperse the tracer material. The six cans containing each tracer represented the diversity of can waste materials: 1 can containing sludge, 2 cans containing cloth and/or paper, 1 can containing metal, 1 can containing concrete/glass, and 1 can containing wood. Placement of tracers in the pit during construction is shown in Figures 13 and 14; the cans containing tracer materials were placed near the center of the pit to ensure that they would be processed by the melt.

6.4 Tracer Placement in Pit 2

Only one tracer material was placed in Pit 2 as shown schematically in Figure 105. The amount of added tracer was Dy_2O_3 - 2.282 kg. The tracer was equally divided and placed into ten paper bags. Each bag was placed into an individual can of waste materials. During placement, the contents of the bag were dumped into the can and a limited attempt made to disperse the tracer material. The ten cans containing each tracer represented the diversity of can waste materials: 3 cans containing sludge, 5 cans containing cloth and/or paper, 1 can containing metal, and 1 can containing concrete/glass. Placement of the tracer cans in the pit during construction is shown in Figure 52; the cans containing tracer materials were placed near the center of the pit to ensure that they would be processed by the melt.

6.5 Tracer Sampling Strategy

Sampling of the following major areas was performed for each test: (a) glass product, (b) confinement hood, (c) off-gas ducting, (d) off-gas scrub solutions, (e) off-gas HEPA and inlet filters, (f) soil and sand used in pit preparations, and (g) soil adjacent to the glass product. Sampling strategies of these areas are described below. Sampling procedures are described in the sampling and analysis plan[29] for the field tests.[a]

---

a. Smears were collected from 100 cm^2 area, a deviation from the sampling and analysis plan.

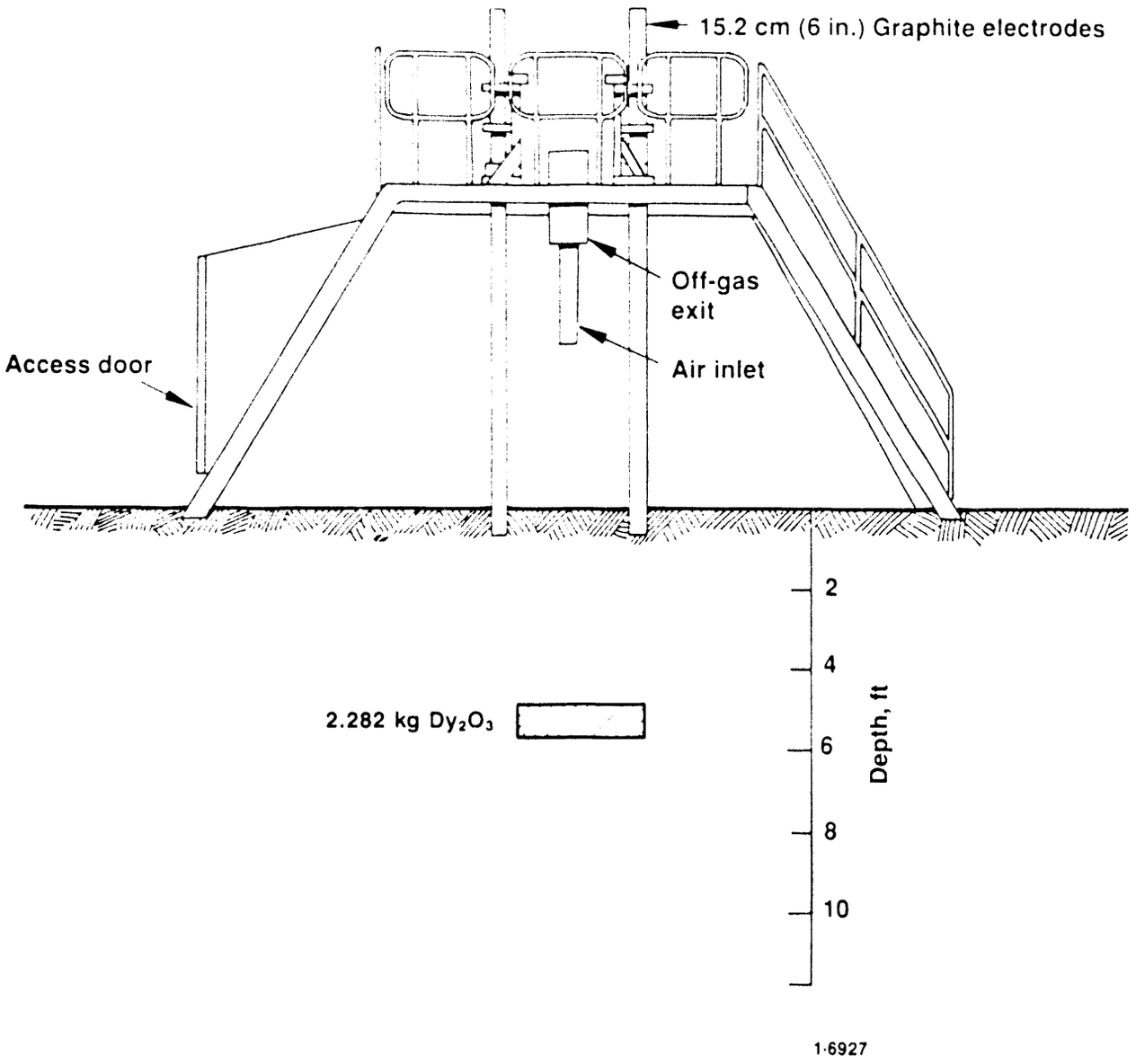

Figure 105. Tracer placement location for Test Pit 2.

Product

Grab and core samples were collected from the product block of each test. The sampling strategy focused on selection of material from different phases observed, and from various spatial locations within the product. See Figures 90 and 91 for the core and sample locations in plan and cross-sectional view for Tests 1 and 2, respectively. No field quality control samples were collected.

Hood

Smears were collected from top and side panels of the inside of the hood before and after each test.[a] Three top smears were collected 0.3 m (1 ft) from the edge of the hood and three[b] side smears were collected 0.6 m (2 ft) from the floor. Blank smears were prepared in each sampling episode.

Off-gas Duct

Smears of the off-gas ducting were collected at five locations before and after each test. The approximate locations (1-5) are shown in Figure 106. The samples were collected from the inside 2.5 cm (1 in.) of the entire circumference at each location. Smears were collected in the same sampling episode as hood smears, which included field smear blank preparation.

Off-gas Scrub Solution

Samples of the off-gas scrub solutions were collected at approximately two hour intervals during each test. The samples were collected from both scrub tanks at each sampling time.[c] Eight duplicate samples were collected.

---

a. Sample identification was inferred from sample logbook and chain-of-custody information.

b. In pretest sample for Test 1, two smears and one blank were collected.

c. Sample identification was inferred from the sample logbook, operations log, and chain-of-custody records in cases of discrepancies. Discrepancies that could not be satisfactorily resolved resulted in omission of data points. Some missing data result from no record of tank volumes and sampling times.

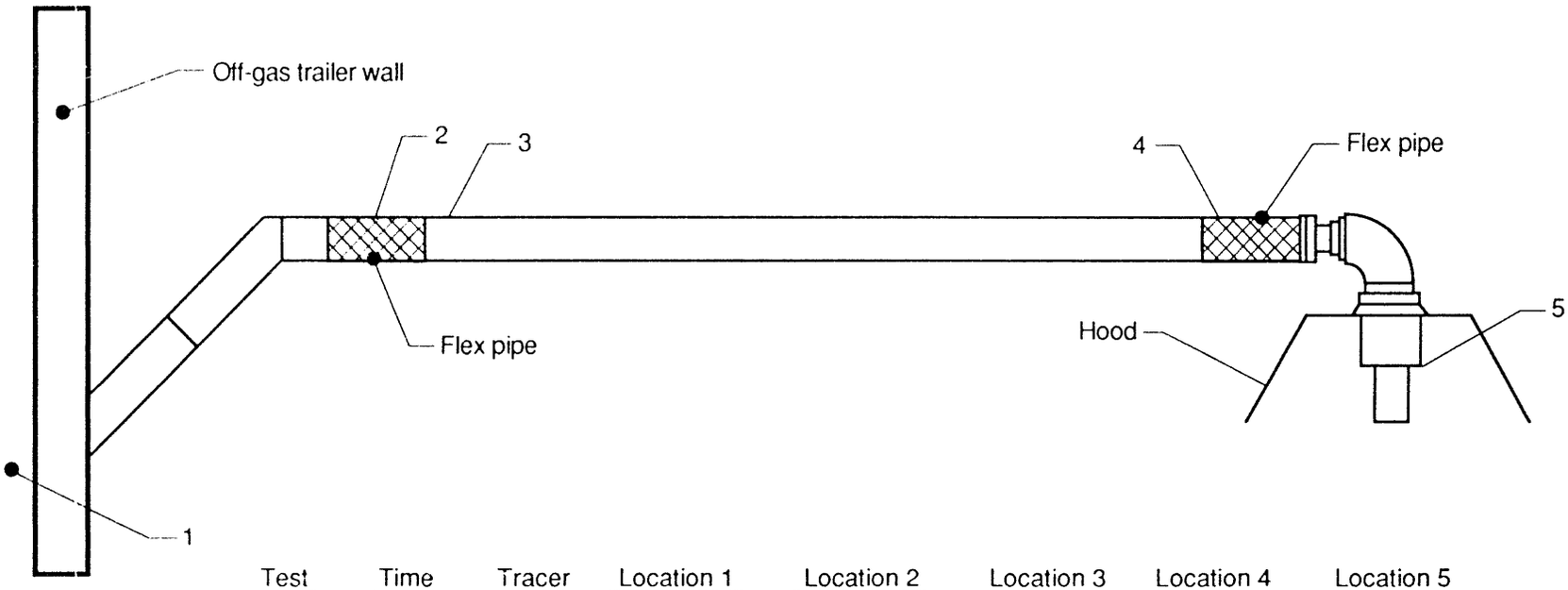

Test	Time	Tracer	Location 1		Location 2		Location 3		Location 4		Location 5	
			Amount (µg)	Flag	Amount (µg)	Flag	Amount (µg)	Flag	Amount (µg)	Flag	Amount (µg)	Flag
Test 1	Pretest	DY	2.2	B	1.0	U	1.0	U	1.0	U	1.0	U
Test 1	Pretest	TB	1.0	U	1.0	U	1.0	U	1.0	U	1.0	U
Test 1	Pretest	YB	1.0	U	1.0	U	1.0	U	1.0	U	1.0	U
Test 1	Post test	DY	5860.0		2370.0		6930.0		3140.0		944.0	
Test 1	Post test	TB	79400.0		35900.0		23200.0		40700.0		5180.0	
Test 1	Post test	YB	24500.0		11300.0		7380		16400.0		1940.0	
Test 2	Post test	DY	2260.0		1650.0		394.0		658.0		343.0	
Test 2	Post test	TB	7450.0		5340.0		438.0		1250.0		921.0	
Test 2	Post test	YB	2090.0		2030.0		274.0		1460.0		418.0	

T91 0479

Figure 106. Schematic showing off-gas duct smear locations and tracer analysis results. (Flag values are defined in Table 28.)

Filters

Eight samples were collected from the primary HEPA filters in the off-gas system and the air inlet filter in the hood.[a] Three samples were collected from the Test 1 air inlet filter, three samples were collected from the Test 2 primary HEPA filter, and two samples were collected from the Test 1 primary HEPA filter. One of each of the sets of three was sampled first and analyzed separately from the remaining samples. A blank of the HEPA filter material from the manufacturer was also submitted for analysis in the second submittal.

Soil

Pretest soil samples were collected from the pile of soil that was used in preparing the test pits. Samples were collected at different locations along the long axis of the pile at different depths; one duplicate sample was collected. In addition, sand used in preparation of the starter path (see Section 1.3.3) for the test pits was sampled in two locations from a pile.

A composite sampling scheme was used in posttest sampling of the soil adjacent to the products from Tests 1 and 2. Composite samples for the sides and bottom of the product blocks at two distances [15.2-20.3 cm (6-8 in.) and 25.4-30.5 cm (10-12 in.)] from the block-soil contact were collected. The number and locations of individual samples that composed each composite varied; the number of individual samples is shown below with the number of splits prepared for each composite. Volumes of individual samples contributing to the composites were not measured.

---

a. The sampling was performed after filters had been removed from the frames and sampled for other analyses. Filter identification was inferred from sampling notes.

	TEST 1 side 15.2-20.3 cm	TEST 1 side 25.4-30.5 cm	TEST 1 bottom 15.2-20.3 cm	TEST 1 bottom 25.4-30.5 cm
Samples:	9	9	3	3
Splits:	2	3	2	2

	Test 2 side 15.2-30.5 cm	Test 2 side 25.4-30.5 cm	Test 2 bottom 15.2-20.3 cm	Test 2 bottom 25.4-30.5 cm
Samples:	4	4	6	6
Splits:	2	2	2	3

6.6 Tracer Analysis

All samples were analyzed for Dy, Tb, and Yb, with the exception of Posttest 2 composite soil samples, which were analyzed for Dy only. The EG&G Idaho Environmental Chemistry Unit analyzed all samples, except product samples. Product samples were analyzed by the EG&G Idaho Separations and Chemical Analysis Unit.

Product Analyses

The product tracer analyses were performed by ICP-AES using an ARL 3410 instrument. The preparation of glass samples involved first crushing, then dissolution using HF and nanopure water, followed by two additions of HNO_3 and nanopure water. The metal samples were prepared using the described HF dissolution on metal shavings. The ICP analyses were performed using standard techniques. A multipoint calibration with replicate standard determinations was performed over a suitable concentration range.

The samples were submitted for analysis under chain of custody.[a] No special preservation or storage of the samples was required. The quality control associated with the glass analyses included two internal standards, matrix blanks, duplicate samples, sample spikes, and blank spikes. The

a. Chain of custody was adequate, with the exception that one sample label was misprinted.

quality control associated with the metal analyses consisted of matrix blanks, sample spikes, and blank spikes. The spikes were of analytes other than the tracers.

The quality control procedures and data[a] were reviewed for compliance with acceptable limits. Over one-third of the analyses were found to be suspect for several reasons. No analytical or matrix spikes were performed on any samples submitted for Dy, Tb, or Yb analysis. For all three tracers, selected sample analytical results are suspect because recoveries on associated standards exceeded procedure limits but were not reanalyzed. The reported mean percent error of standards (bias) is 7.4, 0.6, and -0.1 for Yb, Dy, and Tb analysis of glass samples, respectively. The relative standard deviation of the duplicate sample for Dy analysis of glass samples is 7.8%.

Hood, Off-Gas Duct, Scrub Solution, Filter, and Soil Analyses

EPA SW-846 Method 3020 was used for sample preparation of scrub solution and soil samples. A modified method was used for preparation of smear and filter samples. Method 6020-M Rev. 1 was used for analysis with Cesium-133 as the internal standard.[b] The instrumentation used was a VG Elemental PlasmaQuad II+ ICP-MS, equipped with an autosampler. Sample analyses were performed using peak-jumping mode in the pulse-counting detector. Some samples were analyzed in Extended Dynamic Range due to high analyte concentrations in the samples. All reported sample and quality control (QC) results were quantitated using blank subtraction. No isobaric elemental or molecular-ion interferences occurred at the masses of interest for the three rare-earth analytes, so isobaric interference correction factors, though applied, did not affect reported data. Matrix spikes and matrix spike duplicates were not performed on smear samples because of the impossibility of evenly splitting the samples. To obtain indicators of precision and accuracy for smear analyses, two laboratory control samples (spiked clean paper towels of identical brand as the analysis batch) were processed with the samples.

---

a. Only summarized, no raw data was available for review; therefore, initial and continuing calibration of the instrument was not verified.

b. In one instance, rhodium was used as an internal standard because cesium was detected in the sample.

The samples were submitted for analysis under chain of custody. Sample integrity was found to be adequate except in cases where the pH of the scrub samples was greater than two, which could lead to a low bias in the results. Required refrigeration was maintained and holding times were met. Quality control was measured with initial and continuing calibration verification standards, low-level standards, method and calibration blanks, matrix spikes, matrix spike duplicates, and laboratory control samples.

Because of the scoping nature of the IFT as the first testing of ISV processing of buried waste and the intended use of the tracer data as indicators rather than quantification of element retention, a detailed quality control review inclusive of raw data was not performed. However, the quality control procedures and summary statistics were reviewed for compliance with acceptable limits.

All pretest soil samples are associated with out-of-limit spike recoveries for Dy, indicating that the sample bias could be as high as 43%. QC associated with Posttest 2 smear samples showed a small bias in the blanks (on the order of 0.01 ug or less) for Dy, Tb, and Yb. One smear analysis batch had poor matrix spike recoveries; one of the post-digestion matrix spike recoveries was below the lower control limit.

Virtually all scrub solutions had poor matrix spike recoveries because the amounts added to the samples were much less than sample amounts.[a] However, out-of-limit low post digestion matrix spike recoveries occurred in one Test 1 scrub solution batch for Dy, Tb, and Yb and in two Test 2 scrub solution batches for Yb. Samples with high pH occurred in five of eight scrub solution analysis batches; this could result in a low, but unquantifiable, bias in results. One Test 2 scrub solution batch had a contaminated preparation blank (on the order of 0.1 ug/l) for Dy, Tb, and Yb and another had an initial calibration recovery for Tb slightly less than acceptable. Some laboratory control sample recoveries less than 75% were reported for both Test 1 and Test 2 scrub solutions. The poor matrix spike, initial

---

a. In some cases, the matrix spikes are virtual duplicates of the original sample; however, the analysis results show poor precision. Analysts believe this could be due to the presence of solids in the solutions, which affect the representativeness of the splits.

calibration, and laboratory control sample recoveries and contaminated blanks indicate that scrub solution sample results are biased low, in varying amounts. The bias is not estimated here because of the ubiquitous nature of the problems and the scoping nature of the data analysis.

For tracer analysis of the filters, all calibration verification QC, laboratory control sample, and preparation blank results were in control.[a] Matrix spike recovery problems similar to those in scrub solution analyses were experienced for two of the filters, possibly because of inhomogeneous distribution of analytes on filter surfaces and the high absorbency that is characteristic of HEPA filter media.

The analytical results are discussed below by media and ISV system component. Complete listings of data discussed are presented in Appendix A. In the Appendix and following sections, qualifiers to the data may be shown.[b] The qualifiers and their respective definitions are in Table 28.

In analysis of the results, values flagged with a B are used as actual measurements unless otherwise noted and values flagged with a U are treated as less-than-detectable (LTD) measurements.

Table 28. Data qualifiers and definitions

Qualifier	Qualifier Definition
U	Analyte was analyzed for but not detected (value reported as the IDL followed by a U flag)
B	Value is less than the minimum reporting level (MRL) but greater than the IDL (potential for false positives and or low/high bias exists)
N	Matrix spike or duplicate matrix spike recovery not within control limits
*	Duplicate analysis not within control limits

a. Relative percent difference between duplicates for Tb, 38%, is the exception.

b. If the matrix spike amount was much less than the sample amount and the recovery was not within control limits, the flag 'N' was not reported by the laboratory. ISV product analyses were flagged only as less-than-detection where appropriate; an overall quality flag is reported here with the data.

6.7 Test 1 Tracer Results

Product

Glass, crystalline, and metal phases of each test product were analyzed for Dy, Tb, and Yb. Analysis results are given in Table 29. The table also identifies the analysis results that have questionable quality, as discussed above. With one exception, the tracers were detected in every sample; the exception has questionable analytical quality.

Table 30 gives estimates of the mean (or average) and 90% confidence limits for the mean for glass and crystalline product samples. To compute the statistics, questionable data were removed from the data set. The results imply the following:

- there is a 90% chance that the true mean concentration of Dy in the nonmetal phases of the product is between 172 and 201 ug/g
- there is a 90% chance that the true mean concentration of Tb in the nonmetal phases of the product is between 209 and 267 ug/g
- there is a 90% chance that the true mean concentration of Yb in the nonmetal phases of the product is between 325 and 396 ug/g.

The confidence interval width is influenced by the number and variability of samples; the interval widths and the data themselves indicate that nonmetal product materials from different block locations have relatively similar tracer amounts.

The mass of the Test 1 product has been estimated at 8267 kg. Using the means from Table 30, the estimated tracer amounts in the product are 1538, 1968, and 3009 g Dy, Tb, and Yb, respectively, or 1765, 2314, and 3398 g Dy_2O_3, Tb_4O_7, and Yb_2O_3, respectively. The respective confidence intervals for the tracer oxide amounts, using the limits in Table 30 and ignoring any

Table 29. Product tracer analyses[a]

Location	Block Location	Phase	DY	DY Flag	TB	TB Flag	YB	YB Flag	DY Quality	TB Quality	YB Quality	Units
TEST 1	1	GLASS	58		42	U	5	U	Q	Q	Q	ug/g
TEST 1	2	GLASS	169		199		320					ug/g
TEST 1	3	GLASS AND DENDRITES	187		227		359					ug/g
TEST 1	4	GLASS, TRACE DENDRITES	224		284		362		Q		Q	ug/g
TEST 1	5	GLASS	192		240		390					ug/g
TEST 1	6	GLASS AND DENDRITES	197		241		374					ug/g
TEST 1	7	GLASS AND DENDRITES	188		233		378		Q	Q	Q	ug/g
TEST 1	8	METAL	6	U	42	U	5	U	Q	Q		ug/g
TEST 2	.	GLASS	195		42	U	6		Q	Q		ug/g
TEST 2	1	VESICULATED GLASS	6	U	42	U	6		Q	Q	Q	ug/g
TEST 2	2	GLASS	84		42	U	5	U	Q	Q		ug/g
TEST 2	3	GLASS	186		42	U	5	U				ug/g
TEST 2	4	GREY PORCELINOUS MATERIAL	183		42	U	5	U		Q		ug/g
TEST 2	5	GLASS AND APHANITIC MATERIAL	182		42	U	5	U		Q		ug/g
TEST 2	6	GLASS AND DEVITRIFIED MATERIAL	177		42	U	5	U		Q		ug/g
TEST 2	7	GLASS	172		42	U	5	U				ug/g
TEST 2	9	DEVITRIFIED GLASS	181		42	U	5	U				ug/g
TEST 2	10	DEVITRIFIED MATERIAL	171		42	U	5	U				ug/g
TEST 2	11	METAL	6	U	42	U	5	U	Q	Q		ug/g
TEST 2	15	GLASS	173		42	U	5	U				ug/g
TEST 2	16	GLASS AND CRYSTALLINE	155		42	U	5	U				ug/g
TEST 2	17	GREY APHANITIC MATERIAL	6	U	42	U	8					ug/g
TEST 2	18	METAL	6	U	42	U	5	U	Q	Q		ug/g

a. Questionable data identified with Q.

Table 30. Nonmetal product tracer analyses means and 90% confidence limits (ug/g). Questionable and less-than-detection data removed.

Location	Tracer	Mean	Lower Limit	Upper Limit
Test 1	DY	186.250	171.891	200.609
Test 1	TB	238.200	208.928	267.472
Test 1	YB	360.750	325.484	396.016
Test 2	DY	175.556	169.756	181.355
Test 2	YB	7.000	0.686	13.314

uncertainty (possibly substantial) in the product mass value, are (1632, 1907), (2032, 2596), and (3059, 3728). These estimates far exceed the tracer amounts buried in the pits: 1336 g for Dy_2O_3, 1337 g for Tb_4O_7, and 1331 g for Yb_2O_3. Possible explanations for these estimates being severely biased include (a) bias of the estimate of the product mass and (b) unknown laboratory bias.

An additional source of error is the use of the entire mass of the block in estimating the amounts of tracer. Although the product sample data indicated a relative homogeneous distribution of tracers in the block, these samples were taken from regions where convective mixing is expected. It is possible that areas where convective mixing would be expected to be less, such as near edges of the melt, may have a reduced concentration of tracer.

Hood

Field blank analyses, which include hood smear analyses, are given in Table 31. The pretest blank measurements are under less-than-detection limits. Blanks collected after Test 1 have some contamination of Tb and Yb, indicating a possible bias in smear results for these analytes. Table 32 gives the tracer analyses for all hood smears, with the general hood area identified. All pretest 1 tracer measurements are less-than-detection; the posttest 1 samples are detected at amounts 130 ug and greater. There is an obvious difference between pretest and posttest smear results, even when the bias indicated in the blanks is considered; this difference is evidence that material from ISV does accumulate in the hood.

Mean amounts of tracers accumulated on the top and sides of the hood during Test 1 are provided in Table 33. The table also gives the standard deviation of the data and the coefficient of variation, which is 100 times the sample means and were not significantly different between top and side for Dy, Tb, and Yb. The 90% confidence intervals for smear average amounts (ug) in

Table 31. Field blank analyses

Location	Time	Media	Tracer	Amount	Flag	Units
Test 1	Pretest	Hood Smear	DY	1.00	U	UG
Test 1	Pretest	Hood Smear	TB	1.00	U	UG
Test 1	Pretest	Hood Smear	YB	1.00	U	UG
Test 1	Posttest	Hood Smear	DY	1.00	B	UG
Test 1	Posttest	Hood Smear	TB	10.40		UG
Test 1	Posttest	Hood Smear	YB	5.00		UG
Test 2	posttest	Hood Smear	DY	0.23		UG
Test 2	Posttest	Hood Smear	TB	0.23		UG
Test 2	Posttest	Hood Smear	YB	0.26		UG

Table 32. Hood smear analyses

Location	Type	Hood Location	Area	DY	Dy Flag	TB	Tb Flag	YB	Yb Flag	Units
TEST 1	PRETEST	1	TOP	1.00	U	1.00	U	1.00	U	UG
TEST 1	PRETEST	2	TOP	1.00	U	1.00	U	1.00	U	UG
TEST 1	PRETEST	3	TOP	1.00	U	1.00	U	1.00	U	UG
TEST 1	PRETEST	4	SIDE	1.00	U	1.00	U	1.00	U	UG
TEST 1	PRETEST	5	SIDE	1.00	U	1.00	U	1.00	U	UG
TEST 1	POSTTEST	1	TOP	696.00		393.00		929.00		UG
TEST 1	POSTTEST	2	TOP	617.00		130.00		929.00		UG
TEST 1	POSTTEST	3	TOP	629.00		248.00		366.00		UG
TEST 1	POSTTEST	4	SIDE	457.00		258.00		691.00		UG
TEST 1	POSTTEST	5	SIDE	660.00		406.00		862.00		UG
TEST 1	POSTTEST	6	SIDE	1200.00		792.00		868.00		UG
TEST 2	POSTTEST	1	TOP	500.00		292.00		450.00		UG
TEST 2	POSTTEST	2	TOP	1360.00		255.00		1100.00		UG
TEST 2	POSTTEST	3	TOP	390.00		285.00		607.00		UG
TEST 2	POSTTEST	4	SIDE	23.80		10.30		26.70		UG
TEST 2	POSTTEST	5	SIDE	15.70		10.10		19.00		UG
TEST 2	POSTTEST	6	SIDE	657.00		520.00		634.00		UG

Table 33. Hood tracer analysis statistics

				TRACER								
				DY			TB			YB		
				CONCENTRATION			CONCENTRATION			CONCENTRATION		
LOCATION	MEDIA	AREA	UNITS	MEAN	STANDARD DEVIATION	COEFFICIENT OF VARIATION	MEAN	STANDARD DEVIATION	COEFFICIENT OF VARIATION	MEAN	STANDARD DEVIATION	COEFFICIENT OF VARIATION
[illegible]	[illegible]	[illegible]	[illegible]	772.33	384.03	49.72	485.33	275.70	56.81	807.00	100.50	12.45
	MEAN											
		[illegible]	[illegible]	647.33	42.57	6.58	257.00	131.73	51.26	741.33	325.05	43.85
[illegible]	[illegible]	[illegible]	[illegible]	293.17	467.94	158.48	160.13	294.33	183.40	226.57	352.87	155.74
	MEAN											
		[illegible]	[illegible]	750.00	531.13	70.82	277.33	19.66	7.09	713.00	339.17	47.57

the standard deviation to mean ratio.[a] A statistical test[b] confirmed that the hood after the test is (502, 919) for Dy, (182, 561) for Tb, and (595, 954) for Yb.

The surface area for the inside of the hood has been estimated at approximately 34.5 m^2 (371 ft^2). The hood smears, reported in ug, represent an approximate 0.01 m^2 area. It follows that the total estimated tracer amounts in the hood are 2.45 g for Dy, 1.28 g for Tb, and 2.67 g for Yb. The associated 90% confidence intervals for these mean amounts, assuming there is no variability in the surface area measurements, are (1.73, 3.17) for Dy, (0.63, 1.93) for Tb, and (2.05, 3.3) for Yb.

Off-gas Duct

The analytical results for smears taken inside the off-gas duct between the hood and the off-gas trailer are presented with a schematic of the sample locations (see Figure 106). Field blank data, shown in Table 31 and discussed above, apply to off-gas duct data. Pretest measurements in the duct are all less-than-detection or below the minimum reporting limit (MRL). Posttest 1 smears show tracers detected at amounts of 944 ug and greater. As in the hood, there is an obvious difference between pretest and posttest smear results; this difference is evidence that material from ISV does accumulate in the duct. Tb appears to occur at an order of magnitude greater than Dy. The data are insufficient to make inferences concerning accumulation trends and patterns.

The duct inside surface area has been estimated at 7.57 m^2 (81.5 ft^2). As for the hood, each smear represents an approximate 0.01 m^2 area. Using the duct surface area together with the means of the smears,[c] the total tracer amounts in the duct are 2.9 g Dy, 28 g Tb, and 9.3 g Yb. The following cautions are in order concerning this calculation. The calculation uses the

---

a. Also known as the relative standard deviation.

b. Student's test for the difference in two means at a significance level of 0.05 was used.

c. The means used are 3849 ug for Dy, 36876 ug for Tb, and 12304 ug for Yb.

average of the smear analyses; the average is not considered representative of the duct as a whole because of the location of the samples. The presence of bend sections of piping and reducing and expanding sections will produce flow patterns which likely result in a nonuniform and complex deposition of particulates (including any tracers present) on pipe walls. The sampling locations of the smeared samples were not chosen from the evaluation of likely flow patterns. Therefore, the estimate of deposition amounts based on the use of an overall surface area is only an order of magnitude estimate. Also, the flex pipe section had a surface of woven metal fiber; it is questionable whether a representative smear can be collected in flex pipe, which was one of the sampling locations. Smear surface area from flex pipe is expected to be different from the surface area of a smear from a standard smooth pipe. Because of the reasons stated above, the authors caution the reader concerning the accuracy of the estimate for the total tracer amount in the duct.

Off-gas Scrub Solution

Field duplicates of scrub solution samples are given in Table 34. The coefficients of variation between duplicate samples[a] range between 0.00 and 16.53 (duplicate analyses were within 0.00 and 16.53% of the mean of the duplicates) for Test 1, with one exception. Note that the coefficient of variation is inherently less than relative percent difference (RPD) typically reported by laboratories; thus, the stated range falls well within the 20% RPD limit of the analytical method. The exception, duplicate 4, was collected prior to the first start of Test 1 and was analyzed in the same batch as eight samples during Test 1. The reader should recognize that results presented below for Test 1 scrub solutions may reflect the poor precision observed in this duplicate set.

The tracer amounts given here are the sum of the amounts in the two scrub tanks in the off-gas system. To estimate the amounts in each scrub tank, solution concentrations are multiplied with tank volumes. The tank volume readings, however, are considered to be quite imprecise, and possibly biased.

---

a. No data are available for duplicate set number 3. Due to test restarts, duplicates 1, 4, and 5 are not duplicates of data represented here, but are of scrub solution media and from one of the sample analysis groups that include data presented here, and so are given.

Table 34. Field duplicate analysis statistics

				TRACER								
				DY			TB			YB		
				(AMOUNT)			(AMOUNT)			(AMOUNT)		
QC	LOCATION	MEDIA	UNITS	MEAN	STANDARD DEVIATION	COEFFICIENT OF VARIATION	MEAN	STANDARD DEVIATION	COEFFICIENT OF VARIATION	MEAN	STANDARD DEVIATION	COEFFICIENT OF VARIATION
DUPLICATE 1	TEST 1	SCRUB SOLUTION	UG/L	4.80	0.71	14.73	0.77	0.13	16.53	2.60	0.42	16.32
DUPLICATE 2	TEST 1	SOIL	MG/KG	2.10	0.14	6.73	0.37	0.03	7.64	0.93	0.08	8.41
DUPLICATE 4	TEST 1	SCRUB SOLUTION	UG/L	4.65	1.91	41.06	0.74	0.28	38.22	2.45	0.92	37.52
DUPLICATE 5	TEST 1	SCRUB SOLUTION	UG/L	1.35	0.07	5.24	0.20	0.00	0.00	0.72	0.00	0.00
DUPLICATE 6	TEST 1	SCRUB SOLUTION	UG/L	3.25	0.07	2.18	0.51	0.01	2.77	1.85	0.07	3.82
DUPLICATE 7	TEST 2	SCRUB SOLUTION	UG/L	2000.00	113.14	5.66	4225.00	304.06	7.20	4825.00	304.06	6.30
DUPLICATE 8	TEST 2	SCRUB SOLUTION	UG/L	2844.50	2977.63	104.68	10770.00	12770.35	118.57	5395.00	5395.22	100.00
DUPLICATE 9	TEST 2	SCRUB SOLUTION	UG/L	1130.00	84.85	7.51	2800.00	480.83	17.17	2820.00	56.57	2.01

This leads to noise in the results examined here, of which the reader should be aware. In addition, the analytical quality control indicates that bias is present, in differing amounts.

The results for Test 1 are plotted against hours from the start of the test in Figure 107.[a] In addition, the figure shows the depth of the melt front and tracer burial depths. The pattern shown in the plot does illustrate progressive release of the tracers with melt depths that correspond with tracer burial depths. For Dy, the release occurred at approximately the same time that the melt reached the burial depth. For Tb, the release occurred an hour or more after the melt is believed to have reached Tb burial depth. The amount of Yb in the scrub tanks increased when the melt reached the tracer burial depth, but increased further more than an hour later. The lag times observed could be a function of the melt column through which the tracer traveled to reach the off-gas system; however, the tracer burial depths are estimated (±6 in.) and could lead to as much as a three hour time window on average for release. Nonuniform releases are likely due to processing factors; penetration of cans containing tracer may have occurred at different times during processing at a particular burial depth. There also appears to be evidence that the tracer levels in the tanks dropped off after peak releases, indicating that some amount of the tracers continued past the scrub solution in the off-gas system. Note that the release amounts observed do vary with tracer type (higher with greater burial depth), despite the fact that equal amounts were buried; the reason for this is unknown.

Table 35 gives pretest and posttest tracer amounts in the scrub solution. Pretest values are actually the first measurement after the start of Test 1, and posttest 1 values are simply measurements taken prior to Test 2. Posttest 1 tracer amounts in the scrub solution provide estimates of tracer retention in the scrub tanks for the test. The estimates are 0.9 g for Dy, 1.9 g for Tb, and 2.0 g for Yb. No direct estimates of uncertainty in these numbers are available; however, field duplicate precision in other samples is approximately 5-7%. The analytical quality control statistics indicate that bias is low in scrub solution numbers.

a. Data points that measured LTD are plotted as the reported detection limit.

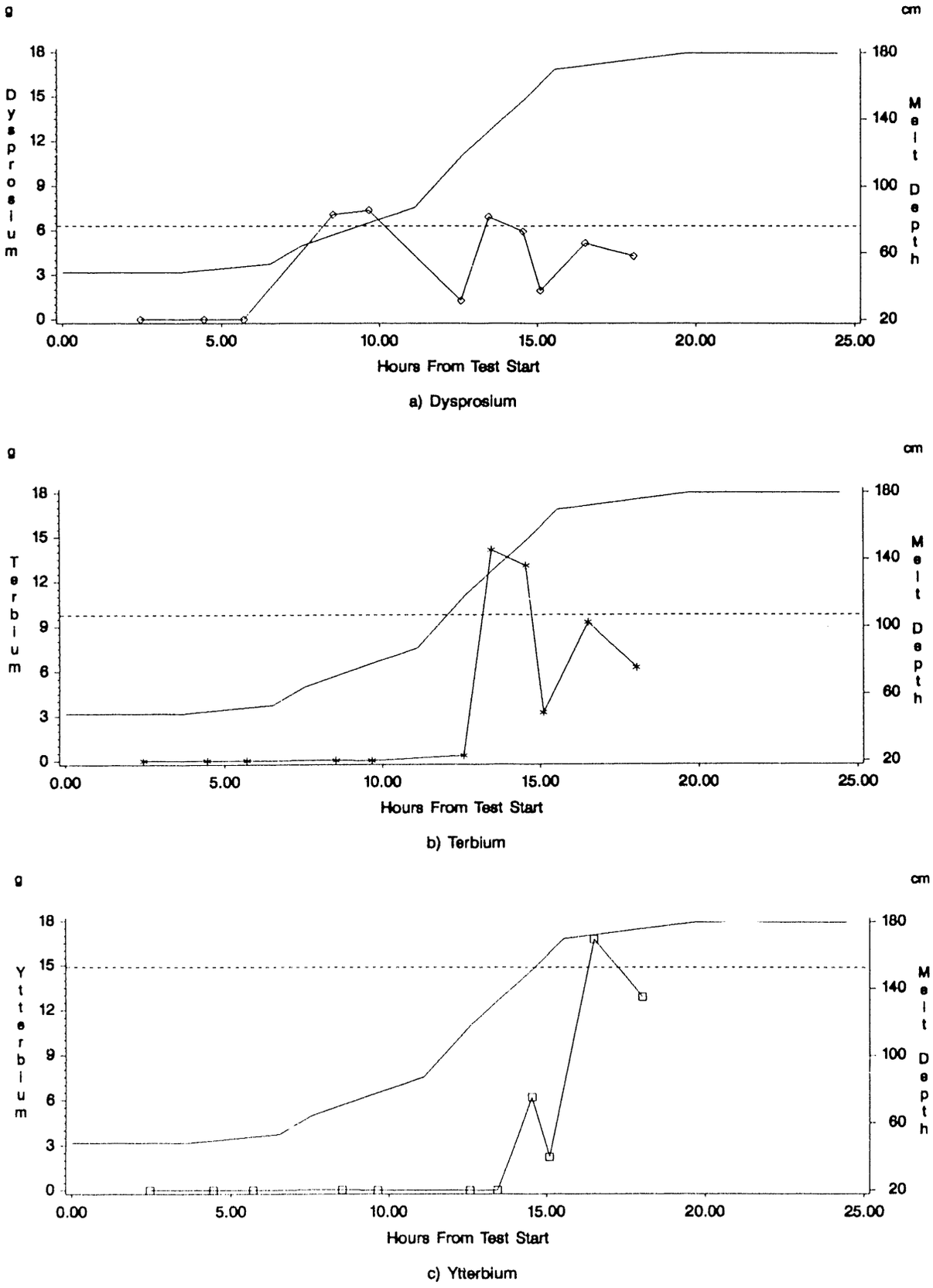

Figure 107. Amounts of tracer in scrub solution and melt depth as a function of time during Test 1. Dashed line shows depth of burial of tracer, (a) Dysprosium, (b) Terbium, (c) Ytterbium.

Table 35. Scrub solution analysis summary

Location	Time	Media	Dy (ug)	Tb (ug)	Yb (ug)
Test 1	Posttest	Scrub Solution	898200	1936600	2043800.0
Test 1	Pretest	Scrub Solution	153	34	95.2
Test 2	Posttest	Scrub Solution	705516	1928640	1547280.0
Test 2	Pretest	Scrub Solution	898200	1936600	2043800.0

Review of the data presented in Table 35, Figure 107, and Table 36 indicate that there is the potential for significant underestimation of the scrub solution tracer amounts. At the temperature of the scrub solution it would be expected that little, if any, tracer would be able to pass further downstream. This is consistent with the data presented below which show little tracer collected on the primary HEPA filters. However, the data shown in Figure 107 indicate a trend of decreasing tracer amount for the samples collected at the end of the test. In addition, the posttest scrub samples shown in Table 35 indicate amounts much lower than the last samples shown in Figure 107. Since the posttest samples were collected several weeks after completion of the test, it is likely that settling of sediment in the tank may have resulted in a lower amount being collected in the samples. (It should be noted that the tracer materials are insoluble in water.) The possibility of material settling may also account for the lower values shown in Figure 107 for samples collected later in the test.

Table 36. Tracer concentration on primary HEPA and air inlet filters, in mg/kg.

Location	Filter Location	Analysis Group		DY	DY Flag	TB	TB Flag	YB	YB Flag
Test 1	HEPA	2		0.95	U	0.95	U	0.11	B
Test 1	HEPA	2		0.98	U	0.98	U	0.28	B
Test 1	INLET	2		134.0		0.34	B	0.19	B
Test 1	INLET	2		209.0		1.2		0.37	B
Test 1	INLET	1		263.0		1.2		0.42	B
Test 2	HEPA	2		0.47	B	0.95	B	0.98	B
Test 2	HEPA	2		0.92	B	4.3		2.2	
Test 2	HEPA	1		1.0		4.0		2.3	
Blank	-	2	0.93	U	0.93	U	0.93	U	

If it is assumed that, once collected in the scrub solution, tracer did not leave the scrub solution, then the maximum amounts shown in Figure 107 may represent a better estimate of the collected tracers. In this case the amounts estimated in the scrub solutions would be higher: 7.3 g for Dy, 14 g for Tb, 16.8 g for Yb.

The abcve considerations point out that there may be significant limitations on data collected from the scrub tanks. These tanks are in the system as operational equipment and are not designed for the purpose of sampling. The potential for nonuniform mixing and settling exists and complicates interpretation of data as shown above. Given these limitations, it may be advantageous in future testing to use isokinetic sampling schemes for off-gas sampling, and rely less on sampling of the scrub solutions.

Filters

Table 36 gives filter tracer analysis results. For Test 1, the primary HEPA filter had less-than-detection Dy and Tb, and Yb at low concentrations. The Test 1 inlet air filter, however, had comparatively high Dy. The Tb and Yb levels in the air filter were detected but were relatively low. No tracer was detected in the blank filter material.

A 90% confidence interval for Dy concentration on the test 1 air inlet filter is (92.8, 311.2) mg/kg. The interval width reflects the sample-to-sample variability observed. The analysis results indicate that the hood pressurizations were sufficient to reverse air flow direction in the area of the inlet filter and deposit tracer-bearing particulates. Although pressurizations occurred during processing of all the tracers, the data show a higher amount of Dy than the other tracers which were buried at greater depth. This is consistent with the hypothesis that materials buried at more shallow depths are more likely to be transported into the off-gas system. The greater depth of melt at later times of the test may act to reduce the amount of material released into the off-gas system from containers buried at greater depth. (Note, however, that the data for tracer in the scrub solution show larger amounts of the tracers buried at greater depths, see Figure 107.) In addition, the fact that tracer was transported to the air inlet filter suggests that entrainment may be a significant mechanism for transport. Other mechanisms such as volatization of material would not result in material being deposited on the air inlet filter. This material could only be transported to the filter during the time periods when the hood experienced positive pressure sufficient to cause air backflow down the air inlet line.

Soil

Field duplicates were collected and analyzed for pretest soil, and the results are presented in Table 34. Coefficients of variation of 6.7 to 8.4 are reported for the tracer analyses. As for scrub solution field duplicates, the stated range falls well within the 20% RPD limit of the analytical method.

Table 37 gives the tracer analysis results for all soil and sand samples. All tracers were detected in all of the samples except Posttest 1 samples, all but one of which had less-than-detection Tb measurements. One of the Posttest 1 samples had a Yb less-than-detection measurement.

To determine whether or not there is a difference between pretest and posttest tracer levels, first, pretest soils are examined to determine whether amounts differ between sampling depths, so that the data can be pooled to compare with posttest samples. A statistical test[a] indicated that there are no significant differences between depths 1 and 2 in samples from the pretest soil pile.

The pretest-posttest comparison strategy is to compare the average of pretest soils with each posttest composite split average. Averages are given in Table 38. Composite values are not combined because they represent unique conditions adjacent to the product block. The comparisons omit tracer analyses from pretest sand samples; this is considered a conservative approach because the sand appears to have higher tracer amounts than pretest soils. A series of statistical tests that controlled the testing error were performed.[b] No significant differences between pretest and individual posttest sample means were detected; however, the reader is cautioned as follows:

---

a. Student's test for the difference in two means at a significance level of 0.05 was used.

b. Student's tests were performed using a Bonferroni family confidence level of 95% for Dy for both tests and also for Yb for Test 1.

Table 37. Soil tracer analyses

Location	Time	Soil Location	Depth	Dy	Dy Flag	Tb	Tb Flag	Yb	Yb Flag	Units
TEST 1	PRETEST	1	1	1.80		0.31	B	0.76		MG/KG
TEST 1	PRETEST	2	2	2.20		0.37	B	0.92		MG/KG
TEST 1	PRETEST	3	1	2.40		0.40	B	1.00		MG/KG
TEST 1	PRETEST	3	2	2.20		0.39	B	0.98		MG/KG
TEST 1	PRETEST	3	2	2.00		0.35	B	0.87		MG/KG
TEST 1	PRETEST	4	3	1.90		0.35	B	0.85		MG/KG
TEST 1	PRETEST			3.20		0.56		1.30		MG/KG
TEST 1	PRETEST			3.50		0.62		1.40		MG/KG
TEST 1	POSTTEST	BOTTOM, 12 in		2.50	B	1.00	U	2.80	B	MG/KG
TEST 1	POSTTEST	BOTTOM, 12 in		2.30	B	0.99	U	1.50	B	MG/KG
TEST 1	POSTTEST	BOTTOM, 6 in		2.70	B	1.00	U	1.10	B	MG/KG
TEST 1	POSTTEST	BOTTOM, 6 in		2.60	B	1.00	U	1.20	B	MG/KG
TEST 1	POSTTEST	SIDE, 12 in		2.40	B	0.97	U	1.20	B	MG/KG
TEST 1	POSTTEST	SIDE, 12 in		2.70	B	1.00	U	6.80	B	MG/KG
TEST 1	POSTTEST	SIDE, 12 in		2.40	B	1.10	B	1.00	U	MG/KG
TEST 1	POSTTEST	SIDE, 6 in		2.40	B	1.00	U	1.00	B	MG/KG
TEST 1	POSTTEST	SIDE, 6 in		2.50	B	0.98	U	1.10	B	MG/KG
TEST 2	POSTTEST	BOTTOM, 12 in		2.60	B	.		.		MG/KG
TEST 2	POSTTEST	BOTTOM, 12 in		2.50	B	.		.		MG/KG
TEST 2	POSTTEST	BOTTOM, 12 in		2.70	B	.		.		MG/KG
TEST 2	POSTTEST	BOTTOM, 6 in		2.60	B	.		.		MG/KG
TEST 2	POSTTEST	BOTTOM, 6 in		2.30	B	.		.		MG/KG
TEST 2	POSTTEST	SIDE, 12 in		2.20	B	.		.		MG/KG
TEST 2	POSTTEST	SIDE, 12 in		2.20	B	.		.		MG/KG
TEST 2	POSTTEST	SIDE, 6 in		2.00	B	.		.		MG/KG
TEST 2	POSTTEST	SIDE, 6 in		2.00	B	.		.		MG/KG

Table 38. Soil tracer analysis means and 90% confidence limits

Location	Time	Media	Soil Location	Dy Mean	Dy Standard Error	Dy Lower Limit	Dy Upper Limit	Yb Mean	Yb Standard Error	Yb Lower Limit	Yb Upper Limit	Units
TEST 1	PRETEST	SAND		3.35000	0.15000	2.40294	4.29706	1.35000	0.05000	1.03431	1.66569	MG/KG
TEST 1	PRETEST	SOIL		2.08333	0.09098	1.90000	2.26667	0.89667	0.03639	0.82333	0.97000	MG/KG
TEST 1	POSTTEST	SOIL	BOTTOM, 12 IN.	2.40000	0.10000	1.76862	3.03138	2.15000	0.65000	-1.95394	6.25394	MG/KG
TEST 1	POSTTEST	SOIL	BOTTOM, 6 IN.	2.65000	0.05000	2.33431	2.96569	1.15000	0.05000	0.83431	1.46569	MG/KG
TEST 1	POSTTEST	SOIL	SIDE, 12 IN.	2.50000	0.10000	2.20800	2.79200	3.00000	1.90088	-2.55053	8.55053	MG/KG
TEST 1	POSTTEST	SOIL	SIDE, 6 IN.	2.45000	0.05000	2.13431	2.76569	1.05000	0.05000	0.73431	1.36569	MG/KG
TEST 2	POSTTEST	SOIL	BOTTOM, 12 IN.	2.60000	0.05774	2.43141	2.76859	.	.	.	.	MG/KG
TEST 2	POSTTEST	SOIL	BOTTOM, 6 IN.	2.45000	0.15000	1.50294	3.39706	.	.	.	.	MG/KG
TEST 2	POSTTEST	SOIL	SIDE, 12 IN.	2.20000	0.00000	2.20000	2.20000	.	.	.	.	MG/KG
TEST 2	POSTTEST	SOIL	SIDE, 6 IN.	2.00000	0.00000	2.00000	2.00000	.	.	.	.	MG/KG

- any difference is confounded by possible high bias in laboratory pretest Dy measurements

- statistical detection of a difference in means is dependent on the number of samples (few samples can only detect a large difference) and also on the error risk assumed in performing the tests

- the composite sampling method used does not provide a good estimate of the spatial variability that may be present.

Each composite represents a relatively large volume of soil and has detectable Dy and Yb. No attempt is made here to estimate the amount of tracers in the soil, which is expected to contribute to error in the mass balance calculations.

6.8 Test 1 Tracer Summary

The tracer concentration appears to be relatively evenly distributed throughout the vitreous and crystalline phases in the product. The tracer concentrations reported are 172-201 ug/g for Dy, 209-267 ug/g for Tb, and 325-396 ug/g for Yb, which correspond to respective amounts of 1538, 1968, and 3009 g in the product. The latter numbers substantially exceed the buried amounts (1164 g for Dy, 1137 g for Tb, and 1169 g for Yb). However, it should be noted that the calculation of total product amounts is based on the entire product mass. Although data from core samples show homogeneity of the product, it is likely that areas near the edges of the melt, where convective mixing is less, may contain reduced concentrations of tracers.

Tracers were found to have been deposited in the hood and no significant difference was detected between the top and bottom smear averages. The estimated total amounts are 1.73-3.17 g for Dy, 0.63-1.93 g for Tb, and 2.05-3.3 g for Yb. The tracer Dy was found on the air inlet filter, indicating that entrainment could be a significant transport mechanism. Tracers were also found to have been deposited in the off-gas duct. Order of

magnitude calculations indicate that approximately 3 g of Dy, 28 g Tb, and 9 g of Yb may have accumulated in the duct during Test 1.

Results of tracer analysis of off-gas scrub solutions show that tracers occur in the scrub solution as the melt reaches the depth of tracer burial. The fate of the tracers in the scrub solution is unclear; however, the primary HEPA filter downstream contained little or no tracer.

Based on limited posttest soil sampling, it appears that there are no significant differences between tracer pretest soil concentrations and concentrations derived from soil samples collected at specific distances from the block.

The product appears to account for most of the originally buried amounts of tracers; however, because the product analyses were performed at a different laboratory than all other analyses, this could account for some of the observed distribution. The relative amounts of the tracers (Yb > Tb > Dy) in the scrub solution is similar to relative tracer amounts in the product; this curiosity at present has no explanation.

6.9 Test 2 Tracer Results

Product

The results of tracer analysis of product samples from Test 2 are given with Test 1 data in Table 29. As expected, all Tb and Yb measurements, which were not added to Pit 2, are reported as less-than-detection (there are three exceptions, but the reported values are very low). Note that no Dy is detected in metal samples; however, because the data have questionable quality, it is not necessarily proven that this is indicative of a pattern in the partitioning of Dy in the phases of the product.

Table 30 gives 90% confidence limits for the mean of glass and crystalline samples with results that are of acceptable quality.[a] The limits for Dy are (170, 181), which is a relatively small interval. This indicates there is small variation in Dy between samples, which in turn suggests that Dy is relatively evenly distributed throughout the nonmetal phases of the product. The Dy confidence interval overlaps substantially with that for Test 1, indicating that there is no difference between nonmetal product sample means between tests. This is especially interesting since the amount of Dy added to Pit 2 was greater than that added to Pit 1.

The mass of the Test 2 product has been estimated at 17,430 kg; the amount of Dy in the product is estimated at 2,929-3,155 g, or 3,362-3,621 g Dy_2O_3. As in the calculations for Test 1, these values greatly exceed the amount originally buried (2282 g Dy_2O_3). However, as noted for Test 1, the total product amounts are based on the assumption of homogeneity throughout the entire product mass. Although the data from case samples show homogeneity of the product, it is likely that areas near the edges of the melt, where convective mixing is less, may contain reduced concentrations of tracers.

Hood

Table 31 shows that hood smear blanks for Test 2 had detectable amounts of Dy, Tb, and Yb. The amounts detected are at levels lower than the detection limit in Test 1, however. The results in Table 32 of the hood tracer analyses show detectable amounts for all three tracers, although two of the side smears are anomalously low. Table 33 gives the means and estimates of variability of the data. As for Test 1, there is not a significant difference between averages of the top and sides of the hood. A 90% confidence interval for the mean of smears in the hood in ug is (82, 900) for Dy. This range is lower than the Dy interval for Posttest 1, indicating that there is higher variability in Posttest 2 smears.

The top of the hood shows apparent decreases in smear means from Test 1 to Test 2 for Dy, Tb, and Yb, but there is not a significant difference in the

---

a. One Dy data point, of grey, ferritic material, was removed from the data set used for the calculation because it was reported as less-than-detection; this was slightly too high to be part of the glass.

means. This result is unexpected because Dy was added to the Test 2 pit. There are at least two possible explanations for this. Either Dy did not accumulate in the hood during Test 2 or the movement of the hood between tests caused Dy to be removed from hood panels, and a comparable amount was added during the test. Laboratory biases are believed to be too small to account for the observed pattern.

A smear was taken of an electrode inside the hood after Test 2. The sampled electrode was one of two (A2 and B2) that showed a red-flaked coating of soft rust-colored flakes. Tracer analysis results of the electrode smear are given in Table 38. Relative to other smears collected in the hood after Test 2, this single sample appears low but similar to two of the hood side smears.

Using hood surface area calculations and the Posttest 2 hood smear data, the estimated amount of Dy in the hood after Test 2 is 0.28-3.1 grams. This amount is not appreciably different from the amount calculated for Posttest 1.

Off-gas Duct

The tracer analyses for off-gas duct smears are presented in Figure 106. The data are insufficient to determine a pattern or meaningful average. There does appear to be a difference between Posttest 1 and Posttest 2 data points; however, this difference cannot be confirmed with the available data. Note that Dy is present at the same order of magnitude as the other tracers, which was not added to the pit. This phenomenon can be seen in the Test 2 hood data also.

A sample of a large barnacle-like buildup of solids at the inlet to the venturi was collected. Tracer analysis[a] of the material is given in Table 39. The buildup indicates heavy particle loading during operations.

---

a. Analytical quality control was adequate except that laboratory control sample was not run. Matrix spike recoveries are poor, but post digestion matrix spike recoveries are acceptable.

Table 39. Miscellaneous tracer analyses

Location	Time	Smear Location	Dy	Dy Flag	Tb	Tb Flag	Yb	Yb Flag	Units
TEST 2	POSTTEST	ELECTROBE SMEAR	1.80		10.20		11.60		UG
TEST 2	POYTTEST	TRAILER PORT	2.20		149.00		123.00		MG/KG

An estimate for the amount of Dy in the off-gas duct calculated as for Test 1 with the accompanying qualifications is 0.8 grams.[a] This value is an order of magnitude less than that calculated for Test 1.

Off-gas Scrub Solution

The tracer analytical results for field duplicates are presented in Table 34. The results for duplicate set numbers 7 and 9 are acceptable (see Section 6.7), but the error in duplicate set number 8 is extremely high (duplicate analyses were 100% of the mean of the duplicates or greater).

The method for calculating the amounts in the Test 2 scrub tanks is the same as for Test 1; tank volumes are used and are believed to introduce error in the results. In addition, there was a tank overflow during Test 2, which calls into question the reliability of all of the data. Heavy particulate loading in the off-gas is believed to be responsible for scrub tank delta pressure level indicator line plugging and the difficulty in getting good flow rate through tank sample lines. Separately, the analytical quality control indicates that bias is present in differing amounts.

The available, if questionable, tracer amounts are plotted in Figure 108 with hours from the start of the test. The depth of the melt front and Dy burial depth are also shown. There is no apparent release of Dy during the test, and all three tracers exhibit a similar pattern. There is also no apparent difference[b] between pretest and posttest (actually last available data point) values, which are shown in Table 35. The magnitudes of the amounts in the scrub tanks during the test are all much less than peak values for Test 1. The data appear to represent residual tracer amounts from Test 1. Note that the three tracers show the same general pattern. Since terbium oxide and ytterbium oxide were not added to Test Pit 2, their total amounts in the scrub solution would be expected to be relatively constant. The fact that

---

a. The mean value used is 1061 ug.

b. No direct estimates of uncertainty are available to test this hypothesis.

all three tracers show the same pattern may reflect an inaccurate level indication. During processing, the tank level fluctuates based on relative amounts of evaporation and condensation in the scrub system. Inaccurate level measurements would equally affect the calculated amounts of any elements not being added or subtracted from the system. This is possibly the case for the data shown in Figure 108.

Despite the above considerations regarding the tank level measurement, the data for dysprosium in Figure 108 suggest that a significant amount of Dy did not enter the off-gas system during Test 2.

Filters

The primary HEPA filter tracer analysis for Test 2 is given in Table 36. All of the tracers were detected, even those added to Test Pit 1 and not Test Pit 2. The tracer added to Test Pit 2 (Dy) was present at levels comparable to those added to Test Pit 1 and not Test Pit 2, indicating that Test 2 may not have contributed to HEPA filter tracer amounts. The upper 90% confidence limit for Dy, 1.28 mg/kg, implies that only about 4.3 mg Dy was retained on the 3.36 kg filter.

Soil

Table 36 shows that Dy was detected in posttest 2 composite soil samples. As in the posttest 1 soils, there are no differences between the mean Dy concentration in pretest soils and the mean of composite splits for each compositing situation (means the given in Table 37). The comments concerning the meaning of the "no differences" statement that are discussed in the soil section for Test 1 apply here. That is, differences may be present and simply not detected with the sampling strategy used and potential for laboratory bias in sample results.

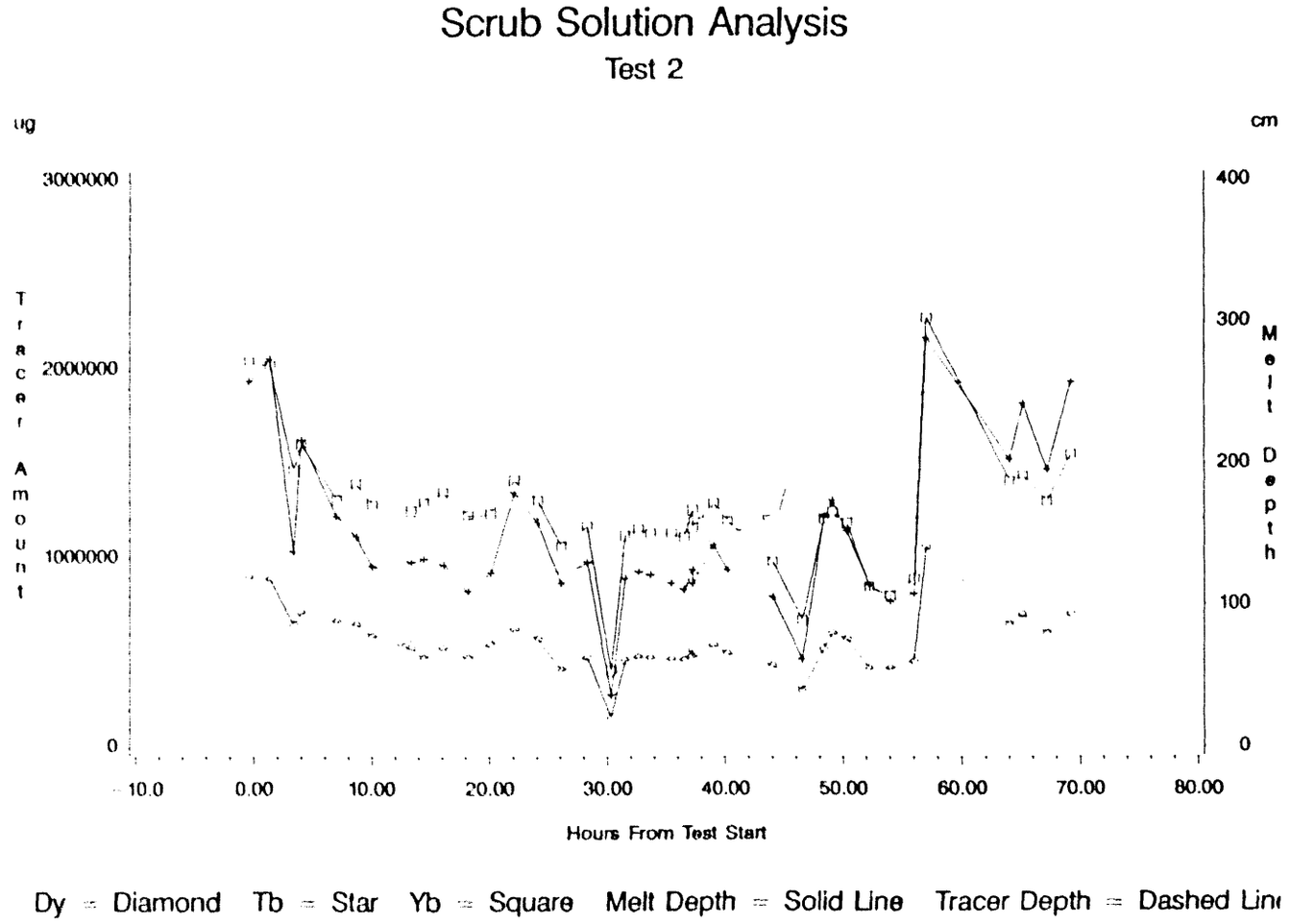

Figure 108. Amounts of tracers Dy, Tb, and Yb in scrub solution and melt depth during Test 2. Dashed line shows depth of burial of Dy.

6.10 Test 2 Tracer Summary

As in Test 1, the Dy concentration of the nonmetal phases of product appears to be relatively evenly distributed in the product. The Dy concentrations reported are 170-181 ug/g, which corresponds to 2929-3155 total grams of Dy in the Test 2 product. Also as in Test 1, the latter number is considered to be in error, considering that it substantially exceeds the buried amounts. The observed concentrations do not appear to be different from those observed in Test 1.

Hood and duct smear data and HEPA filter data indicate that Dy may not have entered the off-gas system. This may also be supported by scrub tank data, but quality control problems complicate this assessment.

Based on limited posttest soil sampling (the same as in Test 1), it appears that there are no significant differences between tracer pretest soil concentrations and concentrations derived from soil samples collected at specific distances from the block.

6.11 General Summary of Test Tracer Results

The tracer study results were reviewed to determine if differences in tracer behavior during ISV processing could be concluded to result from the differences in pit configuration between the two tests or operational differences during ISV processing of the two pits. Significant differences between the configuration of the two pits that may likely influence release characteristics include the additional 0.6 m (2 ft) of overburden in Pit 2, and the stacked layered waste in Pit 2 as compared to the randomly-dumped Pit 1 waste. Significant operational differences between the two tests include the more rapid processing of Pit 1 as compared to Pit 2. Test 2 operations were intended to minimize the pressurizations observed in Test 1. In Test 2, the stacked can region was observed to have heated up in a relatively uniform manner with few transient spikes as compared to Test 1.

The differences in pit configuration and test operations could well have influenced released tracer amounts. However comparison between tests is confounded by the use of three different tracers in Test 1 as compared to one tracer in Test 2. Also, the one common tracer between the two tests (Dy_2O_3) was buried at different depths in the two tests. Additionally, several aspects of the sampling for Test 2 restrict interpretation. The use of the posttest smear data from Test 1 as pretest smear data for Test 2 is suspect. It is possible that material may have been lost during movement of the hood (after posttest 1 smearing) and the data suggest this possibility and reduces the confidence in the hood smear data for Test 2. The scrub data results from Test 2 are also called into question by the problems experienced with the tank level transducer.

Despite the sampling concerns, the data suggest that tracer release for Test 2 is lower than Test 1. This is possible due to the test difference noted above which may act to promote retention of elements in the glass. A less quiescent melt with more active gas releases, such as in Test 1, may promote more entrainment and release of elements into the off-gas system.

Previous data from ISV tests at PNL (see Reference 2) have suggested that elements at greater depth are retained preferentially in the melt. This is consistent with the apparent reduced release of tracer in Test 2 compared to Test 1. However as indicated above, there are too many differences between tests to allow for conclusions regarding effect of depth on released amounts for these tests. Also it is noteworthy that the data from Test 1 show that the tracers at greater depth were released into the off-gas system in greater amounts. Since the three Test 1 tracers were different chemical elements, the different released amounts may possibly be entirely due to chemical transport in the tracers. It appears that further testing is warranted to establish the relationship, if any, between element release and initial depth below ground surface.

A direct extrapolation of these test results to plutonium behavior is not possible. Empirical data do not exist from which quantitative predictions of Pu behavior could be drawn from data involving rare-earth tracers. Nevertheless the data presented indicate that the vast majority of the tracer

elements are retained in the melt; this is consistent with previous data reported by PNL (see Reference 2) for Pu and other elements. Order-of-magnitude estimates for amounts of tracer materials released into the off-gas system for Test 1 were several grams to several tens of grams. This corresponds to up to several percent of the amounts initially added to the pit.

Further experimental work will be necessary if it is desired to make quantitative estimates of Pu release during buried waste ISV processing.

7. ANALYTICAL MODELING OF HOOD TRANSIENTS

Hood pressure and temperature spikes were observed in both Test 1 and Test 2 (see Figures 22 and 70). In several instances the pressure spikes were of sufficient magnitude to result in positive pressure within the hood plenum.

The occurrence of pressure and temperature spikes during processing of buried waste was a key observation from these tests. There has been some previous data for ISV of combustible materials (see Reference 2) but the data did not show the sharp spikes observed in these tests. The occurrence of pressure and temperature spikes within the hood plenum is of concern because of the potential to exceed the design limits of the hood. Additionally, the occurrence of positive pressure in the hood provides a driving force for gas release from the hood that bypasses the off-gas treatment system. Such gas release has the potential to release hazardous materials to the environment.

The current tests, being designed to simulate representative SDA buried waste conditions, were not specifically designed to collect data for determining the mechanisms which resulted in the hood plenum transients. Nevertheless, an attempt has been made to model the transients analytically in order to understand the contributing factors for the spikes.

7.1 Energy Flows in the Hood

Figure 109 shows a model of the energy inflows and outflows to the hood plenum. The energy flows are described as follows:

1. Energy convection due to inlet airflow. This energy flow into the hood plenum can be estimated based on knowledge of ambient temperature and inlet airflow rate. However, no direct measurement of inlet airflow is available. Measurements of flow were taken at the stack outlet. However, note the following equation:

$$\dot{m}_{stack} = \dot{m}_{inlet} + \dot{m}_{melt}$$

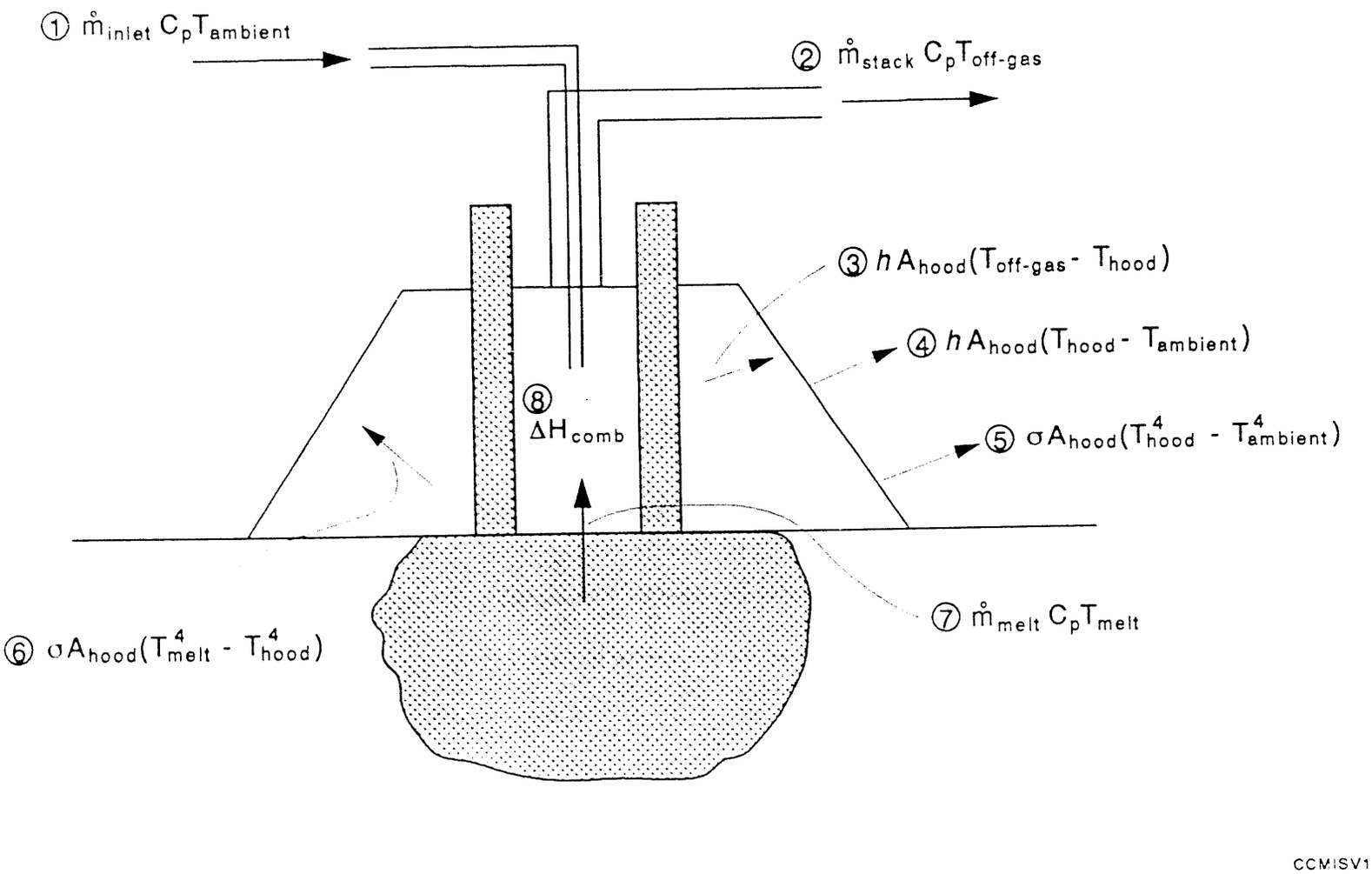

Figure 109. Schematic of energy flows in the hood plenum.

The relative contributions to the total flow of $\dot{m}_{inlet}$ and $\dot{m}_{melt}$ are not known. Additionally, the inlet flow itself is a combination of flow through the inlet air line and leakage flow through the hood panels or through the soil. In order to obtain an accurate measurement of $\dot{m}_{inlet}$, it would be necessary to measure flow in the inlet air line and eliminate (minimize) leakage flow through the hood and soil. The total amount of $\dot{m}_{melt}$ is a result of gases released directly from the melt as well as gases released along the sides of the melt; the temperatures of these two streams will be different. (It is assumed that direct measurement of $\dot{m}_{melt}$ is not feasible; it could be calculated if accurate measurements of $\dot{m}_{stack}$ and $\dot{m}_{inlet}$ were available.)

2. Energy convection due to air outflow. This energy flow is available because stack flowrate and temperature were recorded and off-gas temperature was recorded. It would be preferable (in future tests) to measure both temperature and flowrate in the off-gas pipe, as opposed to using the stack flowrate measurement.

3. Convection of heat from the off-gas air in the plenum to the hood surface. The driving force for this mode of heat transfer is the temperature difference between the plenum internal air and the hood surface. The air flow within the hood will result in forced convection; however the overall contribution of this heat transfer mode is probably lower than the other contributors.

4. Convection of heat from the hood surface to ambient air. The driving force for this mode of heat transfer is the temperature difference between the hood surface and the external ambient air. The overall contribution of this heat transfer mode is probably small relative to other contributors.

5. Radiation from the hood surface to the environment. This energy term can be calculated based on knowledge of the hood external surface temperature and ambient temperature.

6. Radiation from the melt surface to the hood and (particulate-laden) air. This term cannot be directly quantified from the available data; however it may be a significant contributor to plenum heatup, particularly when the melt cold cap is disrupted. Data from the processing of the instrumental can in Test 2 (see Section 4.4.1) suggest that steam release and associated cold cap disruption and subsequent radiation may have resulted in the observed hood plenum heatup. This hypothesis is also supported by data from an underground tank ISV test in which plenum heatup was observed in the absence of combustible materials.[33]

7. Superheat of gases released from the melt. This term cannot be directly quantified because no value for $\dot{m}_{melt}$ is available (see above). Were a value for $\dot{m}_{melt}$ available, an estimate of the gas temperature could be used in order to approximate the energy contribution of the hot gases being introduced into the plenum. It is possible this term may be a significant source of energy during transient surge releases of gases from the melt. Particularly in the case of steam release from the melt (where no heat of combustion contributes), the relative amount of superheat energy may be large. As indicated above, steam release likely contributed to some transient hood heatup observed in these tests.

8. Heat of combustion of pyrolysis gases being oxidized at the melt surface. The energy resulting from combustion of pyrolysis gases in the presence of oxygen introduced by the air inlet line is a major contributor to hood temperature and pressure spikes.

7.2 Modeling Uncertainties

Attempts to analytically model the transient spikes within the hood were hampered by the inability to validate key assumptions in the models used. Several areas of notable uncertainty were as follows:

- Inability to differentiate between radiative heating and combustion. Initial thoughts were that radiation was negligible as a mechanism of gas and hood heatup and resultant pressurization. However, this assumption has been called into question. Preliminary evaluation of a pilot-scale ISV test conducted at Hanford (see Reference 33) indicated that radiation may be signififcant as a heatup mechanism. It is postulated that gas release from the melt may disrupt the cold cap and increase the amount of radiative flux. Although clean air would be largely transparent to the radiation, the presence of large amounts of particulate in the air may result in absorption of the radiation and rapid heatup.

- Inability to quantify gas release rates from the melt. Original analytical efforts focussed on determining gas release rates from the melt that would result in the observed hood response. These attempts assumed complete combustion as one mechanism for energy input. Other mechanisms were heat capacitance of the gas released from the melt, and convective flows of inlet and outlet air. The assumption of complete combustion is not valid; the data showing off-gas spikes of CO, CO_2 and O_2 indicate that combustion is not complete. Thus, it was not possible to determine gas release rates from the melt by inference from pressure/temperature spikes. Note that it is not possible to directly calculate gas release rates from the melt because the rate of air inflow was not monitored; only the stack flowrate was measured. Air inflow is not a straightforward measurement due to the large magnitude of leakage through hood joints and through the soil around the base of the hood. In addition, the gas released from the melt may either be released by bubbling up through the melt itself, or by flowing through the porous dry soil zone at the periphery of the melt and being released at the edges of the melt surface. The temperature of released gas will be different depending upon its release path.

The above discussion indicates that the attempt to analytically model the temperature and pressure transients within the hood and obtain a quantitative match with the data was not fruitful. This is not particularly surprising since the tests were not designed to obtain separate effects data on transients. These tests were the first field tests conducted on buried waste and, as such, provided the first data indicating that pyrolysis gas release and subsequent combustion of buried combustible waste may result in significant spikes of pressure and temperature in the hood. Further tests will be necessary to delineate the physical mechanisms of gas release from the melt and combustion. Understanding these mechanisms is necessary in order to have the necessary degree of understanding and predicive capability to support ISV processing on contaminated buried waste.

7.3 Discussion of Differences Between Tests

Several qualitative differences between the transient pressure and temperature spikes in Test 1 and Test 2 should be noted. In general, the spikes observed in Test 1 were more numerous and more severe. This may be due to the faster melt rate, less overburden, and absence of uniform heatup of the waste region for Test 1 as compared to Test 2. Additional testing and/or analytical modeling will be required to establish the differences in off-gas transients under different operational and waste pit configurations.

An additional noteworthy observation is that spiking appeared to be less severe at later times during the test. This would support hypothesis that greater overburden may result in lessening of transient spikes. During later parts of a test, the amount of melted glass is larger. This may offer some buffering of gas release rates from the melt and thus act to reduce the severity of spikes. Again, further testing and modeling is needed to confirm this hypothesis and establish the significant physical mechanisms.

7.4 Recommendations for Future ISV Off-Gas Tests

Based on the results of analytical efforts for these tests, some recommendations can be made for test design and data collection for future test efforts. These are as follows:

- Quantify completeness of combustion within the hood by more accurate measurement of off-gas composition. The composition should be measured in the off-gas line upstream of the scrub system.

- Obtain accurate measurements of air inflow. This may require careful attention to prevention of leakage through the soil at the base of the hood. A flow measurement device should be placed in the air inlet line.

- Determine/estimate the magnitude of the transient heatup contribution due to radiation from the melt to the hood and plenum gases. As indicated above, there is evidence that radiation may provide a significant contribution to hood transients.

- Determine the magnitude of plenum heatup resulting from release of superheated steam (or other gas) from the melt (or from sides of the melt) into the hood plenum. The heatup from the gases must be decoupled from the increase of radiation energy which may result from melt bubbling disrupting the melt surface.

- Consideration should be given to design of techniques to measure rates of gas release through the melt or around the sides of the melt.

It is anticipated that future testing and analytical studies will provide insight required to understand the mechanisms resulting in hood plenum heatup and pressurizations. Based on this understanding designs may incorporate features to reduce or prevent transient positive pressure spikes within the hood.

8. CONCLUSIONS

Based on analyses of test data, the following conclusions are made relative to the application of ISV to buried waste.

General

- In situ vitrification is a feasible technology for application to buried wastes. The process incorporated and dissolved simulated waste containers into the melt to produce a durable glass and crystalline product. The electrode feed technology was successful in processing the high metal content waste.

- Refinements in equipment design are needed for production scale processing equipment.

ISV Processing

- The small volume of glass in Test 1 due to extensive subsidence (densification) resulted in electrical instabilities for the intermediate-scale transformer during periods of gas releases and encounters with waste containers in the melt. A large volume of glass associated with a large-scale application combined with independent two-phase control of the transformer, and uncoated electrodes will likely result in electrically balanced transformer operations.

- Because the coated graphite electrodes in Test 1 stuck to the frozen layer of glass covering the melt, uncoated graphite electrodes appear to be preferable to silica-based coated graphite electrodes. This sticking created unacceptable electrical conditions with the inability to adjust electrode positions. The extent (rate) of graphite oxidation of uncoated electrodes appears to be acceptable.

- Consistent with the rapid rate of downward melt growth experienced in the two tests, the volume of water vapor condensed in the process off-gas treatment system nearly exceeded the evaporative capability of the intermediate-scale system. Large-scale machine designs for buried wastes will require an increased evaporative capability relative to current designs to prevent the accumulation of secondary liquid wastes.

- Evidence does not support the likelihood of underground fires, unless there is a sufficent oxygen source from outside of the melt boundaries. Even with oxygen present, the consequences of underground fires in buried waste are expected to be minor due to their localized nature.

- Subsidence of the vitrified area was significant relative to previous ISV applications. This densification resulted in the uncovering of adjacent waste material along the perimeter of the vitrified zone. It is desirable to incorporate into the equipment design the ability to add glass-forming materials (soil) during processing to prevent adjacent waste from being uncovered. The hazards of posttest activities would be increased if uncovered wastes exists.

- Incomplete processing of the waste may occur at the edges of the vitrified zone. For a production-scale application of ISV to buried wastes, sequential overlapping processing locations would result in multiple blocks being fused together into a single large monolith.

- Increased levels of particulate generation in the off-gas were apparent relative to previous ISV applications at contaminated soil sites. Consequently, the design of a large-scale system should address the particulate buildup that was observed in the small diameter piping, tanks, and scrubber spray nozzles.

- Stacked metal waste layers or large metal objects offer the potential to promote lateral and vertical heat transfer. Soil

provides a high resistance to heat transfer, which results in steep thermal gradients near the melt front boundary. In stacked waste layers or high metal regions, thermal energy may be more readily transferred away from the immediate melt front boundary. In Test 2, the downward melt growth, as evidenced by electrode depth, was slowed while the stacked can region was heating up. It appeared that the downward melt growth was hindered until the stacked can region had sufficiently heated to vaporize water present in the region, then the downward progression of the melt resumed. A positive aspect of this phenomenon is that the stacked can layer in Test 2 gradually heated and released pressurized gases to the surrounding soil well ahead of the advancing melt front. This apparently resulted in a decrease in the severity of the temperature and pressure spikes compared to those observed in Test 1.

Hood Pressure and Temperature Spikes

- A robust off-gas processing system will be required to effectively contain the off-gases inside the hood. The hood must be designed to accommodate the relatively slow developing pressure spikes created by gas releases from containers, combustion, and thermal expansion of gas. The pressure spikes experienced in Tests 1 and 2 were not characteristic of detonations that produce rapid pressure spikes. The hood must be capable of withstanding contact from splatter of molten glass and must be capable of accommodating short duration gas temperatures in excess of 700°C.

- Test 1 results indicated that waste buried at greater depths had less impact on the transient temperature and pressure spikes than waste buried near the surface. Consequently, it is desirable to incorporate a means into the equipment design to add glass-forming materials during processing. In addition, an adequate amount of cover soil over the buried waste is essential to ensure adequate glass volume exists as glass flows into voids. Sufficient glass volume will buffer the effects of the transient temperature and pressure spikes and act to limit electrical instabilities.

- Further testing and analyses will be necessary to delineate the physical mechanisms of gas release from the melt and combustion. Understanding these mechanisms is necessary in order to have the necessary degree of understanding and predictive capability to support ISV processing on contaminated buried waste. Future test and data collection design should provide for measurement of heat transfer effects from combustion, radiation, and superheat of melt gases. Hood inlet and outlet flows and composition require accurate measurement.

ISV Product

- Based on MCC-1 leach testing data, the durability of the IFT waste form is comparable to obsidian and granite, and 4 to 10 times more durable (based on MCC-1 testing) than typical high-level nuclear waste glasses.

- Preliminary results from intrinsic rate constant measurements using pH stat/ISE and soxhlet extraction methods showed that the intrinsic dissolution rates of the ISV samples range from 0.01 to 0.06 $g/(m^2 \cdot d)$ at 90°C and pH 7. These intrinsic dissolution rate values are 10 to 100 times smaller than measured for a typical borosilicate nuclear waste glass.

- During cooling, devitrification occurred within the glass monolith producing a feather-like crystalline phase called augite. The mineral augite, a variety of clinopyroxene, is a calcium-magnesium-iron rich silicate. Augite is a common, naturally occurring pyroxene found in volcanic rocks, such as the basaltic rocks found at the INEL, which have compositions and cooling histories similar to the vitrified material in the Intermediate Field Tests reported here.

- Differences in durability corresponded to the degree of crystallinity in the samples. Samples that appeared to the eye to be completely devitrified (approximately 50% volume) show consistently lower releases for Ca, Mg, Al, and Si compared with

samples that analyzed x-ray amorphous. The releases of Ca and Mg are as much as two to three times smaller for the other devitrified samples. This difference may be due to smaller dissolution rates for the glass matrix, the crystalline phase(s), or both. Smaller dissolution rate constants appear to be the most likely cause for the smaller releases observed with the devitrified IFT samples. Because most of the ISV monolith is devitrified and no waste component segregation was observed, the lower release rates for the devitrified phase of the ISV waste form will result in a lower (than all glassly phase) overall release source term for heath-based risk assessments.

- Solids characterization of the ISV products showed that the ISV melts are reducing waste, resulting in Fe^{2+}/Fe ratios >90%. Under equivalent closed-system conditions, as might occur during the slow migration of water through cracks in the solid mass, the reaction of the ISV glass with water reduces the redox potential to the lower stability limit of water. Under these conditions, several redox sensitive elements, such as Se and Pu, are expected to be sequestered in an alteration layer on the glass surface resulting in a smaller predicted release rate than calculated from the matrix dissolution rate alone.

- TCLP testing was conducted to document that the ISV waste form could be disposed of in a landfill. The IFT waste forms do not exhibit hazardous characteristics of TCLP toxicity. In most cases, the TCLP results are below detection limits or 10 to 100 times lower than the maximum acceptable concentrations. Two metal samples (taken from the bottom of pit 2) have TCLP leachate concentrations 10% to 20% of the maximum acceptable concentration for chromium. This is thought to be due to the stainless steel in the samples.

Tracer Study

- Order-of-magnitude estimates for amounts of tracer materials released into the off-gas system for Test 1 were several grams to several tens of grams. This corresponds to up to several percent of the amounts initially added to the pit. The data suggest that during buried waste ISV processing, the release of rare-earth tracers in the melt is greater than values previously reported for plutonium release during processing of contaminated soil. These tests are inconclusive regarding the amount of expected Pu release associated with ISV processing of buried waste. Additional efforts are required to assess the adequacy of these tracers to simulate Pu compounds found in buried waste. Similarly, additional theoretical insight is needed in understanding the mechanisms of contaminant release from the melt.

9. REFERENCES

1. D. A. Arrenholz and J. L. Knight, A Brief Analysis and Description of Transuranic Wastes in the Subsurface Disposal Area of the Radioactive Waste Management Complex at INEL, EGG-WTD-9438, February 1991.

2. J. L. Buelt et al., In Situ Vitrification of Transuranic Wastes: Systems Evaluation and Applications Assessment, Battelle Pacific Northwest Laboratory, PNL-4800, Supplement 1, 1987.

3. K. H. Oma et al., In Situ Vitrification of Transuranic Wastes: Systems Evaluation and Applications Assessment, Battelle Pacific Northwest Laboratory, PNL-4800, 1983.

4. J. O. Low, Annual Technology Assessment and Progress Report for the Buried Transuranic Waste Program at the Idaho National Engineering Laboratory, EGG-2429, December 1989.

5. T. L. Clements, Jr., Content Code Assessments for INEL Contact-Handled Stored Transuranic Wastes, WM-F1-82-021, October 1982.

6. J. R. Bishoff and R. J. Hudson, Early Waste Retrieval Final Report, EG&G Idaho, Inc., TREE-1321, August 1979.

7. K. B. McKinley and J. D. McKinney, Initial Drum Retrieval Final Report, EG&G Idaho, Inc., TREE-1286, August 1978.

8. S. S. Koegler, Disposal of Hazardous Wastes by In Situ Vitrification, Battelle Pacific Northwest Laboratory, PNL-6281, 1987.

9. S. O. Bates, In Situ Vitrification Waste Form Product Evaluation Strategy, EGG-WTD-9148, August 1990.

10. U.S. Environmental Protection Agency, "Toxicity Characteristic Leaching Procedure (TLCP)." 40-CFR-268, Appendix I, U.S. Federal Register. Washington, D.C., 1988, Pg. 724-738.

11. U.S. Federal Register, Vol 55 #61, March 29, 1990, pp. 11798-11877.

12. B. P. McGrail, S. O. Bates, "An Evaluation of In-Situ Vitrification for Remediation of a Buried Waste Site," Seventh International Conference on the Physics of Non-Crystalline Solids, Cambridge, England, August 1991.

13. Materials Characterization Center, "MCC-1P Static Leach Test Method." In Nuclear Waste Materials Handbook. Test Methods. DOE/TIC-11400, Rev. 7, Technical Information Center, Springfield, Virginia, 1986.

14. Materials Characterization Center, "MCC-3S Agitated Powder Leach Test Method." In Nuclear Waste Materials Handbook. Test methods. DOE/TIC-11400, Rev. 7, Technical Information Center, Springfield, Virginia, 1986.

15. C. M. Jantzen, and N. E. Bibler, Product Consistency Test (PCT) for DWPF Glass: Part 1. Test Development and Protocol, DPST-87-575, Savannah River Laboratory, Aiken, South Carolina, 1987.

16. J. L. Dussossoy, "R7T7 Glass initial Dissolution Rate Measurements Using a High-Temperature Soxhlet Device." In Scientific Basis for Nuclear Waste Management XIV, Materials Research Society, Pittsburgh, Pennsylvania, 1991.

17. C. H. Kindle, and M. R. Kreiter, Comprehensive Data Base of High-Level Nuclear Waste Glasses-September 1987 Status Report. Volume 1 - Discussion and Glass Durability Data. PNL-6353, Vol 1. Pacific Northwest Laboratory, Richland, Washington, 1987.

18. B. Grambow, "A General Rate Equation for Nuclear Waste Glass Corrosion." In Scientific Basis for Nuclear Waste Management XIV, Materials Research Society, Pittsburgh, Pennsylvania, 1985.

19. B. P. Mcgrail, A conjoint Geochemical-Mass Transport Model for Near-Field Radionuclide Release Calculations, PNL-6174, Pacific Northwest Laboratory, Richland, Washington, 1987.

20. J. G. Carter, S. O. Bates, and G. D. Maupin, In Situ Vitrification of Oak Ridge National Laboratory Soil and Limestone, PNL-6174, Pacific Northwest Laboratory, Richland, Washington, 1987.

21. B. C. Bunker, G. W. Arnold, E. K. Beauchamp, and D. E. Day, "Mechanisms for Alkali Leaching In Mixed Na-K Silicate Glasses." J. Non.-Cryst. Solids, 58:295-322, 1983.

22. N. Kawanishi, H. Igarashi, H. Nagaki, and N. Tsunoda, Leaching Test on Chemical Durability of Glasses Containing Simulated High Level Wastes, PNCT N831-80-01, Power Reactor and Nuclear Fuels Corporation, Japan, 1980.

23. K. Ishiguro, F. Kamei, N. Sasaki, and H. Nagaki, Long-Term Soxhlet Leach Tests of Simulated Waste Glasses (I). PNCT N831-83-01, Power Reactor and Nuclear Fuels Corporation, Japan, 1983.

24. F. Delage, F. and J. L. Dussossoy, "R7T7 Glass Initial Dissolution Rate Measurements Using a High-Temperature Soxhlet Device." In Scientific Basis for Nuclear Waste Management XIV, Materials Research Society, Pittsburgh, Pennsylvania, 1991.

25. B. C. Bunker, G. W. Arnold, E. K. Beauchamp, and D. E. Day, "Mechanisms for Alkali Leaching in Mixed Na-K Silicate Glasses." J. Non-Cryst. Solids, 58:295-322, 1983.

26. J. Schott, R. A. Berner, and E. L. Sjoberg, "Mechanism of Pyroxene and Amphibole Weathering - I. Experimental Studies on Iron-Free Minerals." *Geochim. Cosmochim, Acta* 45:2123-2135, 1981.

27. C. M. Eggleston, M. F. Hochella, and G. A. Parks, "Sample Preparation and Aging Effects on the Dissolution Rate and Surface Composition of Diopside." *Geochim. Cosmochim. Acta* 53:797-804, 1989.

28. T. J. Wolery, EO3NR - A computer Program for Geochemical Aqueous Speciation-Solubility Calculations: User's Guide and Documentation. UCRL-53414, Lawrence Livermore Laboratory, Livermore, California, 1983.

29. P. R. Stoots and C. E. Edinborough, In Situ Vitrification Intermediate-Scale Sampling and Analysis Plan, Rev 4, EGG-WM-8661, November 1990.

30. R. L. Hooker, Incinerator Carryover Tests with Dysprosium as a Stand-In for Plutonium, DPST-81-603, 1981.

31. P. G. Shaw and G. G. Loomis, Plutonium Contamination Control Studies During a Glove-Box Scale Simulated Excavation of TRU Buried Waste, EGG-WM-8289, October 1989.

32. J. E. Flynn, et al., Annual Report on TRU Waste Form Studies with Special Reference to Iron-Enriched Basalt, EGG-FM-5366, June 1981.

33. L. E. Thompson, "Underground Storage Tank Remediation by use of In-Situ Vitrification," Proceeding of Waste Management '91, Tucson, Arizona, March 1991.

APPENDIX A
TRACER DATA

SAMPLE	LOCATION	TIME	DATE	HOUR	MEDIA	LOCATION IN MEDIA	TANK VOLUME	FIELD QC	Dy	Dy FLAG	Tb	Tb FLAG	Yb	Yb FLAG	UNITS
IJ010A901D	TEST 1	PRETEST	31MAY1990	.	DUCT SMEAR	1	.		2.20	B	1.00	U	1.00	U	UG
IJ009A901D	TEST 1	PRETEST	31MAY1990	.	DUCT SMEAR	2	.		1.00	U	1.00	U	1.00	U	UG
IJ008A901D	TEST 1	PRETEST	31MAY1990	.	DUCT SMEAR	3	.		1.00	U	1.00	U	1.00	U	UG
IJ011A901D	TEST 1	PRETEST	31MAY1990	.	DUCT SMEAR	4	.		1.00	U	1.00	U	1.00	U	UG
IJ007A901D	TEST 1	PRETEST	31MAY1990	.	DUCT SMEAR	5	.		1.00	U	1.00	U	1.00	U	UG
IJ006A901H	TEST 1	PRETEST	31MAY1990	.	HOOD SMEAR		.	blank	1.00	U	1.00	U	1.00	U	UG
IJ001A901H	TEST 1	PRETEST	31MAY1990	.	HOOD SMEAR	1	.		1.00	U	1.00	U	1.00	U	UG
IJ002A901H	TEST 1	PRETEST	31MAY1990	.	HOOD SMEAR	2	.		1.00	U	1.00	U	1.00	U	UG
IJ003A901H	TEST 1	PRETEST	31MAY1990	.	HOOD SMEAR	3	.		1.00	U	1.00	U	1.00	U	UG
IJ004A901H	TEST 1	PRETEST	31MAY1990	.	HOOD SMEAR	4	.		1.00	U	1.00	U	1.00	U	UG
IJ005A901H	TEST 1	PRETEST	31MAY1990	.	HOOD SMEAR	5	.		1.00	U	1.00	U	1.00	U	UG
IA001A90	TEST 1	PRETEST	07JUN1990	.	SOIL	1	.		1.80		0.31	B	0.76		MG/KG
IA002A90	TEST 1	PRETEST	07JUN1990	.	SOIL	2	.		2.20		0.37	B	0.92		MG/KG
IA003A90	TEST 1	PRETEST	07JUN1990	.	SOIL	3	.		2.40		0.40	B	1.00		MG/KG
IA004A90	TEST 1	PRETEST	07JUN1990	.	SOIL	3	.	dup2	2.20		0.39	B	0.98		MG/KG
IA004B90	TEST 1	PRETEST	07JUN1990	.	SOIL	3	.	dup2	2.00		0.35	B	0.87		MG/KG
IA005A90	TEST 1	PRETEST	07JUN1990	.	SOIL	4	.		1.90		0.35	B	0.85		MG/KG
ID001A901A0	TEST 1	PRETEST	12JUN1990	1800	SCRUB SOLUTION	TANK 1	110	dup4	6.00		0.94	B	3.10		UG/L
ID003A901A0	TEST 1	PRETEST	12JUN1990	1800	SCRUB SOLUTION	TANK 1	110	dup4	3.30		0.54	B	1.80	B	UG/L
ID002A901B0	TEST 1	PRETEST	12JUN1990	1800	SCRUB SOLUTION	TANK 2	120	dup5	1.30	B	0.20	B	0.72	B	UG/L
ID004A901B0	TEST 1	PRETEST	12JUN1990	1800	SCRUB SOLUTION	TANK 2	120	dup5	1.40	B	0.20	B	0.72	B	UG/L
ID005A901A1	TEST 1		12JUN1990	2100	SCRUB SOLUTION	TANK 1	122	dup1	5.30		0.86	B	2.90		UG/L
ID005B901A1	TEST 1		12JUN1990	2100	SCRUB SOLUTION	TANK 1	122	dup1	4.30		0.68	B	2.30		UG/L
IA006A90	TEST 1	PRETEST	14JUN1990	.	SAND		.		3.20		0.56		1.30		MG/KG
IA007A90	TEST 1	PRETEST	14JUN1990	.	SAND		.		3.50		0.62		1.40		MG/KG
ID001A901A1	TEST 1	PRETEST	14JUN1990	1600	SCRUB SOLUTION	TANK 1	165	dup3	.		.		.		
ID003A901A1	TEST 1	PRETEST	14JUN1990	1600	SCRUB SOLUTION	TANK 1	165	dup3	.		.		.		
ID033A901A1	TEST 1	PRETEST	14JUN1990	1800	SCRUB SOLUTION	TANK 1	160	dup6	3.20		0.50	B	1.80	B	UG/L
ID033B901A1	TEST 1	PRETEST	14JUN1990	1800	SCRUB SOLUTION	TANK 1	160	dup6	3.30		0.52	B	1.90	B	UG/L
ID034A901B1	TEST 1	PRETEST	14JUN1990	1800	SCRUB SOLUTION	TANK 2	170		0.90	B	0.20	U	0.56	B	UG/L
ID035A901A1	TEST 1		14JUN1990	2000	SCRUB SOLUTION	TANK 1	130		3.60		0.56	B	2.10		UG/L
ID036A901B1	TEST 1		14JUN1990	2000	SCRUB SOLUTION	TANK 2	160		1.30	B	0.20	U	0.70	B	UG/L
ID037A901A1	TEST 1		14JUN1990	2155	SCRUB SOLUTION	TANK 1	143		3.20		0.48	B	1.80	B	UG/L
ID038A901B1	TEST 1		14JUN1990	2155	SCRUB SOLUTION	TANK 2	119		0.68	B	0.20	U	0.42	B	UG/L
ID039A901A1	TEST 1		15JUN1990	5	SCRUB SOLUTION	TANK 1	150		45500.00		200.00	B	197.00	B	UG/L
ID040A901B1	TEST 1		15JUN1990	5	SCRUB SOLUTION	TANK 2	165		1470.00		10.00	U	10.00	U	UG/L
ID041A901A1	TEST 1		15JUN1990	153	SCRUB SOLUTION	TANK 1	166		42200.00		10.00	U	10.00	U	UG/L
ID042A901B1	TEST 1		15JUN1990	153	SCRUB SOLUTION	TANK 2	193		1800.00		10.00	U	10.00	U	UG/L
ID043A901A1	TEST 1		15JUN1990	407	SCRUB SOLUTION	TANK 1	155		5570.00		939.00		10.00	U	UG/L
ID044A901B1	TEST 1		15JUN1990	407	SCRUB SOLUTION	TANK 2	250		1630.00		757.00		10.00	U	UG/L

SAMPLE	LOCATION	TIME	DATE	HOUR	MEDIA	LOCATION IN MEDIA	TANK VOLUME	FIELD QC	Dy	Dy FLAG	Tb	Tb FLAG	Yb	Yb FLAG	UNITS
ID045A901A1	TEST 1		15JUN1990	500	SCRUB SOLUTION	TANK 1	200		33200.00		69700.00		15.00	B	UG/L
ID046A901B1	TEST 1		15JUN1990	500	SCRUB SOLUTION	TANK 2	200		1440.00		750.00	U	10.00	U	UG/L
ID047A901A1	TEST 1		15JUN1990	605	SCRUB SOLUTION	TANK 1	184		30500.00		69800.00		33100.00		UG/L
ID048A901B1	TEST 1		15JUN1990	605	SCRUB SOLUTION	TANK 2	235		1390.00		825.00		530.00		UG/L
ID049A901A1	TEST 1		15JUN1990	718	SCRUB SOLUTION	TANK 1	215		7420.00		13800.00		8050.00		UG/L
ID050A901B1	TEST 1		15JUN1990	718	SCRUB SOLUTION	TANK 2	230		1550.00		1110.00		2170.00		UG/L
ID051A901A1	TEST 1		15JUN1990	803	SCRUB SOLUTION	TANK 1	202		23900.00		44300.00		80100.00		UG/L
ID052A901B1	TEST 1		15JUN1990	803	SCRUB SOLUTION	TANK 2	239		1400.00		1260.00		2500.00		UG/L
ID053A901A1	TEST 1		15JUN1990	1015	SCRUB SOLUTION	TANK 1	185		21200.00		31900.00		54900.00		UG/L
ID054A901B1	TEST 1		15JUN1990	1015	SCRUB SOLUTION	TANK 2	280		1260.00		1190.00		3160.00		UG/L
IJ022A901D	TEST 1	POST TEST	25JUN1990	.	DUCT SMEAR	1	.		5860.00		79400.00		24500.00		UG
IJ021A901D	TEST 1	POST TEST	25JUN1990	.	DUCT SMEAR	2	.		2370.00		35900.00		11300.00		UG
IJ020A901D	TEST 1	POST TEST	25JUN1990	.	DUCT SMEAR	3	.		6930.00		23200.00		7380.00		UG
IJ023A901D	TEST 1	POST TEST	25JUN1990	.	DUCT SMEAR	4	.		3140.00		40700.00		16400.00		UG
IJ019A901D	TEST 1	POST TEST	25JUN1990	.	DUCT SMEAR	5	.		944.00		5180.00		1940.00		UG
IJ012A901H	TEST 1	POST TEST	25JUN1990	.	HOOD SMEAR		.	blank	1.00	B	10.40		5.00		UG
IJ013A901H	TEST 1	POST TEST	25JUN1990	.	HOOD SMEAR	1	.		696.00		393.00		929.00		UG
IJ014A901H	TEST 1	POST TEST	25JUN1990	.	HOOD SMEAR	2	.		617.00		130.00		929.00		UG
IJ015A901H	TEST 1	POST TEST	25JUN1990	.	HOOD SMEAR	3	.		629.00		248.00		366.00		UG
IJ016A901H	TEST 1	POST TEST	25JUN1990	.	HOOD SMEAR	4	.		457.00		258.00		691.00		UG
IJ017A901H	TEST 1	POST TEST	25JUN1990	.	HOOD SMEAR	5	.		660.00		406.00		862.00		UG
IJ018A901H	TEST 1	POST TEST	25JUN1990	.	HOOD SMEAR	6	.		1200.00		792.00		868.00		UG
7808229001	TEST 1	POST TEST	20AUG1990	.	FILTER		.	SPLIT1	0.95	U	0.95	U	0.11	B	MG/KG
7808229001	TEST 1	POST TEST	20AUG1990	.	FILTER		.	SPLIT1	0.98	U	0.98	U	0.28	B	MG/KG
7808229002	TEST 1	POST TEST	20AUG1990	.	FILTER		.	SPLIT2	134.00		0.34	B	0.19	B	MG/KG
7808229002	TEST 1	POST TEST	20AUG1990	.	FILTER		.	SPLIT2	209.00		1.20		0.37	B	MG/KG
7808229002	TEST 1	POST TEST	20AUG1990	.	FILTER		.	SPLIT2	263.00		1.20		0.42	B	MG/KG
HEPA BLANK	TEST 1	POST TEST	20AUG1990	.	FILTER		.	BLANK	0.93	U	0.93	U	0.93	U	MG/KG
IB010A901	TEST 1	POST TEST	02OCT1990	.	SOIL	BOTTOM, 12 IN.	.		2.50	B	1.00	U	2.80	B	MG/KG
IB010B901	TEST 1	POST TEST	02OCT1990	.	SOIL	BOTTOM, 12 IN.	.		2.30	B	0.99	U	1.50	B	MG/KG
IB011A901	TEST 1	POST TEST	02OCT1990	.	SOIL	BOTTOM, 6 IN.	.		2.70	B	1.00	U	1.10	B	MG/KG
IB011B901	TEST 1	POST TEST	02OCT1990	.	SOIL	BOTTOM, 6 IN.	.		2.60	B	1.00	U	1.20	B	MG/KG
IB008A901	TEST 1	POST TEST	02OCT1990	.	SOIL	SIDE, 12 IN.	.		2.40	B	0.97	U	1.20	B	MG/KG
IB008B901	TEST 1	POST TEST	02OCT1990	.	SOIL	SIDE, 12 IN.	.		2.70	B	1.00	U	6.80	B	MG/KG
IB008C901	TEST 1	POST TEST	02OCT1990	.	SOIL	SIDE, 12 IN.	.		2.40	B	1.10	B	1.00	U	MG/KG
IB009A901	TEST 1	POST TEST	02OCT1990	.	SOIL	SIDE, 6 IN.	.		2.40	B	1.00	U	1.00	B	MG/KG
IB009B901	TEST 1	POST TEST	02OCT1990	.	SOIL	SIDE, 6 IN.	.		2.50	B	0.98	U	1.10	B	MG/KG
IC013C901W	TEST 1	POST TEST	.	.	PRODUCT	1	.		58.00		42.00	U	5.00	U	UG/G
IC044B901W	TEST 1	POST TEST	.	.	PRODUCT	2	.		169.00		199.00		320.00		UG/G
IC044D901W	TEST 1	POST TEST	.	.	PRODUCT	3	.		187.00		227.00		359.00		UG/G

SAMPLE	LOCATION	TIME	DATE	HOUR	MEDIA	LOCATION IN MEDIA	TANK VOLUME	FIELD QC	Dy	Dy FLAG	Tb	Tb FLAG	Yb	Yb FLAG	UNITS
IC044H901W	TEST 1	POST TEST	.	.	PRODUCT	4	.		224.00		284.00		362.00		UG/G
IC048D901W	TEST 1	POST TEST	.	.	PRODUCT	5	.		192.00		240.00		390.00		UG/G
IC048F901W	TEST 1	POST TEST	.	.	PRODUCT	6	.		197.00		241.00		374.00		UG/G
IC048H901W	TEST 1	POST TEST	.	.	PRODUCT	7	.		188.00		233.00		378.00		UG/G
IH061D901W	TEST 1	POST TEST	.	.	PRODUCT	8	.		6.00	U	42.00	U	5.00	U	UG/G
ID001A901A02	TEST 2	PRETEST	11JUL1990	1515	SCRUB SOLUTION	TANK 1	110		5200.00		13100.00		11300.00		UG/L
ID002A901B02	TEST 2	PRETEST	11JUL1990	1515	SCRUB SOLUTION	TANK 2	140		2330.00		3540.00		5720.00		UG/L
ID003A901A02	TEST 2		11JUL1990	1621	SCRUB SOLUTION	TANK 1	126		4840.00		13500.00		10700.00		UG/L
ID004A901B02	TEST 2		11JUL1990	1621	SCRUB SOLUTION	TANK 2	130		2150.00		2720.00		5180.00		UG/L
ID005A901A12	TEST 2		11JUL1990	1821	SCRUB SOLUTION	TANK 1	112		3850.00		7190.00		8650.00		UG/L
ID006A901B12	TEST 2		11JUL1990	1821	SCRUB SOLUTION	TANK 2	130		1660.00		1760.00		3830.00		UG/L
ID007A901A12	TEST 2		11JUL1990	1900	SCRUB SOLUTION	TANK 1	140		3620.00		10100.00		8040.00		UG/L
ID008A901B12	TEST 2		11JUL1990	1900	SCRUB SOLUTION	TANK 2	131		1590.00		1600.00		3640.00		UG/L
ID009A901A12	TEST 2		11JUL1990	2200	SCRUB SOLUTION	TANK 1	122		3970.00		8560.00		7550.00		UG/L
ID010A901B12	TEST 2		11JUL1990	2200	SCRUB SOLUTION	TANK 2	127		1430.00		1370.00		3070.00		UG/L
ID011A901A12	TEST 2		11JUL1990	2339	SCRUB SOLUTION	TANK 1	138		3730.00		7080.00		8020.00		UG/L
ID012A901B12	TEST 2		11JUL1990	2339	SCRUB SOLUTION	TANK 2	120		1120.00		1120.00		2370.00		UG/L
ID013A901A12	TEST 2		12JUL1990	140	SCRUB SOLUTION	TANK 1	151		3140.00		5530.00		6930.00		UG/L
ID014A901B12	TEST 2		12JUL1990	140	SCRUB SOLUTION	TANK 2	125		886.00		929.00		1880.00		UG/L
ID015A901A12	TEST 2		12JUL1990	420	SCRUB SOLUTION	TANK 1	104		4070.00		8420.00		9890.00		UG/L
ID016A901B12	TEST 2		12JUL1990	420	SCRUB SOLUTION	TANK 2	142		743.00		723.00		1580.00		UG/L
ID017A901A12	TEST 2		12JUL1990	525	SCRUB SOLUTION	TANK 1	120		3170.00		7310.00		8840.00		UG/L
ID018A901B12	TEST 2		12JUL1990	525	SCRUB SOLUTION	TANK 2	130		710.00		884.00		1800.00		UG/L
ID029A901A22	TEST 2		12JUL1990	744	SCRUB SOLUTION	TANK 1	128		3430.00		6680.00		8780.00		UG/L
ID030A901B22	TEST 2		12JUL1990	744	SCRUB SOLUTION	TANK 2	133		654.00		798.00		1660.00		UG/L
ID031A901A22	TEST 2		12JUL1990	951	SCRUB SOLUTION	TANK 1	78		4320.00		8140.00		10800.00		UG/L
ID032A901B22	TEST 2		12JUL1990	951	SCRUB SOLUTION	TANK 2	183		740.00		1010.00		2080.00		UG/L
ID019A901A12	TEST 2		12JUL1990	1145	SCRUB SOLUTION	TANK 1	75		4830.00		8690.00		10500.00		UG/L
ID020A901B12	TEST 2		12JUL1990	1145	SCRUB SOLUTION	TANK 2	180		1010.00		1470.00		2490.00		UG/L
ID021A901A12	TEST 2		12JUL1990	1345	SCRUB SOLUTION	TANK 1	113		3510.00		8870.00		7710.00		UG/L
ID022A901B12	TEST 2		12JUL1990	1345	SCRUB SOLUTION	TANK 2	232		985.00		1460.00		2330.00		UG/L
ID023A901A12	TEST 2		12JUL1990	1545	SCRUB SOLUTION	TANK 1	126		3320.00		7620.00		7440.00		UG/L
ID024A901B12	TEST 2		12JUL1990	1545	SCRUB SOLUTION	TANK 2	180		853.00		1240.00		2030.00		UG/L
ID025A901A12	TEST 2		12JUL1990	1745	SCRUB SOLUTION	TANK 1	148		2040.00		4740.00		5240.00		UG/L
ID026A901B12	TEST 2		12JUL1990	1745	SCRUB SOLUTION	TANK 2	160		658.00		991.00		1770.00		UG/L
ID027A901A12	TEST 2		12JUL1990	1955	SCRUB SOLUTION	TANK 1	150		2380.00		5220.00		5710.00		UG/L
ID028A901B12	TEST 2		12JUL1990	1955	SCRUB SOLUTION	TANK 2	132		902.00		1460.00		2350.00		UG/L
ID033A901A12	TEST 2		12JUL1990	2118	SCRUB SOLUTION	TANK 1	153	dup7	2080.00		4440.00		5040.00		UG/L
ID033B901A12	TEST 2		12JUL1990	2118	SCRUB SOLUTION	TANK 1	153	dup7	1920.00		4010.00		4610.00		UG/L
ID034A901B12	TEST 2		12JUL1990	2118	SCRUB SOLUTION	TANK 2	134		1170.00		2030.00		3010.00		UG/L

SAMPLE	LOCATION	TIME	DATE	HOUR	MEDIA	LOCATION IN MEDIA	TANK VOLUME	FIELD QC	Dy	Dy FLAG	Tb	Tb FLAG	Yb	Yb FLAG	UNITS
ID035A901A12	TEST 2		12JUL1990	2228	SCRUB SOLUTION	TANK 1	144		1940.00		3940.00		4630.00		UG/L
ID036A901B12	TEST 2		12JUL1990	2228	SCRUB SOLUTION	TANK 2	137		1310.00		2320.00		3280.00		UG/L
ID037A901A12	TEST 2		12JUL1990	2336	SCRUB SOLUTION	TANK 1	154		2050.00		4150.00		4840.00		UG/L
ID038A901B12	TEST 2		12JUL1990	2336	SCRUB SOLUTION	TANK 2	123		1310.00		2310.00		3280.00		UG/L
ID039A901A12	TEST 2		13JUL1990	37	SCRUB SOLUTION	TANK 1	162		1930.00		3830.00		4530.00		UG/L
ID040A901B12	TEST 2		13JUL1990	37	SCRUB SOLUTION	TANK 2	114		1400.00		2490.00		3440.00		UG/L
ID041A901A12	TEST 2		13JUL1990	225	SCRUB SOLUTION	TANK 1	157		1890.00		3650.00		4450.00		UG/L
ID042A901B12	TEST 2		13JUL1990	225	SCRUB SOLUTION	TANK 2	112		1500.00		2570.00		3800.00		UG/L
ID043A901A12	TEST 2		13JUL1990	330	SCRUB SOLUTION	TANK 1	136		1890.00		3520.00		4550.00		UG/L
ID044A901B12	TEST 2		13JUL1990	330	SCRUB SOLUTION	TANK 2	128		1590.00		2720.00		3800.00		UG/L
ID045A901A12	TEST 2		13JUL1990	412	SCRUB SOLUTION	TANK 1	144		2090.00		3940.00		5100.00		UG/L
ID046A901B12	TEST 2		13JUL1990	412	SCRUB SOLUTION	TANK 2	119		1780.00		3050.00		4360.00		UG/L
ID047A901A12	TEST 2		13JUL1990	452	SCRUB SOLUTION	TANK 1	153		1970.00		3680.00		4800.00		UG/L
ID048A901B12	TEST 2		13JUL1990	452	SCRUB SOLUTION	TANK 2	110		1560.00		2690.00		3840.00		UG/L
ID049A901A12	TEST 2		13JUL1990	600	SCRUB SOLUTION	TANK 1	272		861.00		1900.00		2040.00		UG/L
ID050A901B12	TEST 2		13JUL1990	600	SCRUB SOLUTION	TANK 2	196		1560.00		2780.00		3740.00		UG/L
ID051A901A12	TEST 2		13JUL1990	750	SCRUB SOLUTION	TANK 1	242		862.00		1820.00		2050.00		UG/L
ID052A901B12	TEST 2		13JUL1990	750	SCRUB SOLUTION	TANK 2	199		1440.00		2470.00		3500.00		UG/L
ID053A901A12	TEST 2		13JUL1990	1100	SCRUB SOLUTION	TANK 1	162		1190.00		2550.00		2740.00		UG/L
ID054A901B12	TEST 2		13JUL1990	1100	SCRUB SOLUTION	TANK 2	191		1250 00		1980.00		2800.00		UG/L
ID061A901A12	TEST 2		13JUL1990	1330	SCRUB SOLUTION	TANK 1	129	dup9	1190.00		3140.00		2780.00		UG/L
ID061B901A12	TEST 2		13JUL1990	1330	SCRUB SOLUTION	TANK 1	129	dup9	1070.00		2460.00		2860.00		UG/L
ID062A901B12	TEST 2		13JUL1990	1330	SCRUB SOLUTION	TANK 2	210		1410.00		2200 00		3190.00		UG/L
ID063A901A12	TEST 2		13JUL1990	1521	SCRUB SOLUTION	TANK 1	204		1600.00		4440.00		3780.00		UG/L
ID064A901B12	TEST 2		13JUL1990	1521	SCRUB SOLUTION	TANK 2	160		1190.00		1930.00		2710.00		UG/L
ID065A901A12	TEST 2		13JUL1990	1645	SCRUB SOLUTION	TANK 1	244		1770.00		4200.00		3570.00		UG/L
ID066A901B12	TEST 2		13JUL1990	1645	SCRUB SOLUTION	TANK 2	207		819.00		1330.00		1780.00		UG/L
ID067A901A12	TEST 2		13JUL1990	1758	SCRUB SOLUTION	TANK 1	308		1350.00		2880.00		2770.00		UG/L
ID068A901B12	TEST 2		13JUL1990	1758	SCRUB SOLUTION	TANK 2	215		723.00		1160.00		1530.00		UG/L
ID069A901A12	TEST 2		13JUL1990	1914	SCRUB SOLUTION	TANK 1	264		1180.00		2580.00		2410.00		UG/L
ID070A901B12	TEST 2		13JUL1990	1914	SCRUB SOLUTION	TANK 2	151		700.00		1120.00		1380.00		UG/L
ID071A901A12	TEST 2		13JUL1990	2100	SCRUB SOLUTION	TANK 1	150		1520.00		3180.00		2850.00		UG/L
ID072A901B12	TEST 2		13JUL1990	2100	SCRUB SOLUTION	TANK 2	320		590.00		909.00		1160.00		UG/L
ID073A901A12	TEST 2		13JUL1990	2300	SCRUB SOLUTION	TANK 1	140		1740.00		3550.00		3350.00		UG/L
ID074A901B12	TEST 2		13JUL1990	2300	SCRUB SOLUTION	TANK 2	320		648.00		965.00		1300.00		UG/L
ID075A901A12	TEST 2		13JUL1990	2400	SCRUB SOLUTION	TANK 1	335		1970.00		3910.00		3870.00		UG/L
ID076A901B12	TEST 2		13JUL1990	2400	SCRUB SOLUTION	TANK 2	177		2250.00		4810.00		5500.00		UG/L
ID077A901A12	TEST 2		14JUL1990	205	SCRUB SOLUTION	TANK 1	200		3480.00		9380.00		7560.00		UG/L
ID079A901A12	TEST 2		14JUL1990	500	SCRUB SOLUTION	TANK 1	200		1440.00		3830.00		2940.00		UG/L
ID081A901A12	TEST 2		14JUL1990	700	SCRUB SOLUTION	TANK 1	155		1940.00		5580.00		3950.00		UG/L

SAMPLE	LOCATION	TIME	DATE	HOUR	MEDIA	LOCATION IN MEDIA	TANK VOLUME	FIELD QC	Dy	Dy FLAG	Tb	Tb FLAG	Yb	Yb FLAG	UNITS
ID082A901B12	TEST 2		14JUL1990	700	SCRUB SOLUTION	TANK 2	360		950.00		1820.00		2200.00		UG/L
ID083A901A12	TEST 2		14JUL1990	847	SCRUB SOLUTION	TANK 1	186		1680.00		5450.00		3120.00		UG/L
ID084A901B12	TEST 2		14JUL1990	847	SCRUB SOLUTION	TANK 2	391		987.00		2040.00		2180.00		UG/L
ID085A901A22	TEST 2		14JUL1990	1050	SCRUB SOLUTION	TANK 1	163		1330.00		4300.00		2750.00		UG/L
ID086A901B22	TEST 2		14JUL1990	1050	SCRUB SOLUTION	TANK 2	456		834.00		1670.00		1850.00		UG/L
ID087A901A22	TEST 2	POST TEST	14JUL1990	1252	SCRUB SOLUTION	TANK 1	161		2220.00		7700.00		4720.00		UG/L
ID088A901B22	TEST 2	POST TEST	14JUL1990	1252	SCRUB SOLUTION	TANK 2	518		672.00		1330.00		1520.00		UG/L
ID089A901A12	TEST 2	POST TEST	14JUL1990	1532	SCRUB SOLUTION	TANK 1	178	dup8	4950.00		19800.00		9210.00		UG/L
ID089B901A12	TEST 2	POST TEST	14JUL1990	1532	SCRUB SOLUTION	TANK 1	178	dup8	739.00		1740.00		1580.00		UG/L
IJ034A901D	TEST 2	POST TEST	23JUL1990	.	DUCT SMEAR	1	.		2260.00		7450.00		2090.00		UG
IJ033A901D	TEST 2	POST TEST	23JUL1990	.	DUCT SMEAR	2	.		1650.00		5340.00		2030.00		UG
IJ032A901D	TEST 2	POST TEST	23JUL1990	.	DUCT SMEAR	3	.		394.00		438.00		274.00		UG
IJ035A901D	TEST 2	POST TEST	23JUL1990	.	DUCT SMEAR	4	.		658.00		1250.00		1460.00		UG
IJ031A901D	TEST 2	POST TEST	23JUL1990	.	DUCT SMEAR	5	.		343.00		921.00		418.00		UG
IJ037A9011	TEST 2	POST TEST	23JUL1990	.	ELECTRODE SMEAR		.		6.00		10.20		11.60		UG
IJ024A901H	TEST 2	POST TEST	23JUL1990	.	HOOD SMEAR		.	blank	0.23		0.23		0.26		UG
IJ025A901H	TEST 2	POST TEST	23JUL1990	.	HOOD SMEAR	1	.		500.00		292.00		450.00		UG
IJ026A901H	TEST 2	POST TEST	23JUL1990	.	HOOD SMEAR	2	.		1360.00		255.00		1100.00		UG
IJ027A901H	TEST 2	POST TEST	23JUL1990	.	HOOD SMEAR	3	.		390.00		285.00		607.00		UG
IJ028A901H	TEST 2	POST TEST	23JUL1990	.	HOOD SMEAR	4	.		23.80		10.30		26.70		UG
IJ029A901H	TEST 2	POST TEST	23JUL1990	.	HOOD SMEAR	5	.		15.70		10.10		19.00		UG
IJ030A901H	TEST 2	POST TEST	23JUL1990	.	HOOD SMEAR	6	.		657.00		520.00		634.00		UG
IJ036A9011	TEST 2	POST TEST	23JUL1990	.	TRAILER PORT		.		56.90		149.00		123.00		MG/KG
7808229003	TEST 2	POST TEST	20AUG1990	.	FILTER		.	SPLIT3	0.47	B	0.95	B	0.98	B	MG/KG
7808229003	TEST 2	POST TEST	20AUG1990	.	FILTER		.	SPLIT3	0.92	B	4.30		2.20		MG/KG
7808229003	TEST 2	POST TEST	20AUG1990	.	FILTER		.	SPLIT3	1.00		4.00		2.30		MG/KG
IB004A9012	TEST 2	POST TEST	04OCT1990	.	SOIL	BOTTOM, 12 IN.	.		2.60	B	.		.		MG/KG
IB004B9012	TEST 2	POST TEST	04OCT1990	.	SOIL	BOTTOM, 12 IN.	.		2.50	B	.		.		MG/KG
IB004C9012	TEST 2	POST TEST	04OCT1990	.	SOIL	BOTTOM, 12 IN.	.		2.70	B	.		.		MG/KG
IB003A9012	TEST 2	POST TEST	04OCT1990	.	SOIL	BOTTOM, 6 IN.	.		2.60	B	.		.		MG/KG
IB003B9012	TEST 2	POST TEST	04OCT1990	.	SOIL	BOTTOM, 6 IN.	.		2.30	B	.		.		MG/KG
IB001A9012	TEST 2	POST TEST	04OCT1990	.	SOIL	SIDE, 12 IN.	.		2.20	B	.		.		MG/KG
IB001B9012	TEST 2	POST TEST	04OCT1990	.	SOIL	SIDE, 12 IN.	.		2.20	B	.		.		MG/KG
IB002A9012	TEST 2	POST TEST	04OCT1990	.	SOIL	SIDE, 6 IN.	.		2.00	B	.		.		MG/KG
IB002B9012	TEST 2	POST TEST	04OCT1990	.	SOIL	SIDE, 6 IN.	.		2.00	B	.		.		MG/KG
IC086C901E	TEST 2	POST TEST	.	.	PRODUCT	.	.		195.00		42.00	U	6.00		UG/G
IC006C901E	TEST 2	POST TEST	.	.	PRODUCT	1	.		6.00	U	42.00	U	6.00		UG/G
IC007D901E	TEST 2	POST TEST	.	.	PRODUCT	2	.		84.00		42.00	U	5.00	U	UG/G
IC026D901E	TEST 2	POST TEST	.	.	PRODUCT	3	.		186.00		42.00	U	5.00	U	UG/G
IC026F901E	TEST 2	POST TEST	.	.	PRODUCT	4	.		183.00		42.00	U	5.00	U	UG/G

SAMPLE	LOCATION	TIME	DATE	HOUR	MEDIA	LOCATION IN MEDIA	TANK VOLUME	FIELD QC	Dy	Dy FLAG	Tb	Tb FLAG	Yb	Yb FLAG	UNITS
IC026I901E	TEST 2	POST TEST	.	.	PRODUCT	5	.		182.00		42.00	U	5.00	U	UG/G
IC026M901E	TEST 2	POST TEST	.	.	PRODUCT	6	.		177.00		42.00	U	5.00	U	UG/G
IC027D901E	TEST 2	POST TEST	.	.	PRODUCT	7	.		172.00		42.00	U	5.00	U	UG/G
IC037D901E	TEST 2	POST TEST	.	.	PRODUCT	9	.		181.00		42.00	U	5.00	U	UG/G
IC037I901E	TEST 2	POST TEST	.	.	PRODUCT	10	.		171.00		42.00	U	5.00	U	UG/G
IH037J901E	TEST 2	POST TEST	.	.	PRODUCT	11	.		6.00	U	42.00	U	5.00	U	UG/G
IC043D901E	TEST 2	POST TEST	.	.	PRODUCT	15	.		173.00		42.00	U	5.00	U	UG/G
IC043I901E	TEST 2	POST TEST	.	.	PRODUCT	16	.		155.00		42.00	U	5.00	U	UG/G
IC043J901E	TEST 2	POST TEST	.	.	PRODUCT	17	.		6.00	U	42.00	U	8.00		UG/G
IH074D901E	TEST 2	POST TEST	.	.	PRODUCT	18	.		6.00	U	42.00	U	5.00	U	UG/G

END

DATE FILMED

01/10/92